CHAPTER ONE

INTRODUCTION

1.1 Background of the Study

The development of modern society and industry has led to a stronger demand for engineers with specialized knowledge in corrosion. There are a number of reasons for this: The application of new material requires new corrosion knowledge. Industrial production has led to pollution, acidification and increased corrosivity of water and the atmosphere. Stronger materials, thinner cross-sections and more accurate calculation of dimensions make it relatively more expensive to add a corrosion allowance to the thickness. The development of industrial sectors like nuclear power production and offshore oil and gas extraction has required stricter rules and corrosion control. Considering the future, it should be noticed that most methods for alternative energy production will involve corrosion problems. Aluminium and mild steel are solid substances obtained from the mother earth. These two substances are general purpose engineering construction materials mostly used as a result of their natural properties like rigidity, ductility, tensile strength conduct of heat and electricity etc (Trethewey and Chamberlain, 1995). Mild steel has numerous industrial applications and is mainly used for the corrosion protection of steel. Aluminum, is amphoteric in its behaviour towards acid and alkaline. It is one of the most important non-ferrous metals, which finds extensive use in metallic coatings. Aluminum is the third most abundant element found in nature; first two are oxygen and silicon. It is an important and widely used metal in the transport, construction, packaging and electrical sectors. Aluminum and its alloys are of economic importance because of their low cost, lightness and good corrosion resistance at moderate temperatures (Kotz and Treichel, 1996). They are also widely used in many industries such as reaction vessels, pipes, machinery and chemical batteries because of their advantages (El Maghraby, 2009). According to Refat and Ishaq (2013), aluminum and its alloys are low cost and remarkable materials in industrial technology because of their light weight, high thermal and electrical conductivity as well as high resistance to corrosion in a wide variety of corrosion environments. Generally, corrosion resistance of metals such as aluminum and steel, in corrosive environment, may be attributed to the formation of a protective tightly adhered invisible oxide film on the metal surface (Uppal and Bhatia, 2009).

Mild steel is an alloy that contains medium amount of carbon. Besides carbon, steel contains many chemical elements which are added into iron to form steel of different kinds having various physical properties (Uppal and Bhatia, 2009). Mild steel is a medium carbon steel

with carbon content of 0.2 – 0.5% (Aggarwal, 2010). It is used for structural applications. It is wieldable, which expands its possible applications. It is widely used in the manufacturing of installations for petroleum, fertilizers, and in other industries. In most cases, operations within these industries such as pickling, acid cleaning, and acid descaling involves contact between mild steel and aggressive solution (such as acids, salts and bases). Mild steel can be hardened by heat treatment, and it has a good machining properties. It is used for the production of lightly stressed machine fittings, shafts, turbine motors, railways axels, crank shafts, and fish plates, cross heads, pipes and drums.

Although, the economic importance of these metals are hindered by corrosion activities. Hence the corrosion of metals is often considered as an inconvenience because it implies a change of the objects/metals in the course of time. The metallurgical extraction of the metal from its ore is the removal of the metal from its stable compound form to become an unstable, artificial form. That instability is the desire of those metals to return to their more stable, natural state (Green and Perry, 2008).

Aluminum, being an industrially important metal, is subject to corrosion in service by various corrosive agents of which the aqueous acids are the most dangerous (Kumar *et al.,* 2010). It is reactive towards oxygen that it immediately forms a passive surface layer of aluminum oxide upon being exposed to air (Trethewey and Chamberlain, 1995). Mild steel is vulnerable to rust. Prathibha *et al* (2012) examined corrosion inhibition of mild steel in HCl medium. Mild steal dissolves according to the reaction (Yuce and Kardas, 2012);

$$Fe_{(s)} + 2HCl_{(aq)} \rightarrow FeCl_{2(aq)} + H_{2(g)}$$

(1.1)

Corrosion of metals results in loss of functional integrity and attractive appearance. Due to enormous costs and health implications associated with corrosion, there is need to device measures that will drastically reduce the rate of corrosion. There are many ways of controlling corrosion, but the one receiving more attention presently is the use of green inhibitors. Generally, an inhibitor can be defined as a chemical substance which, when added in small concentrations or quantity to an environment, minimizes or prevents corrosion. There are inorganic substances like phosphates, chromates, dichromates and arsenates which have been found effective as inhibitors of metal corrosion, but a major disadvantage is that they contain heavy metals which are injurious to health, consequently their use has come under severe criticism.

Owing to the increasing ecological awareness, as well as the strict environmental regulations, and consequently the need to develop environmentally friendly processes, attention is currently focused on the development of "green" alternatives to mitigating corrosion. Green approaches to corrosion mitigation entail the use of substances, techniques, and methodologies that reduce or eliminate the use of products, by-products, solvents, reagents, and so forth that are hazardous to human health or the environment in combating corrosion (Khaledand Al-Mobarak, 2012*;* Uwah *et al.*, 2013; Yaro, 2013). Among the alternative corrosion inhibitors, organic substances containing polar functions with nitrogen, oxygen and/or sulphur atoms in a conjugated system have been reported to exhibit good inhibiting properties (Obot, 2006). Plants have been recognized as sources of naturally occurring compounds (Farooqi *et al.,* 1997). Most of the compounds extracted from plants are used in traditional applications such as pharmaceuticals and biofuels. Furthermore, naturally occurring compounds are of interest, because of they are cost effective, abundant availability and more importantly their environmental acceptability. Due to these advantages, extracts of some common plants and plant products have been tried as corrosion inhibitors for metals and alloys under different environments (Ebenso and Ekpe, 1996; Kliskic *et al.,* 2000; Ebenso *et al.,* 2004; Abdel-Gaber *et al.,* 2006). The qualities mentioned above have made plants become an important source of a wide range of eco-friendly (green) corrosion inhibitors.

Despite the broad spectrum of organic compounds available as corrosion inhibitors, the successful utilization of plant extracts that provide a rich source of naturally synthesized chemical compounds and that can be extracted by simple procedures with low cost as well as biodegradable in nature is a promising alternative (Kang *et al.,* 2012). The use of phytochemicals as corrosion inhibitors can be traced back to 1960s when tannins and their derivatives were used to protect corrosion of steel, iron and other tools (Buchweishaija, 2009).

1.2 Problem Statement

According to World Corrosion Organization, the annual cost of corrosion worldwide is estimated at $2.2 trillion (USD) - more than 3 percent of the world's gross domestic product (GDP) (Hoar TP *et al*. 1971). It has been further estimated that about 20% of this loss could have been saved by better use of existing knowledge in corrosion protection, design etc. In other words, there is a demand for applied research, education, information, transfer of knowledge and technology, and technical development. The cost of corrosion is partly

connected with the efforts to give structures an attractive appearance, it is partly the direct cost of replacement and maintenance and the simultaneous economic loss due to production interruptions, and it includes extra cost of using expensive materials and other measures for the prevention of corrosion and the loss or destruction of products. Besides the financial cost, attention is paid to safety risks and the pollution of the environment due to corrosion. Personnel injuries can occur due to the fracture of structures, the failure of pressure tanks and leakages in containers for poisonous, aggressive or inflammable liquids for instance. Corrosion-control activities are required in practically every area of industry and daily life; from the power plants that produce energy and the wastewater treatment plants to the transportation sector.

Many researches have been carried out to meet these challenges and requirements and considerable engineering activities have been established where careful attention is paid to modern, advanced methods for inspection, monitoring, control and calculation. Corrosion inhibitors (inorganic substances like phosphates, chromates, dichromates and arsenates) are widely used in the industry to reduce the corrosion rate of metals in contact with the aggressive environment. The environmental toxicity of these synthetic corrosion inhibitors have led to the search for eco-friendly corrosion inhibitors as they are safer and have a whole lot of advantages.

The potential usage of *Aspilia africana, Chromolena odorata,* Dennettia tripetala*, Newbrouldia leavis,* Dialium guineense and *Vitex doniana)* leaf extracts discussed in this project is in line with the recent trend of the environment- friendly corrosion inhibitors concept. Also, the corrosive and/or corrosion inhibiting properties of plant extracts; extracts such as tannins, organic amino acids, alkaloids, and organic dyes of plant origin have good corrosion-inhibiting abilities.

1.3 Aim and Objectives

The aim of this work is assessment of inhibition of plant leaf extracts on aluminum and mild steel in acidic and alkaline media using different techniques.

The objectives are to:

1. Determine the functional groups, phytochemicals and molecular compounds of the plant extracts using Fourier transform infra-red (FTIR), Gas chromatography-mass spectrometry (GC-MS) and photochemical analyses.

2. Determine, as well as optimize (using Response surface methodology, RSM) the corrosion inhibition efficiency of the plant extracts on Al and mild steel in an alkaline and acidic media.
3. Evaluate the kinetic/thermodynamic properties of the corrosion inhibition of metals in the alkaline and acid media.
4. Identify the inhibitor types using Potentiodynamic polarization study (PDP) and to investigate their interfacial electrochemical processesusing electrochemical impedance spectroscopy (EIS).
5. Examine the surface morphologies of the metals using Scanning electron microscope, (SEM) and the shifting mechanism of the inhibitors' functional groups using FTIR.
6. Evaluate the molecular properties and the energy interaction of the inhibitors on the metals using quantum chemical study.

1.4 Scope of Work

The scope of this study is to use natural leaf extracts namely*Aspilia africana, Chromolena odorata, Dennettia tripetala, Newbrouldia leavis, Dialium guineense* and *Vitex donianaa*s corrosion inhibitors for aluminum and mild steel in alkaline and acid media. The experimental study is based on weight loss and electrochemical methods.

1.5 Justification of Study

The result of this work will help in developing locally sourced eco-friendly inhibitors for optimum corrosion inhibition of metals in alkaline and acidic media. The plant extracts will be useful as corrosion inhibition additives in alkaline and acid media for cleaning, descaling and pickling metallic structures.

The environmental toxicity of the readily available and commonly used synthetic corrosion inhibitors have fueled the search for eco-friendly corrosion inhibitors.

The potentials of *Aspilia africana, Chromolena odorata, Dennettia tripetala, Newbrouldia leavis, Dialium guineense* and *Vitex donianaa*leaf extracts as bio-based corrosion inhibitors effectively relates this work to the recent trend of environmental- friendly corrosion inhibitor concepts.

CHAPTER TWO

LITERATURE REVIEW

2.1 Meaning of corrosion

The word corrosion is derived from the latin *corrosus* which means eaten away or consumed by degrees; an unpleasant word for an unpleasant process. Corrosion is degradation of materials' properties due to interactions with environments, and corrosion of metals (and many materials for that matter) is inevitable. The fundamental cause or driving force for all corrosion is lowering of a system's Gibbs energy. For instance, in production of almost all metals (and engineering components made of metals) involves adding energy to the system. As a result of this uphill thermodynamic struggle, the metal has a strong driving force to return to its native, low energy oxide state. This return to the native oxide state is known as corrosion and even though it is inevitable, substantial barriers (corrosion control methods) can be used to slow its progress toward the equilibrium state. Thus it is the rate of approach to equilibrium that is often of interest. This rate is controlled not only by the nature of the metals surface, but also by the nature of environment as well as the evolution of both (Shaw and Kelly, 2006). In another interesting view, Trethewey and Chamberlain (1995) further defined corrosion as the destruction of materials caused by chemical or electrochemical action of the surrounding environment. The most common examples of corrosion include rusting, discoloration and tarnishing. Corrosion can only be reduced it cannot be prevented because thermodynamically it is a spontaneous phenomenon.

The economy of any country would be drastically changed if there were no corrosion. For example, automobiles, ships, underground pipelines and house-hold appliances would not require coatings. Corrosion is a fast process and accompanied by number of reactions that change the composition and properties of both metal surface and local environment, for example formation of oxides, diffusion of metal cations into the coating matrix, local pH changes and electrode potential (Acharya *et al.*, 2013).

Corrosion process can be categorized as:

1. Chemical corrosion: This occurs when a metal reacts with dry air or oxygen.
2. Electrochemical corrosion: This occurs in the presence of an electrolyte

2.1.1 Mechanism of corrosion

Considering the mechanism of corrosion, corrosion reaction takes place by two simultaneous reactions: the oxidation of a metal at an anode (a corroded end releasing electron) and the reduction of a substance at the cathode (a protected end receiving electron). In order for the reaction to occur, the following conditions must exist:

1. A chemical potential difference must exist between adjacent sites on a metal surface (or between alloys of a different composition),
2. An electrolyte must be present to provide solution conductivity and as a source of material to be released at the cathode, and
3. An electrical path through the metal or between metals must be available to permit electron flow.

An electrochemical corrosion of iron in contact with water is an example that can be used to describe the electrochemical reactions. In a nearly neutral or slightly acid environment, the water is dissociated into hydrogen ions (H^+) and hydroxyl ions (OH^-) as;

$$H_2O \rightarrow H^+ + OH^- \quad (2.1)$$

When metal is placed in contact with a liquid, surface ionization occurs because of the electric charge difference at the solid-liquid interface. For example ion dissolves in water in the form of positively charged ferrous ions (Fe^{2+}) where

$$Fe \rightarrow Fe^{2+} + 2e^- \quad (2.2)$$

Electrochemically, a chemical substance is oxidized when it loses electrons to a second substance. The electrode at which oxidation takes place is called anode. The electrode at which reduction takes place is called cathode. Hence, oxidation reaction results in the formation of positive charge ferrous ions at the anode. Ferrous ions moving away from the metal surface are further oxidized to ferric ions (Fe^{3+}) as follows:

$$Fe^{2+} \rightarrow Fe^{3+} + e^- \quad (2.3)$$

The positively charged ferric ions are attracted to the negatively charged hydroxyl ions to form corrosion product, $Fe(OH)_3$.

$$Fe^{3+} + 3(OH)^- \rightarrow Fe(OH)_3 \quad (2.4)$$

The rust consists of iron hydroxide or iron oxide hydrates in various states depending on the degree of oxidation and dehydration. The reduction reaction at the cathode must take place concurrently in order to continue the corrosion process. Several reactions are possible and the one that occurs is determined by the environment. Without the presence of air or oxygen, hydrogen ions can be reduced by the excess of electrons at the cathode surface and evolve as molecular hydrogen.

$$2H^+ + 2e^- \rightarrow H_2$$

(2.5)

If hydrogen is not removed from the surface, the cathodic reaction decreases and the corrosion rate is reduced. With the presence of air, the more likely reaction is the reduction of oxygen. Two possible reactions occur:

$$O_2 + 4H^+ + 4e^- \rightarrow 2H_2O$$

(2.6)

$$O_2 + 2H_2O + 4e^- \rightarrow 4(OH)^-$$

(2.7)

2.1.2 Causes of corrosion

Apart from the presence of moisture and acid, the basic reason for metallic corrosion is that metals have the tendency to revert back to their thermodynamically stable state (Dara, 2000).

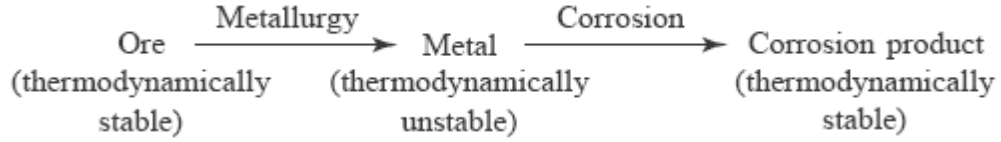

2.2 Types of Corrosion

Generally, there are different types of corrosion, depending on the metal reactions, geometry and physical environments. Corrosion occurs in several widely different forms (Trethewey and Chamberlain, 1995; Green and Perry, 2008; Uppal and Bhatia, 2009; Aggarwal, 2010). According to Trethewey and Chamberlain (1995), any corrosion which occurs at preferred sites of a metal is described as selective attack and it includes grain boundary corrosion, intergranular corrosion, microbiologically induced corrosion (MIC) and selective leaching.

2.2.1. Galvanic corrosion

This type of electrochemical corrosion is also called bimetallic corrosion (Aggarwal, 2010). When two dissimilar metals are connected and exposed to an electrolyte, they will form a galvanic cell. The anodic metal will be oxidised and it will undergo corrosion. Zinc and copper metals connected with each other in an electrolyte medium form a galvanic cell. Zinc acts as anode and undergoes corrosion while cathode will be unaffected.

At anode: $Zn \rightarrow Zn^{++}\, 2e^{-}$[Oxidation] corrosion (2.8)

At cathode: $Cu^{++} \rightarrow +2e^{-}$ [Reduction] unaffected (2.9)

- . Galvanic corrosion can be avoided by coupling metals close to the electrochemical series.
- . Fixing insulating material between two metals.
- By using larger anodic metal and smaller cathodic metal.

Example of galvanic corrosion:

i. Steel screws in brass marine hardware,
ii. Steel pipe connected to copper plumbing,
iii. Steel propeller shaft in bronze bearing,
iv. zinc coating on mild steel,
v. lead–tin solder around copper wires.

2.2.2. Pitting corrosion

Due to crack on the surface of a metal, local straining of metal, sliding under load, chemical attack, there is formation of a local galvanic cell (Trethewey and Chamberlain, 1995). The crack portion acts as anode and rest of the metal surface acts as cathode. It is the anodic area which will be corroded and the formation of a pit is observed.

2.2.3. Stress corrosion

In a metallic structure, if there is a portion under stress, it will act as anode and rest part of the structure will act as cathode. It is now a galvanic system and hence anodic part which is small in area will corrode more. Stress corrosions are observed in the following systems:

- Caustic embrittlement is a type of stress corrosion occurring in steel tank (boiler) at high temperature and in alkaline medium. Boiler water has Na_2CO_3; it will be hydrolysed at high temperature to give NaOH. It flows into hair cracks and crevices. There it reacts with iron and forms Na_2FeO_2 (sodium ferroate) which decomposes to give Fe_3O_4 (ferroferric oxide) and NaOH.

Reaction $3Na_2FeO_2 + 3H_2O \rightarrow Fe_3O_4 + H_2 + 6NaOH$ (2.10)

NaOH thus formed further reacts with iron to cause corrosion. It is called caustic embrittlement. Addition of Na_2SO_4 to boiler water in addition to tannin and lignin to boiler water prevents caustic cracking. By neutralization of excess of alkali with dilute acid (or) control of pH value caustic embrittlement can be controlled.

- Season cracking: It is applied to stress corrosion of copper alloys bronze. Pure copper metal is less sensitive to stress corrosion. However, presence of alloying impurities like P, Zn, Al, etc. results in marked sensitivity for corrosion. Some of the alloys like brass are made of zinc and copper. In the presence of ammonia or amines, zinc and copper undergo inter-granular cracking. These metals form complexes

$[Cu(NH_3)_4]^{++}[Zn(NH_3)_4]^{++}$which appear as corrosion products. Stress corrosion may be reduced:

I. By applying protective coatings
II. Using corrosion inhibitors
III. By stress relief heat treatments

2.2.4. Crevice corrosion

If surface of painted metal is scratched, it will undergo corrosion. The scratched portion acts as small anode and the rest part will act as cathode forming a local cell. Crevice corrosion is formed near joints, rivets and bolts. Changes in the concentration of oxygen/acidic medium cause's crevice corrosion. The attack which occur because part of a metal surface is in a shielded or restricted environment, compared to that of the metal which is exposed to a large volume of electrolyte. Hence crevice corrosion is associated with the geometry of structures such as riveted plates, welded structures and threaded components, contact of metal with non-metallic solids like plastics, rubber and glass; or deposits of sand, dirt or corrosion products (Trethewey and Chamberlain, 1995). The common factor is the initial geometrical arrangement of the solid elements of the system, arising from the way in which the solid components of the system have been assembled or through the surface accumulation of the solid debris. This leads to a heterogeneous distribution of the species dissolved in the electrolyte, which in turn provides the conditions for localized attack. A widely accepted general mechanism for crevice corrosion of stainless steels has been proposed by Fontana and Greene (Shaw and Kelly, 2006).

The steps involved are:

i. Initially the electrolyte is assumed to have uniform composition. Corrosion occurs slowly over the whole of the exposed metal surface, both inside and outside the crevice. Under these conditions, the generation of positive metal ions is counterbalanced electrostatically by the creation of negative hydroxyl ions.

ii. The consumption of dissolved oxygen results in the diffusion of more oxygen from electrolyte surfaces exposed to the atmosphere. Oxygen is more readily replaced at metal surfaces in the bulk electrolyte than at those within the crevice. Within the confined space of

the crevice this lack of oxygen impedes the cathodic process and generation of negative hydroxyl ions is diminished.

iii. The production of excess positive ions in the gap causes negative ions from the bulk electrolyte to diffuse into the crevice to maintain the potential energy at a minimum. In the presence of chlorides, it is likely that complex ions are formed between chloride, metal ions and water molecules. These are thought to undergo hydrolysis (reaction with water), giving the corrosion product and more importantly hydrogen ions which reduce the pH. This is described by Eq. (2.11)

$$M^{Z+} + H_2O \rightarrow MOH^{(Z-1)+} + H^+ \quad (2.11)$$

The equation describes a general hydrolysis reaction. Presence of chloride is well known to be conducive to the development of low pH because of its extremely low tendency to associate with water. Hydrogen chloride dissociates completely in water. Additionally, stainless steels, which rely on the protection of passive films, are unstable in chloride environments. Titanium, another passivating metal has excellent resistance to crevice corrosion because its oxide film is unreactive towards chloride ions.

iv. The increase of hydrogen ion in the concentration accelerates the metal dissolution process, which in turn exacerbates the problem; so does increase of anion concentration within the crevice. An important feature of active crevice corrosion cells is that they are autocatalytic, once started they are self- sustaining. The metal within the crevice is corroding rapidly while that at outside is cathodically protected.

2.2.5. Erosion corrosion

Due to mechanical wear and tear, corrosion occurs on the surface of a metal and is called erosion corrosion. Erosion corrosion is the acceleration or increase in rate of deterioration or attack on a metal because of relative movement between a corrosive fluid and the metal surface. Generally, this movement is quite rapid, and mechanical wear effects or abrasion are involved. Metal is removed from the surface as dissolved ions, or it forms solid corrosion products which are mechanically swept from the metal surface. Sometimes, movement of the environment decreases corrosion, particularly when localized attack occurs under stagnant conditions, but this is not erosion corrosion because deterioration is not increased.

Erosion corrosion is characterized in appearance by grooves, gullies, waves, rounded holes, and valleys and usually exhibits a directional pattern. In many cases, failures because of erosion corrosion occur in a relatively short time, and they are unexpected largely because

evaluation corrosion tests were run under static conditions or because the erosion effects were not considered.

2.2.6. Microbiological corrosion

Some types of bacteria consume oxygen and cause differential aeration type of system which results in corrosion. The corrosion occurs at the portion poor in oxygen concentration. Fungi, algae and bacteria are the major causes of biological corrosion which can cause severe wood rot and metal corrosion (Puckorious, 1978.)

2.2.6.1 Fungi

Fungi are yeasts and molds, fungal growths are found on cooling towers wood, basin walls and in heat exchangers. In wood decay, the cellulose in wood is consumed by organisms until it loses its strength. Fungi are not directly corrosive to metals, however, the deposits of fungi on metal surfaces produce differential concentration cells and interfere with the action of corrosion inhibitors by shielding the metal surface from it, causing corrosion. Wood deterioration can be prevented by impregnation of toxic salts that inhibit fungal growth. Fungi can also be controlled by the periodic application of fungicides such as pentachlorophenol salts or tributyl tin compounds. Chlorine is not effective against these organisms.

2.2.6.2 Algae

Algae, like fungi are relatively large organisms. Algae commonly cause slimy deposits in cooling towers where water and sunlight are present. Deposits of dead algae provide food for bacteria and fungi. Algae are not known to cause corrosion directly, except for occasional occurrences under their deposits. Control can be effected by covering cooling tower decks to prevent sunlight from reaching the tower water, or with chemicals such as chlorine, quaternary ammonium compounds and copper salts.

2.2.6.3 Bacteria

Bacteria associated with corrosion are of two types; aerobic and anaerobic. Aerobic microorganisms readily grow in an environment containing oxygen, while anaerobic species thrive in an environment virtually devoid of atmospheric oxygen. Each type has a specific action and often referred to by its effects on materials. Deterioration and corrosion of materials due to the metabolic activity of microorganisms is quite complicated and in some cases, not fully understood. Corrosion can be explained by any one or more of the following;

a) Producing a corrosive environment.
b) Creating electrolytic concentration cells on the metal surface.

c) Alternating the surface protecting films.
d) Influencing the rate of anodic-cathodic reaction.
e) Changing the environment composition.

Sulfate-reducing bacteria convert water-soluble sulfur compounds to hydrogen sulfide in a slightly acid to alkaline environment. Corrosion of mild steel, stainless steel and copper alloys is due to conversion of iron to iron sulfide. Nickel and nickel-based alloys are severely pitted under a combination of low pH, sulfides, and reducing conditions. Using chlorine to control the bacteria is not effective because the microorganisms are usually covered by slime masses that prevent chlorine from reaching the bacteria. In addition, the sulfides surrounding these microorganisms react with chlorine to form chloride salts that negate the effectiveness of chlorine. Special toxicants such as long-chain fatty-acid amine salts and organic-sulfur compounds (for example, methylene bisthiocynate) are effective in controlling these bacteria.

Another group of microorganisms are the nitrifying (or acid producing) bacteria, which produce nitric acid from ammonia. This results in corrosion of mild steel, copper and aluminum by chemical corrosion in low pH conditions. These microorganisms are not affected by oxygen and do not neutralize corrosion inhibitors such as zinc and chromate. Chlorine as well as many non-oxidizing biocides, is very effective in controlling these bacteria. However, with appreciable amount of ammonia, chlorine may not appear effective; chlorine is neutralized and is unavailable for bacteria control.

2.2.7 Waterline corrosion

It has been observed in the case of an iron tank containing water, that the portion of iron tank just below the water level undergoes corrosion. It is due to the difference in oxygen concentration. Corroding portion is poor in oxygen and acts as anode.

2.2.8 Differential aeration corrosion

If a metal rod is dipped in an electrolyte, the portion dipped in water is poor in oxygen concentration and works as anode which gets corroded and the portion above water acts as cathode which is protected. The system will act as a concentration cell and the chemical reactions for zinc dipped in water.

2.3 Factors that Affect the Rate of corrosion

Corrosion of metals is influenced by so many factors (Green and Perry, 2008; Uppal and Bhatia, 2009). According to Green and Perry (2008), factors that affect corrosion of metals include; solution pH, oxidizing agents, temperature, velocity, nature of film, stream concentration, time and impurities. Furthermore, electrode potential, electrode efficiency,

electrolyte, area ratio, aeration, flow rate, metallurgical condition and composition and stifling effects are factors that influence bimetallic corrosion.

2.3.1 Consequences of corrosion

It may therefore be observed that corrosion is a potent force which destroys economy, depletes resources, affects daily activities and causes costly and untimely failures of plants equipment and components. In most industries, whose facilities are constituted by metallic structures, the phenomenon of corrosion is invariably present. This problem originates very important material and economic losses due to partial or total replacement of equipment and structures, and plant-repairing shutdown.

Corrosion not only has economic implications, but also social implications, and these engage the safety and health of people either working in industries or living in nearby towns. The oil industry in Nigeria is one of the most affected by corrosion because this phenomenon exerts its effects from the very moment of oil extraction is on, causing a constant struggle against it. From the above observations, the consequences of corrosion include:

a. Plant shutdown: Shutdowns of nuclear plants, process plants, power plants and refineries may cause severe problems to industries and consumers.
b. Loss of products/materials: Material losses as corrosion consequences are priced so high that in some countries like the U.S and England, these factors have been estimated from 3-
c. 4% of the GDP. Leaking containers, storage tanks, water and oil transportation lines and fuel tanks cause significant loss of products and may generate severe accidents and hazards.
d. Loss of efficiency: Insulation of heat exchanger turbines and pipelines by corrosion products reduces heat transfer and piping capacity.
e. Contamination: Corrosion products may contaminate chemicals, pharmaceuticals, dyes, packaged goods e.t.c, with dire consequences to consumers.
f. Nuclear hazards: The Chernobyl disaster is a continuing example of transport of radioactive corrosion products in water, fatal to human, animal, and biological lives.

The magnitude of corrosion would depend upon the sensitivity of a particular metal or alloy to a specific environment. For instance, copper corrodes rapidly in the presence of ammonia and it is a serious problem in agricultural areas. Many statues made from bronze have been destroyed (corroded) by ammonia released from fertilizer.

2.4 Corrosive Environments

The environment that causes corrosion is regarded as corrosive environment (Trethewey and Chamberlain, 1995; Aggarwal, 2010). The nature of corrosive environment can be described:

1. pH in the range of 4-10; corrosion rate is fairly independent of pH, but it increases rapidly when the pH falls below 4.
2. Oxygen content; increase in oxygen concentration usually gives an increase in corrosion rate.
3. Flow rate; increased water flow increases oxygen access to the surface and removes protective surface films, so usually increases corrosion, but can sometimes improve access for corrosion- inhibiting reactants.
4. Water type; in general low corrosion rates are found with scale-forming (hard) waters. Aggressive ions which accelerate corrosion are Cl^-, $SO4^{2-}$ but quite complex interactions may occur between the various dissolved species in natural waters.

2 .4.1 Alkaline environment

2.4.1.1 Sodium hydroxide as a corrosive environment

Sodium hydroxide (NaOH) is a white deliquescent compound, usually in form of pellets. Dissolution of sodium hydroxide in water is a highly exothermic reaction in which a large amount of heat is liberated, posing a threat to safety through the possibility of splashing. The resulting solution is usually colorless and odourless with slippery feeling upon contact. Sodium hydroxide reacts with acids to produce water and the corresponding salts. Glass reacts slowly with aqueous sodium hydroxide solutions at ambient temperatures to form soluble silicates. Sodium hydroxide is a popular strong base used in the industry;

i. Sodium hydroxide is used in food processing. The compound is often used in steps for peeling fruits and vegetables, processing cocoa and chocolate, thickening of ice cream and soda processing.
ii. In petroleum industry, sodium hydroxide is used as an additive in drilling mud to increase alkalinity in bentonite mud systems, to increase the mud viscosity, and to neutralize any acid gas which may be encountered in the geological formation as drilling progresses.
iii. Sodium hydroxide is also widely used in the pulping of wood for making paper of regenerated fibers.
iv. It is used in dissolving amphoteric metals and compounds.
v. It is used as esterification and trans- esterification reagent.
vi. It is used as cleaning agent.

2.4.1.2Potassium hydroxide as a corrosive environment

Potassium hydroxide (KOH) is an inorganic compound usually referred to as caustic potash. It is odourless and whitish, and it can be in powder or pellet form. It has strong alkaline properties and contains potassium and hydroxide ions. It is corrosive, and hygroscopic. When solution of KOH comes in contact with metal (such as aluminum), it attacks (corrodes) the metal. KOH has molecular mass, melting point and density of 56g/mol, 380 ^{0}C, and 2.12g/cm^3 (at 25 ^{0}C), respectively.

KOH is produced by adding potassium carbonate to a strong solution of calcium hydroxide. Filtering off the precipitated calcium carbonate and boiling down the solution gives potassium hydroxide.

$$Ca(OH)_2 + K_2CO_3 \rightarrow CaCO_3 + 2KOH \quad (2.12)$$

This method has been largely replaced by the method of electrolysis of potassium chloride solutions.

$$2KCl + 2H_2O \rightarrow 2KOH + Cl_2 + H_2 \quad (2.13)$$

This method is analogous to the manufacture of sodium hydroxide. Potassium hydroxide is produced by methods similar to those used to produce sodium hydroxide. It is used in the manufacture of soap and other potassium compound (Uppal and Bhatia, 2009). It is used in food processing, petroleum, cleaning product, clothing and textile, chemical and petrochemical industries.

2.4.2: Acidic environment

2.4.2.1Hydrochloric acid as a corrosive environment

Hydrochloric acid (HCl) is colourless acid. It has a sharp irritating smell. It has a sour taste. It is heavier than air. It is a monoprotic acid, which means it can ionize only once to give up one H^+ ion in aqueous hydrochloric acid, the H^+ joins with water molecule to form a hydronium ion, H_3O^+.

$$HCl + H_2O \rightarrow H_3O^+ + Cl^- \quad (2.14)$$

The melting and boiling points, density and pH of HCl depend on the concentration or molarity of the HCl in acid solution. Hydrochloric acid as a binary (two-component) mixture of HCl and H_2O has a constant-boiling azeotrope at 20.2 percent HCl and 108.6 ^{0}C.

HCl reacts with iron to form iron chloride and hydrogen. It reacts with zinc to form zinc chloride and hydrogen.

$$Fe + 2HCl \rightarrow FeCl_2 + H_2 \quad (2.15)$$

$$Zn + 2HCl \rightarrow ZnCl_2 + H_2 \quad (2.16)$$

Hydrochloric acid can be manufactured by two main methods (Uppal and Bhatia, 2009). The methods are;

1. Direct synthesis: chlorine and hydrogen react exothermically to form hydrogen chloride gas. The hydrogen chloride gas produced is cooled, and absorbed into water to give hydrochloric acid at the desired concentration.

$$Cl_2 + H_2 \rightarrow 2HCl \quad (2.17)$$

2. Heating rock salt with concentrated H_2SO_4 to 500 ^{0}C.

$$2NaCl + H_2SO_4 \rightarrow Na_2SO_4 + 2HCl \quad (2.18)$$

Other methods of manufacturing HCl include organic by-product synthesis and organic waste incineration (incineration of chlorinated waste).

In general, hydrochloric acid is used;

1. to prepare chloride,
2. as important laboratory reagent, and
3. for pickling of metals.

Pickling of steel is one of the most important applications of hydrochloric acid. It removes rust or iron oxide scale from iron or steel before subsequent processing. Equation (2.22) shows HCl as pickling agent for the pickling of carbon steel grades.

$$Fe_2O_3 + Fe + 6HCl \rightarrow 3FeCl_2 + 3H_2O \quad (2.19)$$

Hydrochloric acid solutions are normally used for pickling of aluminum and electrochemical etching processes that normally lead to substantial loss of metal to corrosion (El Maghraby, 2009; Alinno and Ejikeme, 2012; Ghulamullah, *et al.,* 2015).

2.4.2.2 Tetraoxosulphate vi acid as a corrosive environment

Tetraoxosulphate VI acid is clean, colourless and odourless liquid. It has a molecular weight, density and boiling point of 98g/mol, 1.84g/cm^3 and 337 ^{0}C, respectively. Acid solutions are generally used for removal of undesirable scale and rust in several industrial processes. Tetraoxosulphate VI acid is a strong acid that can be manufactured by two main methods (Uppal and Bhatia, 2009);

1. The contact process,
2. The lead chamber process, which essentially consists of oxidizing a mixture of sulphur dioxide and water to Tetraoxosulphate vi acid using nitric oxide as an oxygen carrier.

$$H_2O + SO_2 + NO_2 \rightarrow H_2SO_4 + NO \quad (2.20)$$

The nitrogen 11 oxide then combines with oxygen to form more nitrogen iv oxide, which is used again;

$$2NO + O2 \rightarrow 2NO_2 \quad (2.21)$$

The effects of sulphuric acid on metal depend on a number of factors, including the type of metal, the concentration of the acid, and the temperature.

Dilute H_2SO_4 will react with any metal that lies above hydrogen in the reactivity series by displacing hydrogen from the acid, releasing it as a gas and forming the sulphate salt of the metal. The metals that come into this category include the alkali metals, such as sodium and potassium, and the alkaline earth metals, like magnesium and calcium, as well as many other common metals, such as iron, nickel, and zinc.

Zinc reacts with concentrated H_2SO_4 and liberate SO_2.

$Zn + 2H_2SO_4 \rightarrow \quad ZnSO4 + 2H_2O + SO_2$

(2.22)

H_2SO_4 and aluminum will react after some delay to produce hydrogen gas and aluminum sulphate.

Tetraoxosulphate VI acid is one of the most important industrial chemicals;

1. The major use of tetraoxosulphate VI acid is in the production of fertilizers.
2. It is widely used in the manufacturing process of a number of chemicals such as edible oils, hydrochloric acid, nitric acid, and aluminum sulphate.
3. It is used to manufacture rayon fibers, cellophane, drug, adhesives, explosives, synthetic rubber, acid dyes, plastics, perfumes, paints and disinfectants.
4. It is also used in de-scaling of steel and non-ferrous plating and purification.
5. Tetraoxosulphate VI acid, at high concentration, is frequently the major ingredient in acidic drain cleaners which are used to remove grease, hair and tissue paper.
6. The process of refining crude oil requires the use of an acid as a catalyst and tetraoxosulphate VI acid is often used in industries for this purpose.
7. It is also used in petroleum refining to wash impurities out of gasoline and other refinery products.
8. Sulfuric acid is used in large quantities by the iron and steel making industry to prevent oxidation, rust and scaling from rolled sheet and billets prior to sale to the automobile and major appliances industry.
9. Tetraoxosulphate VI acid is used in processing metals such as in pickling (cleaning) iron and steel before plating them with tin or zinc (Ghulamullah, *et al.*, 2015).

According to Kang *et al* (2012), acid solutions are often used in industry for cleaning, descaling and pickling of steel structure, processes which are normally accompanied by considerable dissolution of the metal.

2.5 Corrodible Metals

Metal is an element which forms positively charged ion (cation) by loss of electrons from its atom (Aggarwal, 2010). Corrosion is a functional process playing an important role in economics and safety, particularly for metals and alloys (Mistry *et al.*, 2012; Elmsellem *et al.*, 2014). A metal that suffers corrosion is called corrodible. Metals such as aluminum, mild steel and zinc have found wide application in a broad spectrum of industries and machinery; despite their tendency to corrosion.

2.5.1 Aluminum as a corrodible metal

Aluminum is not found native but in combined state (Aggarwal, 2010). It is the third most abundant element found in nature; first two are oxygen and silicon. Aluminum is present to the extent of 7.3% in the earth crust. It occurs as oxides, fluoride, double silicates and basic sulphates. Some of the chief ores of the metal are given below;

(i) Bauxite ($Al_2O_3.H_2O$),

(ii) Cryolite (Na_3AlF_6),

(iii) Corundum (Al_2O_3),

(iv) Felspar ($KAlSi_3O_8$).

(v) Alunite or Alumstone $K_2SO_4.Al_2(SO_4)_3.\ 4Al(OH)_3$.

However, bauxite and cryolite are the chief ores used in the extraction of aluminum. Aluminum is usually isolated from bauxite by electrolysis. The physical properties of aluminum are (Aggarwal, 2010);

(1) It is silvery white metal with a brilliant lustre. It takes a very high polish,

(2) It is a very light metal having specific gravity of 2.7,

(3) It is malleable and ductile and can be rolled into sheets, foils and wires,

(4) It melts at 659 ^{0}C and boils at 2450 ^{0}C.

The chemical properties of aluminum are:

1) Action of acids: Aluminum dissolves readily in hydrochloric acid to form aluminum chloride and hydrogen. The reaction is more vigorous as the acid becomes hotter and more concentrated.

$$2Al + 6HCl \rightarrow 2AlCl_3 + 3H_2\uparrow \qquad (2.23)$$

Dilute sulphric acid reacts slowly with aluminum to form aluminum sulphate and hydrogen.

$$2Al + 3H_2SO_4 \rightarrow Al_2(SO_4) + 3H_2\uparrow$$

(2.24)

On the other hand, hot concentrated sulphuric acid gives Sulphur dioxide with the metal

$$2Al + 6H_2SO_4 \rightarrow Al_2(SO_4)_3 + 6H_2O + 3SO_2\uparrow$$

(2.25)

Nitric acid (dilute as well as concentrated) has no action on pure metal.

2.5.1.1 Action of alkaline

Aluminum readily dissolves in strong alkaline like sodium and potassium hydroxides forming Meta – aluminates or aluminates and liberating hydrogen.

$$2Al + 2NaOH + 2H_2O \rightarrow 2NaAlO_2 + 3H_2\uparrow \quad (2.26)$$

2.5.1.2 Action of water

Pure aluminum is not affected by pure water. Commercial (impure) aluminum is readily corroded by water containing salts (sea water). It decomposes boiling water with the evolution of hydrogen.

$$2Al + 6H_2O \rightarrow 2Al(OH)_2 + 3H_2\uparrow \quad (2.27)$$

Aluminum is an important and widely used metal in the transport, construction, packaging and electrical sectors. Aluminum and its alloys are of economic importance because of their low cost, lightness and good corrosion resistance at moderate temperatures (Kotz and Treichel, 1996). They are also widely used in many industries such as reaction vessels, pipes, machinery and chemical batteries because of their advantages (El Maghraby, 2009). According to Refat and Ishaq (2013), aluminum and its alloys are low cost and remarkable materials in industrial technology because of their light weight, high thermal and electrical conductivity as well as high resistance to corrosion in a wide variety of corrosion environments. Generally, corrosion resistance of metals such as aluminum and steel, in corrosive environment, may be attributed to the formation of a protective tightly adhered invisible oxide film on the metal surface (Uppal and Bhatia, 2009).

A very large proportion of overhead, high voltage, power lines utilize aluminum rather than copper as the conductor on weight grounds. Aluminum and its alloys have also been the prime material of construction for the aircraft industry throughout most of its history. There are now very many examples of its use in commercial vehicles, rail cars both passenger and freight, marine hulls and super structures and military vehicles. Another significant use of aluminum is in packaging for the production of beverage cans. Aluminum is used in buildings for a wide spectrum of applications. These include roofing for factories which incorporate foil vapour barriers, windows and pre-formed sheet cladding features, doors, canopies and fronts for shops and prestigious buildings, architectural hardware and fittings, rainwater goods and replacement windows. Other uses of aluminum include high pressure gas cylinders, machined components, ladders and access equipment, sporting goods, road barriers and signs, domestic and office furniture and lithographic plates. According to

(Rethinnagiri, 2012), aluminum is extensively used in various industrial operations and its corrosion inhibition is of great importance.

2.5.2 Mild steel as corrodible metal

Dubey and Singh (2007) acknowledged that mild steel is employed widely in most industries due to its low cost and availability for the fabrication of various reaction vessels such as cooling tower tanks and pipelines. Besides carbon, steel contains many chemical elements which are added into iron to form steel of different kinds having various physical properties (Uppal and Bhatia, 2009). Mild steel refers to medium carbon steel which is used for structural applications. It is weldable, which expands its possible applications. It is a medium carbon steel with carbon content of 0.2 – 0.5% (Aggarwal, 2010). Other types of steel include soft steel (low carbon steel) with carbon content of 0.05 – 0.2%, hard steel (high carbon steel) with carbon content of 0.5 – 0.7% and very hard steel (very high carbon steel) with carbon content of 0.7 – 1.5%. Mild steel can be hardened by heat treatment, has a good machining properties and it is very good for welding. It is used for the production of lightly stressed machine fittings, armature shafts, turbine motors, railways axels, crank shafts, fish plates, cross heads, pipes and drums. Mild steel is widely used in the manufacturing of installations for petroleum, fertilizers, and in other industries. In most cases, processes within these industries such as pickling, acid cleaning, and acid descaling involves contact between mild steel and aggressive solution (such as acids, salts, and bases). In view of viability of mild steel and its high cost of production and installation, several steps are taken to prolong the life span of the metal in most industries.

2.6 Corrosion prevention techniques

Different methods can be employed to slow or prevent corrosion of metallic structure. The most commonly used methods are protective coatings on metals using organic molecules, plastics, polymers; and cathodic and/or anodic protection using organic or inorganic inhibitors (Koch *et al.*, 2002). Corrosion can be prevented by a number of ways. Some of these are explained below:

2.6.1. Barrier protection

The metal surface is not allowed to come in contact with moisture, oxygen and carbon dioxide. This can be achieved by the following methods:

(i) The metal surface is coated with paint which keeps it out of contact with air; moisture etc. till the paint layer develops cracks.

(ii) By applying film of oil and grease on the surface of the iron tool and machinery, the rusting of iron can be prevented since it keeps the iron surface away from moisture, oxygen and carbon dioxide.

(iii) The iron surface is coated with non-corroding metals such as nickel, chromium aluminium, etc. (by electroplating) or tin, zinc, etc. (by dipping the iron article in the molten metal). This again shuts out the supply of oxygen and water to iron surface.

(IV) The iron surface is coated with phosphate or other chemicals which give a tough adherent insoluble film which does not allow air and moisture to come in contact with iron surface.

2.6.2. Sacrificial protection

Sacrificial protection means covering the iron surface with a layer of metal which is more active (electropositive) than iron and thus prevents the iron from losing electrons. The more active metal loses electrons in preference to iron and converts itself into ionic state. With the passage of time, the more active metal gets consumed but so long as it is present there, it will protect the iron from rusting and does not allow even the nearly exposed surface of iron to react. The metal which is most often used for covering iron with more active metal is zinc and the process is called galvanization.

Iron can be coated with copper by electro-deposition from a solution of copper sulphate or with tin by dipping into molten metal. Now if the coating is broken, iron is exposed and iron being more active than both copper and tin, is corroded. Here iron corrodes more rapidly than it does in the absence of tin. At time, zinc, magnesium and aluminum powders mixed with paints provide decorative protective coatings also.

2.6.3. Electrical protection (cathodic protection)

The iron object to be protected from corrosion is connected to a more active metal either directly or through a wire. The iron object acts as cathode and the protecting metal acts as anode. The anode is gradually used up due to the oxidation of the metal to its ions due to loss of electrons. Hydrogen ions collect at the iron cathode and prevent rust formation. The iron object gets protection from rusting as long as some of the active metal is present. Metals widely used for protecting iron objects from rusting are magnesium, zinc and aluminum which are called sacrificial anodes. Magnesium is often employed in the cathodic protection of iron pipes buried in the moist soil, canals, storage tanks etc. Pieces of magnesium are buried along the pipeline and connected to it by wire.

2.6.4. Using anti-rust solutions

These are alkaline phosphate and alkaline chromate solutions. The alkalinity prevents availability of hydrogen ions. In addition, phosphate tends to deposit an insoluble protective film of iron phosphate on the iron. These solutions are used in car radiators to prevent rusting of iron parts of the engine.

2.6.5. Addition of inhibitors

Corrosion inhibitors are chemical substances that are added to the corrosive environment to reduce or eliminate corrosion. By the addition of corrosion inhibitors to water a simple and inexpensive solution to the corrosion problem is often found. Otherwise, the solution to the corrosion problem may require extensive modification and replacement of equipment or installation of water treatment equipment. Many commercially prepared corrosion inhibitors used in the oil field contain surface active agents. When these are added to a system for the first time, they remove loose deposits of corrosion products. Precautions should be taken to prevent these deposits from accumulating in equipment or in injection wells in order to prevent plugging.

2.7 Corrosion Inhibitors

Corrosion inhibitor is a chemical substance which, when added in small concentration to an environment, minimizes corrosion (Papavinasam, 2000; Nagm *et al.*, 2012a; Green and Perry, 2008). Corrosion inhibitors are used to protect metals from corrosion, including temporary protection during storage or transport as well as localized protection, required, for example, to prevent corrosion that may result from accumulation of small amount of an aggressive phase. Inhibitor selection is based on the metal and the environment. Inhibitors can be classified into environmental conditioners and interfaces inhibitors (Papavinasam, 2000).

Several studies have been reported on the use of non-plant extracts as corrosion inhibitors. Ralston *et al.,* (2008) used vanadium species as corrosion inhibitor for aluminum alloy. Ambrish *et al.,* (2010) used a drug as a corrosion inhibitor for mild steel in acid media (HCl and H_2SO_4). Prathibha *et al.,* (2012) examined the inhibition of mild steel corrosion by non-plant extract (cationic surfactant) in HCl medium used various concentration of drug as corrosion inhibitor of mild steel in HCl solution. The result obtained showed that various concentrations of ampicillin studied inhibited the corrosion of mild steel in solutions of HCl through the mechanism of physiosorption as confirmed by values of activation energy and free energy of adsorption. In another study, Omotioma *et al* (2014)used sodium chromate as corrosion inhibitor of mild steel in natural and oil polluted seawater.

There is great interest in development of eco-friendly corrosion inhibitors. The use of phytochemicals as corrosion inhibitors can be traced back to 1960s when tannins and their derivatives were used to protect corrosion of steel, iron and other tools (Buchweishaija, 2009). Hany *et al* (2012) used vegetable oil as a base material for a synthesized surfactant for carbon steel corrosion inhibitor. Rajam *et al* (2012) evaluated the inhibition efficiency of an aqueous extract of garlic in controlling corrosion of carbon steel in well water in the absence and presence of Zn^{2+} and by mass loss method. Abdallah (2004) examined guar gum as corrosion inhibitor for carbon steel in 1M H_2SO_4 solution using weight loss and Tafel polarization techniques. From the analysis of the experimental results, it was observed that guar acts as an inhibitor for the corrosion of carbon steel in H_2SO_4 solution. The adsorption of guar gum on steel surface in H_2SO_4 solution follows Langmuir adsorption isotherm. The addition of guar shifts the pitting potential of carbon-steel electrode to more positive values indicating an increased resistance to pitting attack.

Plant extracts exhibited moderate to high antioxidant activities. Natural antioxidants may be found in any plant part. Fruits, vegetables, spices, nuts, seeds, leaves, roots and barks are potential sources of natural antioxidants. The plant extract are environmental friendly, non-toxic and readily available. These plant extracts contain several organic compounds which have polar atoms such as O, N, P and S (Rani and Basu, 2012). They are adsorbed into the metal surface through these polar atoms. Adsorptions of these ingredients obey various isotherms. Plant extract has been used to control the corrosion of bronze (Varvara *et al.,* 2010).

Environmentally friendly corrosion inhibitors are biodegradable and do not contain heavy metals or other toxic compounds. Some research groups have reported the successful use of naturally occurring substances to inhibit the corrosion of metals in acidic and alkaline environment. As reported by Znini,*et al,* (2010), several studies have been carried out on the corrosion inhibition of metals by plant extracts. Rosaline-Vimela,*et al,* (2012) examined the corrosion inhibition of mild steel by leaves extract of *Annona muricata, L.* in 1N Hcl. Plant extracts of tobacco from stems, twigs as well as leaves have been reported to show significant corrosion inhibition of aluminum and steel in both saline solutions and strong acids (Davis *et al.,* 2001). Extracts from leaves were investigated and found to be effective corrosion inhibitors for mild steel in 2M HCl solutions. The authors reported maximum inhibition efficiency of 96% with only 0.01% tobacco concentration (100ppm). The tobacco extracts were reported to contain high concentrations of chemical compounds including terpenes, alcohols, polyphenols, carboxylic acids, nitrogen containing compounds and alkaloids that

may exhibit electrochemical activity such as corrosion inhibition. Though many synthetic organic compounds show good corrosion inhibition activities, most of them are toxic and they are often expensive and non-biodegradable (Kang *et al.,* 2012). Cost, health issues and environmental regulation restrictions have now made researchers focus on development of natural products as corrosion inhibitors.

2.7.1 Classification of corrosion inhibitors

Inhibitors are chemicals that react with a metallic surface, or the environment this surface is exposed to, giving the surface a certain level of protection. Inhibitors often work by adsorbing themselves on the metallic surface, protecting the metallic surface by forming a film. Inhibitors are normally distributed from a solution or dispersion. Some are included in protective coating formulation. A qualitative classification of inhibitors is presented in Figure 2.2. Inhibitors can be classified into environmental conditioners and interface inhibitors (Papavinasam, 2000).

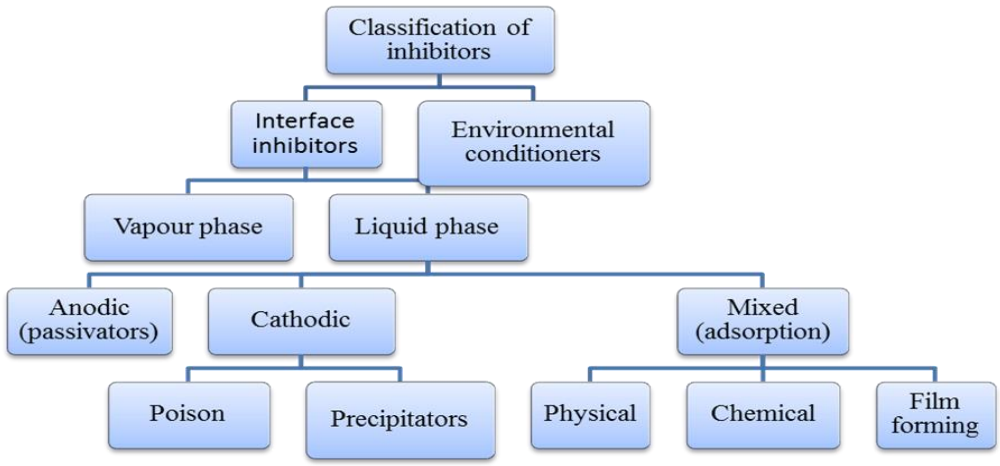

Fig 2.1: Classification of corrosion inhibitors

2.7.1.1 Environmental conditioners (scavengers)

Corrosion can be controlled by removing the corrosive species in the medium. Inhibitors that decrease corrosivity of the medium by scavenging the aggressive substances are called environmental conditioners or scavengers. In near -neutral and alkaline solutions, oxygen reduction is a common cathodic reaction. In such situations, corrosion can be controlled by decreasing the oxygen content using scavengers.

2.7.1.2 Interface inhibitors

Interface inhibitors control corrosion by forming a film at the metal/environment interface. Interface inhibitors can be classified into liquid - and vapor-phase inhibitors.

i. Liquid-phase inhibitors

Liquid-phase inhibitors are classified as anodic, cathodic, or mixed inhibitors, depending on whether they inhibit the anodic, cathodic, or both electrochemical reactions.

ii. Anodic (passivation) inhibitors.

Anodic inhibitors are used in near-neutral solutions where sparingly soluble corrosion products, such as oxides, hydroxides, or salts, are formed (Papavinasam, 2000). They form, or facilitate the formation of, passivation films that inhibit the anodic metal dissolution reaction. Anodic inhibitors are often called passivation inhibitors. Passivation inhibitors cause a large anodic shift of the corrosion potential, forcing the metallic surface into the passivation range. There are two types of passivation inhibitors: oxidizing anions, such as chromate, nitrite, and nitrate, that can passivate steel in the absence of oxygen and the non-oxidizing ions.

These inhibitors are the most effective and consequently the most widely used. Chromate-based inhibitors are the least-expensive inhibitors and were used until recently in a variety of application (recirculation-cooling systems of internal combustion engines, rectifiers, refrigeration units, and cooling towers). Sodium chromate, typically in concentrations of 0.04 to 0.1%, was used for these applications. At higher temperatures or in fresh water with chloride concentrations above 10ppm, higher concentrations are required. If necessary, sodium hydroxide is added to adjust the pH to a range of 7.5 to 9.5. If the concentration of chromate falls below a concentration of 0.016%, corrosion will be accelerated. Therefore, it is essential that periodic colorimetric analysis be conducted to prevent this from occurring. In general, passivation inhibitors can actually cause pitting and accelerate corrosion when concentrations fall below minimum limits. For this reason it is essential that monitoring of the inhibitor concentration be performed.

iii. Cathodic inhibitors

El Quariachi *et al* (2010) reported that *Rosmarinus officinalis* acted as cathodic inhibitor to carbon steel in 0.5 M H_2SO_4. Cathodic inhibitors control corrosion by either decreasing the reduction rate (cathodic poisons) or by precipitating selectively on the cathodic areas (cathodic precipitators). Cathodic poisons, such as sulfides and selenides, are adsorbed on the metal surface; whereas compounds of arsenic, bismuth, and antimony are reduced at the cathode and form a metallic layer (Papavinasam, 2000). Cathodic poisons can cause hydrogen blisters and hydrogen embitterment due to the absorption of hydrogen into steel. Cathodic precipitators increase the alkalinity at cathodic sites and precipitate insoluble compounds on the metal surface. The most widely used cathodic precipitators are the carbonates of calcium and magnesium.

iv. Mixed (organic) inhibitors

Yuce and Kardas (2012) reported 2-thiohydantoin as a mixed type inhibitor of mild steel in 0.1M HCl solution. Great numbers of inhibitors are organic compounds that cannot be designated specifically as anodic or cathodic and are known as mixed inhibitors. The effectiveness of organic inhibitors is related to the extent to which they adsorb and cover the metal surface. Adsorption depends on the structure of the inhibitor, on the surface charge of the metal, and on the type of electrolyte (Papavinasam, 2000).

Mixed inhibitors protect the metal in three possible ways: physical adsorption, chemisorptions and film formation. Physical (or electrostatic) adsorption is a result of electrostatic attraction between the inhibitor and the metal surface. When the metal surface is positively charged, adsorption of negatively charged (anionic) inhibitors is facilitated. Positively charged molecules acting in combination with a negatively charged intermediate can inhibit a positively charged metal. Anions, such as halide ions, in solution adsorb on the positively charged metal surface, and organic cations subsequent adsorb on the dipole. Corrosion of iron in sulphuric acid containing chloride ions is inhibited by quaternary ammonium cations through this synergistic effect. Physically adsorbed inhibitors interact rapidly, but they are also easily removed from the surface. Increase in temperature generally facilitates desorption of physically adsorbed inhibitor molecules. The most effective inhibitors are those that chemically adsorb (chemisorbs), a process that involves charge sharing or charge transfer between the inhibitor molecules and the metal surface. Illustrations of the adsorption of inhibitor on metal surface are shown in Figures 2.2 – 2.4.

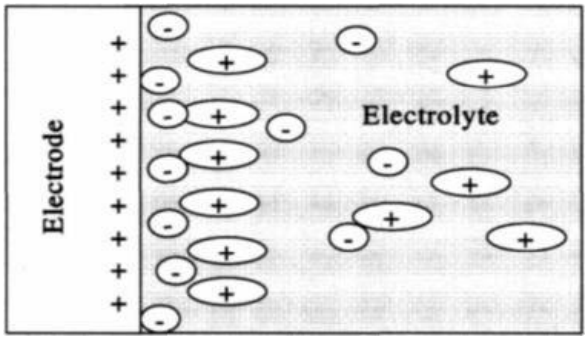

Figure 2.2: Adsorption of negatively charged inhibitor on a positively charged metal surface. *Adopted from Papavinasam (2000).*

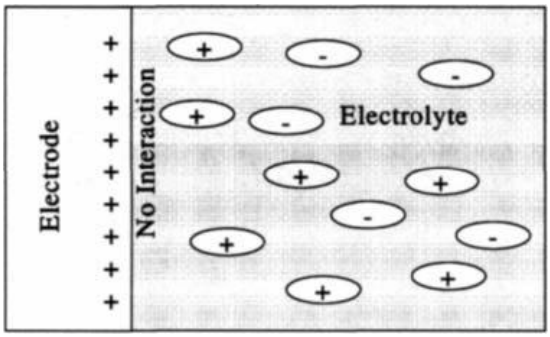

Fig 2.3: Positively charged inhibitor molecule on positively charged metal surface.Adopted from Papavinasam (2000)

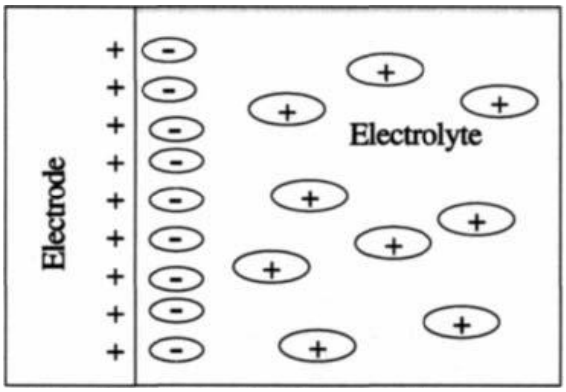

Fig 2.4: Synergistic adsorption of positively charged inhibitor and anion on a positively charged metal surface. Adopted from Papavinasam (2000).

Chemisorption takes place more slowly than physical adsorption. As temperature increases, adsorption and inhibition also increase. Chemisorption is specific and is not completely reversible. Adsorbed inhibitor molecules may undergo surface reactions, producing polymeric films. Corrosion protection increases markedly as the films grow from nearly two-dimensional adsorbed layers to three-dimension films up to several hundred angstroms thick. Inhibition is effective only when the films are adherent, are not soluble, and prevent access of the solution to the metal. Temporary protection against atmospheric corrosion, particularly in closed environments can be achieved using vapor-phase inhibitors (VPI). Substances having low but significant pressure of vapor with inhibiting properties are effective. The VPIs are used by impregnating wrapping paper or by placing them loosely inside a closed container. The slow vaporization of the inhibitor protects against air and moisture. In general, VPIs are more effective for ferrous than non-ferrous metals. V. Precipitation inhibitors

Precipitation-inducing inhibitors are film-forming compounds that have a general action over the metal surface, blocking both anodic and cathodic sites indirectly. Precipitation inhibitors are compounds that cause the formation of precipitates on the surface of the metal, thereby providing a protective film. Hard water that is high in calcium and magnesium is less corrosive than soft water because of the tendency of the salts in the hard water to precipitate

on the surface of the metal and form a protective film. The most common inhibitors of this category are the silicates and the phosphates. Sodium silicate, for example, is used in many domestic water softeners to prevent the occurrence of rust water. In aerated hot water systems, sodium silicate protects steel, copper, and brass. However, protection is not always reliable and depends heavily on pH and a saturation index that depends on water composition and temperature. Phosphates also require oxygen for effective inhibition. Silicates and phosphates do not afford the degree of protection provided by chromates and nitrites; however, they are very useful in situations where nontoxic additives are required.

VI. Volatile corrosion inhibitors

Volatile corrosion inhibitors (VCIs), also called vapor phase inhibitors (VPIs), are compounds transported in a closed environment to the site of corrosion by volatilization from a source. In boilers, volatile basic compounds, such as morpholine or hydrazine, are transported with steam to prevent corrosion in condenser tubes by neutralizing acidic carbon dioxide or by shifting surface pH toward less acidic and corrosive values. In closed vapor spaces, such as shipping containers, volatile solids such as salts of dicyclohexylamine, cyclohexylamine, and hexamethylene-amine are used. On contact with the metal surface, the vapor of these salts condenses and is hydrolyzed by any moisture to liberate protective ions. It is desirable, for an efficient VCI, to provide inhibition rapidly and to last for long periods. Both qualities depend on the volatility of these compounds, fast action wanting high volatility, whereas enduring protection requires low volatility.

2.7.2 Corrosion inhibition mechanism

The majority of inhibitor applications for aqueous, or partly aqueous, systems are concerned with four main types of environment:

i. Aqueous solutions of acids as used in metal-cleaning processes such as pickling for the removal of rust or mill scale during the production and fabrication of metals or in the post service cleaning of metal surfaces.
ii. Natural waters, supply waters, and industrial cooling waters in the near-neutral pH range (5 to 9).
iii. Primary and secondary production of oil and subsequent refining and transport processes.
iv. Atmospheric or gaseous corrosion in confined environments, during transport, storage, or any other confined operation.

Corrosion of metals in neutral solutions differs from that in acid solutions in two important respects. In air-saturated solutions, the main cathodic reaction in neutral solutions is the reduction of dissolved oxygen, whereas in acid solution it is hydrogen evolution. Corroding

metal surfaces in acid solution are oxide-free, whereas in neutral solutions metal surfaces are covered with films of oxides, hydroxides, or salts, owing to the reduced solubility of these species. Because of these differences, substances that inhibit corrosion in acid solution by adsorption on oxide-free surfaces do not generally inhibit corrosion in neutral solution. Typical inhibitors for near-neutral solutions are the anions of weak acids, some of the most important in practice being chromate, nitrite, benzoate, silicate, phosphate, and borate. Passivating oxide films on metals offer high resistance to the diffusion of metal ions, and the anodic reaction of metal dissolution is inhibited. These inhibitive anions are often referred to as anodic inhibitors, and they are more generally used than cathodic inhibitors to inhibit the corrosion of iron, zinc, aluminum, copper, and their alloys in near-neutral solutions. The action of inhibitive anions on the corrosion of metals in near-neutral solution involves the following important functions:

i. Reduction of the dissolution rate of the passivation oxide film.
ii. Repair of the oxide film by promotion of the reformation of oxide.
iii. Repair of the oxide film by plugging pores with insoluble compounds.
iv. Prevention of the adsorption of aggressive anions**.**

2.7.3 Selection of an inhibitor system

Several factors are needed to be considered when choosing an inhibitor including the cost and the amount, easy availability and safety to the environment and its species. The choice of the suitable corrosion inhibitors must follow some aspects including structural and environmental considerations. Structural aspects which belong to the performance of organic inhibitors are related to the chemical structure and physicochemical properties of the compound like functional groups, electron density at the donor atom, p-orbital character, and the electronic structure of the molecule. Structural factors which contribute to the action of inhibitors are chain length, size of the molecule, bonding, aromatic/conjugate, strength of bonding to the substrate, cross-linking ability and solubility in the environment (Rani and Basu, 2012).

Proper choices of inhibitors should be made by matching the appropriate inhibitor chemistry with the corrosion conditions and by selection of appropriate physical properties for the application conditions. Method of application and system characteristics must be considered when selecting physical properties of an inhibitor. Inhibitor selection begins with the choice of physical properties. The physical measurements are those routinely done as part of minimal quality acceptance testing. In choosing between possible inhibitors, the simplest corrosion tests should be done first to screen out unsuitable candidates.

The inhibitor user must employ test procedures that rigorously exclude inferior inhibitors even though some good inhibitors may also be excluded. The challenge in inhibitor evaluation is to design experiments that simulate the conditions of the real-world system. The variables that must be considered include temperature, pressure, and velocity as well as metal properties and corrosive environment chemistry. System corrosion failures are usually localized and attributed to micro conditions at the failure site. Adequate testing must include the most severe conditions that can occur in the system and not be limited to macro or average conditions.

2.7.4 Industrial applications of corrosion inhibitors

According to Mistry,*et al*, (2012), the use of corrosion inhibitor is one of the effective measures for protecting metal surface against corrosion. In oil and gas production industry, internal corrosion of carbon steel pipeline is a well-known phenomenon and a serious problem, and inhibition is the most cost effective and flexible method of corrosion control (Wang *et al.*, 2001).

2.7.4.1 Petroleum production

Corrosion in the hydrocarbon industries may be divided into two types, wet corrosion and dry corrosion. At low temperature, material corrodes due to the presence of an aqueous phase (wet corrosion). At higher temperature (above the boiling point of water), corrosion occurs in the absence of an aqueous phase (dry corrosion). Wet corrosion is influenced by pressure, temperature, and compositions of aqueous, gaseous, and oil phases. In refineries and petrochemical plants, the amount of water is usually small, but the corrosivity is high and is localized at regions where the aqueous phase contacts the metal. The water may contain dissolved hydrogen sulphide (H_2S), carbon dioxide (CO_2), and chloride ions (Cl^-). Corrosion may occur even when the produced water content is as low as 0.1%, or corrosion activity may not begin until after several years of production. Refineries and petrochemical industries employ a variety of film-forming inhibitors to control wet corrosion. Most of the inhibitors are long-chain nitrogenous organic materials, including amines and amides. Water-soluble and water-soluble-oil-dispersible type inhibitors are continuously injected or oil-soluble and oil-soluble-water-dispersible type inhibitors (batch inhibitors) are intermittently applied to control corrosion. Film-forming inhibitors anchor to the metal through their polar group. The non-polar tail protrudes out vertically.

2.7.4.2 Internal corrosion of steel pipelines

Pipelines, operating between oil and gas wells and processing plants, have corrosion problems similar to those in refineries and petrochemical plants. The flow regimes of

multiphase fluids in pipelines influence the corrosion rate. High-velocity flow tends to sweep sediments out of the pipeline, whereas low velocity allows sediments to settle at the bottom, providing sites for pitting corrosion. Internal corrosion of pipelines is controlled by cleaning the pipeline (pigging) and by adding continuous and/or batch inhibitors.

2.7.4.3. Water cooling system

One of the major problems associated with the industrial chill system is corrosion (Sulaiman *et al.*, 2012). Potable water is frequently saturated with dissolved oxygen and is corrosive unless a protective film, or deposit, is formed. Cathodic inhibitors, such as calcium carbonate, silicates, polyphosphates, and zinc salts, are used to control potable water corrosion. Water is used in cooling system in many industries. In a recirculation system, evaporation is the chief source of cooling. As evaporation proceeds, the dissolved mineral salt content increases. Cooling systems may consist of several dissimilar metals and non-metals. Metals picked up from one part of the system can be deposited elsewhere, producing galvanic corrosion. Corrosion is controlled by anodic (passivation) inhibitors.

2.7.4.4 Acids pickling of metals and oil well acidizing

Acids are widely used in pickling, in cleaning of oil refinery equipment and heat exchangers, and in oil well acidizing. Mixed inhibitors are widely used to control acid corrosion.

2.7.4.5 Automobile:

Inhibitors are used in an automobile for two reasons: (1) to reduce the corrosivity of fluid systems (internal corrosion), and (2) to protect the metal surfaces exposed to the atmosphere (external corrosion). Internal corrosion is influenced by the coolants, flow, aeration, temperature, pressure, water impurities and corrosion products, operating conditions, and maintenance of the system.

2.7.4.6 Paints (organic coatings)

Finely divided inhibiting pigments are frequently incorporated in primers. These polar compounds displace water and orient themselves in such a way that the hydrophobic ends face the environment, thereby augmenting the bonding of the coatings on the surface. Other inhibitors used in paints are lead azelate, calcium plumbate and lead sub oxide.

2.7.4.7 Reinforcing steel, tanks and allied materials

Researchers and engineers are continuously in search of cost-effective means to prevent the corrosion of reinforcing steel for the duration of a concrete structure’s design life (Abdurahman *et al.*, 2011). Inhibitors are used to control corrosion in boiler waters, fuel oil tanks, hot chloride dye baths, refrigeration brines, and reinforcing steel in concrete, and they are also used to protect artifacts.

2.7.5 Selected plants as an excellent sources of corrosion inhibitors

Studies have shown that plant extracts are potential eco-friendly corrosion inhibitors (Varvara,*et al.,* 2010; Taleb,*et al.,* 2011; Negm,*et al.,* 2012b). Plant extracts exhibit moderate to high antioxidant activities. Natural antioxidants may be found in any plant part. Fruits, vegetables, spices, nuts, seeds, leaves, roots and barks are potential sources of natural antioxidants. The plant extract are environmental friendly, non-toxic and readily available. Plant extracts contain several organic compounds which have polar atoms such as O, N, P. and S (Rani and Basu, 2012). They are adsorbed into the metal surface through these polar atoms; positive films are formed. Adsorptions of these ingredients obey various isotherms. Plants represent a class of interesting source of compounds currently being explored for use in metal corrosion protection in most systems, as possible replacement of toxic synthetic inhibitors. Phytochemicals of the plants of bitter leaf, mango, neem, pawpaw and tobacco are presented in Table 2.1 (Suleiman, 2011).

Table 2.1: The Analysis of phytochemicals in the hot organic methanol extraction of the extracts.

Phytochemicals	Inference				
	Bitter leaf	Mango	Neem	Pawpaw	Tobacco
Alkaloids	_	+	-	+	+
Tannins	_	+	+	+	+
Steroids	+	-	+	+	+
Terpenoids	-	+	+	+	+
Reducing sugar	-	+	+	-	+
Saponins	+	+	+	-	+
Flavonoids	-	+	+	+	+
Glycosides	+	+	-	+	-

+ = presence, - = absence

The names of selected plants as excellent sources of corrosion inhibitors are *Aspilia africana, Chromolena odarata, Dennettia tripetala, Newbouldia leavis, Dialium guineense*and *Vitex doniana*. Plant-derived substances such as leaves extracts of*Aspilia africana*, *Chromolena odorata*, *Dennettia tripetala*, *Newbouldia leavis*, *Dialium guineense* and *Vitex doniana* plants are of great interest owing to their versatile applications.

2.7.5.1 Aspilia africana

Aspilia Africana is a genus of flowering plants in the daisy family.Historically, *Aspilia africana* was used in Mbaise and most Igbo speaking parts of Nigeria to prevent conception, suggesting potential contraceptive and anti-fertility properties.Leaf extract and fractions of *Aspilia. africana* effectively arrested bleeding from fresh wounds, inhibited microbial growth of known wound contaminants and accelerated wound healing

process.Aspilia*Africana* is thought to be used as herbal medicine by some chimpanzees.The potentials of the leaves of the haemorrhage plant, *Aspilia africana* (*Compositae*) in wound care was evaluated using experimental models. *A. africana*, which is widespread in Africa, is used in traditional medicine to stop bleeding from wounds, clean the surfaces of sores, in the treatment of rheumatic pains, bee and scorpion stings and for removal of opacities and foreign bodies from the eyes(Okoli, *et al.*, 2007).

2.7.5.2 *Chromolena odorata*

Chromolaena odorata is a rapidly growing perennial herb. It has soft stems but the base of the shrub is woody. In shady areas it becomes etiolated and behaves as a creeper, growing on other vegetation. It can then become up to 10 m (33 feet) tall. The plant is hairy and glandular and the leaves give off a pungent, aromatic odour when crushed. The leaves are opposite, triangular to elliptical with serrated edges. Leaves are 4–10 cm long by 1–5 cm wide (up to 4 x 2 inches). Leaf petioles are 1–4 cm long. The white to pale pink tubular flowers are in panicles of 10 to 35 flowers that form at the ends of branches. The seeds are achenes and are somewhat hairy. They are mostly spread by the wind, but can also cling to fur, clothes and machinery, enabling long distance dispersal. Seed production is about 80000 to 90000 per plant. Seeds need light to germinate. The plant can regenerate from the roots. In favorable conditions the plant can grow more than 3 cm per day.Recently *C. odorata* previously known as *Eupatorium odoratum* has been implicated in the larvicidal activity of all the major mosquito vectors (Gade*et al.*,2017).

2.7.5.3 *Newbouldia leavis*

Newbouldia laevis (ogilisi) is a tropical plant belonging to the family of *Bignoniaceae*. It is among the most useful plants in Africa and grows up to 10 m height with a cauliflorous habit. It is an ever greenish plant with a height of approximately 7–8 m high in the West Africa and up to 20 m in Nigeria. The plant has a characteristics shiny dark green leaves with large purple flowers. *Newbouldia laevis* is usually grown as an ornamental tree and planted by cuttings. It is a very popular plant in the African continent and is highly valuable due to its numerous immense benefits to human race. Some parts of Nigeria commonly regard this tree as the tree of fertility or the tree of life. The wood is pale brown, durable, evenly textured and hard and it tends to remain alive for a long time even after cutting it. This makes it viable for usage as posts, woodworks, yam stakes, house posts, firewood and bridges.

2.7.5.4 *Dennettia tripetala* (pepper fruit)

Dennettia tripetala is well known as mmimi by the Igbo people of Nigeria. It is a pungent, pepperish, spicy medicinal plant that is characterized by greenish appearance when unripe but tends to be reddish or pinkish in colour when ripe. Dennettia tripetala tree thrives mainly in the Savannah and rainforest zones while the fruit usually ripens between April and May. Edible mature Dennettia tripetala is mostly chewed raw but can also be used for food preparations and for preparing herbal medicines. Both the fruits, leaves, roots and barks of the *Dennettia tripetala* plant are distinguished by their strong pungent, spicy and pepperish taste, fragrance and aroma (Achinewhu *et al.*, 1995).

2.7.5.5 *Dialium guineense*(velvet tamarind)

Botanicalname:*Dialium guinesses,* 'Icheku' in Igbo. Dialium guineense comes under the *leguminosae* family which is tall, growing under tropical climatic conditions and also bears fruits. The fruits are similar to the grapes and are consumable containing hard shells which must not be consumed. Since the fruit contains tamarind flavor it has its English name as tamarind. Taste is both sweet and sour. When the fruit is dried it becomes powdery and the orange color possess a tangy flavor. Every fruit contains only one firm seed which is flat, circular, brown in color with a width of 7-8 millimeters and a thickness of 3 mm. The seed is a look alike of a watermelons seed having 2 seeds. The seed has a glossy finish and has a coating of starch.

2.7.5.6 Vitex doniana

Vitex doniana(called in English black plum or vitex;in Igbo it is called (ucha akuru)is a medium-sized deciduous tree, 8-18 m high, with a heavy rounded crown and a clear bole up to 5 m. Bark rough, pale brown or greyish-white, rather smooth with narrow vertical fissures. The bases of old trees have oblong scales.Leaves opposite, glabrous, 14-34 cm long, usually with 5 leaflets on stalks 6-14 cm long. Leaflets distinctly stalked, ovate, obovate-elliptic or oblong, entire, 8-22 cm long, 2-9 cm wide. Leaf tips rounded or emarginate, leaf bases cuneate. Dark green above, pale greyish-green below, thickly leathery, with a few scattered stellate hairs on the upper surface, otherwise without hairs. All the plant leaves were identified at the Department of Botany, Nnamdi Azikiwe University, Awka.

2.7.6 Plant phytochemicals

Plant extracts exhibited moderate to high antioxidant activities. Natural antioxidants may be found in any plant part. Fruits, vegetables, spices, nuts, seeds, leaves, roots and barks are potential sources of natural antioxidants. Plant extracts contain several organic compounds which have polar atoms such as O, N, P and S (Rani and Basu, 2012). Alkaloids are group of naturally occurring chemical compounds that contain mostly basic nitrogen. This group also

includes some related compounds with neutral and even weakly acidic properties. Some synthetic compounds of similar structure are also termed alkaloids. In addition to carbon, hydrogen and nitrogen, alkaloids may also contain oxygen, sulphur and more rarely other elements such as chlorine, bromine and phosphorus. Alkaloids are produced by a large variety of organisms including bacteria, fungi, plants and animals. Alkaloids have a wide range of pharmacological activities (Cushnie *et al.*, 2014; Qiu *et al.*, 2014).

Cardiac glycosides are organic compounds containing glycoside (sugar). These glycosides are found as secondary metabolites in several plants, but also in some insects. Flavonoids are class of plant secondary metabolites. Chemically, they have the general structure of a 15-carbon skeleton, which consists of two phenyl rings (A and B) and heterocyclic ring (C). Flavonoids can be classified into three; flavonoids or bioflavonoids, isoflavonoids and neoflavonoids. The three flavonoid classes above are all ketone-containing compounds, and as such, are anthoxanthins (flavons and flavonols). Flavonoids are widely distributed in plants, fulfilling many functions. Some flavonoids have inhibitory activity against organisms that cause plant diseases.

Phenols (phenolics) are class of chemical compounds consisting of a hydroxyl group bonded directly to an aromatic hydrocarbon group. The simplest of the class is phenol, which is also called carbolic acid. Phenolic compounds are classified as simple phenols or polyphenols based on the number of phenol units in the molecule. Phenolic compounds are synthesized industrially; they also are produced by plants and microorganisms, with variation between and within species. Although similar to alcohols, phenols have unique properties and are not classified as alcohols (since the hydroxyl group is not bonded to a *saturated* carbon atom). They have higher acidities due to the aromatic ring's tight coupling with the oxygen and a relatively loose bond between the oxygen and hydrogen. The acidity of the hydroxyl group in phenols is commonly intermediate between that of aliphatic alcohols and carboxylic acids. Phenols have wide range of pharmacological importance(Mishra and Tiwari, 2011; Amorati and Valgimigli, 2012).

Phytic acid (phytate when in salt form), is a saturated cyclic acid. It is the principal storage form of phosphorus in many plant tissues. Catabolites of phytic acid are called lower inositol polyphosphates.Saponins are class of chemical compounds found in particular abundance in various plant species. More specifically, they are amphipathic glycosides grouped by the soap-like foaming they produce when shaken in aqueous solutions. A tannin is an astringent, bitter plant polyphenolic compound that binds to and precipitates proteins and various other organic compounds including amino acids and alkaloids. The term "tannin" by extension is

widely applied to any large polyphenolic compound containing sufficient hydroxyls and other suitable groups (such as carboxyls) to form strong complexes with various macromolecules. The tannin compounds are widely distributed in many species of plants, where they play a role in protection from predation, and perhaps also as pesticides, and in plant growth regulation.

2.8 Techniques for Studying Corrosion Inhibition of Metals

Several techniques, chemical and electrochemical methods, have been used to study the effects of inhibitors on the corrosion of metals in various corrosive media. Latifa and Abdelilah (2007) examined the effect of eugenol on the titanium corrosion in artificial saliva enriched with eugenol at different concentrations. In that study, the corrosion behaviour and titanium surface characterization were investigated by electrochemical measurements and SEM. Anees et al (2009) investigated the effect of temperature and acid concentration on corrosion of low carbon steel in hydrochloric acid media. Thermodynamic parameters of activation and kinetic studies for the corrosion reaction were obtained. The corrosion reaction was appropriately first order reaction. In the work of El Ouariachi,*et a,l* (2010), *Rosmarinus officinalis* essential oil obtained by hydro- distillation was tested as corrosion inhibitor of steel in 0.5M H_2SO_4 using weight loss measurements, and electrochemical polarization methods. Singh and Mukherjee, (2010) investigated the kinetics of mild steel corrosion in aqueous acetic solution using weight loss and polarization techniques steel.

Nadia,*et al,* (2011) examined corrosion protection behaviour of zinc rich epoxy paint in 3% NaCl solution using electrochemical impedance spectroscopy (E1S). The EIS results obtained were interpreted using a model involving the impedance of particle contact to account for the increasing resistance between zinc particles and the electrical resistivity of the binder. In the work of Anthony and Susai, (2012), inhibition of carbon steel in well water by arginine – 2^{2+} systems was investigated. Weight – loss method, photodynamic polarization study, AC impedance measurements, spectrophotometer recording, FTIR spectra analysis, scanning electron microscopy, and analysis by atomic force microscopy were employed in the study. From the weight loss study and surface analysis technique, a suitable mechanism of corrosion inhibition was proposed. Yuce and Kardas, (2012) investigated 2-thiohydantoin as a corrosion inhibitor of mild steel in 0.1m HCl solution. Potentiodynamic polarization, electrochemical impendence spectroscopy and linear polarization resistance measurements were used for the study. From the results, the 2-thiohydantoin acted as a mixed type inhibitor in 0.1M HCl.

In another study, Hany et al, (2012a) explored the corrosion inhibition of carbon steel alloy in 1.0% NaCl saturated with CO_2 by synthesized sulfated fatty acid sodium salt (SFASS) as an anionic surfactant inhibitor. The study employed weight loss measurements, extrapolation of cathodic and anodic Tafel plot and linear polarization resistance techniques. Loto and Poppoola, (2012) used gravimetric and metallographic methods to investigate the effects of tobacco and kola tree extracts on the corrosion inhibition of an aluminum alloy (1200) grade specimens immersed in 0.5M sulphuric acid. Increases in the concentration of the plant extracts gave clear reduction in weight loss and the corrosion rate of the test samples. The corrosion inhibition was associated with the protective film provided on the aluminum alloy's surface by the complex chemical constituents of the plants extracts.

Lebe,*et al.,* (2013), employedgravimetric method to study the adsorption and corrosion inhibition of *Gnetum Africana* leaves extract on carbon steel. In the work of Patel *et al,* (2013), extracts of three plants leaves were investigated as corrosion inhibitor of mild steel in 0.5M H_2SO_4 using chemical and electrochemical methods. Scanning electron microscopic studies were used to provide evidence of improved surface condition, due to the adsorption process. Elmsellem,*et al,* (2014), examined the inhibition effect of new heterocyclic compounds on mild steel corrosion in 1 M HCl. The study includes weight loss measurements, potentiodynamic polarization and electrochemical impedance spectroscopy (EIS) measurements. The molecular structure effect on the corrosion inhibition efficiency was investigated using DFT calculations. The results of the study showed that the inhibition efficiency depends on concentration and molecular structure of the investigated compounds.

Density functional theory (DFT) and time- dependent density functional theory (TD-DFT) were used by Nesrin,*et al,* (2008), to examine the ground-state geometries, absorption wavelengths, oscillation strengths for some hetarylazoindole derivatives. Udhayakala,*et a,l* (2012), investigated the adsorption mechanism and inhibition performance of two pyrimidine derivatives as corrosion inhibitors using density functional theory (DFT). The result showed that the theoretically calculated order of inhibitor efficiency was found to be in close agreement with the experimental order. Mistry,*et al,* (2012), carried out quantum chemical calculations to complement the experimental evidence. John,*et al,* (2013), reviewed and presented the adsorption characterization of mesoporous and microporous materials using methods of density functional theory. Elmsellem,*et al,* (2014), examined the inhibition effect of new heterocyclic compounds on mild steel corrosion in 1 M HCl. The study includes weight loss measurements, potentiodynamic polarization and electrochemical impedance spectroscopy (EIS) measurements. The molecular structure effect on the corrosion inhibition

efficiency was investigated using DFT calculations. The results of the study showed that the inhibition efficiency depends on concentration and molecular structure of the investigated compounds.

Green and Perry, (2008) expressed concern over the indiscriminate use of many electrochemical tests. It was also noted that corrosion is a surface phenomenon, and that the only condition present during any type of corrosion test that is a true representation of real-life circumstance is the open circuit potential (OCP). The OCP is the electrical circuit that exists on the metal surface during the naturally spontaneous accumulation of the electrical potential that forms on the metal surface when exposed to a liquid environment. Any kind of an electrical current that is added to that surface is an artifact that no longer represents the true nature of that corrosion reaction (Green and Perry, 2008).In some cases, researchers do not recognize the dynamic nature of some passive films, corrosion products or deposits from other sources; nor do they even consider the possibility of a change in the surface conditions during the course of their experiment (Green and Perry, 2008).

2.9 Techniques for Analyzing Corrosion Inhibition Study

2.9.1 Corrosion inhibition analysis using density functional theory

Density functional theory provides a powerful tool for computations of the quantum state of atoms, molecules and solids, and of molecular dynamics (Mistry,*et al.,* 2012; Elmsellem,*et al.,* 2014). Density functional methods form the basis of a diversified and very active area of present day's computational atomic, molecular, solid state and even nuclear physics. Its applicability ranges from atoms, molecules and solids to nuclei and quantum and classical fluids. In its original formulation, the density functional theory provides the ground state properties of a system, and the electron density plays a key role. DFT predicts a great variety of molecular properties such as molecular structures, vibrational frequencies, atomization energies, ionization energies, electric and magnetic properties and reaction paths (Nesrin,*et al.,* 2008; Udhayakala,*et al.,* 2012). The original density functional theory has been generalized to deal with many different situations: spin polarized systems, multicomponent systems such as nuclei and electron hole droplets, free energy at finite temperatures, superconductors with electronic pairing mechanisms, relativistic electrons, molecular dynamics, time-dependent phenomena, and excited states.

Quantum chemical methods have already proven to be very useful in determining the molecular structure as well as elucidating the electronic structure and reactivity. Knowledge of the density is all that is necessary for a complete determination of all ground state

molecular properties. The basic relationship of the density functional theory of chemical reactivity is precisely, the one that links the chemical potential of DFT with the first derivative of the energy with respect to the number of electrons, and therefore with the negative of the electronegativity χ (Udhayakala *et al.*, 2012).

$$\mu = \left(\frac{\partial E}{\partial N}\right)_{v(r)} = -\chi \qquad (2.28)$$

Where μ is the chemical potential, E is the total energy, N is the number of electrons, and ν(r) is the external potential of the system.

Hardness (η) has been defined within the DFT as the second derivative of the E with respect to N as (v)r property which measures both the stability and reactivity of the molecule.

$$\eta = \left(\frac{\partial^2 E}{\partial N^2}\right)_{v(r)} \qquad (2.29)$$

Where (v)r and μ are, respectively, the external and electronic chemical potentials.

From the value of the total electronic energy, the ionization potential (IE) and electron affinity (EA) of the inhibitors are calculated using the following equations.

$$IE = E_{N-1} - E_N \qquad (2.30)$$

$$EA = E_N - E_{N+1} \qquad (2.31)$$

Where E is the total electronic energy, N is the number of electrons, and v (r) is the external electrostatic potential that the electrons feel due to the nuclei.

The higher HOMO energy corresponds to the more reactive molecule in the reactions with electrophiles, while lower LUMO energy is essential for molecular reactions with nucleophiles (Khaled, 2010).

$$\chi = -\mu = \frac{IE + EA}{2} \qquad (2.32)$$

$$\eta = \frac{IE - EA}{2} \qquad (2.32)$$

The global softness(S) is the inverse of the global hardness.

$$S = \frac{1}{\eta} \qquad (2.33)$$

Electronegativity, hardness and softness have proved to be very useful quantities in the chemical reactivity theory. When two systems, Fe and inhibitor, are brought together, electrons will flow from lower χ(inhibitor) to higher χ(Fe), until the chemical potentials

become equal. The number of transferred electrons (ΔN) can be determined using the equation below (Khaled, 2010).

$$\Delta N = \frac{\chi_{Fe} - \chi_{inh}}{[2(\eta_{Fe} + \eta_{inh})]} \quad (2.34)$$

Where $\chi_{Fe}$and χ_{inh} denote the absolute electronegativity of iron and inhibitor molecule respectively. η_{Fe} and η_{inh} denote the absolute hardness of iron and the inhibitor molecule respectively.

The global electrophilicity index is given as;

$$\omega = \frac{\mu^2}{2\eta} \quad (2.35)$$

According to the definition, this index measures the propensity of chemical species to accept electrons. A good, more reactive, nucleophile is characterized by lower value of ω; and conversely a good electrophile is characterized by a high value of ω. This new reactivity index measures the stabilization in energy when the system acquires an additional electronic charge ΔN from the environment (Udhayakala,*et al.,* 2012).

The change in electron density is the nucleophilic $f^+(r)$ and electrophilic $f^-(r)$ Fukui functions, which can be calculated using the finite difference approximation:

For nucleophilic attack;

$$f^+(r) = \rho_{N+1}(r) - \rho_N(r) \quad (2.36)$$

For electrophilic attack;

$$f^-(r) = \rho_N(r) - \rho_{N-1}(r) \quad (2.37)$$

Where ρ_{N+1}, ρ_N and ρ_{N-1} are the electronic densities of anionic, neutral and cationic species respectively.

Condensed softness indices allowing the comparison of reactivity between similar atoms of different molecules can be calculated easily starting from the relation between the Fukui function f(r) and the local softness s(r).

$$s(r) = \left(\frac{\partial \rho(r)}{\partial N}\right)_{v(r)} \left(\frac{\partial N}{\partial \mu}\right)_{v(r)} = f(r)S \quad (2.38)$$

From this relation, one can infer that local softness and Fukui function are closely related, and they should play an important role in the field of chemical reactivity.

The energy of the highest occupied molecular orbital (E_{HOMO}) measures the tendency towards the donation of electron by a molecule (Udhayakala *et al.*, 2012). Therefore, higher values of

E_{HOMO} indicate better tendency towards the donation of electron, enhancing the adsorption of the inhibitor on mild steel and therefore better inhibition efficiency. E_{LUMO} indicates the ability of the molecule to accept electrons. The binding ability of the inhibitor to the metal surface increases with increasing of the HOMO and decreasing of the LUMO energy values.

According to the frontier molecular orbital theory (FMO) of chemical reactivity, transition of electron is due to interaction between highest occupied molecular orbital (HOMO) and lowest unoccupied molecular orbital (LUMO) of reacting species

The energy gap, ($\Delta E = E_{LUMO} - E_{HOMO}$) is an important parameter as a function of reactivity of the inhibitor molecule towards the adsorption on the metallic surface. As ΔE decreases, the reactivity of the molecule increases leading to increase in the inhibition efficiency of the molecule. Lower values of the energy difference will render good inhibition efficiency, because the energy to remove an electron from the last occupied orbital will be low. Reportedly, excellent corrosion inhibitors are usually organic compounds which not only offer electrons to unoccupied orbital of the metal but also accept free electrons from the metal. A molecule with a low energy gap is more polarizable and is generally associated with the high chemical activity and low kinetic stability and is termed soft molecule.

The dipole moment (μ in Debye) is another important electronic parameter that results from non-uniform distribution of charges on the various atoms in the molecule. The high value of dipole moment probably increases the adsorption between chemical compound and metal surface. The energy of the deformability increases with the increase in μ, making the molecule easier to adsorb at the Fe surface. Ionization energy is a fundamental descriptor of the chemical reactivity of atoms and molecules. High ionization energy indicates high stability and chemical inertness and small ionization energy indicates high reactivity of the atoms and molecules. Absolute hardness and softness are important properties to measure the molecular stability and reactivity. It is apparent that the chemical hardness fundamentally signifies the resistance towards the deformation or polarization of the electron cloud of the atoms, ions or molecules under small perturbation of chemical reaction. A hard molecule has a large energy gap and a soft molecule has a small energy gap. Normally, the inhibitor with the least value of global hardness (hence the highest value of global softness) is expected to have the highest inhibition efficiency (Udhayakala *et al.*, 2012). For the simplest transfer of electron, adsorption could occur at the part of the molecule where softness (S) has a highest value.

2.9.2 Determination of inhibitor's efficiency by electrochemical techniques

2.9.2.1 Potentiodynamic polarization technique

Singh and Mukherjee (2010) investigated the kinetics of mild steel corrosion in aqueous acetic solution using weight loss and polarization techniques. For the polarization measurements, the inhibition efficiency (IE%) was calculated using Equation (2.47) (Singh and Mukherjee, 2010; Negm,*et al.,* 2012b):

$$\text{IE \%} = \frac{i_{corr(uninh)} - i_{corr(inh)}}{i_{corr(unmh)}} \text{ x } 100 \quad (2.39)$$

Where $i_{corr(uninh)}$ and $i_{corr(inh)}$ are the corrosion current density values without and with inhibitors respectively.

2.9.2.2 Electrochemical impedance spectroscopy technique:

Mehdi Ebadi,*et al.,* (2012); examinedthecorrosion inhibition properties of pyrazolylindolenine compounds on copper surface in acidic media employing electrochemical impedance spectroscopy (EIS), open circuit potential (OCP) and linear scan voltammetry (LSV) techniques. The inhibition efficiency for the electrochemical impedance spectroscopy measurement was evaluated using equation (2.48), (Ebadi,*et al.,* 2012; Fouda, *et al.,* 2014 and Ashassi-Sorkhabi, *et al.,* 2015).

$$IE\% = \frac{R_{ct(inh)} - R_{ct}}{R_{ct(inh)}} \times 100 \quad (2.40)$$

Where, R_{ct} *and* $R_{ct(inh)}$ are the transfer resistance values in the absence and presence of inhibitor respectively.

The R_{ct} can be calculated from the difference in the impedance at lower and higher frequencies (Ashassi-Sorkhabi,*et al.*, 2015).

$$Cdl = \frac{1}{2\pi f_{max} R_{ct}} \quad (2.41)$$

2.9.3 Determination of inhibition efficiency by thermometric method

The reaction number (RN) can be evaluated using Equation (2.49) (Mabrouk,*et al.,* 2011; Eddy *et al.,* 2012).

$$RN = \frac{T_m - T_i}{t} \quad (2.42)$$

Where T_m and T_i are the maximum and initial temperatures (in ^{0}C) respectively, and t is the time in minutes elapsed to reach T_m.

According to Mabrouk,*et al,* (2011), the inhibitor efficiency can be evaluated using Equation (2.46);

$$IE\% = (1 - \frac{RN_{add}}{RN_{free}}) * 100$$

(2.43)

Where RN_{free} and RN_{add} are the reaction numbers for the metal dissolution in free and inhibited corrosive medium respectively.

2.9.4 Efficiency, kinetics and thermodynamic properties of inhibitor by weight loss method

The corrosion rate (Cr), surface coverage (θ) and inhibition efficiency (IE %) were obtained by using the following equations.

$$Cr = \frac{w_i - w_f}{At} \tag{2.44}$$

$$\theta = \frac{\omega_0 - \omega_1}{\omega_0} \tag{2.45}$$

$$IE\% = \frac{\omega_0 - \omega_1}{\omega_0} * 100 \tag{2.46}$$

Where w_i and w_f are the initial and final weight of metal samples respectively; ω_1 and ω_0 are the weight loss values in presence and absence of inhibitor, respectively. A is the total area of the specimen and t is the immersion time. Using Arrhenius equation, the activation energy can be obtained (Octave, 2003; Nwabanne and Okafor, 2011; Nnanna,*et al.*, 2013). The thermodynamic parameters such as heat of adsorption, adsorption equilibrium constant and free energy of adsorption can be obtained using adsorption isotherms (Orubite-Okorosaye and Oforka, 2004; Nwabanne and Okafor, 2011; Alinnor and Ejikeme, 2012; Nnanna,*et al.*, 2013). Adsorption is the adhesion of atoms, ions or molecules from a gas, liquid or dissolved solid to a surface. The process creates a film of the adsorbate on the surface of the adsorbent. Adsorption is a surface phenomenon. It is present in many natural, physical, biological and chemical systems, and is widely used in industrial applications. Adsorption is usually described through isotherms, that is, the amount of adsorbate on the adsorbent as a function of its pressure (if gas) or concentration (if liquid) at constant temperature. The quantity adsorbed is nearly always normalized by the mass of the adsorbent to allow comparison of different materials. Various isotherm models have been developed (Foo and Hameed, 2010; Nwabanne and Okafor, 2011; Alinnor and Ejikeme, 2012; Li and Deng, 2012; Patel *et al.*, 2013). Adsorption isotherms that are most frequently used are Bockris-Swinkel, Dahar-Flory-Huggins, Flory-Huggins, Freundlich, Frumkin, Hill de Boer, Langmuir, and Temkin isotherms (Ezeoke*et al*., 2012).

2.10 Review of Related Work

Recently, Okeoma (2015), in his work, computational and experimental studies of the inhibitive effects of *Newbouldia laevis* extract using magnetic fields on copper corrosion in aqueous acidic media using gravimetric method, found that the magneticfield can work as a dipole by providing the required charges which will suppress the corrosion of copper in the aggressive environment; proved to be a good corrosion inhibitor on copper.

In another interesting work, Nnanna*et al.,* (2012) investigated the inhibition by *Newbouldia leavis* leaf extract of the corrosion of Aluminum in HCL and H_2SO_4 solutions employing only gravimetric technique. The obtained 95.03% efficiency using *Newbouldia leavis* leaf extract as corrosion inhibitor in acidic environments.

Furthermore, Ihebrodike,*et al.,* (2012)reported that the phytochemical constituents of AA were strongly adsorbed on the surface of aluminum, giving rise to a remarkable inhibition efficacy that was observed in the paper titled Experimental and theoretical assessment of the inhibiting action of *Aspilia africana* extract on corrosion of aluminum alloy AA3003 in hydrochloric acid.

In the work of El Ouariachi *et al* (2010)*Rosmarinus officinalis* essential oil obtained by hydro- distillation was tested as corrosion inhibitor of steel in 0.5 H_2SO_4 using weight loss measurements, and electrochemical polarization methods. Results obtained indicate that the corrosion rate was reduced and *Rosmarinus officinalis* oil adsorbed on the metal surface and then inhibited corrosion process. Its inhibition efficiency increases with increasingoil content to reach 61% at 1g/l. Polarization curves showed that *Rosmarinus officinalis* acted as a cathodic inhibitor. The inhibition efficiency of natural oil remains slightly constant with the rise in temperature. Chemical analysis of *Rosmarinus officinalis* was carried out using capillary GC and GC-MS.

Quraishi *et al* (2010) used weight loss, electrochemical impedance spectroscopy, linear polarization and potentiodynamic polarization to study the inhibition of the corrosion of mild steel in hydrochloric acid and suprhuric acid solutions by the extract of *Murraya koenigii* leaves. The thermodynamic parameters showed strong interaction between inhibitor and mild steel surface. The results show that the extract of the leaves could serve as an effective inhibitor of the corrosion of mild steel in hydrochloric and sulphuric acid media.

Furthermore, Ndibe,*et al,* (2011) studied the corrosion inhibition of mild steel in HCl and HNO_3 by acid extract of *Veronica amygdaline* (VA) using weight loss method. The results showed that the rate of corrosion of the metal in the media increased with an increase in the concentration of the acid and decreased with an increase in the concentration of the inhibitor.

VA is an adsorption inhibitor and its adsorption on the surface of mild steel is physically controlled, exothermic,spontaneous and sufficiently fits with Langmuir adsorption isotherm.

In their report, Nwabanne and Okafor, (2011) used weight loss technique to investigate the inhibitive, thermodynamics and adsorptive properties of ethanol extract of *Veronica amygdalina* for the corrosion of mild steel in 0.4M HNO_3 solutions. The inhibition efficiency of the extract decreased as temperature and time of immersion increased, but increased with increase in concentration of extract. The adsorption of the inhibitor on surface of mild steel was exothermic, spontaneous and follows the mechanism of physical adsorption.

Torres,*et al,* (2011) examined the effects of aqueous extracts of spent coffee grounds on the corrosion of carbon steel in a 1 mol L^{-1} HCl. The study reveals that the adsorption process of components of spent coffee grounds extract obeyed the Langmuir adsorption isotherm. In another study, Negm,*et al,* (2012b) derived four environmentally friendly corrosion inhibitors from vanillin and were evaluated gravimetrically and electrochemically as corrosion inhibitors for carbon steel in 1M HCl. The inhibition efficiencies of the inhibitors depend on their concentration and the chemical structures. Also, Abdulwahab,*et a,l* (2012) investigated the corrosion inhibition of an aqueous extract of bitter leaf on aluminum alloy in 0.5M hydrochloric acid solution. The study was carried out using weight loss method. The effects of temperature, time and inhibitor's concentration on the inhibition efficiency of the inhibitor were investigated. The result revealed that corrosion rate was significantly reduced in the presence of all concentrations of the inhibitor.

Gopal *et al* (2012) reported *Parthenium hysterophorus* (*Asteraceae* family) plant leaves extract as a corrosion inhibitor of mild steel in HCl. They employed weight loss measurements, Tafel polarization and electrochemical impedance spectroscopy techniques in analyzing the effect of the plant extract on steel corrosion. In the study, a significant decrease in corrosion rate is observed using water extract of *parthemium hysterophorus* plant as inhibitor. The maximum potential of the extract was obtained at 1100mg/l with 84% efficiency. It was found that adsorption of *Parthemium hysterophours* extract follows Langmuir isotherm model. UV – vis spectra and SEM images were used to explore the mechanism of the corrosion inhibition.

In a study by Li and Deng, (2012), weight loss, potentiodynamic polarization, electrochemical impedance spectroscopy and scanning electron microscopy methods were used to investigate the inhibition effect of *Dendrocalamus brandisii* leave extraction (DBLE) on the corrosion of aluminium in HCl and H_3PO_4 solutions. The results of the experiment show that DBLE is a good inhibitor in 1.0M HCl, while a moderate inhibitor in H_3PO_4.

Vasudha and Shanmuga, (2013) investigated the corrosion inhibition efficiency of dry *Polyalthia longitolia* (Asoka tree) leaves in 1N HCl medium by exploring weight loss and temperature studies. Effect of temperature on the corrosion behaviour of mild steel in the presence of plant extract was studied. Inhibition was found to increase with increase in concentration of the extract. Adsorption of extract molecules on mild steel surface obeyed the Langmuir, Temkin, Freundlich adsorption isotherms. The results obtained prove that the leaves extract of *Polyalthia longifolia* is a good corrosion inhibitor having efficiency of 87% at 1.5% inhibitor concentration.

Nnanna, *et al*, (2013) examined the adsorption of *Gnetum Africana* leaves extract and corrosion inhibition of carbon steel in hydrochloric acid solutions. The effects of time, temperature and inhibitor's concentration on the inhibition efficiency were examined. The experimental data complied with the Langmuir and Temkin adsorption isotherms and the negative values of the Gibb's free energy of adsorption obtained suggested that inhibitor molecules have been spontaneously adsorbed on to the carbon steel.

However, Rajendran, *et al.,* (2005), in their paper titled, Corrosion inhibition by plant extracts- an overview described the inhibitive activity of ethanolic extracts from leaves of *Chromolena odorata* as eco-friendly corrosion inhibitor of aluminium in 2M HCL using hydrogen evolution and thermometric technique.

Also, for mild steel in H_2SO_4 solutions,*Chromolena odorata*worked as a corrosion inhibitor and the inhibition efficiency increased as theconcentration of extract but decreased with temperature. Inhibition efficiency of 99% at 303K and 89% at 333K respectively at a concentration of 5%v/v of the extract was achieved, (Lame,*et al.*, 2013, Obot and Obi-Egbedi, 2010).

2.11 Research gap

It is imperative that a lot of works have been done on corrosion inhibition of metals using natural inhibitors which are plant origin due their eco-friendly nature.

Although several studies have been carried out on phytochemical screening, the results differ as a result of the biochemical variations within species, geographical locations, mode of extraction and solvent used. It is important to adopt test techniques of corrosion inhibition of metals with detailed understanding of the inhibitors. Also, there is need to obtain eco-friendly plant extracts for corrosion inhibition of metals in both acid and alkaline media.

Plant-derived substances such as extracts of *Aspilia africana, Chromolena odorata, Newbouldia laevis, Dennettia tripetala, Dialium guineense* and *Vitex doniana* plants are of great interest owing to their availability and the need to explore their versatile applications.

However, in this research work *Dennettia tripetala, Dialium guineense* and *Vitex doniana* are new inhibitors while *Aspilia africana, Chromolena odorata, Newbouldia laevis*have been used before by others. The study will include the determination of the types of the inhibitors and shifting mechanism of the functional groups of the inhibitors for the corrosion inhibition process, the transfer charge and the quantum chemical calculations.

Gravimetric, electrochemical and quantum chemical studies of aluminum and mild steel corrosion inhibition by natural leaf extracts of *Aspilia africana* leaf,*Chromolena odorata, Newbouldia leavis,Dennettia tripetala, Diallium guineense*and *Vitex doniana* has not been previously studied.

CHAPTER THREE

MATERIALS AND METHODS

3.1 Materials and Equipment

3.1.1 Materials

- Metals:

(a) Aluminum alloy with composition of Si (0.25%), Fe (0.02%), Zn (0.05%), Mn (0.04%) Mg (0.03%), V (0.04%), Ti (0.02%), Cu (0.03%), Cr (0.02%), Al (99.5%) (b) mild steel with composition of P (0.02%), Mn (0.11%), Si (0.02%), S (0.02%), Cu (0.01%), C (0.23%), Ni (0.02), Cr (0.01%) and Fe (99.56 %).

Reagents: KOH, NaOH, HCl and H_2S0_4acetone, distilled water etc. All the chemicals used for this experiment were of analytical grade.

Plant leaves extract: *Aspilia africana, Chromolena odorata, Newbouldia laevis, Dennettia tripetala, Dialium guineense* and *Vitex doniana*

- Equipment:

(a) Fourier transform infrared spectrophotometer (SHIMADZU, Model: IR affinity- 1; S/N: A2137470136 SI).

(b) Gas chromatography-mass spectrometer (GC MS -QP2010 PLUS, SHIMADZU, Japan).

© Potentiostat/galvanostat 263 electrochemical system workstation

(d) SEM – model: Rhenom Prox, Phenom World Eindhoven, Netherlands and

(e) Design expert and DFT software

(f) Glass wares, electronic weighing balance, water bath, memmert oven, stop watch.

(g) Others: knife, plastic bucket, grinding machine, filter paper, thread, masking tape, emery papers etc

3.2 Methods

3.2.1 Preparation of Alkaline and Acid Solutions

The solutions of 1M NaOH, 1M KOH 1M HCl and 1M H_2SO_4were separately prepared using distilled water. The solutions were prepared with the aid of electronic weighing balance, volumetric flask and beakers. 1M NaOH was prepared by dissolving 40g of NaOH in 1 liter of distilled water. 1M KOH was prepared by dissolving 56g of KOH in 1 liter of distilled water. 85.91 ml HCl (36% pure, specific gravity of 1.18) was added to 600 ml of distilled water in 1 liter measuring cylinder. The solution was made up to 1 liter with addition of distilled water. For the preparation of 1M H_2SO_4, 54.35 ml H_2SO_4 (98% pure, specific gravity of 1.84) was added to 700 ml of distilled water in 1 liter measuring cylinder. The solution was made up to 1 liter with addition of distilled water.

3.3 Extraction of the Plant Extracts

Leaves of *Aspilia Africana* and *Chromolena odorata* were collected from Nnamdi Azikiwe University, Awka, whereas *Newbouldia laevis, Dennettia tripetala, Dialium guineense* and *Vitex doniana*were sourced from Isuaniocha, Anambra State, Nigeria. These leaves were identified at Department of Botany, Nnamdi Azikiwe University, Awka. The Leaves were separately sun dried for three days. After sun drying, the dried leaves were separately ground to increase the surface area and stored in closed containers. 20 grams of each of the ground plant leaveswere measured and soaked in 500ml of ethanol (99.7% v/v) for 24 hours. At the end of the 24 hours, each plant mixture was filtered. The filtrate obtained is a mixture of the

plant extract and the ethanol. The plant extract obtained in ethanol solvent was concentrated by evaporating the ethanol from the mixture. Each of the plant extract was weighed and stored for the corrosion inhibition study.

3.4 Metals Preparation

The metals were cut into coupons; Aluminum (5cm x 4cm x 0.06cm) and mild steel (5cm x 4cm x 0.1cm). The coupons were cleaned followed by polishing with emery paper to expose shining polished surface. To remove any oil and organic impurities, the coupons were degreased with acetone and finally washed with distilled water, dried in air and then stored in desiccators. Accurate weight of each coupon was taken using electronic weighing balance and the initial weight was recorded. The coupons were labeled in a manner to avoid any mix up.

3.5 Characterization of the Plant Extracts

3.5.1 Instrumental analysis

3.5.1.1 FTIR analysis of the plant extracts

FTIR spectrophotometer is a powerful instrument used in identifying the type of bonding especially functional groups existing in an organic compounds El Ouariachi, et al, (2010). Extracts contain organic compounds and these organic compounds are adsorbed on the metal surface providing protection against corrosion. Therefore, the FTIR analysis can be suitable in predicting whether organic inhibitors are adsorbed or not adsorbed; FTIR spectra were used to support the fact that corrosion inhibition of mild steel in acid medium is due to the adsorption of inhibitor molecules on the aluminum and mild steel surfaces as well as providing new bonding information on the metal surface after immersion in inhibited KOH, NaOH, HCL and H_2SO_4 solutions.

The isolated inhibitor, as well as the protective film that form over aluminum and mild steel surfaces by the inhibitor molecule, was analyzed separately using FTIR spectroscopy using the KBr pellet method. The specimens (aluminum and mild steel) were immersed respectively in the corrosive medium consisting of 0.2-1.0g/l of the inhibitor for 8hrs, which resulted in formation of a fine protective film over the aluminum and mild steel surfaces. Further, the film were carefully scratched from the aluminum and mild steel surfaces and analyzed by FTIR spectroscopy. The analysis was carried out by using Perkin Elmer System FTIR instrument.

3.5.1.2 GC MS Analysis of the Plant Extracts

Chemical analysis of each of the plant extracts was carried out using gas chromatography-mass spectrometer (GCMS-QP2010, SHIMADZU). The method used for the gas

chromatography-mass spectrometry analysis is similar to that of El Ouariachi,*et al, (*2010) and Rosaline-Vimela,*et al,* (2012). The analysis was carried out at National Research Institute for Chemical Technology (NARICT), Zaria. The gas chromatography-mass spectrometer combined the features of gas chromatography (GC) and mass spectrometry (MS) to identify different substances within a test sample of each plant extract. In the GC, the plant extract was separated into individual substances when heated. The heated substances were carried through a column with an inert gas. As the separated substances emerged from the column opening, they flew into the MS. The MS identified the compounds of the plant extract by the mass of the analyte molecule.

3.5.1.3 Scanning Electron Microscopy (SEM) analysis of metals

Scanning electron microscopy (SEM) was used for monitoring the surface morphological changes. In this study, polished aluminum and mild steel coupons were immersed in 1 M HCL, H_2SO_4, KOH and NaOH media respectively in the absence and presence of the 0.2-1.0g/l of the inhibitor for 8hrs. Then the specimen were cleaned with distilled water, dried in acetone and used for the analysis.

3.5.2 Phytochemical analysis of the plant extracts

Methods used by Marcano and Hasenawa (1991) and Mayuri (2012) were adopted for the phytochemical analysis of the plant extracts.

3.5.2.1 Qualitative Analysis of the Plant Extracts

Qualitative Analysis was done on the extracts from the six plants used for this study in order to dictate the presence of somephytochemical components responsible for hindering the corrosion of metals in acid / alkaline environments. Some of these components present in the extracts are; cardiac glycosides, was detected by appearance of brown ring when One drop of $FeCl_3$and1ml conc. H_2SO_4 was added. Flavonoids,appearance of yellow colour by adding 5ml of NH_4OH to 1ml conc. $H_2SO_4$to the test sample. By adding a few drops of 1% (w/v) solution of ferric chloridefollowed by 1% (w/v) gelatin in sodium chloride of the sameconcentration. The formation of a precipitate indicated the presence of polyphenols confirmed the presence of polyphenols. Tannins showed green colour appearance when A few drops of 0.1% $FeCl_3$ were added to test sample in oven at100°C for 15min. Formation of emulsion of the oil or froth to the sample indicated saponins and for alkaloids, is (Orange-brown ppt) using Dragendorff's reagent or (Cream ppt) in case of Mayer's reagent,indicated the presence of alkaloids.

3.5.2.2 Quantitative analysis of the plant extracts

(i) Alkaloids

20ml of 10% acetic acid in ethanol was added to 1g of sample. The mixture was shaken and allowed to settle for 4 hours. It was then filtered. The filtrate was evaporated to about a quarter of its original volume. One drop of concentrated ammonia was added. The precipitate formed was filtered through a weighed filter paper. The filter paper was left to dry in the oven at 60^{o}C. The filter paper was weighed after drying it to constant weight.

$$Alkaloid = \left(\frac{w_r - w_f}{w_0}\right) \quad (3.1)$$

Where w_r is the weight of filter paper + residue, w_f is the weight of filter paper, and w_0 is the weight of the sample analyzed.

(ii) Cardiac glycosides

1g of the extract was placed in the oven at 100 ^{0}C for 15min. 1ml of the extract was added to 2ml glacial acetic acid plus one drop of $FeCl_3$. Also, 1ml conc. H_2S0_4 was added. The absorbance of the resulting solution was measured at 410nm.

(iii). Flavonoids

0.5ml of 2% $AlCl_3$ methanol solution was added to 0.05ml sample solution. After 1hrs at room temperature, yellow colour appeared indicating the presence of flavonoids. Flavonoids content as mg/g quereetin was determined.

(iv). Phenols

0.2% formic acid was added to 2g of the extract and left to settle for 2 minutes. It was then filtered. With the aid of pipette, 2ml of the extract was put into a test tube and 0.5ml folin-ciocalteau reagent was added. It was left for 20 minutes for colour development. The absorbance at 765nm was read and the concentration for a standard graph was obtained. It is expressed as GAE/g (Gallic Acid Equivalent).

(v) Phytate

Ferric ammonium sulphate was added to 0.5ml of extract in a text tube. The test tube was heated in water bath for 30 minutes. It was cooled and centrifuged. To 1ml of the supernatant, 1.5 ml of 2,2-bipyridine solution was added. Measurement was carried out at 519nm, with distilled water as blank.

(vi). Saponins

1g of sample 15 ml ethanol was added and put in a water bath at 55^{o}C for 4 hours. It was filtered and washed the residue with 20% ethanol twice. The extract was reduced to about 5 ml in the oven. 5ml of petroleum ether was added to the concentrated extract inside a separating funnel. The petroleum ether layer was discarded and 3ml of butanol was added to it. It was washed with 5ml of 5% sodium chloride. The butanol was later poured onto a weighed petri dish. It was put in the oven to evaporate to dryness, and the residue was weighed.

(vii). Tannins

1g of the sample was extracted with 25ml of the solvent mixture of 8:2 acetone: 10% glacial acetic acid for 5 hours. It was filtered and the absorbance measured at 500nm. The absorbance of the reagents blank was also measured. A standard graph with 10, 20, 30, 40, 50 mg/100g of tannic acid was drawn. The concentration of tannin (taking into consideration any dilution factor) was obtained

3.6Weight Loss (Gravimetric) Method of Corrosion Inhibition Study

The weight loss method was carried out at different temperatures (303-343K) using different concentrations of the plant extracts. The weighed metal coupons were separately immersed in 250 ml open beakers containing 200ml of 1M NaOH, 1M KOH, 1M HCl and 1M H_2SO_4 respectively for control experiment. Then weighed metal coupons were separately immersed in 250 ml open beakers containing 200 ml of 1M NaOH, 1M KOH, 1M HCl and 1M H_2SO_4 with different concentrations of plant extracts. The variation of weight loss was monitored periodically at various temperatures and in different media, in the absence (control) and presence of different concentrations of the plant extracts. The coupons were taken out at 1, 2, 4, 6 and 8 hours respectively and immersed in acetone, scrubbed with a bristle brush under running water, dried and reweighed. The weight loss was calculated in grammes as the difference between the initial weight and the weight after the removal of the corrosion product. The experimental readings were recorded. The weight loss (Δw) was measured. Corrosion rate (CR) and inhibition efficiency (IE) were obtained using equations (3.4), (3.5) and (3.6) respectively. The surface coverage was obtained using Equation (3.7) Negm, et al, (2012b).

$$\Delta w = w_i - w_f \tag{3.1}$$

$$CR = \frac{w_i - w_f}{At} \tag{3.2}$$

$$IE\% = \frac{\omega_0 - \omega_1}{\omega_0} * 100 \quad (3.3)$$

$$\theta = \frac{\omega_0 - \omega_1}{\omega_0} \quad (3.4)$$

Where w_i and w_f are the initial and final weight of metal samples respectively; ω_1 and ω_0 are the weight loss values in presence and absence of inhibitor, respectively. A is the total area of the specimen and t is the immersion time.The reaction number (RN) was also evaluated using Equation (3.4a) (Mabrouk *et al*, 2011; Eddy *et al*, 2012).

$$RN = \frac{T_m - T_i}{t} \quad (3.4a)$$

Where T_m and T_i are the maximum and initial temperatures (in ^{0}C) respectively, and t is the time in minutes elapsed to reach T_m.

The inhibitor efficiency was determined using Equation (3.4b) (Mabrouk *et el*, 2011)

$$IE\% = (1 - \frac{RN_{add}}{RN_{free}}) * 100 \quad (3.4b)$$

Where RN_{free} and RN_{add} are the reaction numbers for the metal dissolution in free and inhibited corrosive medium respectively. Fig 3.1 represents the experimental set up for different methods of corrosion used.

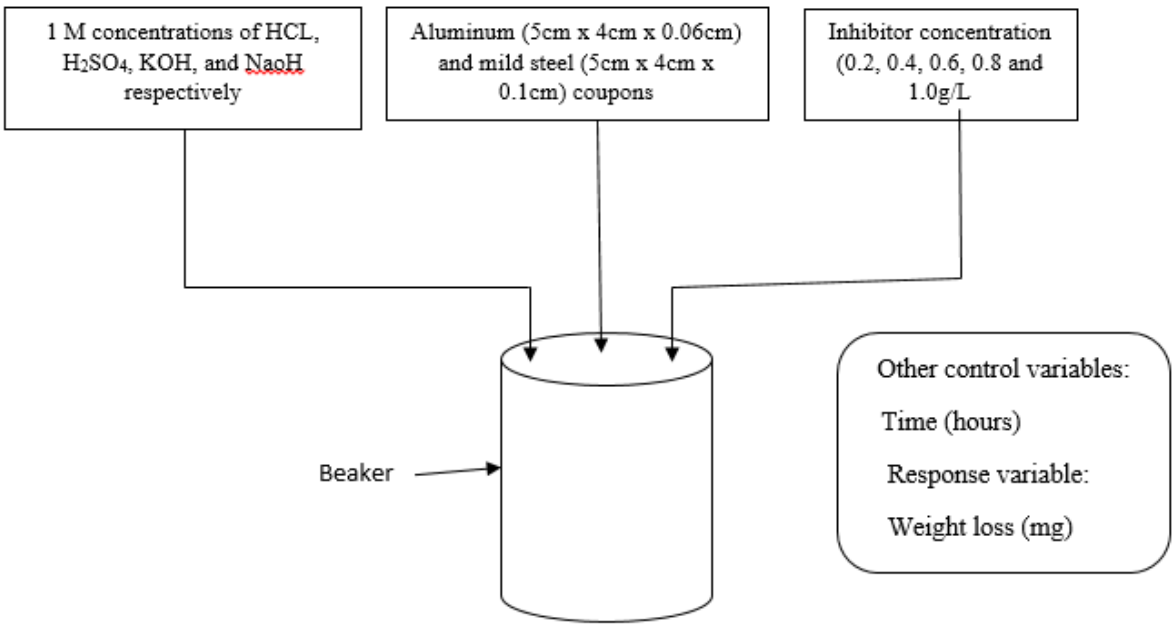

Fig 3.1: Flow process of the experimental setup

3.6.1 Effect of Temperature on Corrosion Rate

Effect of temperature on the corrosion rate was described using Arrhenius equation;

$$CR = Ae^{-E_a/RT} \tag{3.5}$$

Where CR is the corrosion rate of the metal, A is the pre-exponential factor, E_a is the activation energy, R is the gas constant.

Equation (3.5) can be linearized.

$$\ln(CR) = lnA - (E_a/R)(\frac{1}{T}) \tag{3.6}$$

Considering the corrosion rates of the metal at T_1 and T_2 as CR_1 and CR_2, then Equation [3.6] can be expressed by Equation (3.7) (Octave, 2003; Nwabanne and Okafor, 2011; Nnanna *et al.*, 2013).

$$\ln\left(CR_2/CR_1\right) = (E_a/2.303R)(\frac{1}{T_1} - \frac{1}{T_2}) \tag{3.7}$$

3.6.2. Thermodynamic parameter for the adsorption process

Ebenso, etal, (2008), Orubite-Okorosaye and Oforka, (2004) and Nwabanne and Okafor, (2011), evaluated the heat of adsorption Q_{ads} (kJmol^{-1}) using Equation (3.8).

$$Q_{ads} = 2.303R\left[\log\left(\frac{\theta_2}{1-\theta_2}\right) - \log\left(\frac{\theta_1}{1-\theta_1}\right)\right] * \frac{T_2.T_1}{T_2-T_1} \tag{3.8}$$

Where R is the gas constant, θ_1 and θ_2 are the degree of surface coverage at temperatures T_1 and T_2 respectively.Q_{ads} = heat of adsorption.

3.6.3 Adsorption isotherms

The data obtained for the degree of surface coverage were used to test for the applicability of different adsorption isotherms such as Langmuir, Frumkin, Temkin and Flory-Huggins isotherms.

1. Langmuir isotherm

Langmuir isotherm can be expressed by Equation (3.9) (Nwabanne and Okafor, 2011; Li and Deng, 2012; Patel *et al.*, 2013).

$$\frac{C}{\theta} = \frac{1}{K} + C \quad (3.9)$$

Where C is the concentration of the inhibitor, K is the adsorption equilibrium constant and θ is the degree of surface coverage.

Linearizing (3.9) gives;

$$log\frac{C}{\theta} = \log C - logK \quad (3.10)$$

2. Frumkin isotherm

Frumkin adsorption isotherm can be expressed according to equation (3.11) (Nwabanne and Okafor, 2011).

$$\log\left((C) * \left(\frac{\theta}{1-\theta}\right)\right) = 2.303logK + 2\alpha\theta \quad (3.11)$$

Where K is the adsorption-desorption constant and α is the lateral interaction term describing the interaction in adsorbed layer.

3. Temkin isotherm

Temkin isotherm can be expressed by equation (3.12) (Nwabanne and Okafor, 2011).

$$\theta = -\frac{2.303logK}{2a} - \frac{2.303logC}{2a} \quad (3.12)$$

Where K is the adsorption equilibrium constant, a is the attractive parameter, θ is the degree of surface coverage, C is the concentration of the inhibitor.

4. Flory-Huggins isotherm

The Flory-Huggins isotherm can be expressed by Equation (3.13) (Nwabanne and Okafor, 2011; Alinnor and Ejikeme, 2012).

$$\log(\frac{\theta}{C}) = \log K + xlog(1-\theta) \quad (3.13)$$

where x is the size parameter and is a measure of the number of adsorbed water molecules substituted by a given inhibitor molecule.

The free energy of adsorption (ΔG_{ads}) was calculated according to equation (3.14) (Nwabanne and Okafor, 2011; Alinnor and Ejikeme, 2012).

$$\Delta G_{ads} = -2.303RTlog(55.5K) \quad (3.14)$$

Where R is the gas constant, T is temperature, K is the equilibrium constant for the adsorption process and 55.5 represents the concentration of water in acidic and alkaline solution respectively.

3.6.4 Weight loss Method using Response Surface Method

Response surface method in design expert software was used to design the experiment for the weight loss method. Inhibitor concentration, temperature and time were the considered factors while weight loss, corrosion rate and inhibition efficiency were the expected responses of the study. The RSM was used to analyze the responses. The ANOVA and graphical analyses of the inhibition efficiencies were carried out. The mathematical models in terms of coded form were obtained. The models in terms of coded factors were used to make predictions about the response for given levels of each factor. The high levels of the factors were coded as +1 and the low levels of the factors were coded as -1.

3.7 Electrochemical Studies

Aluminum and mild steel coupons used for the electrochemical experiment were cut and prepared in such a way that only 1cm was left uncovered for easy removal of the coupons at the end of each experimental run. The electrodes used were polished with emery papers ranging from 600 to 1000, rinsed with distilled water, degreased by ethanol, dried in acetone. Electrochemical experiment were conducted in a three electrode corrosion cell using a VERSASTAT 300 complete dc voltametry and corrosion system with V3 studio software for electrochemical impedance spectroscopy. Then, potentiodynamic/Galvanostat corrosion system with E-chem software was used for potentiodynamic polarization experiments. A graphite rod was used as counter electrode and a saturated calomel electrode (SCE) was used as reference electrode. The latter was connected via a luggins capillary. Impedance measurement were performed in aerated and unstirred solutions at the end of 1800 s at 30 ± 1^0 C. Impedance measurements were made at corrosion potentials (E_{corr}) over a frequency range of 100KHz-0.1 Hz with a signal amplitude perturbation of 5 mV (Oguzie, *et al.,* 2012and Ihebrodike,*et al.,* 2011). The inhibition efficiencies (*IE %*) for different inhibitor concentrations were calculated from Nyquist plots using the equation:

$$IE\% = \left(\frac{R_{ct(inh)} - R_{ct}}{R_{ct(inh)}}\right) x\ 100 \qquad (3.15)$$

Where R_{ct} and $R_{ct\ (inh)}$ denotes charge transfer resistance in the absence and presence of the inhibitor.

Potentiodynamic polarization

n studies were carried out in the potential range ± 250 mV versus corrosion potential at a scan rate of 0.333 mVs^{-1} for mild steel and -250 to +400 mV for aluminum. Each test was run in

triplicate to verify the reproducibility of the data. All experiments were carried out in freshly prepared solution at a temperature of 30±^{o}C (Chidiebere,*et al.,* 2014; Oguzie *et al,* 2010). The inhibition efficiency was determined using equation (3.16).

$$IE\% = \frac{i_{corr\ (unin\ h)} - i_{corr\ (in\ h)}}{i_{corr\ (unin\ h)}} \times 100$$

(3.16)

Where $i_{corr(uninh)}$ and $i_{corr(inh)}$ are the corrosion current density values without and with inhibitors, respectively.

3.8 Quantum Chemical Study

All theoretical calculations were performed using the density functional theory (DFT) electronic structure programs Forcite and DMol3 as contained in the Materials Studio 4.0 software (Accelrys, Inc.).The following quantum chemical indices were calculated: the energy of the highest occupied molecular orbital (E_{HOMO}), the energy of the lowest unoccupied molecular orbital (E_{LUMO}) and the energy gap ($\triangle E = E_{LUMO} - E_{HOMO}$).

CHAPTER FOUR

RESULTS AND DISCUSSION

4.1Instrumental Analysis

4.1.1 Fourier transform infrared spectrophotometer (FTIR) analysis

FTIR spectrum of the pure plant extracts and corrosion products with the plant extracts (scratched metal oxides film) were shown in Appendix A1-A6. The peaks, intensities and assignments of the FTIR analyses of the pure plant extracts and corrosion products with the plant extracts are presented in Tables 4.1- 4.6. The shift/disappearance of some functional groups observed in the scratched metal oxides films shown in Tables 4.1- 4.6 were as a result of the active functional groups that actually inhibit the metals during corrosion process.

(i) Table 4.1:Peak, intensity and assignment of FTIR analysis of pure and*Dennettia tripetala*extracts and scratched oxide film using NaOH.

Dennettia tripetala leaves extract			Scratched Al oxide film		
Peak (cmol2/kJ2)	Intensity	Assignment	Peak (cmol2/kJ2)	Intensity	Assignment
576.36	1.4333	C=C-H, Ar-H bend out of plane	613.36	1.8791	C=C-H, Ar-H bend out of plane

825.48	1.2858	C=C-H, Ar-H bend out of plane	860.24	2.0199	C=C-H, Ar-H bend out of plane
1134.60	2.1934	C-H bend in plane	983.68	3.7293	C=C-H, Ar-H bend out of plane
1258.44	2.3642	C-O stretch	1168.84 1261.42	3.3746 2.8867	C-O stretch
1567.08	1.9817	C=C stretch, C=N stretch	1415.72	2.5189	C=C
1813.32	2.1475	C=O stretch	1724.32 1878.62	2.0579 2.4582	C=O stretch
1938.60	2.7587	C=O stretch	1724.32 1878.62	2.0579 2.4582	C=O stretch
2058.50	2.4065	C≡C stretch, C≡N stretch	2187.22 2310.66	2.0436 2.5063	C≡C stretch, C≡N stretch
2242.44	2.3609	C≡C stretch, C≡N stretch	2187.22 2310.66	2.0436 2.5063	C≡C stretch, C≡N stretch
2367.24	1.7943	C≡C stretch, C≡N stretch	2156.36 2310.66	2.4119 2.1299	C≡C stretch, C≡N stretch
3601.80	1.735	O-H stretch	3483.34 3575.92	2.4463 2.3126	O-H stretch

Table 4.1 presents the analysis of pure *Dennettia tripetala* extract and scratched Al oxide film. The FTIR spectra of adsorbed protective layer formed on Al surface after immersion in O.5M NaOH containing 0.4g/l extracts of *Dennettia tripetala* extract revealed that the O –H stretching at 3601.80 cmol2/kJ2shifted to 3480.34 cmol2/kJ2and from 2367.24 to 2156.36 cmol2/kJ2C≡C stretch, C≡N stretch and 1938.60 cmol2/kJ2 is identified as an C=O bending and was found to shift to 1724.32 cmol2/kJ2 on the adsorbed film of the *Dennettia tripetala* spectra and from 1258.26cmol2/kJ2 to 1168.84 cmol2/kJ2C–O shift on the adsorbed film. Also, a shift from 825.06 to 860.17 cmol2/kJ2due to a C=H bending and a rare shift from 572.75 to 630 cmol2/kJ2was observed due to a C=H stretching. The result indicates thatthe adsorption of the inhibitors took place via –OH stretching, N–H bending, C–O stretching for extracts, and –C, C–H:C–H bending and C–C stretching (in ring) and is in line withChidiebere, et al, (2015).

(ii) Table 4.2:Peak, intensity and assignment of FTIR analysis of *Dialium guineense* leaves extract and scratched Al oxide film in NaOH.

Dialium guineense leaves extract			scratched Al oxide film.		
Peak (cmol2/kJ2)	Intensity	Assignment	Peak (cmol2/kJ2)	Intensity	Assignment
581.64	1.5377	C=C-H, Ar-H bend out of plane	613.36	1.8791	C=C-H, Ar-H bend out of plane
763.08	2.1753	C=C-H, Ar-H bend out of plane	613.36	2.908	C≡C-H, C-H bend
887.88	2.964	C=C-H, Ar-H bend out of plane	860.24	2.0199	C=C-H, Ar-H bend out of plane
1195.08	2.4171	C-H bend in plane	983.68	3.7293	C=C-H, Ar-H bend out of plane
1319.88	2.1638	C-H bend in plane	937.39	2.6214	C=C-H, Ar-H bend out of plane
1442.76	2.6399	N-O asymmetric stretch	1292.28	2.1001	N-O symmetric stretch

1633.80	1.9191	C=C stretch, C=N stretch	1662.6	2.2599	C=C stretch, C=N stretch
1873.80	2.8225	C=O stretch	1724.32	2.0579	C=O stretch
			1878.62	2.4582	
2244.36	2.8358	C≡C stretch, C≡N stretch	2187.22	2.0436	C≡C stretch, C≡N stretch
			2310.66	2.5063	
3623.88	1.9735	O-H stretch	3483.34	2.4463	O-H stretch
			3575.92	2.3126	

Table 4.2 presents the analysis of *Dialium guineense* leaves extract and scratched Al oxide film. The FTIR spectra of adsorbed protective layer formed on Al surface after immersion in O.5M NaOH containing 0.4g/l extracts of *Dialium guineense* revealed that the O –H stretching at 3623.88 cmol2/kJ2shifted to 3575.92 cmol2/kJ2and from 1442.2 N-O asymmetric stretch to 1292.28 cmol2/kJ2N-O symmetric stretch on adsorbed film. 1319.88 C-H is identified as bend in plane and was found to shift 937.39 cmol2/kJ2C=C-H, Ar-H bend out of plane on the adsorbed filmof*Dialium guineense*. Also, a shift from 763.08 C=C-H, Ar-H bend out of plane is identified as C≡C-H, C-H bend and was found to shift to 613.34 cmol2/kJ2 on the adsorbed film of the *Dialium guineense* spectra and from 581.64cmol2/kJ2 =C-H, Ar-H bend out of plane to 618.36 cmol2/kJ2C=C-H, Ar-H bend out of plane shift on the adsorbed film. The result proves thatthe adsorption of the inhibitors took place via –OH stretching, N–H bending, C–O stretching for extracts, and –C, C–H:C–H bending and C–C stretching.

(iii) Table 4.3:Peak, intensity and assignment of FTIR analysis of *Newbouldia leavis*extract and scratched mild steel oxide film using KOH.

Newbouldia leavis leaves extract			scratched mild steel oxide film.		
Peak (cmol2/kJ2)	Intensity	Assignment	Peak (cmol2/kJ2)	Intensity	Assignment
1003.77	1.1243	C-H bend in plane	921.96	2.6189	C=C-H, Ar-H bend out of plane
1269.46	1.1964	C-O stretch	1168.84	3.3746	C-O stretch
			1261.42	2.8867	
1435.09	0.2010	N-O asymmetric stretch	1292.28	2.1001	N-O symmetric stretch
1619.13	2.7641	C=C stretch, C=N stretch	1600.88	2.617	C=C stretch, C=N stretch
2O27.20	2.44843	C≡C stretch, C≡N stretch	2187.22	2.0436	C≡C stretch, C≡N stretch
			2310.66	2.5063	
2436.90	2.654	C≡C stretch, C≡N stretch	2156.36	2.6264	C≡C stretch, C≡N stretch
			2403.24	2.6979	
2761.99	1.4541	C-H stretch	2804.42	2.8647	C-H stretch
3119.74	1.7401	C-H stretch	3174.74	2.5713	C-H stretch
3675.66	5.5670	O-H stretch	3329.04	4.1986	O-H stretch

Furthermore, Table 4.3 presents the analysis of pure *Newbouldia leavis* leaves extract and scratched mild steel oxide film.. O-H stretches showed peaks of 3675.66cmol2/kJ2 shifted to O-H stretch (3329.04 cmol2/kJ2); C-H stretch (2761.99-3119.74 cmol2/kJ2) shifted to C-H stretch 3174.74 cmol2/kJ2 and C≡C, C≡N stretches shifted to 2187.22 C≡C, C≡N aromatic stretches, N-O (1435.09 cmol2/kJ2)asymmetric stretch shifted to N=O (1292.28 cmol2/kJ2) symmetric stretch. C-H bend in plane (1003.77 cmol2/kJ2) shifted to 921.96 cmol2/kJ2. C=H-H, Ar-H bend out of plane. The adsorption operation in this analysis indicated that the extracts were adsorbed on the surface of the metal.

(iv) Also, Table 4.4 shows the analysis of pure *Aspilia africana* leaves extract and scratched mild steel oxide film using HCL. The characteristics bands at (762.07-880.56 cmol2/kJ2) C=C-H Ar-H bend out of plane shifted to (860.24cmol2/kJ2) C≡C-H, C-H bend; C-H bend in plane at 1006. 12 - 1166.66cmol2/kJ2) shifted toC=C-H, Ar-H bend out of plane at (921.23 - 983.68cmol2/kJ2). C=C stretch, C=N stretch at (1674.96 cmol2/kJ2) shifted to 1662.66 cmol2/kJ2); the unique band at 1900.26 cmol2/kJ2keto group (C=O) shifted to 1724.32 cmol2/kJ2and the C≡C, C≡N stretches at (2234.82 – 2487.43cmol2/kJ2) shifted to (2186.12 – 2310.66 cmol2/kJ2). The O-H stretch band at (3370.18 – 3796.57 cmol2/kJ2) shifted to (3390.76 – 3622.21 cmol2/kJ2) and C-H stretch at (2742.24 – 3131.62 cmol2/kJ2) shifted to (280.42 – 3174.74 cmol2/kJ2). These observations imply that the green inhibtors are strongly adsorbed over the MS surface and protect it from the direct attack of aggressive HCL medium.

Table 4.4: Peak, intensity and assignment of FTIR analysis of *Aspilia africana* leaves extract and scratched mild steel oxide film using HCL.

Aspilia africana leaves extract			scratched mild steel oxide film.		
Peak (cmol2/kJ2)	Intensity	Assignment	Peak (cmol2/kJ2)	Intensity	Assignment
762.07	2.7832	C=C-H, Ar-H bend out of plane	613.36	2.908	C≡C-H, C-H bend
880.56	0.4387	C=C-H, Ar-H bend out of plane	860.24	2.0199	C=C-H, Ar-H bend out of plane
1006.12	0.9814	C-H bend in plane	921.96	2.6189	C=C-H, Ar-H bend out of plane
1166.66	0.7413	C-H bend in plane	983.68	3.7293	C=C-H, Ar-H bend out of plane
1674.96	0.7845	C=C stretch, C=N stretch	1662.6	2.2599	C=C stretch, C=N stretch
1900.26	0.8761	C=O stretch	1724.32	2.0579	C=O stretch
2234.82	2.2814	C≡C stretch, C≡N stretch	2187.12	2.0436	C≡C stretch, C≡N stretch

2487.43	1.8451	C≡C stretch, C≡N stretch	2156.36 2310.66	2.4119 2.1299	C≡C stretch, C≡N stretch
2742.24	1.8671	C-H stretch	2804.42	2.8647	C-H stretch
3131.62	2.1580	C-H stretch	3174.74	2.5713	C-H stretch
3370.18	1.5634	O-H stretch,	3390.76	2.6024	O-H stretch
3543.59	1.3234	O-H stretch	3483.34	2.4463	O-H stretch
3796.57	2.0812	O-H stretch	3622.21	2.5632	O-H stretch

(v) Table 4.5:Peak, intensity and assignment of FTIR analysis of *Chromolena odorata* leaves extract and scratched mild steel oxide film using H_2S0_4

Chromolena odorata leaves extract			scratched mild steel oxide film		
Peak (cmol2/kJ2)	Intensity	Assignment	Peak (cmol2/kJ2)	Intensity	Assignment
710.74	0.7108	C=C-H, Ar-H bend out of plane	705.94	1.7303	C=C-H, Ar-H bend out of plane
944.32	0.6730	C=C-H, Ar-H bend out of plane	860.24 952.82	1.7859 2.1501	C=C-H, Ar-H bend out of plane
1263.36	0.5542	C-O stretch	1168.84 1261.42	3.3746 2.8867	C-O stretch
1506.36	0.7327	N-O asymmetric stretch	1323.14	2.073	N-O symmetric stretch
2146.66	0.7906	C≡C stretch, C≡N stretch	2187.22 2310.66	2.0436 2.5063	C≡C stretch, C≡N stretch
2364.37	0.7906	C≡C stretch, C≡N stretch	2187.22 2310.66	2.0436 2.5063	C≡C stretch, C≡N stretch
3015.07	2.4052	C-H stretch	2989.58	2.693	C-H stretch
3377.27	2.1385	O-H stretch	3452.48	2.4329	O-H stretch
3603.00	0.8516	O-H stretch	3483.34 3575.92	2.4463 2.3126	O-H stretch

Also, pure plant extract and its scratched protective film formed over mild steel were screened by FTIR spectroscopy, and the result obtained depicted a characteristic band at 3603.00 3377.27 cmol2/kJ2 (O-H stretch) shifted to 3575.92 – 3452.48 cmol2/kJ2; 3015.07 cmol2/kJ2(C-H stretch) shifted to 2989.58cmol2/kJ2(C-H stretch); 2364.37 – 2146.66 cmol2/kJ2(C≡C, C≡N stretches) shifted to 2310.66-2187.22 cmol2/kJ2(C≡C, C≡N stretches); 1506.36 cmol2/kJ2 (N-O asymmetric stretch) shifts to 1323.14 cmol2/kJ2 (N-O asymmetric stretch). Thus, FTIR studies have paved the way to identify the active sites of coordination in a multiring molecule.

(vi) Table 4.6:Peak, intensity and assignment of FTIR analysis of *Vitex doniana* leaves extract and scratched mild steel oxide film using NaOH .

Vitex doniana leaves extract			scratched mild steel oxide film		
Peak (cmol2/kJ2)	Intensity	Assignment	Peak (cmol2/kJ2)	Intensity	Assignment
864.01	0.5249	C=C-H, Ar-H bend out of plane	860.24	2.0199	C=C-H, Ar-H bend out of plane
1003.76	0.7209	C-H bend in plane	921.96	2.6189	C=C-H, Ar-H bend out of plane

1269.45	0.5542	C-O stretch	1168.84 1261.42	3.3746 2.8867	C-O stretch
1435.09	0.7215	N-O asymmetric stretch	1292.28	2.1001	N-O symmetric stretch
2027.20	0.7906	C≡C stretch, C≡N stretch	2187.22 2310.66	2.0436 2.5063	C≡C stretch, C≡N stretch
2200.26	1.3988	C≡C stretch, C≡N stretch	2156.36 2310.66	2.4119 2.1299	C≡C stretch, C≡N stretch
2438.50	1.6445	C≡C stretch, C≡N stretch	2156.36 2403.24	2.6264 2.6979	C≡C stretch, C≡N stretch
2761.99	1.8599	C-H stretch	2804.42	2.8647	C-H stretch
3119.73	2.1082	O-H stretch, C-H stretch	3082.16	4.0661	O-H stretch, C-H stretch
3675.86	1.0272	O-H stretch	3545.06	3.7989	O-H stretch
3911.59	1.8632	O-H stretch	3699.36	2.1468	O-H stretch

Finally, Table 4.6 presents the analysis of pure *Vitex doniana*leaves extract and scratched mild steel oxide film. O-H stretches showed peaks of (3119.73- 3911.59cmol2/kJ2) shifts to O-H stretch (3082.16-3699.36 cmol2/kJ2); C-H stretch (2761.99cmol2/kJ2) shifted to C-H stretch (2804.42 cmol2/kJ2) and C≡C, C≡N stretches (2027.22-2438.50 cmol2/kJ2) shifted to (2187.22- 2403.24 cmol2/kJ2) C≡C, C≡N aromatic stretches, N-O (1435.09cmol2/kJ2) asymmetric stretch shifted to(1292.28 cmol2/kJ2) N=O symmetric stretch. C-H bend in plane (1003.76) shifted to 921.96 cmol2/kJ2. C=H-H, Ar-H bend out of plane. The adsorption operation in this analysis indicated that the extracts were adsorbed on the surface of the metal. Finally, Tables 4.1 – 4.6 presents the active ingredients in the plant extracts responsible for inhibiting the metals and the shifting/disappearance of some bonds/peaks or functional groups after corrosion inhibition process confirmed the peaks that actually inhibited the materials.

4.1.2 **Gas Chromatography-Mass Spectrometry (GC-MS) analysis**

The phytocomponents present in the leaf ethanolic extracts of *Aspilia africana*, *Chromolena odorata*, *Newbouldia laevis*, *Dennettia tripetala, Dialium guineense* and *Vitex doniana* were identified by GC-MS analysis, GC-MS running time is 40min. The active compounds in the leaf ethanolic extract of the plants, their retention time (RT), molecular formula, molecular weight and concentration is provided in **Table 4.7- 4.12.**

Table 4.7: Gas Chromatography-Mass Spectrometry analysis**of** *Dennettia tripetala***leaf extracts**

The gas chromatogram shows the relative concentrations of various compounds getting eluted as a function of retention time. The heights of the peaks indicate the relative concentrations of the components present in the plant. GC-MS analysis revealed the presence

of 32 compounds. Sterols, stanols and Terpenoids were the most prominent compounds detected. The major compounds detected were 9,19-Cyclolanost-24-en-3-ol (16.09%), 2,5,5-Triphenyl-4-methoxyimidazole (10.87%), Beta-Sitosterol (8.81%), Stigmast-4-en-3-one(7.26%), Phytol (5.62%), Bicyclo[3.1.1] heptane, 2,6,6-trimethyl-, (1.alpha.,2.beta.,5.alpha.) (4.34%), Acetamide, 2-(1-isoquinolinylthio) -N,N-dimethyl- (4.20%), Cholest-4-en-3-one (4.06%),

The carbonyl group and the carbon double bonds present in the Dennettia tripetala leaf extract suggest that the Dennettia tripetala leaf extract inhibited the corrosion of mild steel. The presence of the aromatic group also suggests the Dennettia tripetala leave extract as good corrosion inhibitor on aluminum and mild steel.

(ii) The aqueous extract of *Dialium guineense* leaf extract revealed several peaks which represents different compounds as shown in Table 4.8 of Gas Chromatography-Mass Spectrometry analysis. The peaks in the chromatogram were integrated and were compared with the database of spectrum of known components stored in the Gas Chromatography-Mass Spectrometry library. The carbonyl group and the carbon double bonds present in the Dennettia tripetala leaf extract suggest that the Dennettia tripetala leaf extract inhibited the corrosion of Al.

Table 4.8: Gas Chromatography-Mass Spectrometry analysis **of** *Dialium guineense* **leaf extracts**

(iii) The compound has a 4-carbon structure and the molecular formula. Its isomers include isobutanol, 2-butanol, and *tert*-butanol. Butanol is one of the group of "fusel alcohols" (from the German for "bad liquor"), which have more than two carbon atoms and have significant solubility in water. The compound is used in butter, cream, fruit, rum, whiskey, ice cream and ices, candy, baked goods and cordials. The largest use of *n*-butanol is as an industrial intermediate, particularly for the manufacture of butyl acetate. 2,6-Di-*tert*-butylphenol is the major fraction, constituting above 4% of the chemical constituents of the studied plant extract. The compound is colourless solid alkylated phenol and its derivatives are used industrially as UV stabilizer and as an antioxidant for hydrocarbon-based products ranging from petrochemicals to plastics. Illustrative of its usefulness, it prevents gumming in aviation fuels. 6-Di-*tert*-butylphenol is also a precursor to more complex compounds used as antioxidants and light-protection agents. Also, closely related aromatic compounds were identified. The compounds included, (1-butylheptyl) benzene, (1-ethylnonyl) benzene, (1-methyldecyl) benzene and 91-pentylheptyl) benzene. The major similarity in these

compounds is that they are aromatic compounds built from different hydrocarbon chains attached to benzene ring.

Table 4.9: Gas Chromatography-Mass Spectrometry analysisof*Vitex doniana* leaf extracts

Table 4.10: Gas Chromatography-Mass Spectrometry analysisof*Newbouldia leavis*leaf extracts

(iv) The compounds present in *Newbouldia leavis* leaf extract support the corrosion application of the plant. The study revealed major compounds present in all of the extracts. Identification of these compounds in the plant serves as the basis in determining the possible health benefits of the plant leading to further studies.

Table 4.11: Gas Chromatography-Mass Spectrometry analysisofChlomolena odoarataleaf extracts

(v) The aqueous extract of *Chlomolena odoarata* leaf revealed several peaks which represents different compounds as shown in Table 4.11 of Gas Chromatography-Mass Spectrometry analysis. The peaks in the chromatogram were integrated and were compared with the database of spectrum of known components stored in the Gas Chromatography-Mass Spectrometry library.

Table 4.12: Gas Chromatography-Mass Spectrometry analysis**of** *Aspilia africana* leaf extracts**.**

Nowadays, the study of the organic compounds from plants and their activity has increased. The combination of a best separation technique (GC) with the best identification technique (MS) made GC-MS an ideal technique for qualitative analysis for volatile and semi-volatile compounds.The GC-MS analysis revealed that the extract is mainly composed of oxygenated hydrocarbons, alkane hydrocarbon, and predominantly phenolic hydrocarbons and tannins. Phytochemical analysis by GC-MS revealed the presence of palmitic acid, tannins, hydrocarbons, aldehydes, fatty acid esters, fatty acid amide, terpenoids, terpene alcohol, and phytol as the major compound groups.

4.1.3 Metal surface study using Scanning electron microscopy(SEM)

Scanning electron microscopy (SEM) provides a pictorial representation of the metal surfaces studied. To understand the nature of the surface film in the absence and presence of inhibitors and the extent of corrosion of the metals.The micrographs of the corroded metals in the

corrosive media (absence) and in the presence of the plant extracts are presented in Plate 4.1 - 4.5. Looking at the corroded metals for all themedia used, there were significant differences in the morphology of the metal surfaces in the presence and absence of the plant extracts. The electron micrographs revealed that the metal surfaceswere strongly damaged owing to corrosion in the absence of the inhibitor, but in the presence of inhibitor, there is a much smaller damage on the surface. This is attributed to the formation of a good protective film on the metal surfaces by the inhibitors (Shanthi and Rajendran, 2013). The micrographs have close correlation with the results obtained from the weight loss method. This is in agreement with the previous study by Loto and Popoola, (2012). The surface-nature of the corroded metals in the presence and absence of the plant extracts shows that the inhibitors surpressed the corrosion process.

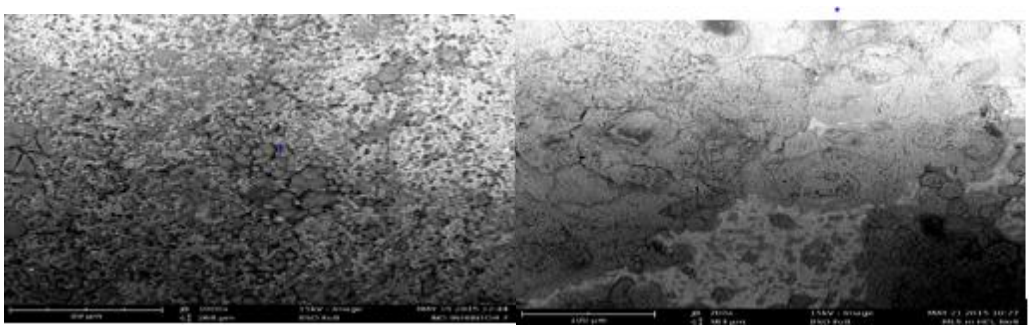

(a) (b)

Plate 4.1: The micrograph of corroded mild steel surface in HCl,(a) without *Newbouldialaevis*leaf extract (b) with *Newbouldia laevis*leaf extract.

The morphology of the Al surface in plate 4.1a reveals that, in the absence of inhibitors, the surface was highly damaged, with areas of typical uniform corrosion on the Al surface. Although, in the presence of green inhibitors plate 4.1b, the rate of corrosion was surpressed, due the formation of an adsorbed film of the inhibitor on the Al surface. The protective nature of the film is reflected in the inhibition efficiency measurements obtained in the chemical and electrochemical methods.

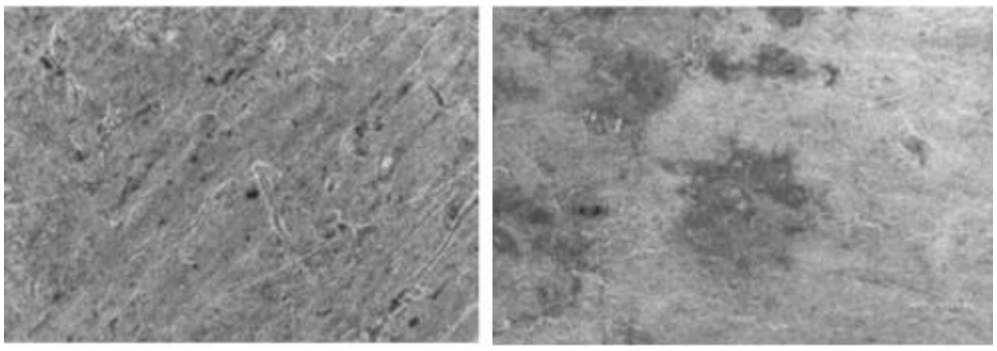

(a) (b)

Plate 4.2:The micrograph of corroded Al surface in NaOH, (a) without *Aspilia africana*leaf extract (b) with *Aspilia africana* leaf extract

Plate (4.2b) shows the protected Al surface after addition of green inhibitors, whereby the surface damage has diminished in comparison to the blank material. This is attributed to a good protective film on the Al surface.

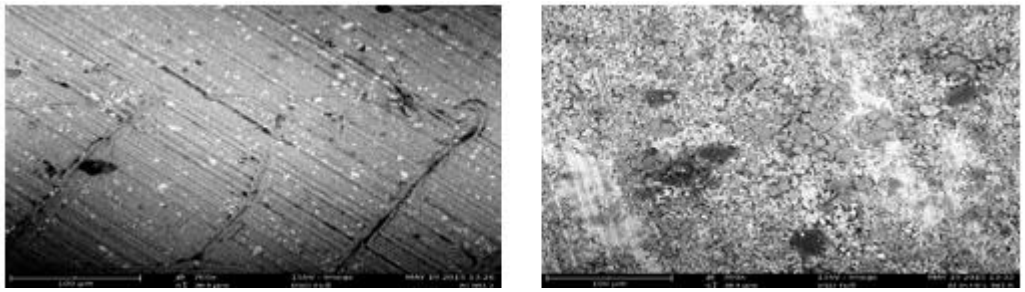

(a) (b)

Plate 4.3:The micrograph of corroded Al surface in HCl, (a) without *Vitex doniana*leaf extract (b) with *Vitex doniana*leaf extract.

Parallel features on the polished Al surface before exposure to the corrosive solution (plate 4.3a). the SEM image revealed a severe damage on the Al surface due to metal dissolution.it appears that material dissolution began on grain boundaries and it is known that grain boundaries are active sites where dislocations and other lattice defects are accumulated, so that Al oxide deposition is likely to be initiated on grain boundaries to be later spread on all the surface.

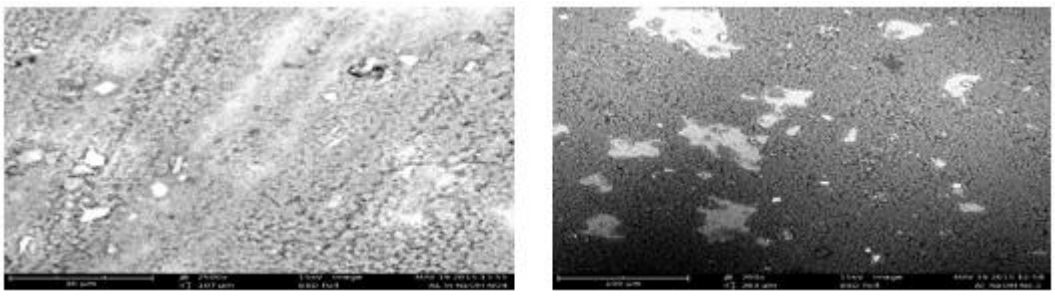

(a) (b)

Plate 4.4:The micrograph of corroded Al surface in KOH, (a) without *Dennettia tripetala* leaf extract (b) with *Dennettia tripetala* leaf extract.

Plate 4.4b shows that the corrosion is highly minimized by green inhibitors. The micrograph also reveal that the formation of a protective layer over all the metal surface is the reason for corrosion inhibition by the plant extract.

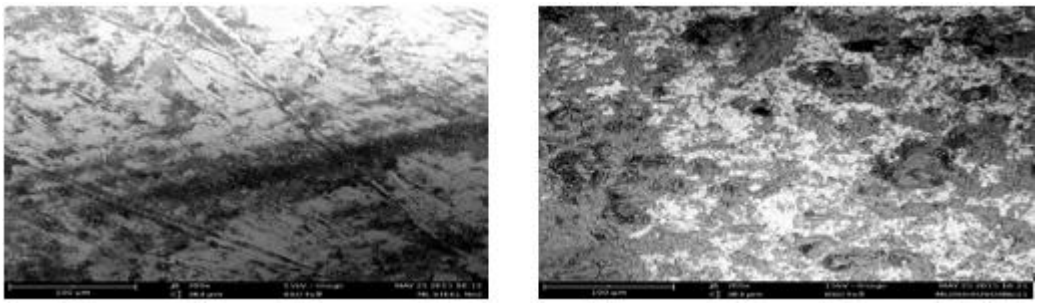

(a) (b)

Plate 4.5:The micrograph of corroded mild steel surface in H_2SO_4, (a) without *Dialium guineense*leaf extract (b) with *Dialium guineense* leaf extract.

From plate 4.5a, it was observed that the surface was very rough and severely damaged in the absence of inhibitor while in 4.5b the surface was transformed into smoother, more uniform deposits with patches upon addition of *Dialium guineense*leaf extract.

4.2 Phytochemical Results

In Table 4.13, the qualitative analysis of the extracts show that the phytochemicals of alkaloids, cardiac glycosides, flavonoids, phenolics, phytates, saponins and tanins are present in the extracts at various degrees. The qualitative results of the extract phytochemicals are denoted with symbols; +++ (highly concentrated), ++ (concentrated), + (in traces), and – (absence or too little to be observed qualitatively). The difference in the results may be attributed to biochemical variations of the plant species (Ojezele and Agunbiade, 2013).

Table 4.13: Qualitative analysis of the plant extracts

Parameters	*Aspilia africana* leaves	*Chromolena odorata* leaves	*Newbouldia leavis* leaves	*Dennettia tripetala* leaves	*Dialium guineense* leaves	*Vitex doniana*
Alkaloids	+	+	+	+	+	+
Cardiac glycosides	-	-	+	-	+	-
Flavonoids	++	++	++	++	++	++
Phenolics	+	++	+	++	++	++
Phytates	+	+	+	+	+	+
Saponins	++	++	++	++	++	++
Tannins	++	++	++	++	++	++

The phytochemical components have been analyzed qualitatively in our laboratory by the common methods using chemicals.Flavonoids, cardiac glycosides, tannins, phenolics, phytates, alkaloids and saponins were found in the leaf extracts presented in Table 4.13.

Again, Table 4.14 indicates the amount/quantity of each phyotcomponents present in 1m of the extracts.

Table 4.14: Quantitative analysis of the plant extracts

Parameters	*Aspilia africana* leaves	*Chromolena odorata* leaves	*Newbouldia leavis* leaves	*Dennettia tripetala* leaves	*Dialium guineense* leaves	*Vitex doniana* leaves
Alkaloids (mg/100g)	203.9	324.2	360.5	290.2	83.3	377.9
Cardiac glycosides (mg/100g)	10.0	8.3	53.3	81.0	70.0	20.11
Flavonoids (mgCE/100g)	417.20	140.0	367.47	152.27	365.0	351.53
Phenolics (GAE/g)	38.0	27.5	52.50	108.46	24.9	63.50
Phytates (mg/100g)	78.3	33.3	43.3	46.7	50.0	12.34
Saponins (mg/100g)	24.71	55.0	49.21	39.3	11.7	44.23
Tannins (mg/100g)	76.9	60.0	82.36	115.0	270.0	72.1

4.3 Weight Loss Studies

4.3.1 Effect of Concentration

Appendix B show the result of weight loss, corrosion rate (CR) and in inhibition efficiency of metals (aluminum and mild steel) in alkaline and acid media using various plant extracts (*Aspilia africana* leaf, *Chromolena odorota*, *Newbouldia leavis*,*Dennttia tripetala*, *Dialium guineense*and *Vitex doniana*). These were evaluated using equations (3.1), (3.2) and (3.3) respectively. The highest inhibition efficiency of 88.88% were obtained with Al in NaOH using *Aspilia africana* leaf and 89.38% from mild steel in KOH using *Newbouldia leavis*Figures 4. 1 – 4.8.The same figures present the result of the effects of concentration of the inhibitors on the reaction number (RN) and the inhibition efficiency (IE) for the metals in the alkaline and acid media for all the plant extracts. The value of the reaction number was evaluated as a function of the ratio of change in temperature to the maximum time attained (equations 3.4a and 3.4b). The mild steel did not corrode in the alkaline media at a temperature of 30°C. For each of the media (NaOH, KOH, HCl and H_2SO_4), reaction number was evaluated in the absence and presence of various concentrations of the plant extracts. The concentration of the plant extracts (inhibitors) ranged from 0.2 to 1.0 g/l. Increase in concentration of the inhibitor lowers the reaction number. This is in agreement with the observation made by Mabrouk,*et al,* (2011). The inhibition efficiency of each of the plant extracts (*Aspilia africana* leaf, Chromolena odorota, *Newbouldia leavis*,*Dennettia tripetala*, *Dialium guineense*and *Vitex doniana*) for the metals (aluminium and mild steel) in the alkaline and acid media were obtained as function of reaction number (in the absence and presence of the plant extracts). Increase in concentration increases the inhibition efficiency of the plant extracts. It shows that inhibition efficiency is inversely related to the reaction number in terms of their relationship to the concentration of the plant extract.

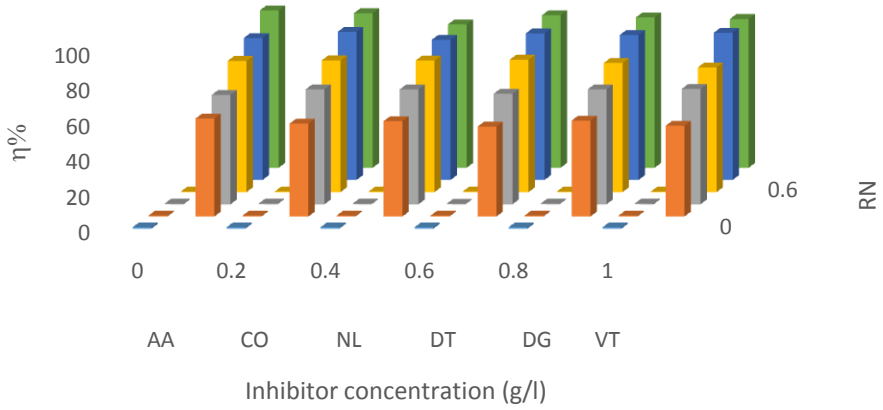

Fig 4.1: Effect of concentration of the extracts on the IE (%) and RN of Al in NaOH at 303K

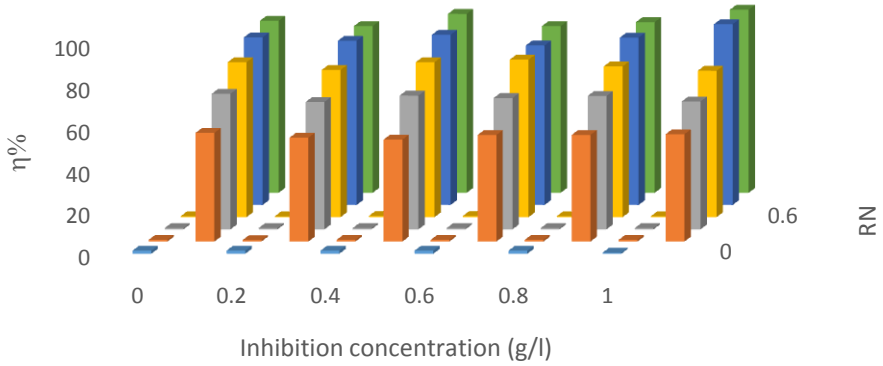

Fig 4.2: Effect of concentration of the extracts on the IE (%) and RN of Al in KOH at 303K

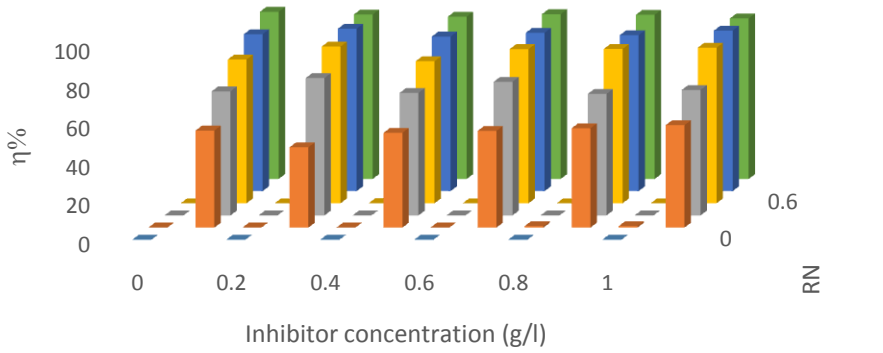

Fig 4.3: Effect of concentration of the extracts on the IE (%) and RN of Al in HCL at 303K

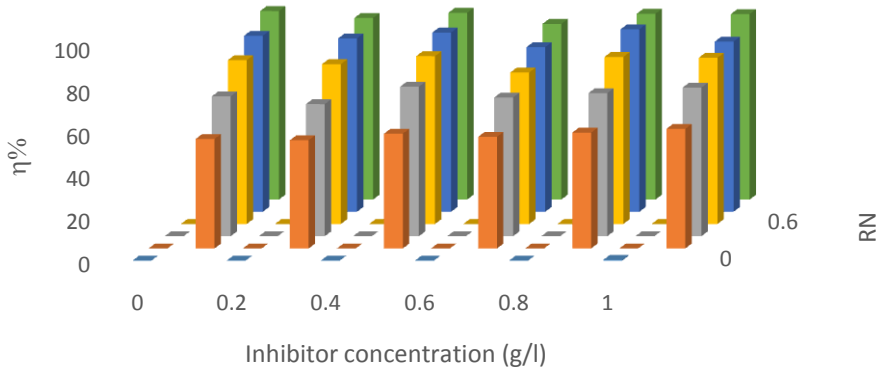

Fig 4.4: Effect of concentration of the extracts on the IE (%) and RN of Al in H_2SO_4 at 303K

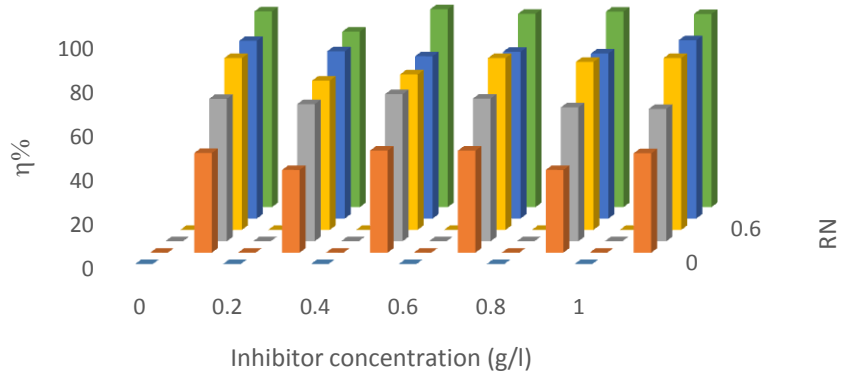

Fig 4.5: Effect of concentration of the extracts on the IE (%) and RN of mild steel in NaOH at 303K

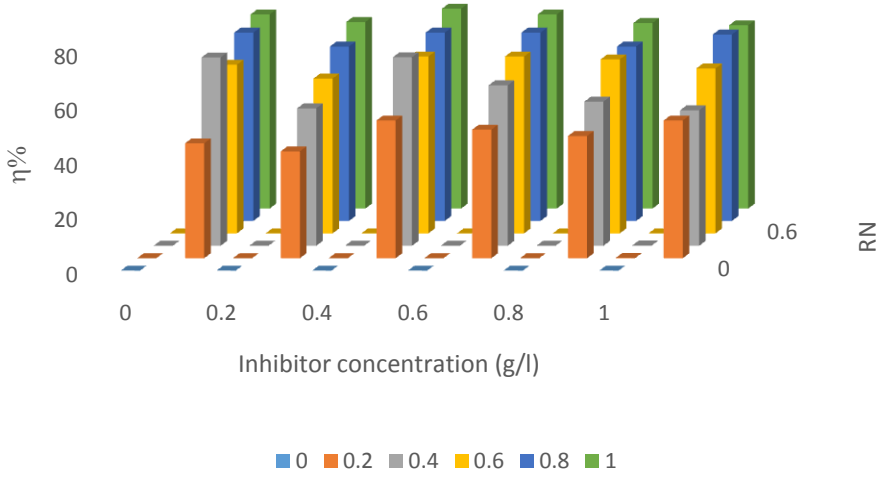

Fig 4.6: Effect of concentration of the extracts on the IE (%) and RN of mild steel in KOH at 303K

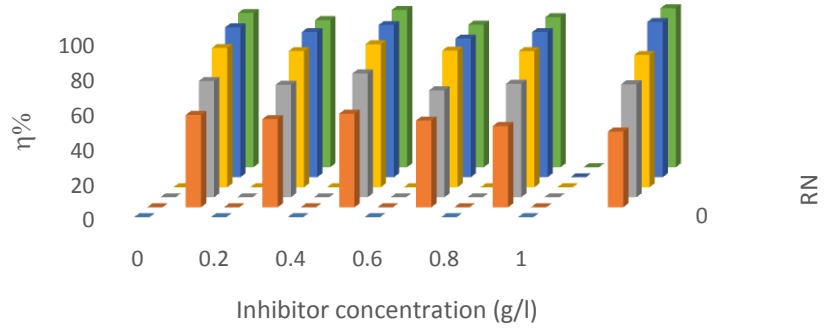

Fig 4.7: Effects of concentration of the extracts on the IE (%) and RN of mild steel in HCL at 303K

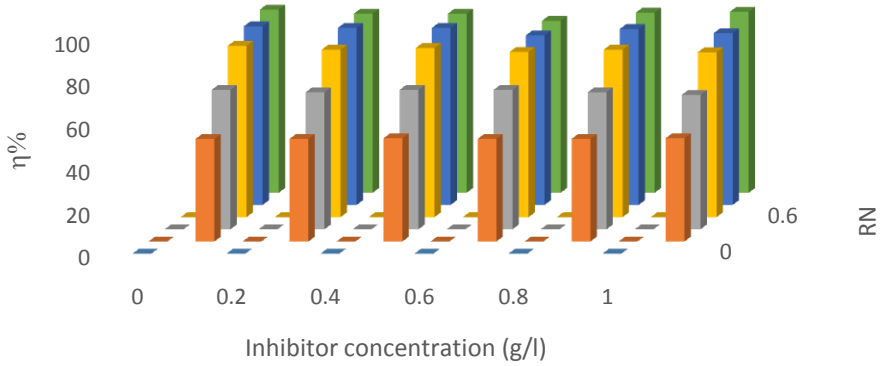

Fig 4.8: Effects of concentration of the extracts on the IE (%) and RN of mild steel in H_2SO_4 at 303K

4.3.2 The inhibition efficiency (IE) and degree of surface coverage (θ) of the metals in the alkaline and acid media with plant extract.

The inhibition efficiency and degree of surface coverage of the metals in the alkaline and acid media with plant extracts are presented in Tables 4.15 – 4.22. In all cases, the inhibition efficiency increases with increase in concentration of the plant extract. The inhibition efficiency however, decreaseswith increase in temperature in all the cases studied. These observations are in agreement with previous studies (El Ouariachi *et al.,* 2010;Ndibe *et al.,* 2011; Abdulwahab *et al.,* 2012). Similar trend was noticed in the relationship between the degree of surface coverage and the concentration of the plant extract. The degree of surface coverage is useful for further analyses of the experimental data using adsorption isotherms (Languirm, Frumkin, Temkin and Flory-Huggins isotherms).

For the corrosion inhibition of Al in NaOH, the inhibition efficiency is in the order of *Newbouldia leavis* (83.74%) >*Aspilia africana* (83.40%) >*Vitex doniana* (80.45%) >*Dialium*

guineense (80.23%) >*Chromolena odorata* (79.74%)>*Dennettia tripetala* (78.91%). In the corrosion inhibition of Al in KOH, HCl and H_2SO_4, *Newbouldia leavis*extract has the highest inhibition efficiency of 85.75%,*Vitex doniana* 85.94% and *Chromolena odorata* 83.68% respectively. For the mild steel in HCl media, inhibition efficiency of *Newbouldia leavis*, (87.55%) >*Vitex doniana*,(80.44%) >*Dialium guineense* (80.29%) respectively were achieved by various plant extracts. Plant inhibitors of this high inhibition efficiency can be employed as inhibition additives in drilling fluids fomulation, oil well acidizing, pipeline pigging and other metallic maintenance operations.

Table 4.15: The inhibition efficiency (IE) and degree of coverage (θ) of Al in NaOH with plant extracts.

At temperature of 303 K; metal area of 5cm*3cm; immersion time of 8.5hr, NaOH												
Inhibitor conc. (g/l)	*Aspilia africana* leaves extract		*Chromolena odorata* leaves extract		*Newbouldia leavis* leaves extract		*Dennettia tripetala* leaves extract		*Dialium guineense* leaves extract		*Vitex doniana* leaves extract	
	IE (%)	θ	IE (%)	θ	IE (%)	θ	IE (%)	θ	IE (%)	θ	IE (%)	θ
0.2	55.02	0.5002	45.27	0.4527	55.16	0.5516	45.27	0.4527	48.45	0.4845	49.20	0.4920
0.4	65.38	0.6538	65.38	0.6538	66.12	0.6612	65.47	0.6547	65.38	0.6538	66.38	0.6638
0.6	69.43	0.6943	69.43	0.6943	80.07	0.8007	69.28	0.6928	69.25	0.6925	69.25	0.6925
0.8	80.07	0.8007	79.40	0.7940	80.23	0.8023	76.74	0.7674	76.74	0.7674	77.32	0.7723
1.0	83.40	0.8340	79.74	0.7974	83.74	0.8374	78.91	0.7891	80.23	0.8023	80.45	0.8045
At temperature of 323 K; metal area of 5cm*3cm; immersion time of 8.5hr												
	IE (%)	θ	IE (%)	θ	IE (%)	θ	IE (%)	θ	IE (%)	θ	IE (%)	θ
0.2	45.23	0.4524	44.26	0.4426	45.40	0.4540	44.17	0.4417	44.45	0.4445	45.21	0.4521
0.4	59.65	0.5965	59.34	0.5934	59.18	0.5918	59.34	0.5934	59.18	0.5918	60.72	60.72
0.6	63.13	0.6313	62.66	0.6266	64.26	0.6426	62.66	0.6266	63.13	0.6313	61.42	0.6142
0.8	64.29	0.6429	64.62	0.6462	65.21	0.6521	64.62	0.6462	64.55	0.6455	65.21	0.6521
1.0	68.12	0.6812	64.55	0.6455	68.89	0.6689	64.15	0.6415	65.09	0.6509	66.65	0.6665
At temperature of 343 K; metal area of 5cm*3cm; immersion time of 8.5 hr												
	IE (%)	θ	IE (%)	θ	IE (%)	θ	IE (%)	θ	IE (%)	θ	IE (%)	θ
0.2	43.03	0.4303	42.65	0.4265	45.21	0.4521	44.65	0.4465	45.12	0.4512	45.34	0.4534
0.4	55.02	0.5502	54.74	0.5474	55.21	0.5521	54.74	0.5474	56.74	0.5674	57.53	0.5753
0.6	57.33	0.5733	57.61	0.5761	58.24	0.5824	57.61	0.5761	58.24	0.5824	58.67	0.5867
0.8	61.39	0.6139	61.05	0.6105	61.39	0.6139	61.36	0.6136	61.78	0.6178	62.21	0.6221
1.0	62.11	0.6211	61.47	0.6147	62.26	0.6226	61.60	0.6160	61.39	0.6139	62.26	0.6226

Table 4.16: The inhibition efficiency (IE) and degree of surface coverage (θ) of Al in KOH with plant extracts.

At temperature of 303 K; metal area of 5cm*3cm; immersion time of 8.5 hr, KOH												
Inhibitor conc. (g/l)	*Aspilia africana* leaves extract IE (%)	θ	*Chromolena odorata* leaves extract IE (%)	θ	*Newbouldia leavis* leaves extract IE (%)	θ	*Dennettia tripetala* leaves extract IE (%)	θ	*Dialium guineense* leaves extract IE (%)	θ	*Vitex doniana* leaves extract IE (%)	θ
0.2	43.25	0.4325	43.25	0.4325	43.42	0.4342	43.40	0.4340	42.13	0.421	43.14	0.4314
0.4	55.71	0.5571	54.12	0.5412	55.24	0.5524	55.24	0.5524	55.31	0.553	55.43	0.5543
0.6	73.10	0.7310	70.62	0.7062	70.34	0.7034	73.10	0.7310	73.10	0.731	72.15	0.7215
0.8	75.63	0.7563	75.75	0.7575	75.41	0.7541	75.75	0.7575	75.29	0.752	75.82	0.7582
1.0	79.40	0.7940	76.53	0.7653	85.75	0.8575	79.18	0.7918	78.64	0.786	80.43	0.8043
At temperature of 323 K; metal area of 5cm*3cm; immersion time of 8.5hr												
	IE (%)	θ	IE (%)	θ	IE (%)	θ	IE (%)	θ	IE (%)	θ	IE (%)	θ
0.2	40.62	0.4062	40.62	0.4062	40.81	0.4081	41.21	0.4121	40.41	0.404	41.84	0.4184
0.4	50.10	0.5010	50.17	0.5017	50.93	0.5093	50.11	0.5011	50.12	0.501	50.96	0.5096
0.6	67.30	0.6730	67.02	0.6702	67.30	0.6730	67.06	0.6706	67.06	0.670	67.88	0.6788
0.8	69.52	0.6952	68.61	0.6861	70.17	0.7017	68.67	0.6867	68.86	0.688	69.87	0.6987
1.0	70.34	0.7034	67.54	0.6754	70.34	0.7034	67.80	0.6780	68.64	0.686	68.89	0.6889
At temperature of 343 K; metal area of 5cm*3cm; immersion time of 8.5hr												
	IE (%)	θ	IE (%)	θ	IE (%)	θ	IE (%)	θ	IE (%)	θ	IE (%)	θ
0.2	41.03	0.4103	41.03	0.4103	42.21	0.4221	41.34	0.4134	41.34	0.413	42.31	0.4231
0.4	50.32	0.5032	50.40	0.5040	50.45	0.5045	50.45	0.5045	50.54	0.505	50.55	0.5055
0.6	62.57	0.6257	62.23	0.6223	62.42	0.6242	62.42	0.6242	63.03	0.630	63.48	0.6348
0.8	63.54	0.6354	63.82	0.6382	63.63	0.6363	63.51	0.6351	63.60	0.636	63.86	63.86
1.0	65.81	0.6581	65.54	0.6554	66.40	0.6640	65.44	0.6544	65.43	0.654	65.16	0.6516

Table 4.17: The inhibition efficiency (IE) and degree of surface coverage (θ) of Al in HCl with plant extracts.

Inhibitor conc. (g/l)	*Aspilia africana* leaves extract		*Chromolena odorata* leaves extract		*Newbouldia leavis* leaves extract		*Dennettia tripetala* leaves extract		*Dialium guineense* leaves extract		*Vitex doniana* leaves extract	
	IE (%)	θ	IE (%)	θ	IE (%)	θ	IE (%)	θ	IE (%)	θ	IE (%)	θ
0.2	45.60	0.4560	45.03	0.4503	45.64	0.4564	45.32	0.4532	45.32	0.4532	45.78	0.4578
0.4	68.15	0.6815	68.15	0.6815	68.53	0.6853	68.15	0.6815	68.15	0.6815	68.15	0.6815
0.6	80.69	0.8069	80.51	0.8051	80.69	0.8069	80.69	0.8051	80.73	0.8073	80.74	0.8074
0.8	82.57	0.8257	81.75	0.8175	82.75	0.8275	81.74	0.8174	82.23	0.8223	82.87	0.8287
1.0	84.32	0.8432	84.51	0.8451	84.61	0.8461	85.62	0.8562	85.87	0.8587	85.94	0.8594
	At temperature of 323 K; metal area of 5cm*3cm; immersion time of 8.5hr, HCl											
	IE (%)	θ	IE (%)	θ	IE (%)	θ	IE (%)	θ	IE (%)	θ	IE (%)	θ
0.2	43.38	0.4338	43.60	0.4360	43.82	0.4382	43.38	0.4338	43.38	0.4338	44.52	0.4352
0.4	66.45	0.6645	66.45	0.6645	66.74	0.6674	66.74	0.6674	66.80	0.6680	66.99	0.6699
0.6	72.58	0.7258	72.54	0.7254	72.45	0.7245	72.37	0.7237	72.44	0.7244	72.44	0.7244
0.8	76.26	0.7626	75.68	0.7568	75.68	0.7568	75.68	0.7568	75.23	0.7623	76.19	0.7619
1.0	77.41	0.7741	76.48	0.7648	77.64	0.7764	77.41	0.7741	76.61	0.7661	77.45	0.7745
	At temperature of 343 K; metal area of 5cm*3cm; immersion time of 8.5hr, HCl											
	IE (%)	θ	IE (%)	θ	IE (%)	θ	IE (%)	θ	IE (%)	θ	IE (%)	θ
0.2	39.11	0.3911	38.75	0.3875	39.11	0.3911	39.11	0.3911	40.00	0.4000	40.02	0.4002
0.4	55.80	0.5580	55.80	0.5580	55.80	0.5580	55.80	0.5580	55.84	0.5584	55.84	0.5584
0.6	61.42	0.6142	60.51	0.6051	61.42	0.6142	60.08	0.6008	60.14	0.6014	60.23	0.6023
0.8	62.71	0.6271	61.38	0.6138	62.52	0.6252	61.86	0.6186	62.71	0.6271	62.71	0.6271
1.0	62.83	0.6283	61.86	0.6186	62.86	0.6286	62.71	0.6271	62.36	0.6236	62.38	62.38

Table 4.18: The inhibition efficiency (IE) and degree of surface coverage (θ) of Al in H_2SO_4 with plant extracts.

Inhibitor conc. (g/l)s	*Aspilia africana* leaves extract		*Chromolena odorata* leaves extract		*Newbouldia leavis* leaves extract		*Dennettia tripetala* leaves extract		*Dialium guineense* leaves extract		*Vitex doniana* leaves extract	
	IE (%)	θ	IE (%)	θ	IE (%)	θ	IE (%)	θ	IE (%)	θ	IE (%)	θ
0.2	49.12	0.4912	49.54	0.4954	48.95	0.4895	49.40	0.4940	49.68	0.4968	49.68	0.4968
0.4	65.76	0.6576	55.45	0.5545	65.76	0.6576	55.45	0.5545	55.45	0.5545	56.43	0.5643
0.6	77.41	0.7741	77.42	0.7742	76.10	0.7610	76.10	0.7610	77.04	0.7704	77.28	0.7728
0.8	83.16	0.8316	83.16	0.316	82.31	0.8231	83.25	0.8325	83.33	0.8333	83.33	0.8333
1.0	83.01	0.8301	83.68	0.8368	83.68	0.8368	82.52	0.8252	82.37	0.8237	83.34	0.8334
	At temperature of 323 K; metal area of 5cm*3cm; immersion time of 8.5hr, H_2SO_4											
	IE (%)	θ	IE (%)	θ	IE (%)	θ	IE (%)	θ	IE (%)	θ	IE (%)	θ
0.2	44.81	0.4481	44.81	0.4481	44.63	0.4463	44.57	0.4457	44.00	0.4400	44.25	0.4425
0.4	56.12	0.5612	56.48	0.5648	56.31	0.5631	56.50	0.5650	55.20	0.5520	55.25	0.5525
0.6	62.54	0.6254	62.54	0.6254	62.54	0.6254	62.66	0.6266	62.66	0.6266	62.72	0.6272
0.8	67.82	0.6782	67.82	0.6782	72.87	0.7287	67.82	0.6782	67.84	0.6784	63.51	0.6351
1.0	72.82	0.7282	72.82	0.7282	79.40	0.7940	72.82	0.7844	72.60	0.7260	72.81	0.7281
	At temperature of 343 K; metal area of 5cm*3cm; immersion time of 8.5hr, H_2SO_4											
	IE (%)	θ	IE (%)	θ	IE (%)	θ	IE (%)	θ	IE (%)	θ	IE (%)	θ
0.2	43.26	0.4326	43.26	0.4326	43.37	0.4337	43.37	0.4337	42.06	0.4206	43.70	43.70
0.4	48.56	0.4856	48.56	0.4856	48.56	0.4856	48.56	0.4856	48.56	0.4856	48.45	0.4856
0.6	54.92	0.5492	54.92	0.5492	54.92	0.5492	54.92	0.5492	54.92	0.5492	53.99	0.5399
0.8	64.50	0.6450	59.47	0.5947	64.50	0.6450	59.47	0.5947	59.47	0.5947	59.43	0.5943
1.0	67.89	0.6789	64.50	0.6450	67.89	0.6789	64.50	0.6450	64.50	0.6450	64.65	0.6450

Table 4.19: The inhibition efficiency (IE) and degree of surface coverage (θ) of mild steel in NaOH with plant extracts.

At temperature of 303K; mild steel area of 5cm*3cm; immersion time of 8.5hr, NaOH												
Inhibitor conc. (g/l)	*Aspilia africana* leaves extract IE (%)	θ	*Chromolena odorata* leaves extract IE (%)	θ	*Newbouldia leavis* leaves extract IE (%)	θ	*Dennettia tripetala* leaves extract IE (%)	θ	*Dialium guineense* leaves extract IE (%)	θ	*Vitex doniana* leaves extract IE (%)	θ
0.2	41.20	0.4120	36.90	0.3690	41.20	0.4120	41.10	0.4110	36.90	0.3690	40.89	0.4089
0.4	55.49	0.5549	55.49	0.5549	55.53	0.5553	47.81	0.4781	55.59	0.5559	55.75	0.5575
0.6	61.44	0.6144	61.44	0.6144	61.44	0.6144	61.31	0.6131	61.54	0.6154	61.56	0.6156
0.8	67.28	0.6728	67.28	0.6728	67.41	0.6741	67.45	0.6745	67.69	0.6769	67.83	0.6783
1.0	75.37	0.7537	67.73	0.6773	75.22	0.7522	75.19	0.7519	75.91	0.7591	75.90	0.7590
At temperature of 323 K; mild steel area of 5cm*3cm; immersion time of 8.5hr, NaOH												
	IE (%)	θ	IE (%)	θ	IE (%)	θ	IE (%)	θ	IE (%)	θ	IE (%)	θ
0.2	37.42	0.3742	32.22	0.3222	37.42	0.3742	37.43	0.3743	32.22	0.3222	32.17	0.3217
0.4	44.13	0.4413	44.13	0.4413	44.45	0.4445	45.18	0.4518	38.42	0.3842	38.42	0.3842
0.6	51.19	0.5119	51.19	0.5119	51.25	0.5125	51.25	0.5125	51.19	0.5119	51.19	0.5119
0.8	57.06	0.5706	57.10	0.5710	57.10	0.5710	57.10	0.5710	57.10	0.5710	57.11	0.5711
1.0	63.48	0.6348	57.10	0.5710	63.48	0.6348	57.10	0.5710	57.10	0.5710	57.11	0.5711
At temperature of 343 K; metal area of 5cm*3cm; immersion time of 8.5hr, NaOH												
	IE (%)	θ	IE (%)	θ	IE (%)	θ	IE (%)	θ	IE (%)	θ	IE (%)	Θ
0.2	25.86	0.2586	25.86	0.2586	25.86	0.2586	22.23	0.2223	25.86	0.2586	25.86	0.2586
0.4	40.55	0.4055	35.55	0.3555	40.55	0.4055	40.55	0.4055	31.56	0.3156	31.56	0.3156
0.6	45.30	0.4530	40.55	0.4055	45.33	0.4533	45.60	0.4560	40.55	0.4055	42.19	0.4219
0.8	53.74	0.5374	45.30	0.4530	53.74	0.5374	53.74	0.5374	45.30	0.4530	45.30	0.4530
1.0	53.74	0.5374	53.74	0.5374	53.74	0.5374	53.74	0.5374	45.30	0.4530	45.30	0.4530

Table 4.20: The inhibition efficiency (IE) and degree of surface coverage (θ) of mild steel in KOH with plant extracts.

At temperature of 303 K; mild steel area of 5cm*3cm; immersion time of 8.5hr, KOH												
Inhibitor conc. (g/l)	*Aspilia africana* leaves extract		*Chromolena odorata* leaves extract		*Newbouldia leavis* leaves extract		*Dennettia tripetala* leaves extract		*Dialium guineense* leaves extract		*Vitex doniana* leaves extract	
	IE (%)	θ	IE (%)	θ	IE (%)	θ	IE (%)	θ	IE (%)	θ	IE (%)	θ
0.2	41.52	0.4152	33.28	0.3328	41.25	0.4125	33.28	0.3338	33.28	0.3328	33.17	0.3317
0.4	47.11	0.4711	41.52	0.4152	47.11	0.4711	41.52	0.4152	41.52	0.4152	41.53	0.4253
0.6	54.74	0.5474	47.11	0.4711	54.74	0.5474	47.11	0.4711	47.12	0.4712	49.23	0.4923
0.8	60.43	0.6043	54.74	0.5474	60.43	0.6043	54.74	0.5474	54.74	0.5474	54. 76	0.5476
1.0	60.43	0.6043	60.43	0.6043	65.86	0.6586	60.43	0.6043	60.26	0.6026	65.86	0.6586
At temperature of 323 K; mild steel area of 5cm*3cm; immersion time of 8.5hr, KOH												
	IE (%)	θ	IE (%)	θ	IE (%)	θ	IE (%)	θ	IE (%)	θ	IE (%)	θ
0.2	34.62	0.3462	29.40	0.2940	34.62	0.3462	34.62	0.3462	29.40	0.2940	31.20	0.3120
0.4	40.38	0.4038	40.38	0.4038	40.38	0.4038	40.38	0.4038	40.38	0.4038	41.34	0.4134
0.6	45.83	0.4583	45.83	0.4583	45.83	0.4583	45.83	0.4583	45.83	0.4583	45.83	0.4583
0.8	50.46	0.5046	50.46	0.5046	56.98	0.5698	52.46	0.5046	50.46	0.5046	50.46	0.5046
1.0	56.98	0.5698	50.46	0.5046	62.51	0.6251	50.46	0.5046	50.46	0.5046	52.14	0.5214
At temperature of 343 K; metal area of 5cm*3cm; immersion time of 8.5hr, KOH												
	IE (%)	θ	IE (%)	θ	IE (%)	θ	IE (%)	θ	IE (%)	θ	IE (%)	θ
0.2	20.13	0.2013	20.13	0.2013	23.55	0.2355	20.13	0.2013	20.13	0.2013	23.14	23.14
0.4	36.75	0.3675	31.34	0.3134	36.75	0.3675	36.75	0.3675	31.34	0.3134	31.34	0.3134
0.6	42.39	0.4239	34.80	0.3480	42.39	0.4239	42.39	0.4239	34.80	0.3480	34.80	0.3480
0.8	49.44	0.4944	36.75	0.3675	49.44	0.4944	49.44	0.4944	36.75	0.3875	36.75	0.3875
1.0	49.44	0.4944	45.83	0.4583	56.98	0.5698	49.44	0.4944	42.39	0.4239	42.39	0.4239

Table 4.21: The inhibition efficiency (IE) and degree of surface coverage (θ) of mild steel in HCl with plant extracts

At temperature of 303 K; mild steel area of 5cm*3cm; immersion time of 8.5hr, HCl												
Inhibitor conc. (g/l)	*Aspilia africana* leaves extract IE (%)	θ	*Chromolena odorata* leaves extract IE (%)	θ	*Newbouldia leavis* leaves extract IE (%)	θ	*Dennettia tripetala* leaves extract IE (%)	θ	*Dialium guineense* leaves extract IE (%)	θ	*Vitex doniana* leaves extract IE (%)	θ
0.2	46.56	0.4656	41.62	0.4162	53.22	0.5322	41.62	0.4162	41.62	0.4162	39.62	0.3962
0.4	57.84	0.5784	50.40	0.5040	67.69	0.6769	56.20	0.5620	58.39	0.5839	53..34	0.5334
0.6	69.32	0.6632	61.24	0.6124	70.12	0.7012	63.91	0.6391	53.91	0.6391	63.75	0.6375
0.8	75.41	0.7541	73.55	0.7355	77.18	0.7718	77.18	0.7718	78.10	0.7810	77.45	0.7745
1.0	79.28	0.7928	77.91	0.7791	87.55	0.8755	78.10	0.7810	80.29	0.8029	80.44	0.8044
At temperature of 323 K; mild steel area of 5cm*3cm; immersion time of 8.5hr, HCl												
	IE (%)	θ	IE (%)	θ	IE (%)	θ	IE (%)	θ	IE (%)	θ	IE (%)	θ
0.2	42.91	0.4291	39.16	0.3916	46.15	0.4615	41.96	0.4196	41.96	0.4196	41.43	0.4334
0.4	57.68	0.5768	53.10	0.5310	57.68	0.5768	53.10	0.5310	57.68	0.5768	57.68	0.5768
0.6	69.28	0.6928	64.31	0.6431	69.28	0.6928	66.13	0.6613	69.28	0.6928	65.18	0.6518
0.8	74.51	0.7451	66.13	0.6613	74.51	0.7451	69.22	0.6922	69.93	0.6993	69.90	0.6889
1.0	78.54	0.7854	69.22	0.6922	75.86	0.7586	69.90	0.6990	74.51	0.7451	69.90	0.6990
At temperature of 343 K; metal area of 5cm*3cm; immersion time of 8.5hr, HCl												
	IE (%)	θ	IE (%)	θ	IE (%)	θ	IE (%)	θ	IE (%)	θ	IE (%)	θ
0.2	35.00	0.3500	35.00	0.3500	40.00	0.4000	35.00	0.3500	35.00	0.3500	35.21	0.3521
0.4	53.50	0.5350	50.00	0.5000	53.50	0.5350	50.00	0.5000	53.50	0.5350	53.50	0.5350
0.6	60.00	0.6000	55.00	0.5500	60.00	0.6000	55.00	0.5500	60.00	0.6000	60.00	0.6000
0.8	65.00	0.6500	56.50	0.5650	65.00	0.6500	60.00	0.6000	61.50	0.6150	61.50	0.6150
1.0	66.50	0.6650	60.00	0.6000	68.50	0.6850	61.50	0.6150	65.00	0.6500	65.00	0.6500

Table 4.22: The inhibition efficiency (IE) and degree of surface coverage (θ) of mild steel in H_2SO_4 with plant extracts.

Inhibitor conc. (g/l)	*Aspilia africana* leaves extract		*Chromolena odorata* leaves extract		*Newbouldia leavis* leaves extract		*Dennettia tripetala* leaves extract		*Dialium guineense* leaves extract		*Vitex doniana* leaves extract	
	IE (%)	θ	IE (%)	θ	IE (%)	θ	IE (%)	θ	IE (%)	θ	IE (%)	θ
At temperature of 303 K; mild steel area of 5cm*3cm; immersion time of 8.5hr, H_2SO_4												
0.2	46.54	0.4654	46.54	0.4654	46.54	0.4654	46.54	0.4654	46.54	0.4654	46.56	0.4656
0.4	60.45	0.6045	57.92	0.5792	59.23	0.5923	58.46	0.5846	59.00	0.5900	58.45	0.5845
0.6	71.54	0.7154	71.54	0.7154	71.54	0.7154	71.54	0.7154	71.54	0.7154	72.34	0.7234
0.8	76.15	0.7615	74.62	0.7462	76.92	0.7692	74.62	0.7462	75.38	0.7538	76.42	0.7642
1.0	76.92	0.7692	74.85	0.7485	77.69	0.7769	75.38	0.7538	76.15	0.7615	78.05	0.7805
At temperature of 323K; mild steel area of 5cm*3cm; immersion time of 8.5hr, H_2SO_4												
	IE (%)	θ	IE (%)	θ	IE (%)	θ	IE (%)	θ	IE (%)	θ	IE (%)	θ
0.2	42.75	0.4275	42.75	0.4275	42.75	0.4275	42.75	0.4275	42.75	0.4275	43.23	0.4325
0.4	57.25	0.5725	55.80	0.5580	57.25	0.5725	56.52	0.5652	56.74	0.5674	58.25	0.5825
0.6	68.84	0.6884	68.84	0.6884	68.84	0.6884	68.84	0.6884	68.84	0.6884	70.56	0.7056
0.8	71.01	0.7101	69.57	0.6957	71.01	0.7101	70.29	0.7029	71.01	0.7101	72.81	0.7281
1.0	72.46	0.7246	70.29	0.7029	72.68	0.7268	71.01	0.7101	71.74	0.7174	72.88	0.7288
At temperature of 343 K; metal area of 5cm*3cm; immersion time of 8.5 hr, H_2SO_4												
	IE (%)	θ	IE (%)	θ	IE (%)	θ	IE (%)	θ	IE (%)	θ	IE (%)	θ
0.2	37.76	0.3776	37.76	0.3776	37.76	0.3776	37.76	0.3776	37.76	0.3776	40.47	0.4047
0.4	47.55	0.4755	47.55	0.4755	47.55	0.4755	47.55	0.4755	47.55	0.4755	48.75	0.4875
0.6	65.03	0.6503	63.85	0.6385	65.03	0.6503	64.34	0.6434	64.34	0.6434	66.69	0.6669
0.8	65.24	0.6524	64.34	0.6434	65.24	0.6524	64.55	0.6455	64.55	0.6455	66.80	0.6680
1.0	66.43	0.6643	64.55	0.6455	66.64	0.6664	64.83	0.6483	65.03	0.6503	69.72	0.6972

4.4 Thermodynamics and Adsorption Isotherms

4.4.1. Thermodynamic quantities considered

4.4.1.1 Heat of adsorption for the corrosion inhibition

Heat of adsorption values for the corrosion inhibition of some metals (aluminium and mild steel) in acid and alkaline media (NaOH, KOH, HCl and H_2SO_4),are presented in Tables 4.23 and 4.24. Heat of adsorption as an important thermodynamic parameter, has a direct relationship with the degree of surface coverage. For the corrosion inhibition of these metals an increase in concentration of plant extract increases the negative values of the heat of adsorption. In each of the cases, heat of adsorption is negative indicating that the adsorption of the extract on the metal surface is exothermic (Nwabanne and Okafor, 2011).

Table 4.23: The heat of adsorption for the corrosion inhibition of Al in the alkaline and acid media by various concentrations of plant extracts.

Media	Conc. of the plant extract (g/l)	Heat of adsorption, Q_{ads} (kJ/mol)					
		Aspilia africana leaves extract	*Chromolena odorata* leaves extract	*Newbouldia leavis* leaves extract	*Dennettia tripetala* leaves extract	*Dialium guineense* leaves extract	*Vitex doniana* leaves extract
KOH	0.2	-6.0803	-1.9675	-1.0678	-1.8230	-0.7019	-0.7328
	0.4	-2.2983	-3.2229	-4.1563	-4.1563	-4.1396	-4.2359
	0.6	-8.6276	-8.1599	-7.6943	-10.6362	-10.0725	-20.5666
	0.8	-0.5413	-12.3467	-12.1263	-12.6363	-12.0147	-15.346
	1.0	-2.8909	-11.6475	-24.0579	-15.0671	-14.3756	-17.0103
NaOH	0.2	-3.2150	-2.2983	-8.6276	-0.5413	-2.8909	-3.3475
	0.4	-4.6797	-9.6277	-9.9274	-9.7136	-7.8759	-8.1402
	0.6	-10.4979	-11.0948	-22.8596	-10.9423	-10.3534	-9.9708
	0.8	-12.4674	-19.4405	-20.2443	-15.7984	-15.4148	-15.6181
	1.0	-15.0022	-19.5100	-24.5960	-32.6531	-20.2443	-19.7488
HCL	0.2	-5.7521	-5.5823	-5.7869	-5.5081	-4.7038	-5.0865
	0.4	-11.3996	-11.3996	-11.7791	-11.3996	-11.3646	-11.3646
	0.6	-20.8491	-21.4266	-20.8491	-21.8147	-22.0648	-21.9976
	0.8	-22.3759	-22.3874	-22.8226	-21.9344	-21.8694	-22.8294
	1.0	-25.0041	-26.2089	-25.4539	-27.3155	-28.0802	-5.0865
H_2S0_4	0.2	-5.0999	-5.4629	-4.8561	-5.2451	-6.6439	-5.8761
	0.4	-15.3450	-5.9736	-15.345	-5.9736	-5.9736	-6.8327
	0.6	-22.3438	-22.3561	-20.7571	-20.7571	-21.8893	-22.9937
	0.8	-21.6029	24.9683	-20.3170	-26.3592	-26.4834	-26.5192
	1.0	-18.0971	-22.4152	-19.1401	-20.6301	-20.4061	-21.8818

Table 4.24: The heat of adsorption for the corrosion inhibition of mild steel in the alkaline and acid media by various concentrations of plant extracts.

Media	Conc. of the plant extract (g/l)	Heat of adsorption, Q_{ads} (kJ/mol)					
		Aspilia africana leaves extract	*Chromolena odorata* leaves extract	*Newbouldia leavis* leaves extract	*Dennettia tripetala* leaves extract	*Dialium guineense* leaves extract	*Vitex doniana* leaves extract
KOH	0.2	-15.0710	-14.7488	-17.8002	-14.7488	-10.8493	-10.8010
	0.4	-13.0301	-9.5445	-9.2304	-4.3307	-8.5258	-10.4402
	0.6	3.6112	-11.0645	-10.7370	-4.1278	-9.9526	-12.8994
	0.8	-1.5255	-15.8396	-9.6320	-4.5927	-10.2893	-14.0179
	1.0	-6.8266	-12.7603	-8.1242	-9.6320	-7.0257	-20.8244
NaOH	0.2	-7.561	-11.1646	-15.0710	-19.2825	-11.1646	-14.7942
	0.4	-9.2304	-17.6180	-13.0650	-6.3724	-21.5754	-21.7155
	0.6	-10.7370	-18.3311	-14.1126	-13.7588	-18.4224	-16.9796
	0.8	-9.6320	-19.6488	-12.4644	-12.5038	-20.0525	-20.1910
	1.0	-9.6320	-12.7799	-20.7521	-20.7174	-28.8717	-28.8598
HCL	0.2	-0.0016	-6.0635	-11.5469	-6.0635	-6.0635	-4.0725
	0.4	-0.0008	-0.3457	-12.9489	-5.3858	-4.2903	0.13892
	0.6	-0.0014	-5.5470	-9.6696	-8.0111	-3.5864	-3.4366
	0.8	-0.0029	-16.4468	-12.9517	-17.5661	-17.3519	-16.5394
	1.0	-0.0040	-18.472	-25.3572	-17.3519	-14.5542	-17.1761
H_2S0_4	0.2	-7.8023	-7.8023	-7.8023	-3.3150	-7.8023	-5.3603
	0.4	-11.2852	-9.0218	-9.5013	-1.7591	-9.9827	-8.4539
	0.6	-6.5118	-7.6245	-7.1645	-2.7894	-7.1645	-5.7728
	0.8	-11.4794	-10.5499	-10.3519	-6.6529	-11.2277	-10.2992
	1.0	-11.2626	-10.615	-10.9628	-5.8171	-11.6791	-9.3893

4.4.1.2 Thermodynamic properties

The results of the activation energy (obtained from Appendix C) for the corrosion inhibition of aluminium and mild steel in acid and alkaline media (NaOH, KOH, HCl and H_2SO_4), using different plant extracts are presented in Tables 4.25 and 4.26. The activation energy was determined from Arrhenius equation that relates corrosion rate to the absolute temperature. For the corrosion inhibition of these metals (aluminium and mild steel) in the alkaline and acid media, increase in concentration of plant extract increases the activation energy. The values of the activation energies (Tables 4.25 and 4.26) reveal that the adsorption of ethanol extracts of the plants on the metal surfaces is in line with the mechanism of physical adsorption (Nwabanne and Okafor, 2011). The values of enthalpy (ΔH) on the tables (4.25 and 4.26) were all positive signifying the strength of bond between the adsorbate and adsorbent (Khaled, 2010). More light was thrown by the tables (4.25 and 4.26) as the values of the entropy (ΔS) were all negative showing the disorderliness of the process.

Table 4.25: The activation parameters for the corrosion inhibition of Al in alkaline and acid media using different Concentrations of inhibitors

		Aspilia africana leaves extract			*Chromolena odorata* leaves extract			*Newbouldia leavis* leaves extract			*Dennettia tripetala* leaves extract			*Dialium guineense* leaves extract			*Vitex doniana* leaves extract		
Media	Inhibitor conc. (g/l)	Ea (KJ/mol)	ΔH (KJ/mol)	ΔS (J/mol/K)	Ea (KJ/mol)	ΔH (KJ/mol)	ΔS (J/mol/K)	Ea (KJ/mol)	ΔH (KJ/mol)	ΔS (J/mol/K))	Ea (KJ/mol)	ΔH (KJ/mol)	ΔS (J/mol/K)	Ea (KJ/mol)	ΔH (KJ/mol)	ΔS (J/mol/K)	Ea (KJ/mol)	ΔH (KJ/mol)	ΔS (J/mol/K)
I	0.0	4.26	2.92	-211	62.0	59.0	-40.5	63.4	58.2	-55.7	50.7	51.7	-0.05	47.8	44.6	-40.6	60.6	5.51	-62.2
	0.2	30.6	28.0	-116	67.7	64.3	-45.8	65.1	59.7	-46.0	52.4	50.5	-0.08	56.2	53.8	-39.5	63.1	59.0	-58.0
	0.4	26.9	24.2	-140	64.2	63.3	-39.0	67.5	63.2	-45.5	56.6	53.4	-0.07	54.4	51.5	-48.4	64.2	60.5	-55.7
	0.6	23.9	20.1	-159	69.2	64.4	-45.8	69.2	66.8	-40.1	56.4	54.0	-0.07	50.1	48.0	-50.6	70.4	6.63	-41.1
	0.8	28.7	26.4	-125	70.0	66.5	-46.7	70.0	65.3	-45.4	59.5	55.7	-0.07	49.2	46.4	-48.7	74.4	69.2	-32.5
	1.0	26.5	24.6	-124	68.4	67.4	-45.9	67.0	66.5	-51.0	56.0	53.0	-0.06	49.6	44.5	-40.1	71.1	66.4	-31.3
II	0.0	60.6	57.5	-62.7	68.4	67.4	-45.8	62.0	59.0	-40.2	4.26	2.92	-211	50.7	51.7	-0.05	47.8	44.6	-40.6
	0.2	63.1	59.0	-58.5	67.7	64.3	-45.1	67.7	64.3	-45.8	30.6	28.0	-116	52.4	50.5	-0.08	56.2	53.8	-39.5
	0.4	64.2	60.5	-55.6	64.2	63.3	-39.0	64.2	63.3	-39.6	26.9	24.2	-140	56.6	53.4	-0.07	54.4	51.5	-48.9
	0.6	70.4	67.6	-41.8	69.2	64.4	-45.0	69.2	64.4	-45.9	23.9	20.1	-159	56.4	54.0	-0.07	50.1	48.0	-50.6
	0.8	74.4	69.2	-32.0	70.0	66.5	-46.4	70.0	66.5	-46.0	28.7	26.4	-125	59.5	55.7	-0.07	49.2	46.4	-48.7
	1.0	71.1	66.4	-31.1	68.4	67.4	-45.8	68.4	67.4	-45.9	26.5	24.6	-124	56.0	53/0	-0.06	49.6	44.5	-40.1
III	0.0	63.4	58.2	-55.6	4.26	2.92	-211	50.7	51.7	-0.05	47.8	44.6	-40.6	60.6	57.5	-62.7	62.0	59.0	-40.0
	0.2	65.1	59.7	-46.9	30.6	28.0	-116	52.4	50.5	-0.08	56.2	53.8	-39.5	63.1	59.0	-58.8	67.7	64.3	-45.2
	0.4	67.5	63.2	-45.8	26.9	24.2	-140	56.6	53.4	-0.07	54.4	51.5	-48.4	64.2	60.5	-55.0	64.2	63.3	-39.9
	0.6	69.2	66.8	-40.4	23.9	20.1	-159	56.4	54.0	-0.07	50.1	48.0	-50.6	70.4	67.6	-41.3	69.2	64.4	-45.4
	0.8	70.0	65.3	-45.9	28.7	26.4	-125	59.5	55.7	-0.07	49.2	46.8	-48.7	74.4	69.2	-32.3	70.0	66.5	-46.0
	1.0	67.0	66.5	-51.2	26.5	24.6	-124	56.0	53.0	-0.06	49.6	44.5	-40.1	71.1	66.4	-31.7	68.4	67.4	-45.1
IV	0.0	62.0	59.0	-40.0	60.6	57.5	-62.1	63.4	58.2	-55.0	4.26	2.92	-211	47.8	44.6	-40.6	50.7	51.7	-0.05
	0.2	67.7	64.3	-45.5	63.1	59.0	-58.0	65.1	59.7	-46.8	30.6	28.0	-116	56.2	53.8	-39.5	52.4	50.5	-0.08
	0.4	64.2	63.3	-39.1	64.2	60.5	-55.7	67.5	63.2	-45.0	26.9	24.2	-140	54.4	51.5	-48.4	56.6	53.4	-0.07
	0.6	69.2	64.4	-45.3	70.4	67.6	-41.1	69.2	66.8	-40.5	23.9	20.1	-159	50.1	48.0	-50.6	56.4	54.0	-0.07
	0.8	70.0	66.5	-46.4	74.4	69.2	-32.0	70.0	65.3	-45.2	28.7	26.4	-125	49.2	46.4	-48.7	59.5	55.7	-0.07
	1.0	68.4	67.4	-45.8	71.1	66.4	-31.1	67.0	66.5	-51.9	26.5	24.6	-124	49.6	44.5	-40.1	56.0	53.0	-0.06

KOH[I]; NaOH [II] HCL [III]; H_2S0_4[IV]

Table 4.26: The activation parameters for the corrosion inhibition of mild steel in alkaline and acid media using various concentrations of inhibitors.

	Inhibitor	*Aspilia africana* leaves extract			*Chromolena odorata* leaves extract			*Newbouldia leavis* leaves extract			*Dennettia tripetala* leaves extract			*Dialium guineense* leaves extract			*Vitex doniana* leaves extract		
Media	conc. (g/l)	Ea (KJ/mol)	ΔH (KJ/mol)	ΔS (J/mol/K)	Ea (KJ/mol)	ΔH (KJ/mol)	ΔS (J/mol/K)	Ea (KJ/mol)	ΔH (KJ/mol)	ΔS (J/mol/K)	Ea (KJ/mol)	ΔH (KJ/mol)	ΔS (J/mol/K)	Ea (KJ/mol)	ΔH (KJ/mol)	ΔS (J/mol/K)	Ea (KJ/mol)	ΔH (KJ/mol)	ΔS (J/mol/K)
I	0.0	63.6	56.0	-48.3	67.3	63.8	-60.3	70.5	68.3	-66.0	65.6	61.2	-59.5	67.0	62.4	-60.0	70.4	67.5	-60.2
	0.2	70.1	67.7	-65.4	69.2	66.0	-55.1	69.2	64.0	-61.1	69.2	65.6	-62.5	69.3	65.1	-63.1	70.3	60.9	-56.9
	0.4	70.2	66.9	-61.8	71.6	68.2	-60.0	106	104	-100	69.6	68.0	-65.2	69.7	70.3	-67.3	69.3	59.1	-55.1
	0.6	80.1	78.6	-75.2	78.3	75.7	-70.3	107	101	-97.5	78.3	74.9	-70.8	77.3	74.3	-70.8	75.8	70.8	-65.7
	0.8	105	100	-80.8	97.8	93.8	-88.6	110	106	-89.2	100	94.2	-90.2	89.5	85.3	-81.5	89.1	80.0	-76.0
	1.0	112	106	-90.5	104	98.4	-94.6	52.5	50.2	-48.0	113	90.5	-88.1	108	105	-102	110	101	-96.9
II	0.0	39.8	36.7	-34.1	42.5	40.1	-41.2	41.5	39.9	-38.1	49.1	47.8	-45.3	52.8	50.4	-47.9	53.1	56.6	-54.9
	0.2	51.8	49.3	-46.2	52.5	49.3	-45.8	60.0	58.5	-54.8	51.8	50.1	-49.4	51.5	48.7	-45.8	51.8	36.8	-34.8
	0.4	60.1	58.0	-55.5	60.0	57.6	-55.5	70.1	67.2	-63.9	60.0	57.6	-58.7	60.0	57.8	-54.8	61.0	45.8	-40.6
	0.6	68.0	66.1	-63.6	70.1	68.9	-66.7	72.4	69.1	-66.2	68.9	63.1	-60.4	68.9	61.9	-59.5	68.7	56.4	-53.3
	0.8	70.4	68.1	-65.5	72.4	70.0	-69.9	102	96.0	-92.0	69.6	65.9	-62.2	70.2	69.0	-67.9	70.5	58.9	-54.7
	1.0	81.8	80.0	-78.8	102	100	-101	14.3	11.3	-10.0	71.3	68.2	-63.8	72.6	68.8	-66.3	71.3	68.0	-64.5
III	0.0	14.2	11.1	-25.2	14.6	12.7	-20.1	15.0	12.3	-21.4	15.9	13.1	-10.3	15.1	12.7	-9.12	14.2	10.4	-8.76
	0.2	39.8	36.8	-31.0	54.2	50.6	-51.2	59.7	57.8	-57.3	17.8	14.3	-12.2	33.9	30.8	-31.5	14.8	11.4	-9.66
	0.4	40.1	39.0	-35.9	52.3	49.5	-50.0	70.2	69.9	-71.0	32.7	30.8	-26.5	31.4	29.7	-30.2	21.6	19.5	-17.9
	0.6	63.8	58,6	-55.5	84.1	80.5	-79.7	112	109	-110	64.5	61.0	-57.1	56.9	54.2	-51.5	42.4	40.8	-38.7
	0.8	71.6	68.8	-66.7	87.9	84.1	-79.2	128	123	-120	56.9	53.6	-48.0	60.0	56.8	-54.9	54.7	50.5	-49.3
	1.0	77.5	70.0	-68.1	90.9	85.2	-81.4	135	131	-130	60.0	58.5	-51.8	61.7	66.3	-62.1	50.7	45.9	-40.7
IV	0.0	13.6	10.9	-9.12	18.1	15.7	-14.1	10.4	10.0	-8.90	5.88	3.99	-1.23	10.9	8.88	-6.63	14.4	12.2	-10.2
	0.2	22.3	19.0	-16.3	21.8	18.5	-16.1	21.8	17.9	-14.2	13.6	11.4	-6.86	13.6	11.6	-9.09	20.5	17.2	-13.5
	0.4	19.3	16.3	-17.2	32.4	28.2	-23.3	35.7	31.6	-28.9	21.1	19.1	-15.3	22.0	20.0	-18.6	25.2	23.1	-20.5
	0.6	30.0	27.8	-25.8	34.3	30.4	-27.1	30.9	28.8	-25.3	20.6	16.2	-14.7	20.6	18.5	-15.8	26.0	23.5	-20.4
	0.8	30.2	28.0	-25.2	44.6	39.8	-36.6	51.9	48.2	-45,2	27.5	25,1	-23.7	29.5	26.3	-16.9	31.9	30.7	-26.2
	1.0	35.6	32.6	-30.6	45.1	41.1	-42.1	51.2	47.1	-44.8	29.0	24.6	-21.8	30.1	27.6	-25.5	31.2	31.2	-29.1

4.4.2Adsorption isotherms

Adsorption isotherms are important in understanding the mechanism of corrosion inhibition reactions. In the light of this, four adsorption isotherms namely Flory-Huggins, Frumkin, Langmuir and Temkin were studied and used in modelling the equilibrium data because of their simplicity and easy of linearization. In order to gain more insight in the adsorption process, the goodness-of-fit of the experimental data to the proposed models, the correlation coefficient (R^2), intercept, and slope were calculated using Trendline function in Microsoft Excel software. In addition to these, equilibrium constant (K_{ads}), and free energy of adsorption (ΔG_{ads}), for the adsorption process were evaluated for the four isotherms considered and presented on Tables 27-74 below. It was observed that in all isotherms studied, Temkin isotherm had $R^2 = 1.00$ at 303K and $R^2 \geq 0.99$ at 343K on Tables 4.30, 4.34, 4.38 and 4.42 whereas Flory-Huggins, Frumkin and Langmuir isotherms had $R^2 \geq 0.99$ at 303K and 343K respectively. It can be seen from all the isotherms studied that the value of free energy of adsorption increased from -35KJ/mol on Table 4.47; at 343K (Langmuir isotherm) to -0.12 kJ/mol on Table 4.49 at 303K (Temkin) indicating that the process is exothermic and is in line with Ayssar Nahle, *et al.,* 2010. In all the cases, all the four isotherms considered in this research favours physisorption.

4.4.2.1 Fitting of experimental data into Frumkin isotherm

The plots presented on Appendix D1 – D6 agrees with Frumkin isotherm by producing a linear relationship of log ($C^*((\theta/(1-\theta))$) versus 'θ' (surface coverage of the inhibitors). The calculated values of lateral interaction parameter, 'α' were all positive as can be seen on Tables 4.27 – 4.74 agrees with Sharma, K. K, & Sharma, L. K., (1999); Eddy and Ebenso, 2008.

4.4.2.2 Fitting of experimental data into Temkin isotherm

The plot of surface coverage (θ), versus natural logarithm of concentration (log C), for the corrosion inhibition of the two metals (aluminium and mild steel) studied at varying temperatures and fitted into Temkin isotherm as shown i Appendix D7 – D10 gave a linear relationship which agrees with Ebenso, *et al.,* 2008; etal, Ayssar Nahle, 2010, et al; Khamis, *et al.,* 2013. The value of calculated molecular parameter 'a', equilibrium constant 'K_{ads}' and free energy of adsorption for the adsorption process were determined from the slope and intercept of the straight lines respectively and presented in Tables 4.27- 4.74. Again the negative values of

'a' in all the tables implies a strong repulsive forces between the adsorbed molecules; is in line with Okafor and Yugui Zheng, 2009; Okafor, *et al.*, 2008.

4.4.2.3 Fitting of experimental of Data into Flory- Huggins Isotherm

The plots shown in Appendix D11- D14 is a straight line plot of log (θ/C) against log (1-θ) for the corrosion inhibition of some metals (Aluminium and Mild steel) studied at varying temperatures which is consistent with Flory-Huggins isotherm are shown in AppendixD11- D14. The value of calculated size ratio parameter 'x', for the adsorption process were determined from the slope and intercept of the straight lines respectively and presented in Tables 4.27- 4.74. Also the calculated value of 'x' were all positive as presented in the tables implying that attraction exist between size of the molecules adsorbed on the surface of the metal is capable of retarding the aggressive solutions from eating deep into the metal. It can be observed from the tables that the value of 'x' at 303K were higher than that at 343K signifying that free energy of adsorption decrease as the temperature increase. The value of the size parameter will aid in determining whether the adsorbed extract is bulky. This is in accordance with Nwabanne and Okafor, 2011.

4.4.2.4 Fitting of experimental Data into Langumir Isotherms

The experimental data fitted in D15- D18 reveals that Log (C/θ) versus Log C gave a straight line which conforms to Lagmuir isotherm and in accordance with I.B. Obot, *et al.*, 2015; Punita Mourya, *et al.*, 2014; and M.E. Ikpi, *et al.*, 2012. In order to gain more insight into the study of the isotherms, the adsorption properties; R^2,intercept, slope and free energy of adsorption were shown on Tables 4.27 – 4.74. The R^2 >0.99 signify that the adsorption of the plant extracts obey Langmuir isotherm. Hence, Langmuir adsorption isotherm can be described as an ideal isotherm for physical and chemical adsorption where there is no interaction between the adsorbate and adsorbent as in (Eddy, N.O. and Ebenso, E.E., 2008). The isotherms employed in this work were used to determine equilibrium conditions for corrosion inhibition process. It was also deduced that the process followed Temkin isotherm model it conforms to R^2 equal unity.

4.4.2.5 Adsorption properties

The tables 4.27 – 4.74 show the adsorption parameters and free energy of adsorption for Flory – Huggins, Frumkin, Temkin and Langmuir isotherms.

Table 4.27: Adsorption properties for the corrosion inhibition of Al in KOH by *Aspilia africana* leaves extract.

Adsorption Isotherm	Temperature (K)	R^2	Log K	K_{ads} (mol2/kJ2)	Slope	ΔG_{ads} (kJ/mol)	Isotherm value	
Flory-Huggins Isotherm	303	0.9921	-0.5907	0.2566	1.0936	-6.6924	x	1.094
	343	0.9993	-0.4040	0.3945	0.4986	-8.8026		0.499
Frumkin Isotherm	303	0.9903	-1.0418	0.0908	3.6913	-4.0637	α	1.846
	343	0.9843	-1.1345	0.0734	4.3227	-3.9748		2.161
Temkin Isotherm	303	0.9996	-0.7497	0.1780	0.5374	-5.7709	a	-1.068
	343	0.9991	-1.9829	0.0104	0.3275	1.5674		-3.416
Langumir Isotherm	303	0.9991	0.0928	1.238	0.6074	-10.5982		
	343	0.9969	0.1657	1.4589	0.7006	-12.5328		

Table 4.28: Adsorption properties for the corrosion inhibition of Al in NaOH by *Aspilia africana* leaves extract.

Adsorption Isotherm	Temperature (K)	R^2	Log K	K_{ads}(mol2/kJ2)	Slope	ΔG_{ads} (kJ/mol)	Isotherm value	
Flory-Huggins Isotherm	303	0.9933	-0.5907	0.2566	1.2121	-6.692	x	1.212
	343	0.9843	-0.4395	0.3635	0.474	-8.569		0.474
Frumkin Isotherm	303	0.9937	-6.4668	2.9297	4.881	-12.828	α	2.044
	343	0.9818	-1.2946	0.0507	5.0909	-2.950		2.545
Temkin Isotherm	303	0.9992	-1.8185	0.0152	0.599	0.4285	a	-0.724
	343	0.9156	-2.3864	0.0041	0.2412	4.2245		-4.292
Langumir Isotherm	303	0.9972	0.0820	1.2078	0.6825	-10.595		
	343	0.9963	0.3345	2.1602	0.4870	-13.652		

Table 4.29: Adsorption properties for the corrosion inhibition of Al in H_2SO_4 by *Aspilia africana* leaves extract.

Adsorption Isotherm	Temperature (K)	R^2	Log K	K_{ads} (mol2/kJ2)	Slope	ΔG_{ads} (kJ/mol)	Isotherm value	
Flory-Huggins Isotherm	303	0.9996	-0.6041	0.2488	0.8412	-6.6146	x	0.841
	343	0.9972	-0.2907	0.5120	0.2787	-9.5462		0.279
Frumkin Isotherm	303	0.9895	-1.1691	0.0678	3.9703	-3.3389	α	1.985
	343	0.9738	-1.1309	0.0740	4.3469	-4.0293		2.173
Temkin Isotherm	303	0.9995	-1.7240	0.0189	0.4859	-0.1204	a	-2.370
	343	0.9954	-2.3014	0.0050	0.2697	3.6563		-4.270
Langumir Isotherm	303	0.9893	0.0553	1.1358	0.6565	-10.4405		
	343	0.9911	0.1775	1.5048	0.7117	-12.6211		

Table 4.30: Adsorption properties for the corrosion inhibition of Al in HCL by *Aspilia africana* leaves extract.

Adsorption Isotherm	Temperature (K)	R^2	Log K	K_{ads}(mol 2/kJ2)	Slope	ΔG_{ads} (kJ/mol)	Isotherm value	
Flory-Huggins Isotherm	303	0.9983	-0.8531	0.1402	1.6755	-11.4201	x	1.676
	343	0.9942	-0.4658	0.3421	0.6583	-10.2631		0.658
Frumkin Isotherm	303	0.9801	1.0926	0.0808	3.7214	-13.4307	α	1.857
	343	0.9624	-1.1446	0.0717	4.3721	-15.6633		2.186
Temkin Isotherm	303	1.000	-1.4130	0.0386	0.6417	-9.0018	a	-1.794
	343	0.9930	-3.4084	0.0004	0.3937	-8.7968		-2.925
Langumir Isotherm	303	0.9666	0.0412	1.0995	0.6102	-8.87506		
	343	0.9759	0.1715	1.4842	0.7072	-10.4675		

Table 4.31: Adsorption properties for the corrosion inhibition of Al in KOH by *Chromolena odorata* leaves extract.

Adsorption Isotherm	Temperature (K)	R^2	Log K	K_{ads} (mol2/kJ2)	Slope	ΔG_{ads} (kJ/mol)	Isotherm value	
Flory-Huggins Isotherm	303	0.9921	-0.5907	0.2566	1.0936	-6.6924	x	1.094
	343	0.9993	-0.4040	0.3945	0.4986	-8.8023		0.499
Frumkin Isotherm	303	0.9887	-1.0436	0.0904	3.7295	-4.0887	α	1.865
	343	0.9855	-1.1390	0.0726	4.3433	-3.8367		2.172
Temkin Isotherm	303	0.9996	-0.7497	0.1780	0.5374	-5.7709	a	-1.068
	343	0.9991	-1.9829	0.0104	0.3275	1.5674		-3.416
Langumir Isotherm	303	0.9848	0.0825	1.2092	0.6021	-10.5982		
	343	0.9931	0.1661	1.4589	0.7032	-12.5328		

Table 4.32: Adsorption properties for the corrosion inhibition of Al in NaOH by *Chromolena odorata* leaves extract.

Adsorption Isotherm	Temperature (K)	R^2	Log K	K_{ads} (mol2/kJ 2)	Slope	ΔG_{ads} (kJ/mol)	Isotherm value	
Flory-Huggins Isotherm	303	0.9933	-0.5907	0.2566	1.2121	-0.1836	x	1.212
	343	0.9843	-0.4395	0.3635	0.474	-0.2077		0.474
Frumkin Isotherm	303	0.9881	-5.9378	0.0011	3.8932	0.1933	α	1.947
	343	0.9818	-1.2946	0.0507	5.0909	-0.0715		2.545
Temkin Isotherm	303	0.9992	-1.8185	0.0152	0.599	0.0117	a	-0.724
	343	0.9976	0.0849	1.2159	0.8248	-0.2911		-4.292
Langumir Isotherm	303	0.9976	0.0849	1.2159	0.8248	0.2914		-
	343	0.9975	0.3261	2.1188	0.5379	0.3295		

Table 4.33: Adsorption properties for the corrosion inhibition of Al in H_2S0_4 by *Chromolena odorata* leaves extract.

Adsorption Isotherm	Temperature (K)	R^2	Log K	K_{ads}(mol2/kJ2)	Slope	ΔG_{ads} (kJ/mol)	Isotherm value	
Flory-	303	0.9998	-0.6369	0.2307	0.8829	-6.4243	x	0.883
Huggins	343	0.9971	-0.3402	0.4564	0.3473			0.347
Isotherm						-9.2183		
Frumkin	303	0.9533	-1.0662	0.0859	3.5683	-3.9351	α	1.784
Isotherm	343	0.9832	-1.2587	0.0551	4.9676	-3.1881		2.484
Temkin	303	0.9995	-1.7240	0.0189	0.4859	-0.1204	a	-2.370
Isotherm	343	0.9954	-2.3014	0.0050	0.2697	3.6563		-4.270
Langumir	303	0.9912	0.0553	1.1358	0.6565	-10.4405		
Isotherm	343	0.9975	0.2007	1.5845	0.7572	-12.7683		

Table 4.34: Adsorption properties for the corrosion inhibition of Al in HCL by *Chromolena odorata* leaves extract.

Adsorption Isotherm	Temperature (K)	R^2	Log K	K_{ads}(mol2/kJ2)	Slope	ΔG_{ads} (kJ/mol)	Isotherm value	
Flory-	303	0.9983	-0.8531	0.1402	1.6755	-5.1694	x	1.676
Huggins	343	0.9942	-0.4658	0.3421	0.6583			0.658
Isotherm						-8.3961		
Frumkin	303	0.9796	1.0838	0.0824	3.6985	-3.8303	α	1.849
Isotherm	343	0.9548	-1.1502	0.0708	4.4298	-3.9032		2.215
Temkin	303	1.000	-1.4130	0.0386	0.6417	-1.9196	a	-1.794
Isotherm	343	0.9930	-3.4084	0.0004	0.3937	10.8602		-2.925
Langumir	303	0.9666	0.0412	1.0995	0.6102	-10.3587		
Isotherm	343	0.9759	0.1715	1.4842	0.7072	-12.5819		

Table 4.35: Adsorption properties for the corrosion inhibition of Al in KOH by *Newbouldia leavis* leaves extract.

Adsorption Isotherm	Temperature (K)	R^2	Log K	K_{ads} (mol2/kJ2)	Slope	ΔG_{ads} (kJ/mol)	Isotherm value	
Flory-	303	0.9921	-0.5907	0.2566	1.0936	-6.6927	x	1.094
Huggins	343	0.9993	-0.4040	0.3945	0.4986			0.499
Isotherm						-8.8026		
Frumkin	303	0.9965	-1.0393	0.0913	3.6861	-4.0637	α	1.843
Isotherm	343	0.9852	-1.1601	0.06917	4.41	-3.9748		2.205
Temkin	303	0.9996	-0.7497	0.1780	0.5374	-5.7709	a	-1.068
Isotherm	343	0.9991	-1.9829	0.0104	0.3275	1.5674		-3.416
Langumir	303	0.9848	0.0825	1.2092	0.6021	-10.5982		
Isotherm	343	0.9931	0.1661	1.4589	0.7032	-12.5328		

Table 4.36: Adsorption properties for the corrosion inhibition of Al in NaOH by *Newbouldia leavis* leaves extract.

Adsorption Isotherm	Temperature (K)	R^2	Log K	K_{ads} (mol2/kJ2)	Slope	ΔG_{ads} (kJ/mol)	Isotherm value	
Flory-Huggins Isotherm	303	0.9910	O.6797	4.7830	1.1118	-14.0630	x	1.112
	343	0.9843	-0.4395	0.3635	0.4740	-8.5692		0.474
Frumkin Isotherm	303	0.9862	-6.9746	0.0011	4.3883	7.0449	α	2.194
	343	0.9818	-1.2946	0.0507	5.0909	-2.9507		2.545
Temkin Isotherm	303	0.9992	-1.8185	0.0152	0.599	0.4285	a	-0.724
	343	0.9156	-2.3864	0.0041	0.2412	4.2254		-4.292
Langumir Isotherm	303	0.9996	0.0707	1.1768	0.8746	-10.5298		
	343	0.9975	0.3261	2.1188	0.5379	-13.5971		

Table 4.37: Adsorption properties for the corrosion inhibition of Al in $H_2SO_4$by *Newbouldia leavis*leaves extract.

Adsorption Isotherm	Temperature (K)	R^2	Log K	K_{ads}(mol 2/kJ2)	Slope	ΔG_{ads} (kJ/mol)	Isotherm value	
Flory-Huggins Isotherm	303	0.9998	-0.6783	0.2097	0.9968	-6.1838	x	0.997
	343	0.9971	-0.3894	0.4079	0.4258	-8.8979		0.426
Frumkin Isotherm	303	0.992	-1.1736	0.0671	3.992	-3.3127	α	1.200
	343	0.9731	-1.1325	0.0737	3.3528	-4.0177		1.676
Temkin Isotherm	303	0.9995	-1.7240	0.0189	0.4859	-0.1204	a	-2.370
	343	0.9954	-2.3014	0.0050	0.2697	3.6563		-4.270
Langumir Isotherm	303	0.9913	0.0553	1.1358	0.6565	-10.4405		
	343	0.9963	0.1775	1.5048	0.7117	-12.6211		

Table 4.38: Adsorption properties for the corrosion inhibition of Al in HCL by *Newbouldia leavis* leaves extract.

Adsorption Isotherm	Temperature (K)	R^2	Log K	K_{ads}(mol2/kJ2)	Slope	ΔG_{ads} (kJ/mol)	Isotherm value	
Flory-Huggins Isotherm	303	0.9983	-0.8531	0.1402	1.6755	-5.1694	x	1.676
	343	0.9942	-0.4658	0.3421	0.6583	-8.3961		0.658
Frumkin Isotherm	303	0.9775	-0.9252	0.1188	2.3427	-4.7521	α	1.171
	343	0.9623	-1.3193	0.0479	4.3801	-2.7887		2.190
Temkin Isotherm	303	1.000	-1.4130	0.0386	0.6417	-1.9196	a	-1.794
	343	0.9930	-3.4084	0.0004	0.3937	10.8602		-2.925
Langumir Isotherm	303	0.9666	0.0412	1.0995	0.6102	-10.3587		
	343	0.9759	0.1715	1.4842	0.7072	-12.5819		

Table 4.39: Adsorption properties for the corrosion inhibition of Al in KOH by*Dennettia tripetala*leaves extract.

Adsorption Isotherm	Temperature (K)	R^2	Log K	K_{ads}(mol2/ kJ2)	Slope	ΔG_{ads} (kJ/mol)	Isotherm value	
Flory-	303	0.9921	-0.5907	0.2566	1.0936	-6.6924	x	1.094
Huggins	343	0.9993	-0.4040	0.3945	0.4986			0.499
Isotherm						-8.8026		
Frumkin	303	0.9893	-1.1670	0.0681	3.6862	-3.3500	α	1.843
Isotherm	343	0.9837	-1.1480	0.0711	4.3784	-3.9152		2.189
Temkin	303	0.9996	-0.7497	0.1780	0.5374	-5.7709	a	-1.068
Isotherm	343	0.9991	-1.9829	0.0104	0.3275	1.5674		-3.416
Langumir	303	0.9887	0.0809	1.2048	0.595	-10.5890		
Isotherm	343	0.9897	0.1663	1.4666	0.6964	-12.5478		

Table 4.40: Adsorption properties for the corrosion inhibition of Al in NaOH by *Dennettia tripetala* leaves extract.

Adsorption Isotherm	Temperature (K)	R^2	Log K	K_{ads} (mol2/kJ2)	Slope	ΔG_{ads} (kJ/mol)	Isotherm value	
Flory- Huggins Isotherm	303	0.9910	O.6797	4.7830	1.1118	-14.063	x	1.112
	343	0.9843	-0.4395	0.3635	0.474	-8.5692		0.474
Frumkin Isotherm	303	0.9934	-5.9328	0.0012	3.8859	6.8257	α	1.943
	343	0.9818	-1.2946	0.0507	5.0909	-2.9507		2.545
Temkin Isotherm	303	0.9992	-1.8185	0.0152	0.599	0.4285	a	-0.724
	343	0.9995	0.0611	1.1511	0.8990	-11.8569		-4.192
Langumir Isotherm	303	0.9960	0.3109	2.0460	0.5466	-11.9234		
	343	0.9691	0.2765	1.8902	0.4906	-13.2715		

Table 4.41: Adsorption properties for the corrosion inhibition of Al in H_2SO_4 by *Dennettia tripetala* leaves extract.

Adsorption Isotherm	Temperature (K)	R^2	Log K	K_{ads}(mol 2/kJ2)	Slope	ΔG_{ads} (kJ/mol)	Isotherm value	
Flory-	303	0.9994	-0.7378	0.1829	1.1432	-5.8334	x	1.143
Huggins	343	0.9971	-0.3894	0.4079	0.4258			0.426
Isotherm						-8.8979		
Frumkin	303	0.9794	-1.0773	0.08368	3.7345	-3.8691	α	1.867
Isotherm	343	0.9825	-1.2616	0.0548	4.9784	-3.1725		2.489
Temkin	303	0.9995	-1.7240	0.0189	0.4859	-0.1204	a	-2.370
Isotherm	343	0.9954	-2.3014	0.0050	0.2697	3.6563		-4.270
Langumir	303	0.9913	0.0553	1.1385	0.6565	-10.4464		
Isotherm	343	0.9963	0.2035	1.5977	0.7601	-12.7920		

Table 4.42: Adsorption properties for the corrosion inhibition of Al in HCL by *Dennettia tripetala*leaves extract.

Adsorption Isotherm	Temperature (K)	R^2	Log K	K_{ads}(mol 2/kJ2)	Slope	ΔG_{ads} (kJ/mol)	Isotherm value	
Flory-	303	0.9983	-0.8531	0.1402	1.6755	-11.4201	x	1.676
Huggins	343	0.9942	-0.4658	0.3421	0.6583			0.658
Isotherm						-10.2631		
Frumkin	303	0.9808	-1.0917	0.0810	3.7211	-13.4305	α	1.860
Isotherm	343	0.9648	-1.1620	0.0689	4.4666	-15.7243		2.233
Temkin	303	1.000	-1.4130	0.0386	0.6417	-9.0018	a	-1.794
Isotherm	343	0.9930	-3.4084	0.0004	0.3937	-8.7968		-2.925
Langumir	303	0.9666	0.0412	1.0995	0.6102	-8.8750		
Isotherm	343	0.9813	0.1766	1.4842	0.7 205	-10.5206		

Table 4.43: Adsorption properties for the corrosion inhibition of Al in KOH by*Dialium guineense* leaves extract.

Adsorption Isotherm	Temperature (K)	R^2	Log K	K_{ads}(mol2/ kJ2)	Slope	ΔG_{ads} (kJ/mol)	Isotherm value	
Flory-	303	0.9921	-0.5907	0.2566	1.0936	-6.6924	x	1.094
Huggins	343	0.9993	-0.4040	0.3945	0.4986			0.499
Isotherm						-8.8026		
Frumkin	303	0.9895	-1.0252	0.0944	3.6454	-4.1728	α	1.823
Isotherm	343	0.9806	-1.1415	0.0722	4.3451	-3.9590		2.173
Temkin	303	0.9996	-0.7497	0.1780	0.5374	-5.7709	a	-1.068
Isotherm	343	0.9991	-1.9829	0.0104	0.3275	1.5674		-3.416
Langumir	303	0.9887	0.0809	1.2048	0.595	-10.5890		
Isotherm	343	0.9897	0.1663	1.4666	0.6964	-12.5478		

Table 4.44: Adsorption properties for the corrosion inhibition of Al in NaOH by *Dialium guineense* leaves extract.

Adsorption Isotherm	Temperature (K)	R^2	Log K	k_{ads}(mol2/k J2)	Slope	ΔG_{ads} (kJ/mol)	Isotherm value	
Flory-	303	0.9933	-0.7367	0.1834	1.2121	-5.8462	x	1.212
Huggins	343	0.9843	-0.4395	0.3635	0.474			0.474
Isotherm						-8.5692		
Frumkin	303	0.9937	-6.4668	2.9297	4.881	-12.828	α	2.044
Isotherm	343	0.9818	-1.2946	0.0507	5.0909	-2.9507		2.545
Temkin	303	0.9992	-1.8185	0.0152	0.599	0.4285	a	-0.724
Isotherm	343	0.9156	-2.3864	0.0041	0.2412	4.2223		-4.292
Langumir	303	0.9999	0.0940	1.2417	0.7761	-10.6651		
Isotherm	343	0.9960	0.3109	2.0460	0.5466	-13.4975		

Table 4.45: Adsorption properties for the corrosion inhibition of Al in H_2S0_4 by *Dialium guineense* leaves extract.

Adsorption Isotherm	Temperature (K)	R^2	Log K	K_{ads}(Mol 2/kJ2)	Slope	ΔG_{ads} (kJ/mol)	Isotherm value	
Flory-Huggins Isotherm	303	0.9994	-0.7712	0.1694	1.1961	-5.6461	x	1.196
	343	0.9971	-0.3894	0.4079	0.4258	-8.8979		0.426
Frumkin Isotherm	303	0.9772	1.0764	0.0839	3.7263	-3.8757	α	1.863
	343	0.9897	-1.2275	0.0592	4.8483	-3.3928		2.424
Temkin Isotherm	303	0.9995	-1.7240	0.0189	0.4859	-0.1204	a	-2.370
	343	0.9954	-2.3014	0.0050	0.2697	3.6563		-4.270
Langumir Isotherm	303	0.9912	0.138	1.3740	0.0402	-10.9202		
	343	0.9963	0.2035	1.5977	0.7601	-12.7920		

Table 4.46: Adsorption properties for the corrosion inhibition of Al in HCL by*Dialium guineense* leaves extract.

Adsorption Isotherm	Temperature (K)	R^2	Log K	K_{ads} (mol2/kJ 2)	Slope	ΔG_{ads} (kJ/mol)	Isotherm value	
Flory-Huggins Isotherm	303	0.9983	-0.8531	0.1402	1.6755	-5.1694	x	1.676
	343	0.9942	-0.4658	0.3421	0.6583	-8.3961		0.658
Frumkin Isotherm	303	0.9811	-1.0911	0.0811	3.7174	-3.7902	α	1.859
	343	0.9641	-1.1859	0.0652	4.5506	-3.6682		2.275
Temkin Isotherm	303	1.000	-1.4130	0.0386	0.6417	-1.9196	a	-1.794
	343	0.9930	-3.4084	0.0004	0.3937	10.8602		-2.925
Langumir Isotherm	303	0.9781	0.0963	1.24828	0.4910	-10.6784		
	343	0.9813	0.1766	1.5017	0.7205	-12.6153		

Table 4.47: Adsorption properties for the corrosion inhibition of Al in KOH by *Vitex doniana* leaves extract.

Adsorption Isotherm	Temperature (K)	R^2	Log K	K_{ads}(mol2/kJ2)	Slope	ΔG_{ads} (kJ/mol)	Isotherm value	
Flory-Huggins Isotherm	303	0.9999	-0.0007	0.9934	0.9992	-10.1029	x	1.000
	343	0.9993	-0.4040	0.3945	0.4986	-8.8027		0.499
Frumkin Isotherm	303	0.9926	-1.1969	0.0636	3.6857	-3.1778	α	1.843
	343	0.9749	-1.1585	0.0695	4.4008	-3.8503		2.200
Temkin Isotherm	303	0.9996	-0.7497	0.1780	0.5374	-5.7709	a	-1.068
	343	0.9991	-1.9829	0.0104	0.3275	1.5674		-3.416
Langumir Isotherm	303	0.9887	0.0809	1.2048	0.5950	-10.5890		
	343	0.7203	0.5749	3.7575	0.5093	-35.2312		

Table 4.48: Adsorption properties for the corrosion inhibition of Al in NaOH by *Vitex doniana* leaves extract.

Adsorption Isotherm	Temperature (K)	R^2	Log K	K_{ads}(mol2 /kJ2)	Slope	ΔG_{ads} (kJ/mol)	Isotherm value	
Flory-	303	1.0000	3E-05	1.0001	1.0027	-10.1199	x	1.003
Huggins	343	0.9843	0.4395	2.7511	0.474			0.474
Isotherm						-14.342		
Frumkin	303	0.9937	-6.4668	2.9297	4.881	-12.828	α	2.044
Isotherm	343	0.9818	-1.2946	0.0507	5.0909	-2.9507		2.545
Temkin	303	0.9992	-1.8185	0.0152	0.599	0.4285	a	-0.724
Isotherm	343	0.9889	-5.3094	0.0095	0.2868	1.8256		-4.015
Langumir	303	0.9988	0.0909	1.2328	0.7403	-10.647		
Isotherm	343	0.9961	0.3093	2.0384	0.5608	-13.4868		

Table 4.49: Adsorption properties for the corrosion inhibition of Al in H_2S0_4 by *Vitex doniana*leaves extract.

Adsorption Isotherm	Temperature (K)	R^2	Log K	K_{ads}(mol 2/kJ2)	Slope	ΔG_{ads} (kJ/mol)	Isotherm value	
Flory-	303	0.9990	-0.8294	0.1481	1.2737	-5.3075	x	1.274
Huggins	343	0.9971	-0.3894	0.4079	0.4258			0.426
Isotherm						-8.8971		
Frumkin	303	0.9807	-1.0884	0.0816	3.7577	-3.8057	α	1.879
Isotherm	343	0.9759	-1.2664	0.0541	4.9998	-3.1359		2.500
Temkin	303	0.9995	-1.7240	0.0189	0.4859	-0.1204	a	-2.370
Isotherm	343	0.9954	-2.3014	0.0050	0.2697	3.6563		-4.270
Langumir	303	0.9912	0.0615	1.1521	0.6362	-10.4764		
Isotherm	343	0.9963	0.2035	1.5977	0.7601	-12.7920		

Table 4.50: Adsorption properties for the corrosion inhibition of Al in HCL by *Vitex doniana*leaves extract.

Adsorption Isotherm	Temperature (K)	R^2	Log K	K_{ads}(mo l2/kJ2)	Slope	ΔG_{ads} (kJ/mol)	Isotherm value	
Flory-	303	1.0000	0.0017	1.0039	0.9970	-10.1295	x	1.000
Huggins Isotherm	343	0.9942	-0.4658	0.3421	0.6583	-8.3961		0.658
Frumkin	303	0.9818	-1.0992	0.0796	3.7394	-3.7432	α	1.870
Isotherm	343	0.9640	-1.1858	0.0652	4.5490	-3.6682		2.275
Temkin	303	1.000	-1.4130	0.0386	0.6417	-1.9196	a	-1.794
Isotherm	343	0.9930	-3.4084	0.0004	0.3937	10.8602		-2.925
Langumir	303	0.9781	0.0963	1.24828	0.491	-10.6784		
Isotherm	343	0.9813	0.1766	1.5017	0.7205	-12.6153		

Table 4.51: Adsorption properties for the corrosion inhibition of mild steel in KOH by *Aspilia africana* leaves extract.

Adsorption Isotherm	Temperature (K)	R^2	Log K	K_{ads} (mol2/kJ 2)	Slope	ΔG_{ads} (kJ/mol)	Isotherm value	
Flory-	303	0.9994	-0.1527	0.7036	0.6485	-9.2339	x	0.649
Huggins	343	0.9990	-0.1133	0.7703	0.5564			0.556
Isotherm						-10.7112		
Frumkin	303	0.9651	-0.8973	0.1267	3.8670	-4.9143	α	1.934
Isotherm	343	0.9945	-0.9396	0.1149	4.2480	-5.2842		2.126
Temkin	303	0.9997	-1.3352	0.0462	0.4912	-2.3724	a	-2.344
Isotherm	343	0.9964	0.8193	0.1516	0.4313	-6.0748		-2.670
Langumir	303	0.9959	0.1917	1.5549	0.7069	-11.2314		
Isotherm	343	0.9991	0.6260	4.2267	0.9775	-15.5668		

Table 4.52: Adsorption properties for the corrosion inhibition of mild steel in NaOHby *Aspilia africana*leaves extract.

Adsorption Isotherm	Temperature (K)	R^2	Log K	K_{ads}(mol2/kJ2)	Slope	ΔG_{ads} (kJ/mol)	Isotherm value	
Flory-	303	0.9986	-0.2698	0.5373	1.3579	-8.5544	x	1.358
Huggins Isotherm	343	0.9981	-0.1337	0.7350	0.7409	-10.5774		0.741
Frumkin	303	0.9977	-1.0818	0.0828	3.9841	-3.8425	α	1.992
Isotherm	343	0.9932	-0.9786	0.1050	4.2329	-5.0272		2.116
Temkin	303	0.9986	-1.5162	0.0305	0.4979	-1.3262	a	-2.313
Isotherm	343	0.9890	-1.3129	0.0487	0.4083	-2.8359		-2.820
Langumir	303	0.9993	0.1256	1.3354	0.6242	-10.8484		
Isotherm	343	0.9966	0.2989	1.9902	0.6021	-13.4186		

Table 4.53: Adsorption properties for the corrosion inhibition of mild steel in H_2S0_4 by *Aspilia africana* leaves extract.

Adsorption Isotherm	Temperature (K)	R^2	Log K	K_{ads}(mol2/ kJ2)	Slope	ΔG_{ads} (kJ/mol)	Isotherm value	
Flory-	303	0.9969	-0.7383	0.1827	2.4909	-5.8365	x	2.491
Huggins	343	0.9964	-0.4646	0.3431	1.3573			1.357
Isotherm						-8.4044		
Frumkin	303	0.9915	-1.1254	0.07492	3.9510	-3.5905	α	1.976
Isotherm	343	0.9715	-0.9937	0.1015	3.8315	-4.9305		1.916
Temkin	303	0.9964	-1.1726	0.0672	0.7393	-3.3165	a	-1.558
Isotherm	343	0.9989	-1.1160	0.0766	0.6542	-4.1277		-1.760
Langumir	303	0.9960	0.0931	1.2391	0.6623	-10.6598		
Isotherm	343	0.9992	0.2169	1.6478	0.7482	-12.8801		

Table 4.54: Adsorption properties for the corrosion inhibition of mild steel in HCL by *Aspilia africana* leaves extract.

Adsorption Isotherm	Temperature (K)	R^2	Log K	K_{ads}(mol 2/kJ2)	Slope	ΔG_{ads} (kJ/mol)	Isotherm value	
Flory-	303	0.999	-0.4766	0.3337	1.2869	-7.3543	x	1.287
Huggins	343	0.9999	-0.3887	0.4086	0.9881			0.988
Isotherm						-8.9028		
Frumkin	303	0.9918	-0.8480	0.1419	3.1145	-5.1998	α	1.557
Isotherm	343	0.9606	-1.0013	0.0997	3.771	-4.8795		1.886
Temkin	303	0.9965	-1.3040	0.0497	0.606	-2.5564	a	-1.900
Isotherm	343	0.9986	-1.2995	0.0502	0.5386	-2.9225		-2.138
Langumir	303	0.999	0.0986	1.2549	0.6618	-10.6918		
Isotherm	343	0.9964	0.1541	1.4259	0.6662	-12.4676		

Table 4.55: Adsorption properties for the corrosion inhibition of mild steel in KOH *Chromolena odorata* leaves extract.

Adsorption Isotherm	Temperature (K)	R^2	Log K	K_{ads}(mol 2/kJ2)	Slope	ΔG_{ads} (kJ/mol)	Isotherm value	
Flory-	303	0.9994	-0.1527	0.7036	0.6485	-9.2339	x	0.649
Huggins	343	0.9980	-0.0960	0.8017	0.4325			0.433
Isotherm						-10.8254		
Frumkin	303	0.9856	-1.0357	0.0930	4.3142	-4.1352	α	2.157
Isotherm	343	0.9945	-0.9396	0.1149	4.2480	-5.2842		2.126
Temkin	303	0.9921	-1.4367	0.0366	0.4136	-1.7855	a	-2.784
Isotherm	343	0.9991	-1.332	0.0466	0.3153	-2.7102		-3.651
Langumir	303	0.9960	0.2295	1.6963	0.633	-11.4511		
Isotherm	343	0.9941	0.5105	3.2397	0.8589	-14.8083		

Table 4.56: Adsorption properties for the corrosion inhibition of mild steel in NaOH by *Chromolena odorata* leaves extract.

Adsorption Isotherm	Temperature (K)	R^2	Log K	K_{ads}(mol 2/kJ2)	Slope	ΔG_{ads} (kJ/mol)	Isotherm value	
Flory-	303	0.9986	-0.2698	0.5373	1.3579	-8.5544	x	1.358
Huggins Isotherm	343	0.9981	-0.1337	0.7350	0.7409	-10.5774		0.741
Frumkin	303	0.9413	-1.1572	0.0696	3.9327	-3.4049	α	1.966
Isotherm	343	0.9824	-0.9791	0.1049	4.4578	-5.0245		2.229
Temkin	303	0.9986	-1.5162	0.0305	0.4979	-1.3262	a	-2.313
Isotherm	343	0.9890	-1.3129	0.0487	0.4083	-2.8358		-2.820
Langumir	303	0.9993	0.1256	1.3354	0.6242	-10.8484		
Isotherm	343	0.9974	0.4564	2.8602	0.8107	-14.453		

Table 4.57: Adsorption properties for the corrosion inhibition of mild steel in H_2S0_4 by *Chromolena odorata* leaves extract.

Adsorption Isotherm	Temperature (K)	R^2	Log K	K_{ads}(mol 2/kJ2)	Slope	ΔG_{ads} (kJ/mol)	Isotherm value	
Flory-Huggins Isotherm	303	0.9969	-0.7383	0.1827	2.4909	-5.8365	x	2.491
	343	0.9964	-0.4646	0.3431	1.3573	-8.4044		1.357
Frumkin Isotherm	303	0.9915	-1.1254	0.07492	3.9510	-3.5905	α	1.976
	343	0.9715	-0.9937	0.1015	3.8315	-4.9305		1.916
Temkin Isotherm	303	0.9964	-1.1726	0.0672	0.7393	-3.3165	a	-1.558
	343	0.9989	-1.1160	0.0766	0.6542	-4.1277		-1.760
Langumir Isotherm	303	0.9960	0.0931	1.2391	0.6623	-10.6598		
	343	0.9992	0.2169	1.6478	0.7482	-12.8801		

Table 4.58: Adsorption properties for the corrosion inhibition of mild steel in HCL by *Chromolena odorata* leaves extract.

Adsorption Isotherm	Temperature (K)	R^2	Log K	K_{ads}(mol 2/kJ2)	Slope	ΔG_{ads} (kJ/mol)	Isotherm value	
Flory-Huggins Isotherm	303	0.9991	-0.5717	0.2681	1.7329	-6.8028	x	1.733
	343	0.9986	-0.3044	0.4961	0.6135	-9.4562		0.614
Frumkin Isotherm	303	0.9954	-0.9279	0.1108	3.2829	-4.5764	α	1.641
	343	0.9606	-1.0013	0.0997	3.771	-4.8795		1.886
Temkin Isotherm	303	0.9994	-1.224	0.0597	0.7138	-3.0183	a	-1.613
	343	0.9997	-1.4919	0.0322	0.4029	-1.6559		-2.858
Langumir Isotherm	303	0.9937	0.0731	1.1833	0.7157	-10.5437		
	343	0.983	0.2051	1.6036	0.6743	-12.8026		

Table 4.59: Adsorption properties for the corrosion inhibition of mild steel in KOH by *Newbouldia leavis* leaves extract.

Adsorption Isotherm	Temperature (K)	R^2	Log K	K_{ads}(mol 2/kJ2)	Slope	ΔG_{ads} (kJ/mol)	Isotherm value	
Flory-Huggins Isotherm	303	0.9982	-0.1617	0.6891	0.8019	-9.1814	x	0.802
	343	0.9990	-0.1133	0.7703	0.5564	-10.7112		0.556
Frumkin Isotherm	303	0.985	-0.9514	0.1118	4.1704	-4.5991	α	2.090
	343	0.965	-0.9087	0.1234	4.1781	-5.4878		2.090
Temkin Isotherm	303	0.9997	-1.3352	0.0462	0.4912	-2.3724	a	-2.344
	343	0.9964	0.8193	0.1516	0.4313	-6.0748		-2.670
Langmuir Isotherm	303	0.9959	0.1917	1.5549	0.7069	-11.2318		
	343	0.9991	0.6260	4.2267	0.9775	-15.5668		

Table 4.60: Adsorption properties for the corrosion inhibition of mild steel in NaOH by *Newbouldia leavis* leaves extract.

Adsorption Isotherm	Temperature (K)	R^2	Log K	K_{ads}(mol 2/kJ2)	Slope	ΔG_{ads} (kJ/mol)	Isotherm value	
Flory-	303	0.9993	-0.2606	0.5488	1.2593	-8.6078	x	1.259
Huggins	343	0.9981	-0.1337	0.7350	0.7409			0.741
Isotherm						-10.5774		
Frumkin	303	0.9979	-1.0830	0.0826	3.9884	-3.8364	α	1.994
Isotherm	343	0.9933	-0.9787	0.1050	4.2329	-5.0272		2.116
Temkin	303	0.9986	-1.5162	0.0305	0.4979	-1.3262	a	-2.313
Isotherm	343	0.9890	-1.3129	0.0487	0.4083	-2.8359		-2.820
Langumir	303	0.9993	0.1256	1.3354	0.6242	-10.8484		
Isotherm	343	0.9890	0.3886	2.4468	0.7519	-14.0077		

Table 4.61: Adsorption properties for the corrosion inhibition of mild steel in H_2S0_4 by *Newbouldia leavis* leaves extract.

Adsorption Isotherm	Temperature (K)	R^2	Log K	K_{ads}(mol 2/kJ2)	Slope	ΔG_{ads} (kJ/mol)	Isotherm value	
Flory-	303	0.9969	-0.7383	0.1827	2.4909	-5.8365	x	2.491
Huggins	343	0.9964	-0.4646	0.3431	1.3573			1.357
Isotherm						-8.4044		
Frumkin	303	0.9915	-1.1254	0.07492	3.9510	-3.5905	α	1.976
Isotherm	343	0.9715	-0.9937	0.1015	3.8315	-4.9305		1.916
Temkin	303	0.9964	-1.1726	0.0672	0.7393	-3.3165	a	-1.558
Isotherm	343	0.9989	-1.1160	0.0766	0.6542	-4.1277		-1.760
Langumir	303	0.9960	0.0931	1.2391	0.6623	-10.6598		
Isotherm	343	0.9992	0.2169	1.6478	0.7482	-12.8801		

Table 4.62: Adsorption properties for the corrosion inhibition of mild steel in HCL by *Newbouldia leavis*leaves extract.

Adsorption Isotherm	Temperature (K)	R^2	Log K	K_{ads}(mol 2/kJ2)	Slope	ΔG_{ads} (kJ/mol)	Isotherm value	
Flory-	303	0.9991	-0.5717	0.2681	1.7329	-6.8028	x	1.733
Huggins	343	0.9999	-0.3887	0.4086	0.9881			0.988
Isotherm						-8.9028		
Frumkin	303	0.9515	-0.8072	0.1553	3.1879	-5.4271	α	1.594
Isotherm	343	0.9743	-0.9613	0.10932	3.6861	-5.1422		1.843
Temkin	303	0.9994	-1.224	0.0597	0.7138	-3.0183	a	-1.613
Isotherm	343	0.9986	-1.2995	0.0502	0.5386	-2.9225		-2.138
Langumir	303	0.9884	0.1115	1.2927	0.5934	-10.7665		
Isotherm	343	0.9964	0.1541	1.4259	0.6662	-12.4676		

Table 4.63: Adsorption properties for the corrosion inhibition of mild steel in KOH by *Dennettia tripetala* leaves extract.

Adsorption Isotherm	Temperature (K)	R^2	Log K	K_{ads}(mol 2/kJ2)	Slope	ΔG_{ads} (kJ/mol)	Isotherm value
Flory-	303	0.9982	-0.1617	0.6891	0.8019	-9.1814	x 0.802
Huggins	343	0.9990	-0.1133	0.7703	0.5564		0.556
Isotherm						-10.7112	
Frumkin	303	0.9858	-1.0301	0.0933	4.3081	-4.1433	α 2.154
Isotherm	343	0.9945	-0.9396	0.1149	4.2480	-5.2842	2.126
Temkin	303	0.9921	-1.4367	0.0366	0.4136	-1.7855	a -2.784
Isotherm	343	0.9964	0.8193	0.1516	0.4313	-6.0748	-2.670
Langumir	303	0.9968	0.2060	1.6069	0.5963	-11.3147	
Isotherm	343	0.9998	0.4140	2.5942	0.4421	-14.1745	

Table 4.64: Adsorption properties for the corrosion inhibition of mild steel in NaOH by *Dennettia tripetala* leaves extract.

Adsorption Isotherm	Temperature (K)	R^2	Log K	K_{ads}(mol 2/kJ2)	Slope	ΔG_{ads} (kJ/mol)	Isotherm value
Flory-	303	0.9993	-0.2606	0.5488	1.2593	-8.6078	x 1.259
Huggins	343	0.9981	-0.1337	0.7350	0.7409		0.741
Isotherm						-10.5774	
Frumkin	303	0.9871	-1.0115	0.0974	3.7682	-4.2517	α 1.884
Isotherm	343	0.9934	-0.9338	0.1165	4.0216	-5.3237	2.011
Temkin	303	0.9986	-1.5162	0.0305	0.4979	-1.3262	a -2.313
Isotherm	343	0.9890	-1.3129	0.0487	0.4083	-2.8359	-2.820
Langumir	303	0.9993	0.1256	1.3354	0.6242	-10.8484	
Isotherm	343	0.9834	0.4204	2.6327	0.7982	-14.2166	

Table 4.65: Adsorption properties for the corrosion inhibition of mild steel in H_2S0_4 by *Dennettia tripetal* leaves extract.

Adsorption Isotherm	Temperature (K)	R^2	Log K	K_{ads}(mol 2/kJ2)	Slope	ΔG_{ads} (kJ/mol)	Isotherm value
Flory-	303	0.9969	-0.7383	0.1827	2.4909	-5.8365	x 2.491
Huggins	343	0.9964	-0.4646	0.3431	1.3573		1.357
Isotherm						-8.4044	
Frumkin	303	0.9915	-1.1254	0.07492	3.9510	-3.5905	α 1.976
Isotherm	343	0.9715	-0.9937	0.1015	3.8315	-4.9305	1.916
Temkin	303	0.9964	-1.1726	0.0672	0.7393	-3.3165	a -1.558
Isotherm	343	0.9989	-1.1160	0.0766	0.6542	-4.1277	-1.760
Langumir	303	0.9960	0.0931	1.2391	0.6623	-10.6598	
Isotherm	343	0.9992	0.2169	1.6478	0.7482	-12.8801	

Table 4.66: Adsorption properties for the corrosion inhibition of mild steel in HCL by *Dennettia tripetala* leaves extract.

Adsorption Isotherm	Temperature (K)	R^2	Log K	K_{ads}(mol 2/kJ2)	Slope	ΔG_{ads} (kJ/mol)	Isotherm value	
Flory-	303	0.999	-0.4766	0.3337	1.2869	-7.3543	x	1.287
Huggins	343	0.9987	-0.3478	0.4490	0.8121			0.812
Isotherm						-9.1717		
Frumkin	303	0.9969	-0.9801	0.1047	3.5424	-4.4338	α	1.771
Isotherm	343	0.9743	-0.9613	0.10932	3.6861	-5.1422		1.843
Temkin	303	0.9965	-1.3040	0.0497	0.606	-2.5564	a	-1.900
Isotherm	343	0.9997	-1.3674	0.0429	0.4829	-2.4743		-2.385
Langumir	303	0.9902	0.0850	1.2162	0.5857	-10.6128		
Isotherm	343	0.968	0.1628	1.4548	0.6228	-12.5248		

Table 4.67: Adsorption properties for the corrosion inhibition of mild steel in KOH by *Dialium guineense*leaves extract.

Adsorption Isotherm	Temperature (K)	R^2	Log K	K_{ads}(mol 2/kJ2)	Slope	ΔG_{ads} (kJ/mol)	Isotherm value	
Flory-	303	0.9994	-0.1527	0.7036	0.6485	-9.2339	x	0.649
Huggins	343	0.9980	-0.0960	0.8017	0.4325			0.433
Isotherm						-10.8251		
Frumkin	303	0.9851	-1.0304	0.09323	4.3054	-4.1414	α	2.153
Isotherm	343	0.9813	-0.8959	0.1271	3.7129	-5.5720		1.857
Temkin	303	0.9921	-1.4367	0.0366	0.4136	-1.7855	a	-2.784
Isotherm	343	0.9991	-1.332	0.0466	0.3153	-2.7102		-3.651
Langumir	303	0.9963	0.2300	1.6982	0.6341	-11.4539		
Isotherm	343	0.9997	0.5674	3.6932	0.9203	-15.1819		

Table 4.68: Adsorption properties for the corrosion inhibition of mild steel in NaOH by *Dialium guineense* leaves extract.

Adsorption Isotherm	Temperature (K)	R^2	Log K	K_{ads}(mol 2/kJ2)	Slope	ΔG_{ads} (kJ/mol)	Isotherm value	
Flory-	303	0.9999	-0.2741	0.5320	1.493	-8.5295	x	1.493
Huggins	343	0.9981	-0.1337	0.7350	0.7409			0.741
Isotherm						-10.5774		
Frumkin	303	0.9971	-1.0072	0.0984	3.7194	-4.2774	α	1.860
Isotherm	343	0.9808	-1.0432	0.0905	5.0237	-4.6034		2.512
Temkin	303	0.9986	-1.5162	0.0305	0.4979	-1.3262	a	-2.313
Isotherm	343	0.9890	-1.3129	0.0487	0.4083	-2.8359		-2.820
Langumir	303	0.9993	0.1256	1.3354	0.6242	-10.8484		
Isotherm	343	0.9991	0.5739	3.7489	0.9716	-15.2247		

Table 4.69: Adsorption properties for the corrosion inhibition of mild steel in H_2S0_4 by *Dialium guineense* leaves extract.

Adsorption Isotherm	Temperature (K)	R^2	Log K	K_{ads}(mol2/kJ2)	Slope	ΔG_{ads} (kJ/mol)	Isotherm value	
Flory-Huggins Isotherm	303	0.9969	-0.7383	0.1827	2.4909	-5.8365	x	2.491
	343	0.9964	-0.4646	0.3431	1.3573	-8.4044		1.357
Frumkin Isotherm	303	0.9915	-1.1254	0.07492	3.9510	-3.5905	α	1.976
	343	0.9715	-0.9937	0.1015	3.8315	-4.9305		1.916
Temkin Isotherm	303	0.9964	-1.1726	0.0672	0.7393	-3.3165	a	-1.558
	343	0.9989	-1.1160	0.0766	0.6542	-4.1277		-1.760
Langumir Isotherm	303	0.9960	0.0931	1.2391	0.6623	-10.6598		
	343	0.9992	0.2169	1.6478	0.7482	-12.8801		

Table 4.70: Adsorption properties for the corrosion inhibition of mild steel in HCL by*Dialium guineense* leaves extract

Adsorption Isotherm	Temperature (K)	R^2	Log K	K_{ads}(mol2/kJ2)	Slope	ΔG_{ads} (kJ/mol)	Isotherm value	
Flory-Huggins Isotherm	303	0.999	-0.4766	0.3337	1.2869	-7.3543	x	1.287
	343	0.9987	-0.3478	0.4490	0.8121	-9.1717		0.812
Frumkin Isotherm	303	0.9932	-0.9290	0.1178	3.4016	-4.7308	α	1.701
	343	0.9743	-0.9613	0.10932	3.6861	-5.1422		1.843
Temkin Isotherm	303	0.9965	-1.3040	0.0497	0.606	-2.5564	a	-1.900
	343	0.9997	-1.3674	0.0429	0.4829	-2.4743		-2.385
Langumir Isotherm	303	0.9902	0.085	1.2162	0.5857	-10.6128		
	343	0.968	0.1628	1.4548	0.6228	-12.5248		

Table 4.71: Adsorption properties for the corrosion inhibition of mild steel in KOH by *Vitex doniana* leaves extract.

Adsorption Isotherm	Temperature (K)	R^2	Log K	K_{ads}(mol 2/kJ2)	Slope	ΔG_{ads} (kJ/mol)	Isotherm value	
Flory-Huggins Isotherm	303	0.9994	-0.1527	0.7036	0.6485	-9.2339	x	0.649
	343	0.9980	-0.0960	0.8017	0.4325	-10.8251		0.433
Frumkin Isotherm	303	0.9861	-1.0737	0.08439	4.5843	-3.8904	α	2.292
	343	0.9735	-0.8452	0.1428	3.4571	-5.9042		1.729
Temkin Isotherm	303	0.9921	-1.4367	0.0366	0.4136	-1.7855	a	-2.784
	343	0.9991	-1.332	0.0466	0.3153	-2.7102		-3.651
Langumir Isotherm	303	0.9897	0.2060	01.6069	0.5963	-11.3147		
	343	0.9991	0.6260	4.2267	0.9775	-15.5668		

Table 4.72: Adsorption properties for the corrosion inhibition of mild steel in NaOH by *Vitex doniana* leaves extract.

Adsorption Isotherm	Temperature (K)	R^2	Log K	K_{ads}(mol 2/kJ2)	Slope	ΔG_{ads} (kJ/mol)	Isotherm value	
Flory-	303	0.9996	-0.2905	0.5123	1.5246	-8.4344	x	1.525-
Huggins	343	0.9981	-0.1337	0.7350	0.7409			0.741
Isotherm						-10.5774		
Frumkin	303	0.9978	-1.0714	0.0848	3.9376	-3.9026	α	1.969
Isotherm	343	0.9753	-1.0342	0.0924	4.9453	-4.6626		2.472
Temkin	303	0.9986	-1.5162	0.0305	0.4979	-1.3262	a	-2.313
Isotherm	343	0.9890	-1.3129	0.0487	0.4083	-2.8359		-2.820
Langumir	303	0.9993	0.1256	1.3354	0.6242	-10.8484		
Isotherm	343	0.9988	0.5291	3.3814	0.9021	-14.9304		

Table 4.73: Adsorption properties for the corrosion inhibition of mild steel in H_2S0_4 by *Vitex doniana* leaves extract.

Adsorption Isotherm	Temperature (K)	R^2	Log K	K_{ads}(mol2/kJ2)	Slope	ΔG_{ads} (kJ/mol)	Isotherm value	
Flory-	303	0.9969	-0.7383	0.1827	2.4909	-5.8365	x	2.491
Huggins	343	0.9964	-0.4646	0.3431	1.3573			1.357
Isotherm						-8.4044		
Frumkin	303	0.9915	-1.1254	0.07492	3.9510	-3.5905	α	1.976
Isotherm	343	0.9715	-0.9937	0.1015	3.8315			1.916
						-4.9305		
Temkin	303	0.9964	-1.1726	0.0672	0.7393	-3.3165	a	-1.558
Isotherm	343	0.9989	-1.1160	0.0766	0.6542			-1.760
						-4.1277		
Langumir	303	0.9960	0.0931	1.2391	0.6623	-10.6598		
Isotherm	343	0.9992	0.2169	1.6478	0.7482	-12.8801		

Table 4.74: Adsorption properties for the corrosion inhibition of mild steel in HCL by *Vitex doniana* leaves extract.

Adsorption Isotherm	Temperature (K)	R^2	Log K	K_{ads}(MO L2/KJ2)	Slope	ΔG_{ads} (kJ/mol)	Isotherm value	
Flory-	303	0.999	-0.4766	0.3337	1.2869	-7.3543	x	1.287
Huggins	343	0.9987	-0.3478	0.4490	0.8121			0.812
Isotherm						-9.1717		
Frumkin	303	0.9969	-0.9801	0.1047	3.5424	-4.4338	α	1.771
Isotherm	343	0.9606	-1.0013	0.0997	3.771	-4.8795		1.886
Temkin	303	0.9965	-1.3040	0.0497	0.606	-2.5564	a	-1.900
Isotherm	343	0.9997	-1.3674	0.0429	0.4829	-2.4743		-2.385
Langumir	303	0.9939	0.0859	1.2187	0.5434	-10.618		
Isotherm	343	0.9696	0.1632	1.4561	0.6265	-12.5273		

4.5Response Surface Methodology

4.5.1 Results of the weight loss method using RSM

The responses of weight loss, corrosion rate and inhibition efficiency to the factors of inhibitor's concentration, temperature and time for the corrosion inhibition of the metals in media with the plant extracts are presented in Tables 4.75 – 4.82. The data show the variation of weight loss with concentration, temperature and time for the corrosion inhibition of the metals (aluminum and mild steel) in the alkaline and acid media (NaOH, KOH, HCl and H_2SO_4). The weight loss increased with increase in temperature and time of immersion but decreased with an increase in the concentration of the plant extracts (*Aspilia africana* leaf, *Chromolena odorata*, *Newbouldia leavis*, *Dennettia tripetala*, *Dialium gunineense* and *Vitex doniana*). Similar trends were noticed in the variation of corrosion rate with concentration, temperature and time. Decrease in corrosion rate with increase in concentration of the inhibitor is an indication that the plant extracts inhibited the corrosion of the metals in the alkaline and acid media. Increase in concentration increases the inhibition efficiency. Also, inhibition efficiency reduces as temperature rises. These observations are in agreement with previous studies of El Ouariachi *et al.*,2010;Ndibe *et al.*, 2011; Abdulwahab *et al.*, 2012. The high inhibition efficiency values of 85.23% (in NaOH), 78.43% (in KOH), 70.07% (in HCL) and 64.07% (in H_2SO_4) were achieved by using *Dialium gunineense* leaf extract as corrosion inhibition of aluminum in the alkaline and acid media. Similarly, high values of inhibition efficiency of other plant extracts (*Vitex doniana*, *Chromolena odorata*, *Aspilia africana*,*Newbouldia leavis* and *Dennettia tripetala*) as corrosion inhibition of aluminium in NaOH, KOH, HCl and H_2SO_4 media were obtained.

Table 4.75: RSM result of corrosion inhibition of Al in KOH using *Dialium guineense* leaves extract

Std	Run	Factor 1 KOH conc (mol	Factor 2 Inhibitor con. (g/l)	Factor 3 Time (hrs)	Factor 4 Temperature (K)	Response 1 Weight loss (g)	Response 2 Corrosion rate (g/cm^2hr)	Response 3 Inhibitor efficiency (%)
6	1	2	0.025	6.25	313	0.36	6	61.43
19	2	1.5	0.01	4.5	323	0.36	6	71.43
12	3	2	0.055	2.75	333	0.14	7	73.58
13	4	1	0.025	6.25	333	0.33	5.5	63.81
25	5	1.5	0.04	4.5	323	0.36	6	51.43
4	6	2	0.055	2.75	313	0.45	4.5	73.37
2	7	2	0.025	2.75	313	0.36	6	66.43
15	8	1	0.055	6.25	333	0.28	14	58.88
29	9	1.5	0.04	4.5	323	0.98	9.8	54
24	10	1.5	0.04	4.5	343	0.31	15.5	62.33
27	11	1.5	0.04	4.5	323	0.587	5.87	56.46
14	12	2	0.025	6.25	333	0.863	8.63	56.4
7	13	1	0.055	6.25	313	0.36	6	71.43
30	14	1.5	0.04	4.5	323	0.42	21	50
26	15	1.5	0.04	4.5	323	0.86	14.33	56.3
22	16	1.5	0.04	8	323	0.33	16.5	37.74
16	17	2	0.055	6.25	333	0.36	6	51.43
10	18	2	0.025	2.75	333	0.29	2.9	71.99
8	19	2	0.055	6.25	313	0.24	12	68
20	20	1.5	0.07	4.5	323	0.31	5.17	75.4
18	21	2.5	0.04	4.5	323	0.36	6	77.43
11	22	1	0.055	2.75	333	0.36	6	78.43
9	23	1	0.025	2.75	333	0.14	7	70.58
3	24	1	0.055	2.75	313	0.33	5.5	69.81
28	25	1.5	0.04	4.5	323	0.36	6	51.43
17	26	0.5	0.04	4.5	323	0.45	4.5	73.37
23	27	1.5	0.04	4.5	303	0.36	6	61.43
5	28	1	0.025	6.25	313	0.28	14	57.88
1	29	1	0.025	2.75	313	0.98	9.8	54
21	30	1.5	0.04	1	323	0.31	15.5	52.33

Table 4.76: RSM result of corrosion inhibition of Al in HCl using *Newbouldia leavis* leaves extract

Std	Run	Factor 1 Acid conc (mols)	Factor 2 Inhibitor conc (g/l)	Factor 3 Time (hrs)	Factor 4 Temperature (K)	Response 1 Weight loss (g)	Response 2 Corrosion rate g/cm^2hr)	Response 3 Inhibitor efficiency (%)
15	1	1	0.055	6.25	333	0.45	5.17	61.63
28	2	1.5	0.04	4.5	323	0.41	6.83	69.63
25	3	1.5	0.04	4.5	323	0.28	6.83	68.58
7	4	1	0.055	6.25	313	0.98	7	68.56
21	5	1.5	0.04	1	323	0.53	5.5	49.63
11	6	1	0.055	2.75	333	0.45	6.83	83.37
20	7	1.5	0.07	4.5	323	0.41	6.83	67.63
19	8	1.5	0.01	4.5	323	0.28	14	55.88
1	9	1	0.025	2.75	313	0.98	9.8	44
10	10	2	0.025	2.75	333	0.53	8.83	72.41
24	11	1.5	0.04	4.5	343	0.59	5.9	68.29
23	12	1.5	0.04	4.5	303	0.863	8.63	46.4
26	13	1.5	0.04	4.5	323	0.41	6.83	69.63
4	14	2	0.055	2.75	313	0.42	21	40
22	15	1.5	0.04	8	323	0.86	14.33	56.3
2	16	2	0.025	2.75	313	0.33	16.5	37.74
6	17	2	0.025	6.25	313	0.41	6.83	67.63
27	18	1.5	0.04	4.5	323	0.3	3	68.37
13	19	1	0.025	6.25	333	0.24	12	50
12	20	2	0.055	2.75	333	0.31	5.17	75.4
5	21	1	0.025	6.25	313	0.45	6.83	67.63
14	22	2	0.025	6.25	333	0.41	6.83	59.63
18	23	2.5	0.04	4.5	323	0.28	7	73.58
8	24	2	0.055	6.25	313	0.98	5.5	69.56
30	25	1.5	0.04	4.5	323	0.53	6.83	69.63
9	26	1	0.025	2.75	333	0.45	6.83	73.37
17	27	0.5	0.04	4.5	323	0.41	6.83	75.63
29	28	1.5	0.04	4.5	323	0.28	14	68.88
3	29	1	0.055	2.75	313	0.98	9.8	48
16	30	2	0.055	6.25	333	0.53	8.83	62.41

Table 4.77: RSM result of corrosion inhibition of mild steel in NaOH using *Dennettia tripetala* leaves extract

Std	Run	Factor 1 NaOH conc (mol)	Factor 2 Inhibitor conc (g/l)	Factor 3 Time (hrs)	Factor 4 Temperature (K)	Response 1 Weight loss (g)	Response 2 Corrosion rate (g/cm^2hr)	Response 3 Inhibitor efficiency (%)
4	1	2	0.055	2.75	313	0.03	0.094	34.4
26	2	1.5	0.04	4.5	323	0.04	0.125	32.53
30	3	1.5	0.04	4.5	323	0.053	0.11	34.29
11	4	1	0.055	2.75	333	0.03	0.063	55
12	5	2	0.055	2.75	333	0.033	0.069	47.86
22	6	1.5	0.04	8	323	0.013	0.081	35
15	7	1	0.055	6.25	333	0.03	0.094	36.4
20	8	1.5	0.07	4.5	323	0.03	0.094	23.4
7	9	1	0.055	6.25	313	0.017	0.106	40.33
3	10	1	0.055	2.75	313	0.027	0.169	25.54
21	11	1.5	0.04	1	323	0.03	0.094	43.4
10	12	2	0.025	2.75	333	0.027	0.084	54.06
8	13	2	0.055	6.25	313	0.013	0.081	43.48
28	14	1.5	0.04	4.5	323	0.037	0.116	35.09
27	15	1.5	0.04	4.5	323	0.03	0.094	33.4
2	16	2	0.025	2.75	313	0.017	0.053	54.05
24	17	1.5	0.04	4.5	343	0.03	0.094	43.4
6	18	2	0.025	6.25	313	0.013	0.027	65
9	19	1	0.025	2.75	333	0.007	0.044	55
17	20	0.5	0.04	4.5	323	0.03	0.063	40
14	21	2	0.025	6.25	333	0.03	0.094	33.4
13	22	1	0.025	6.25	333	0.04	0.125	34.53
25	23	1.5	0.04	4.5	323	0.053	0.11	32.29
19	24	1.5	0.01	4.5	323	0.03	0.063	55
5	25	1	0.025	6.25	313	0.033	0.069	52.86
23	26	1.5	0.04	4.5	303	0.013	0.081	43
18	27	2.5	0.04	4.5	323	0.03	0.094	43.4
29	28	1.5	0.04	4.5	323	0.03	0.094	43.4
1	29	1	0.025	2.75	313	0.017	0.106	38.33
16	30	2	0.055	6.25	333	0.027	0.169	25.54

Table 4.78: RSM result of corrosion inhibition of mild steel in H_2SO_4 using *Chromolena odorata* leaves extract

Std	Run	Factor 1 Acid conc (mol)	Factor 2 Inhibitor conc (g/l)	Factor 3 Time (hrs)	Factor 4 Temperature (K)	Response 1 Weight loss (g)	Response 2 Corrosion rate (g/cm^2hr)	Response 3 Inhibitor efficiency (%)
8	1	2	0.055	2.75	313	0.4	1.25	62.6
26	2	1.5	0.04	4.5	323	0.4	1.313	63.82
30	3	1.5	0.04	4.5	323	0.42	0.896	63.84
11	4	1	0.055	2.75	333	0.43	1.313	65.62
12	5	2	0.055	2.75	333	0.21	1.625	57.17
22	6	1.5	0.04	8	323	0.26	2.019	44.88
15	7	1	0.055	6.25	333	0.4	1.25	59.6
20	8	1.5	0.07	4.5	323	0.35	1.09	64.65
7	9	1	0.055	6.25	313	0.62	1.938	37.37
3	10	1	0.055	2.75	313	0.4	1.25	59.6
21	11	1.5	0.04	1	323	0.4	1.25	49.6
10	12	2	0.025	2.75	333	0.38	2.375	43.48
8	13	2	0.055	6.25	313	0.25	1.563	52.9
28	14	1.5	0.04	4.5	323	0.327	0.681	64.85
27	15	1.5	0.04	4.5	323	0.89	1.854	63.76
2	16	2	0.025	2.75	313	0.27	1.688	47.79
24	17	1.5	0.04	4.5	343	0.507	1.056	57.55
6	18	2	0.025	6.25	313	0.72	1.5	47.62
9	19	1	0.025	2.75	333	0.4	1.25	59.6
17	20	0.5	0.04	4.5	323	0.4	1.25	59.6
14	21	2	0.025	6.25	333	0.4	1.25	59.6
13	22	1	0.025	6.25	333	0.42	1.313	66.82
25	23	1.5	0.04	4.5	323	0.43	0.896	63.84
19	24	1.5	0.01	4.5	323	0.21	1.313	56.62
5	25	1	0.025	6.25	313	0.26	1.625	45.17
23	26	1.5	0.04	4.5	303	0.4	2.019	42.88
18	27	2.5	0.04	4.5	323	0.35	1.25	59.6
29	28	1.5	0.04	4.5	323	0.62	1.09	64.65
1	29	1	0.025	2.75	313	0.4	1.938	47.37
16	30	2	0.055	6.25	333	0.4	1.25	59.6

Table 4.79: RSM result of corrosion inhibition of mild steel in HCL using *Vitex doniana* leaves extract

Std	Run	Factor 1 Acid conc (mol)	Factor 2 Inhibitor conc (g/l)	Factor 3 Time (hrs)	Factor 4 Temperature (K)	Response 1 Weight loss (g)	Response 2 Corrosion rate (g/cm^2hr)	Response 3 Inhibitor efficiency (%)
14	1	2	0.025	6.25	333	0.037	0.231	44.78
9	2	1	0.025	2.75	333	0.08	0.167	66
16	3	2	0.055	6.25	333	0.077	0.16	54.8
28	4	1.5	0.04	4.5	323	0.047	0.147	59.41
22	5	1.5	0.04	8	323	0.047	0.147	58.41
13	6	1	0.025	6.25	333	0.047	0.147	61.41
6	7	2	0.025	6.25	313	0.057	0.209	47.14
30	8	1.5	0.04	4.5	323	0.053	0.11	62.94
19	9	1.5	0.01	4.5	323	0.017	0.106	67.18
11	10	1	0.055	2.75	333	0.04	0.125	60
7	11	1	0.055	6.25	313	0.037	0.231	52.78
12	12	2	0.055	2.75	333	0.08	0.167	60
4	13	2	0.055	2.75	313	0.077	0.16	38.8
26	14	1.5	0.04	4.5	323	0.047	0.147	59.41
1	15	1	0.025	2.75	313	0.047	0.147	48.41
5	16	1	0.025	6.25	313	0.047	0.147	58.41
21	17	1.5	0.04	1	323	0.057	0.209	52.14
24	18	1.5	0.04	4.5	343	0.053	0.11	60.94
27	19	1.5	0.04	4.5	323	0.017	0.106	60.18
29	20	1.5	0.04	4.5	323	0.04	0.125	60
3	21	1	0.055	2.75	313	0.037	0.231	35.09
25	22	1.5	0.04	4.5	323	0.047	0.147	60.41
10	23	2	0.025	2.75	333	0.04	0.125	56.6
18	24	2.5	0.04	4.5	323	0.07	0.219	38.05
20	25	1.5	0.07	4.5	323	0.047	0.147	62.41
8	26	2	0.055	6.25	313	0.047	0.147	48.41
23	27	1.5	0.04	4.5	303	0.057	0.356	32.97
17	28	0.5	0.04	4.5	323	0.037	0.231	51.95
15	29	1	0.055	6.25	333	0.033	0.069	65.91
2	30	2	0.025	2.75	313	0.13	0.271	45

Table 4.80: RSM Result of corrosion inhibition of Al in KOH using *Aspilia africana* leaves extract

Std	Run	Factor 1 Alkaliconc (mol)	Factor 2 Inhibitor conc (g/l)	Factor 3 Time (hrs)	Factor 4 Temperature (K)	Response 1 Weight loss (g)	Response 2 Corrosion rate (g/cm^2hr)	Response 3 Inhibitor efficiency (%)
2	1	2	0.025	2.75	313	0.31	31	56.67
3	2	1	0.055	2.75	313	0.33	33	68.52
22	3	1.5	0.04	8	323	0.33	33	64.52
26	4	1.5	0.04	4.5	323	0.73	73	57.56
30	5	1.5	0.04	4.5	323	0.33	33	55.52
10	6	2	0.025	2.75	333	0.46	92	46.33
19	7	1.5	0.01	4.5	323	0.83	55.33	61.63
16	8	2	0.055	6.25	333	0.13	26	65.79
4	9	2	0.055	2.75	313	0.33	33	74.52
28	10	1.5	0.04	4.5	323	0.293	19.53	56.36
9	11	1	0.025	2.75	333	0.28	28	60.44
8	12	2	0.055	6.25	313	0.33	33	64.52
5	13	1	0.025	6.25	313	0.58	58	47.63
11	14	1	0.055	2.75	333	0.33	33	62.52
29	15	1.5	0.04	4.5	323	1.3	86.67	59.9
14	16	2	0.025	6.25	333	0.33	33	64.52
25	17	1.5	0.04	4.5	323	0.63	42	56.73
24	18	1.5	0.04	4.5	343	0.297	59.4	56.96
17	19	0.5	0.04	4.5	323	0.237	47.4	45.63
1	20	1	0.025	2.75	313	0.413	27.53	65
21	21	1.5	0.04	1	323	0.31	31	66.67
13	22	1	0.025	6.25	333	0.33	33	54.52
12	23	2	0.055	2.75	333	0.33	33	56.52
6	24	2	0.025	6.25	313	0.73	73	60.56
23	25	1.5	0.04	4.5	303	0.33	33	64.52
15	26	1	0.055	6.25	333	0.46	92	45.33
7	27	1	0.055	6.25	313	0.83	55.33	45.63
18	28	2.5	0.04	4.5	323	0.13	26	55.79
27	29	1.5	0.04	4.5	323	0.33	33	55.52
20	30	1.5	0.07	4.5	323	0.293	19.53	71.36

4.5.2 The ANOVA results of the response surface method

The ANOVA results of the two metals (aluminum and mild steel) in alkaline and acid media (KOH, NaOH, H_2S0_4, and HCL) using leaves extract (*Aspilia africana*, *Chromolena odorata*,*Newbouldia leavis*, *Dennettia tripetala*, *Dialium guineense* and *Vitex doniana*) are displayed on Tables 4.81– 4.86 below. From the Tables, it was observed that the Model F-values ranging from 8.90 to 1.487E+006implies the model is significant. There is onlya 0.01% chance that an F-value this large could occur due to noise.Values of "Prob > F" less than 0.0500 indicate model terms are significant.In this case AB, AC, AD, BC, BD, CD, A^2, B^2 are significant model terms.Values greater than 0.1000 indicate the model terms are not significant. The "Pred

R-Squared" ranging from 0.7358 to 1.000 is in reasonable agreement with the "Adj R-Squared" ranging from 0.7922 to 1.000; i.e. the difference is less than 0.2. "Adeq Precision" measures the signal to noise ratio. A ratio greater than 4 is desirable. The ratio of 12.348 to 5264.68 indicates an adequate signal. These models can be used to navigate the design spaces.

Table 4.81: ANOVA for corrosion inhibition of Al in KOH using *Dennettia tripetala* leaves extract.

ANOVA for Response Surface Quadratic model
Analysis of variance table [Partial sum of squares - Type III]

Source	Sum of Squares	Df	Mean Square	F Value	p-value Prob > F	
Model	1443.15	14	103.08	8.90	< 0.0001	Significant
A-Acid/base conc.	*24.91*	*1*	*24.91*	*2.15*	*0.1633*	
B-Inhibitor conc.	*505.36*	*1*	*505.36*	*43.61*	*< 0.0001*	
C-Time	*348.16*	*1*	*348.16*	*30.05*	*< 0.0001*	
D-Temperature	*522.39*	*1*	*522.39*	*45.08*	*< 0.0001*	
AB	*0.36*	*1*	*0.36*	*0.031*	*0.8619*	
AC	*12.41*	*1*	*12.41*	*1.07*	*0.3172*	
AD	*9.41*	*1*	*9.41*	*0.81*	*0.3818*	
BC	*10.45*	*1*	*10.45*	*0.90*	*0.3574*	
BD	*2.38*	*1*	*2.38*	*0.21*	*0.6569*	
CD	*6.14*	*1*	*6.14*	*0.53*	*0.4779*	
A^2	*0.023*	*1*	*0.023*	*1.942E-003*	*0.9654*	
B^2	*0.74*	*1*	*0.74*	*0.064*	*0.8044*	
C^2	*0.20*	*1*	*0.20*	*0.018*	*0.8963*	
D^2	*0.091*	*1*	*0.091*	*7.855E-003*	*0.9306*	
Residual	173.81	15	11.59			
Lack of Fit	*40.96*	*10*	*4.10*	*0.15*	*0.9939*	*not significant*
Pure Error	*132.85*	*5*	*26.57*			
Cor Total	1616.96	29				
Std. Dev.	3.40	R-Squared		0.8925		
Mean	59.10	Adj R-Squared		0.7922		
C.V. %	5.76	Pred R-Squared		0.7358		
PRESS	427.21	Adeq Precision		12.348		
-2 Log Likelihood	137.84	BIC		188.86		
		AICc		202.12		

Table 4.82: ANOVA for corrosion inhibition of mild steel in NaOH using *Dennettia tripetala* leaves extract

ANOVA for Response Surface Reduced Quadratic model
Analysis of variance table [Partial sum of squares - Type III]

Source	Sum of Squares	df	Mean Square	F Value	p-value Prob > F	
Model	2815.35	12	234.61	20.77	< 0.0001	Significant
A-Acid conc	*29.48*	*1*	*29.48*	*2.61*	*0.1246*	
B-Inhibitor concentration	*838.75*	*1*	*838.75*	*74.24*	*< 0.0001*	
C-Time	*102.09*	*1*	*102.09*	*9.04*	*0.0080*	
D-Temperature	*5.41*	*1*	*5.41*	*0.48*	*0.4981*	
AB	*63.12*	*1*	*63.12*	*5.59*	*0.0303*	
AD	*224.55*	*1*	*224.55*	*19.88*	*0.0003*	
BD	*184.28*	*1*	*184.28*	*16.31*	*0.0009*	
CD	*1079.12*	*1*	*1079.12*	*95.52*	*< 0.0001*	
A^2	*118.31*	*1*	*118.31*	*10.47*	*0.0049*	
B^2	*57.82*	*1*	*57.82*	*5.12*	*0.0371*	
C^2	*57.82*	*1*	*57.82*	*5.12*	*0.0371*	
D^2	*164.89*	*1*	*164.89*	*14.60*	*0.0014*	
Residual	192.06	17	11.30			
Lack of Fit	*105.15*	*12*	*8.76*	*0.50*	*0.8464*	*not significant*
Pure Error	*86.91*	*5*	*17.38*			
Cor Total	3007.41	29				

Std. Dev.	3.36	R-Squared	0.9361
Mean	41.11	Adj R-Squared	0.8911
C.V. %	8.18	Pred R-Squared	0.7923
PRESS	624.64	Adeq Precision	18.378
-2 Log Likelihood	140.84	BIC	185.05
		AICc	189.59

Table 4.83: ANOVA for corrosion inhibition of mild steel in HCL using *Aspilia africana* leaves extract

ANOVA for Response Surface Reduced Quadratic model
Analysis of variance table [Partial sum of squares - Type III]

Source	Sum of Squares	df	Mean Square	F Value	p-value Prob > F	
Model	1820.57	5	364.11	126.35	< 0.0001	Significant
A-Acid conc	*55.94*	*1*	*55.94*	*19.41*	*0.0002*	
B-Inhibitor concentration	*981.25*	*1*	*981.25*	*340.49*	*< 0.0001*	
C-Time	*536.19*	*1*	*536.19*	*186.06*	*< 0.0001*	
D-Temperature	*223.26*	*1*	*223.26*	*77.47*	*< 0.0001*	
C^2	*23.93*	*1*	*23.93*	*8.30*	*0.0082*	
Residual	69.17	24	2.88			
Lack of Fit	*61.83*	*19*	*3.25*	*2.22*	*0.1925*	*not significant*
Pure Error	*7.34*	*5*	*1.47*			
Cor Total	1889.73	29				

Std. Dev.	1.70	R-Squared	0.9634
Mean	58.78	Adj R-Squared	0.9558
C.V. %	2.89	Pred R-Squared	0.9165
PRESS	157.74	Adeq Precision	41.353
-2 Log Likelihood	110.20	BIC	130.60

	AICc	125.85

Table 4.84: ANOVA for corrosion inhibition of Al in NaOH using *Dennettia tripetala* leaves extract.

ANOVA for Response Surface Quadratic model

Analysis of variance table [Partial sum of squares - Type III]

Source	Sum of Squares	df	Mean Square	F Value	p-value Prob>F	
Model	917.12	14	65.51	19.79	<0.0001	Significant
A-Acid/base conc.	*318.21*	*1*	*318.21*	*96.12*	*<0.0001*	
B-Inhibitor conc.	*165.53*	*1*	*165.53*	*50.00*	*<0.0001*	
C-Time	*43.44*	*1*	*43.44*	*13.12*	*0.0025*	
D-Temperature	*366.05*	*1*	*366.05*	*110.57*	*<0.0001*	
AB	*4.07*	*1*	*4.07*	*1.23*	*0.2850*	
AC	*1.056E-003*	*1*	*1.056E-003*	*3.190E-004*	*0.9860*	
AD	*1.36*	*1*	*1.36*	*0.41*	*0.5308*	
BC	*4.32*	*1*	*4.32*	*1.30*	*0.2714*	
BD	6.14	1	6.14	1.85	0.1934	
CD	*0.68*	*1*	*0.68*	*0.20*	*0.6577*	
A^2	*1.49*	*1*	*1.49*	*0.45*	*0.5122*	
B^2	*1.78*	*1*	*1.78*	*0.54*	*0.4752*	
C^2	*9.115E-003*	*1*	*9.115E-003*	*2.753E-003*	*0.9588*	
D^2	*5.48*	*1*	*5.48*	*1.66*	*0.2177*	
Residual	49.66	15	3.31			
Lack of Fit	*44.26*	*10*	*4.43*	*4.10*	*0.0664*	*not significant*
Pure Error	*5.40*	*5*	*1.08*			
Cor Total	966.78	29				

Std. Dev.	1.82	R-Squared	0.9486
Mean	54.74	Adj R-Squared	0.9007
C.V. %	3.32	Pred R-Squared	0.7283
PRESS	262.72	Adeq Precision	17.905
-2 Log Likelihood	100.26	BIC	151.27
		AICc	164.54

Table 4.85: ANOVA for corrosion inhibition of mild steel in H_2SO_4 using *Chromolena odorata* leaves extract

ANOVA for Response Surface Reduced Quadratic model
Analysis of variance table [Partial sum of squares - Type III]

Source	Sum of Squares	df	Mean Square	F Value	p-value Prob > F	
Model	2291.98	12	191.00	58.53	< 0.0001	Significant
A-Acid conc	*36.19*	*1*	*36.19*	*11.09*	*0.0040*	
B-Inhibitor concentration	*31.99*	*1*	*31.99*	*9.80*	*0.0061*	
C-Time	*221.37*	*1*	*221.37*	*67.84*	*< 0.0001*	
D-Temperature	*5.52*	*1*	*5.52*	*1.69*	*0.2107*	
AB	*198.46*	*1*	*198.46*	*60.82*	*< 0.0001*	
AC	*93.46*	*1*	*93.46*	*28.64*	*< 0.0001*	
AD	*1076.00*	*1*	*1076.00*	*329.76*	*< 0.0001*	
BC	*417.28*	*1*	*417.28*	*127.88*	*< 0.0001*	
BD	*67.28*	*1*	*67.28*	*20.62*	*0.0003*	
CD	*50.87*	*1*	*50.87*	*15.59*	*0.0010*	
A^2	*45.20*	*1*	*45.20*	*13.85*	*0.0017*	
C^2	*37.99*	*1*	*37.99*	*11.64*	*0.0033*	
Residual	55.47	17	3.26			
Lack of Fit	*50.87*	*12*	*4.24*	*4.61*	*0.0515*	*not significant*
Pure Error	*4.60*	*5*	*0.92*			
Cor Total	2347.46	29				

Std. Dev.	1.81	R-Squared	0.9764
Mean	56.79	Adj R-Squared	0.9597
C.V. %	3.18	Pred R-Squared	0.8874
PRESS	264.30	Adeq Precision	38.479
-2 Log Likelihood	103.58	BIC	147.79
		AICc	152.33

Table 4.86: ANOVA for corrosion inhibition of mild steel in HCL using *Newbouldia leavis* leaves extract

ANOVA for Response Surface Reduced Quadratic model
Analysis of variance table [Partial sum of squares - Type III]

Source	Sum of Squares	df	Mean Square	F Value	p-value Prob > F	
Model	2950.83	13	226.99	74.84	< 0.0001	significant
A-Acid conc	*37.38*	*1*	*37.38*	*12.32*	*0.0029*	
B-Inhibitor concentration	*184.76*	*1*	*184.76*	*60.92*	*< 0.0001*	
C-Time	*27.03*	*1*	*27.03*	*8.91*	*0.0087*	
D-Temperature	*448.68*	*1*	*448.68*	*147.94*	*< 0.0001*	
AB	*225.53*	*1*	*225.53*	*74.36*	*< 0.0001*	
AC	*25.58*	*1*	*25.58*	*8.43*	*0.0104*	
AD	*32.35*	*1*	*32.35*	*10.67*	*0.0049*	
BC	*774.09*	*1*	*774.09*	*255.23*	*< 0.0001*	
BD	*144.54*	*1*	*144.54*	*47.66*	*< 0.0001*	
A^2	*53.16*	*1*	*53.16*	*17.53*	*0.0007*	
B^2	*18.63*	*1*	*18.63*	*6.14*	*0.0247*	
C^2	*618.78*	*1*	*618.78*	*204.02*	*< 0.0001*	
D^2	*451.22*	*1*	*451.22*	*148.78*	*< 0.0001*	
Residual	48.53	16	3.03			
Lack of Fit	*31.84*	*11*	*2.89*	*0.87*	*0.6097*	*not significant*
Pure Error	*16.68*	*5*	*3.34*			
Cor Total	2999.35	29				

Std. Dev.	1.74	R-Squared	0.9838
Mean	58.97	Adj R-Squared	0.9707
C.V. %	2.95	Pred R-Squared	0.9439
PRESS	168.41	Adeq Precision	30.315
-2 Log Likelihood	99.56	BIC	147.18
		AICc	155.56

4.5.3 Model equations for the inhibition efficiency

The mathematical models for inhibition efficiency of the plant extracts as corrosion inhibitors of the metals in the alkaline and acid media are shown in equations (4.1) – (4.48). The models were obtained by employing RSM tools of designexpert software. Each model showed the relationship among the inhibition efficiency (IE), inhibitor concentration (A), temperature (T) and time (C). The mathematical models in terms of coded factors were obtained using the optimization tool of the RSM. The models in terms of coded factors predict the response for given levels of each factor.

The positive signs in the models signified synergistic effect, while the negative signs signified antagonistic effect. In all the models, the highest power of at least one of the variables is 2, which showed that the mathematical models are quadratic equations. The concentration (A), temperature (T) and time (C) were all significant terms of the models. Factors A and B were synergistic model terms because the coefficients have positive sign, while factor C is

antagonistic because the coefficient sign is negative. The model equations for the corrosion inhibition of aluminum in the alkaline and acid media, were displayed in equations 4.1- 4.24, the interactive behaviour between A and B was synergistic to the models because the coefficients of their products were positive; equations (4.1-4.8), (4.14 and 4.16), (4.19), (4.20), (4.23) and (4.24). The antagonistic equations are (4.15), (4.21), (4.9), (4.11) and (4.22). Mathematical models for the corrosion inhibition of mild steel in the alkaline and acid media are presented in equations (4.25) – (4.48). The interactive behaviour between the concentration (A) and time (C) was antagonistic to the models equations (4.27), (4.29), (4.30), (4.36-4.39) and (4.41 - 4.48). Furthermore, the synergistic equations are (4.40), (4.26), (4.34), (4.25), (4.28), (4.32) – (4.31). From the models, the concentration (A) was responsible for the quadratic form of the models. The equations showed that A and B were jointly responsible for the quadratic form of the models.

The general model equations with combined significant and insignificant terms are presented in equations (E1) – (E48) of Appendix E. Considering the significant terms, the modelequations for the corrosion inhibition of the metals presented in equations (4.1) – (4.48) were obtained by eliminating P-values > 0.05 as can be seen on the ANOVA Tables above. From the statistical analysis, there was only a 0.01% chance that large F-value could occur due to noise. Source of noise may be attributed to non-controlable factors of oxygen content and flow rates of the inhibitors' functional groups.

The model for the corrosion inhibition of Al in KOH by *Aspilia africana* leaves extract is;

$$IE=+420.30+11.10A+620.67B- 69.96C -0.99D+323.83A*B+6.05A*C -94.28B*C +0.18C*D -8.02A^2+8626.98B^2+0.56C^2 \quad (4.1)$$

The model for the corrosion inhibition of Al in NaOH by *Aspilia africana* leaves extract is;

$$IE=+254.09+132.12A-11983.12B+7.05C-0.46D-1.68A*C-0.37A*D+265.59B*C +33.43B*D -0.06C*D+0.38C^2 \quad (4.2)$$

The model for the corrosion inhibition of Al in H_2SO_4 by *Aspilia africana* leaves extract is;

$$IE=+707.43-102.40A-14691.79B+25.76C-2.05D-127.50A*B+4.064A*C+0.23A*D-137.76 B*C+50.19B*D-0.08C*D+3.94A^2 -8559.03B^2 \quad (4.3)$$

The model for the corrosion inhibition of Al in HCL by *Aspilia africana* leaves extract is; IE=+615.80+37.67A─501.71B─19.39C─3.22D+67.50A*B─0.05A*C─0.15A*D─10.38B*C+1.37B*D+0.06C*D+2.47A^2─300.00B^2─2.04C^2+4.78D^2 (4.4)

The model for the corrosion inhibition of Al in KOH by *Chromolena odorata* leaves extract is; IE=+29.98+123.72A+2677.90B─6.90C +0.26D+411.17A*B+7.87A*C ─0.44A*D ─63.67B*C ─10.98B*D+0.15C*D ─8.15A^2+9023.80B^2+0.24C^2 (4.5)

The model for the corrosion inhibition of Al in NaOH by *Chromolena odorata* leaves extract is;IE=+4313.70─226.46A+818.07B+56.87C─26.47D─257.67A*B─2.12A*C+0.80A*D+80.19B*C─0.15C*D+11299.20B^2─0.39C^2 +0.04D^2 (4.6)

The model for the corrosion inhibition of Al in H_2SO_4 by *Chromolena odorata* leaves extract is; IE=+541.39─17.79A─14047.70B+30.73C─1.55D+4.10A*C─158.00B*C+47.07B*D─0.087C*D─5019.44B^2 ─0. (4.7)

The model for the corrosion inhibition of Al in HCL by *Chromolena odorata* leaves extract is; IE=+3521.89+30.43A+6073.81B─ 9.85C─22.14D+6.99A*C ─94.47B*C ─14.92B*D ─20.02A^2 ─10784.13B^2+0.035D^2 (4.8)

The model for the corrosion inhibition of Al in KOH by *Newbouldia leavis* leaves extract is; IE=+2645.01─512.18A─629.21B─80.59C─12.33D─88.50A*B─4.61A*C+1.68A*D+122.00B*C+0.26C*D+3319.04B^2─0.49C^2+0.01D^2 (4.9)

The model for the corrosion inhibition of Al in NaOH by *Newbouldia leavis* leaves extract is; IE=─84.91+21.41A─5935.78B+56.96C+0.35D+299.58A*B─5.15A*C+17.23B*D─0.15C*D─5.48A+0.20C (4.10)

The model for the corrosion inhibition of Al in H_2SO_4 by *Newbouldia leavis* leaves extract is; IE=─6213.70+42.411A+7688.41B+10.76C+37.59D+279.00A*B─5.20A*C─51.28B*C─24.28B*D─6.92A^2─0.056D^2 (4.11

The model for the corrosion inhibition of Al in HCL by *Newbouldia leavis* leaves extract is; IE= ─3995.23─82.21A─1411.52B+210.17C+22.17D─138.33A*B+2.47A*C+0.18A*D+7.62B*D ─0.62C*D+5.26A^2 ─8430.55B^2 ─1.33C^2 ─0.299D^2 (4.12)

The model for the corrosion inhibition of Al in KOH by *Dennettia tripetala* leaves extract is; IE= +186.884 +2.037A +305.917B +2.5317C ─ 0.466D. (4.13)

The model for the corrosion inhibition of Al in NaOH by *Dennettia tripetala*leaves extract is; IE = +64.794─7.282A + 175.083B─0.896C +0.390D (4.14)

The model for the corrosion inhibition of Al in H_2SO_4 by *Dennettia tripetala* leaves extract is; IE =+9741.47+337.008A─2518.30B+73.44C─61.96D+573.25A*B+5.58A*C─1.08A*D+164.13B*C+6.12B*D ─ 0.324C*D ─ 9.002A^2 ─ 8924.53B^2 +3.059C^2 + 0.099D^2 (4.15)

The model for the corrosion inhibition of Al in HCl by *Dennettia tripetala* leaves extract is; IE = +1904.69+854.94A - 828.622B - 15.460D +560.86AB - 2.69AD+0.03022D^2 (4.16)

The model for the corrosion inhibition of Al in KOH by *Dialium gunineense* leaves extract is; IE=+356.31+70.39A─10317.58B+0.77C─1.11D─457.83A*B─104.71B*C+34.68B*D─17.06A^2 +0.26C^2 (4.17)

The model for the corrosion inhibition of Al in NaOH by *Dialium gunineense* leaves extract is;

$IE=-2429.37+56.34A+10451.02B+14.42C+13.67D-175.91A*B-2.10A*C-0.31A*D-84.35B*C-27.52B*D+23.23A^2-11272.68B^2-0.98C^2-0.02D^2$ (4.18)

The model for the corrosion inhibition of Al in H_2SO_4 by *Dialium gunineense* leaves extract is;

$IE=-1838.11+173.18A-5680.33B+49.14C+10.93D+258.17A*B-4.15A*C-0.39A*D+18.71B*D-0.11C*D-13.77A^2-7870.37B^2-0.70C^2-0.016D^2$ (4.19)

The model for the corrosion inhibition of Al in HCL by *Dialium gunineense* yleaves extract is;

$IE=+1858.82+86.12A+4602.10B+76.25C-13.21D-1.94A*C-0.43A*D-18.05B*D-0.21C*D+23.15A^2+23518.98B^2-0.59C^2+0.02D^2$ (4.20)

The model for the corrosion inhibition of Al in KOH by *Vitex doniana* leaves extract is;

$IE=+1475.08-156.22A+5231.50B-12.21C-8.29D+289.67A*B+0.43A*D+126.47B*C-18.91B*D+4.25A^2-311.51B^2+1.01C^2+0.01D^2$ (4.21)

The model for the corrosion inhibition of Al in NaOH by *Vitex doniana* leaves extract is;

$IE=-1567.81-311.76A-4219.69B-59.63C+12.78D+643.00A*B+3.76A*C+0.85A*D+134.67A*C+6.68B*D+0.16C*D-4.76A^2+8032.47B^2-0.35C^2-0.023D^2$ (4.22)

The model for the corrosion inhibition of Al in H_2SO_4 by *Vitex doniana* leaves extract is;

$IE=+2441.37-220.64A+11259.24B-24.98C-15.03D-0.62A*D-152.21B*C-35.40B*D+0.062C*D+6.59A^2+10440.28B+1.100C^2+0.024D^2$ (4.23)

The model for the corrosion inhibition of Al in HCL by *Vitex doniana* leaves extract is;

$IE=+400.21-306.62A+5965.18B-65.59C-0.59D+972.67A*B+2.14A*C+0.57A*D-24.69B*D+0.17C*D+21.60A^2+10327.77B^2+0.94C^2$

(4.24)

The model for the corrosion inhibition of mild steel in KOH by *Aspilia africana* leaves extract is:

$IE=+414.51-98.50A-637.19B-61.76C-0.80D+480.833A*B+2.27A*C+0.15C*D+20.97A^2+0.99C^2$ (4.25)

The model for the corrosion inhibition of mild steel in NaOH by *Aspilia africana* leaves extract is;IE=+2349.01−57.77A−554.27B−7.69C−13.95D+397.33A*B+13.96A^2+0.72C^2+0.02D^2(4.26)

The model for the corrosion inhibition of mild steel in H_2SO_4 by *Aspilia africana* leaves extractis;IE=−1287.41+11.62A+1403.72B+44.60C+7.28D−380.75A*B+1.50A*C+117.73B*C −0.13C*D−13075.00B^2 −0.71C^2−0.01D^2 (4.27)

The model for the corrosion inhibition of mild steel in HCL by *Aspilia africana* extract is; IE=−68.22+3.05A+426.28B+0.02C+0.30D+0.29C^2 (4.28)

The model for the corrosion inhibition of mild steel in KOH by *Chromolena odorata* leaves extractis;IE=+607.53+209.51A−7663.49B+141.18C−2.08D−0.64A*D+19.86B*D−0.43C*D+1 223.25B^2(4.29)

The model for the corrosion inhibition of mild steel in NaOH by *Chromolena odorata* leaves extractis;IE=+1584.66+205.34A−8677.31B+142.51C−11.45D−164.83A*B−0.69A*C+22.63B* D−0.46C*D+5.68A^2+16864.81B^2+0.42C^2+0.02D^2 (4.30)

The model for the corrosion inhibition of mild steel in H_2SO_4 by *Chromolena odorata* leaves extract,is;IE=−3832.91+206.88A+2295.94B−48.59C+23.13D+254.58A*B+2.27A*C−0.66A*D − 134.50B*C −5.01B*D+0.19C*D−4.48A^2−3826.39B^2 −1.37C^2 −0.03D^2 (4.31)

The model for the corrosion inhibition of mild steel in HCL by *Chromolena odorata* extract is; IE=−3461.82+150.15A−3678.03B−19.73C+21.39D+253.00A*B+3.20A*C−0.54A*D−200.76 B*C+11.20B*D+0.09C*D +9252.38B^2− 1.08C^2−0.03D^2 (4.32)

The model for the corrosion inhibition of mild steel in KOH by *Newbouldia leavis* leaves extractis;IE=−475.06−2987.36B+141.65C+1.61D+8.66B*D−0.43C*D−0.34C^2(4.33)

The model for the corrosion inhibition of mild steel in NaOH by *Newbouldia leavis* leaves extract

is;IE=+201.30+282.83A─4918.38B+142.41C─3.82D─311.92A*B─2.98A*C─0.83A*D+12.60B*D─0.44C*D+4.64A^2+12940.28B^2+0.30C^2+0.01D^2

(4.34)

The model for the corrosion inhibition of mild steel in H_2SO_4 by *Newbouldia leavis* leaves extract is; IE=─85.64+148.17B+1.71C+0.42D─0.29C^2 (4.35)

Tnhe model for the corrosion inhibition of mild steel in HCL by *Newbouldia leavis* extract is; IE=─4230.51+79.53A─6138.62B+21.78C+26.25D+500.58A*B+1.44A*C─0.28A*D─264.97B*C+20.03B*D ─ 5.56A^2+3662.50B^2─1.55C^2 ─0.04D^2(4.36)

The model for the corrosion inhibition of mild steel in KOH by *Dennettia tripetala* leaves extract is;IE=+558.32+178.16A─8729.76B+150.15C─1.93D─0.55A*D+23.10B*D─0.46C*D+12470.37B^2 (4.37)

The model for the corrosion inhibition of mild steel in NaOH by *Dennettia tripetala* leaves extractis;IE=+1896.19+229.90A─7820.96B+146.13C─13.56D─264.83A*B─0.95A*B─0.75B*D +22.62B*D ─0.47C*D+8.31A^2+6452.78B^2+0.47C^2+0.02D^2 (4.38)

The model for the corrosion inhibition of mild steel in H_2SO_4 by *Dennettia tripetala* leaves extract

is;IE=+2502.53+19.96A─3844.93B─13.93C+16.28D+454.58A*B─229.71B*C+13.32B*D+0.10C*D─1.07C^2 ─0.03D^2(4.39)

The model for the corrosion inhibition of mild steel in HCL by *Dennettia tripetala* leaves extract is;IE=─3510.09+159.93A─3911.93B─17.55C+21.63D+253.00A*B+2.92A*C─0.57A*D─191.23B*C+12.03B*D+0.09C*D─0.03A^2+8275.92B^2─1.08C^2─0.03D^2 (4.40)

The model for the corrosion inhibition of mild steel in KOH by*Dialium guineense* leaves extract is;IE=─2756.77─14.97A+637.59B+10.86C+16.61D─2.95A*C─127.48B*C─0.03D^2 (4.41)

The model for the corrosion inhibition of mild steel in NaOH by *Dialium guineense* leaves extractis;IE=+2550.66─286.91A─3916.83B+14.94C─13.97D+116.58A*B─2.30A*C+097A*D ─138.07B*C+16.09B*D─6.61A^2─9525.46B^2─0.49C^2+0.02D^2 (4.42)

The model for the corrosion inhibition of mild steel in H_2SO_4 by *Dialium guineense* leaves extractis;IE=─3403.40─107.82A+1870.91B─7.06C+21.91D─560.83A*B+3.30A*C+0.40A*D+ 43.47B*C─4.48A^2─13997.62B^2─0.04D^2
(4.43)

The model for the corrosion inhibition of mild steel in HCL by*Dialium guineense* extract is; IE=─4843.86─93.91A+6584.18B─2.36C+30.11D─937.41A*B+3.51A*C+0.37A*D+42.69B*C ─10.19B*D─25130.09B^2─0.63C^2─0.05D^2 (4.44)

The model for the corrosion inhibition of mild steel in KOH by *Vitex doniana* leaves extractis;IE=772.54─107.20A+2680.03B─58.62C+6.15D+356.42A*B+1.54A*C+0.28A*D+42. 65B*C ─9.49B*D+0.18C*D ─4141.67B^2─0.58C^2 ─0.011D^2 (4.45)

The model for the corrosion inhibition of mild steel in NaOH by *Vitex doniana* leaves extract is;IE=─1636.73─114.77A+5645.72B─18.73C+10.60D+296.83A*B─1.99A*C+0.38A*D─2.14 B*C─16.26C*D+0.11A^2 ─9961.11B^2 ─1.34C^2 ─0.02D^2
(4.46)

The model for the corrosion inhibition of mild steel in H_2SO_4 by *Vitex doniana* leaves extract is;IE=─2692.00+129.66A─742.18B+82.64C+14.86D+258.58A*B─2.02A*C─0.31A*D+72.35 B*C ─0.25C*D ─10.77A^2 ─0.02D^2
(4.47)

The model for the corrosion inhibition of mild steel in HCL by *Vitex doniana* extract is;

$$IE=-3939.07+129.44A-5959.93B+68.9C+23.33D+241.17A*B-2.44A*C-0.27A*D+76.86B*C+14.92B*D-0.19C*D-15.58A^2+4681.48B^2-0.43C^2-0.03D^2 \quad (4.48)$$

4.5.4 Graphical analysis of the inhibition efficiency, IE (%), using RSM

The graphical analysis or 3-D surface plots was employed in this work to determine the relationship between the factors (time, temperature, inhibitor and acid/alkaline concentrations) and response (inhibition efficiency) using design expert 10.0 software. The 3-D surface plot of the inhibition efficiency of the various inhibitors or plant extracts (*Aspilia africana*, *Chromolena odorata*, *Newbouldia leavis*, *Dennettia tripetala*, *Dialium guineense* and *Vitex doniana*) with the metals (aluminum and mild steel) in different aggressive environments (KOH, NaOH,H_2SO_4 and HCl) were presented in Figures 4.9 – 4.15. The remaining graphs of similar trends are presented in Appendix F1 –F8. Plots of predicted values versus actual experimental values were used to test the significance of the models. In all the cases studied, the predicted versus actual plots gave linear relationshionship indicating the actual experimental values is in consistent with the predicted. Corrosion inhibition of the metals (Al and mild steel) in various media (NaOH, KOH, HCl and H_2SO_4) with various concentrations of the plants extracts (*Aspilia african*, *Chromolena odorata*, *Newbouldia leavis*, *Dennettia tripetala*, *Dialium guineense* and *Vitex doniana*) showed that increase in concentration increases the inhibition efficiency. However, inhibition efficiency reduces as temperature increases. These observations are in agreement with previous studies of El Ouariachi *et al.*, 2010;Ndibe *et al.*, 2011; Abdulwahab *et al.*, 2012. The graphs of the inhibition efficiency versus concentration, temperature and time are in quadratic forms. Analysis of variance, mathematical model equations and optimization (sections 4.2, 4.4 and 4.5) were also used to elucidate more on the inhibition efficiency. The analysis of variance helped in identifying the models significance terms. The powers of the variables were used to confirm the quadratic models. The graphs displayed the inhibition efficiency of the plant extracts as a function of factors of acid/alkaline concentration, inhibitor concentration, temperature and time. The interactive behaviour of the acid/alkaline concentration,inhibitor concentration, temperature and time were also identified.

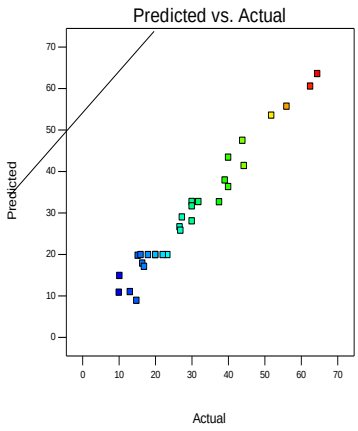

(a)

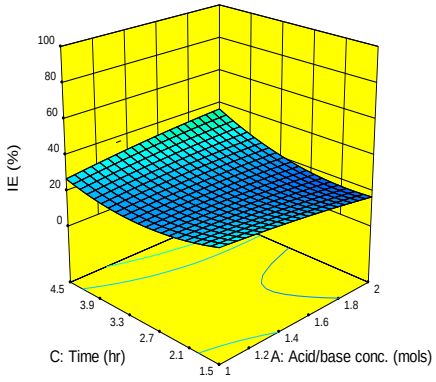

(b)

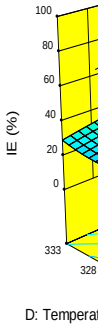

(c)

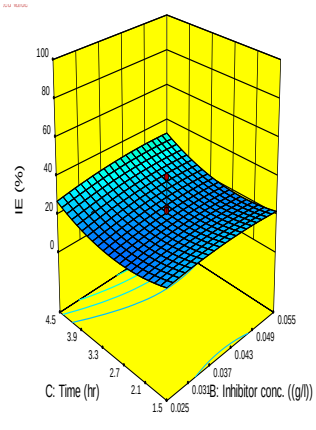

(d)

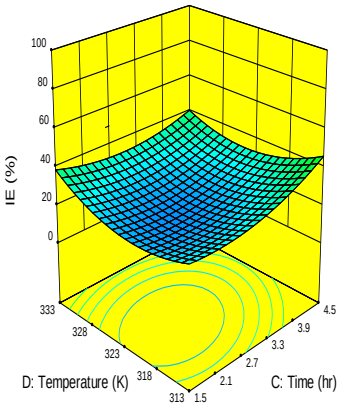

(e)

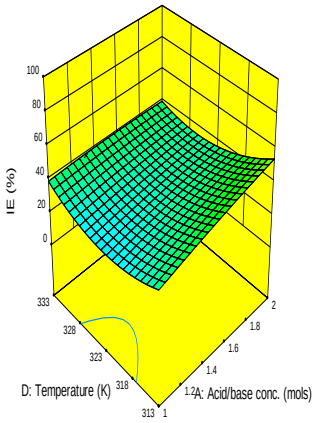

(f)

Fig 4.9 (a-f): IE (%) of *Dennetia tripetala* leaves extract as corrosion inhibitor of Al in H_2SO_4. (a) Predicted versus Actual IE (%), b) IE (%) versus time and acid concentration (c)IE (%) versus temperature and inhibitor concentration. (d)IE (%) versus temperature and time, (e) IE

(%) versus time and inhibitor concentration. (F) IE (%) versus temperature and acid/base concentration.

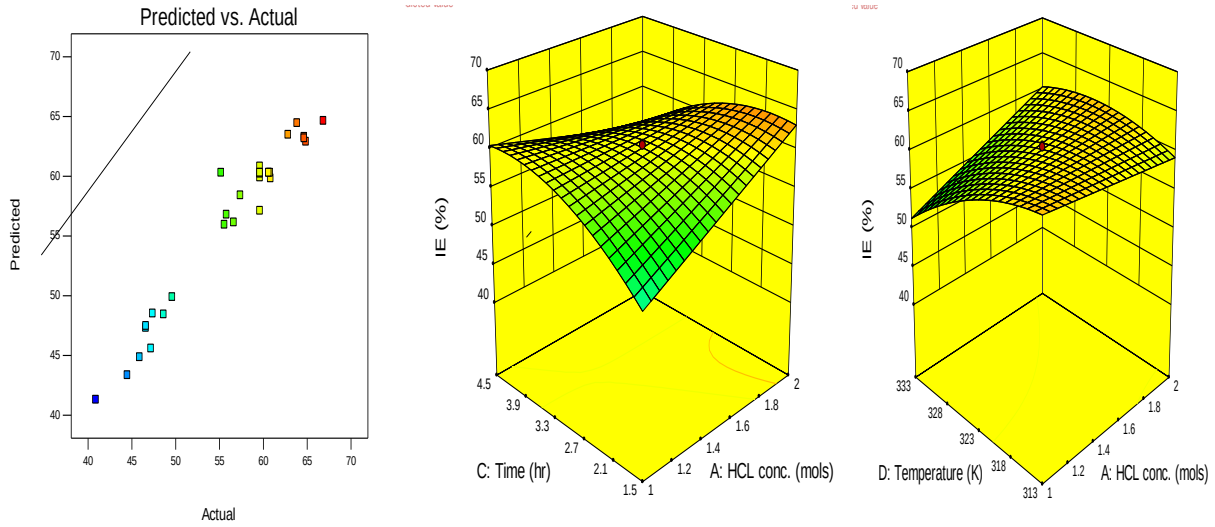

(a) (b) (C)

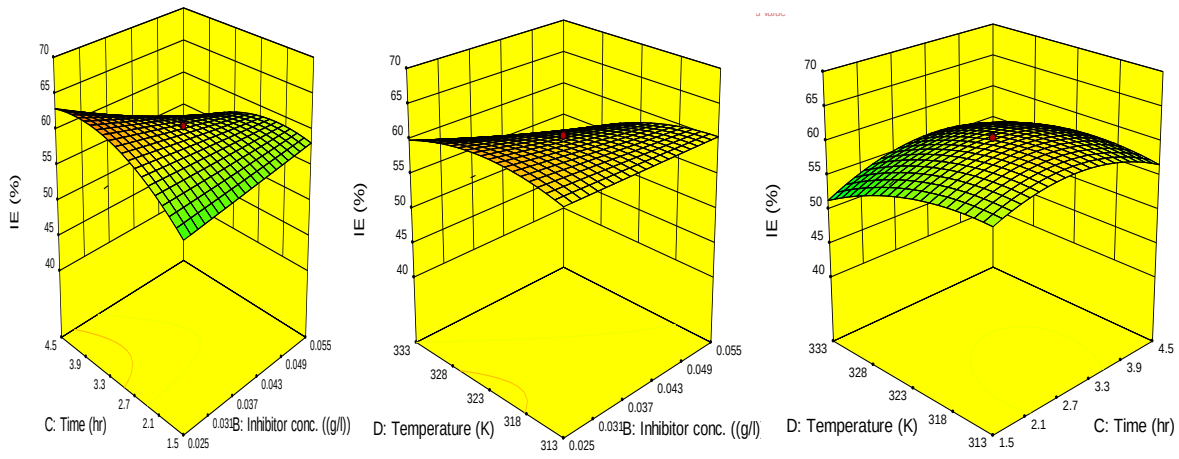

(d) (e) (f)

Fig 4.10 (a-f): IE (%) of *Dennetia tripetala* leaves extract as corrosion inhibitor of mild steel in HCl.

a) Predicted versus Actual (b) IE (%) versus time and acid concentration. (c) IE (%) versus temperature and acid concentration. (d) IE (%) versus time and inhibitor concentration. (e) IE (%) versus temperature and inhibitor concentration. (f) IE (%) versus time and inhibitor concentration.

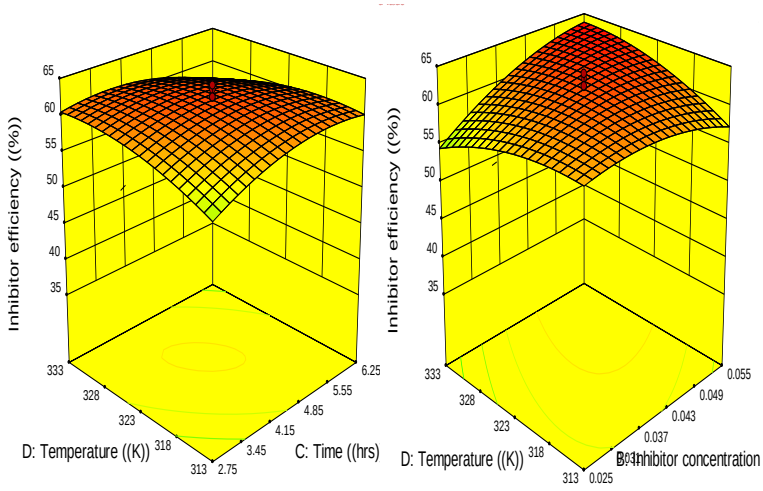

(a) (b)

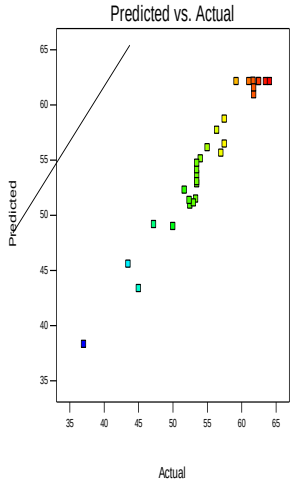

(c)

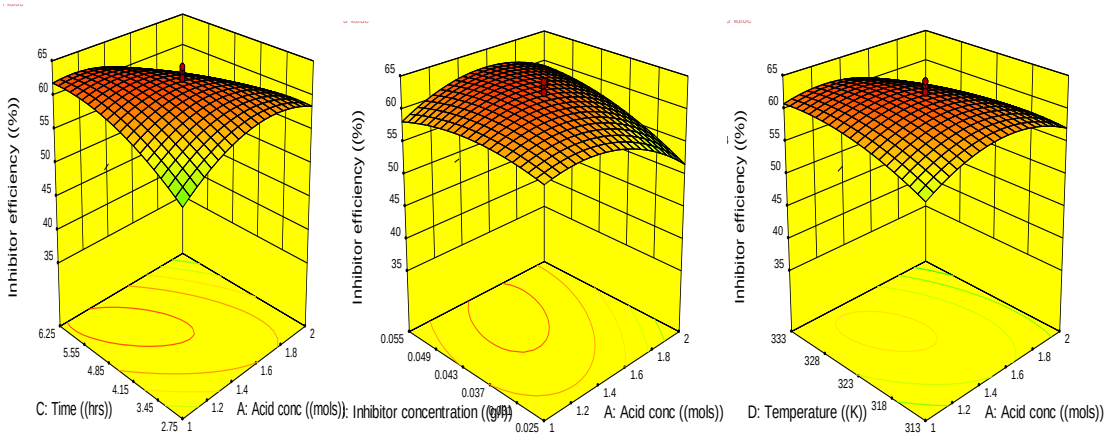

(d) (e) (f)

Fig 4.11(a-f): IE (%) of *Dialium guineense* leaves extract as corrosion inhibitor of Al in H_2SO_4.
a) IE (%) versus time and temperature. b) IE (%) versus temperature and inhibitor concentration (c) Predicted versus Actual (d) IE (%) versus time and acid concentration. (e) IE (%) versus acid concentration and acid concentration (f) IE (%) versus temperature and acid concentratio

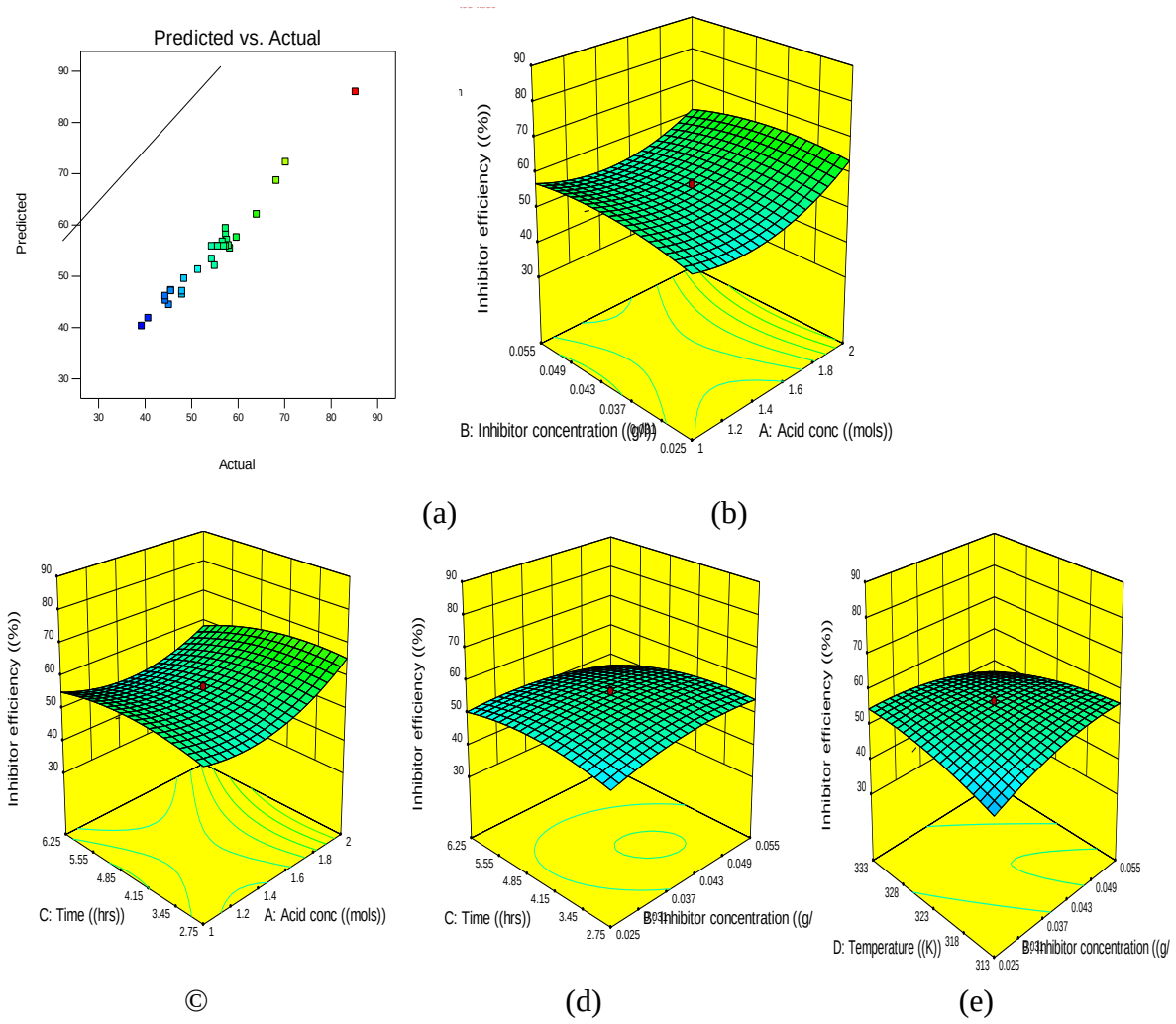

Fig 4.12(a-e): IE (%) of *Aspilia africana* leaves extract as corrosion inhibitor of Al in KOH.
(a) Predicted versus Actual (b) IE (%) versus inhibitor concentration and acid concentration.
(c) IE (%) versus time and acid concentration. (d) IE (%) versus time and inhibitor concentration.
(e) IE (%) versus temperature and inhibitor concentration.

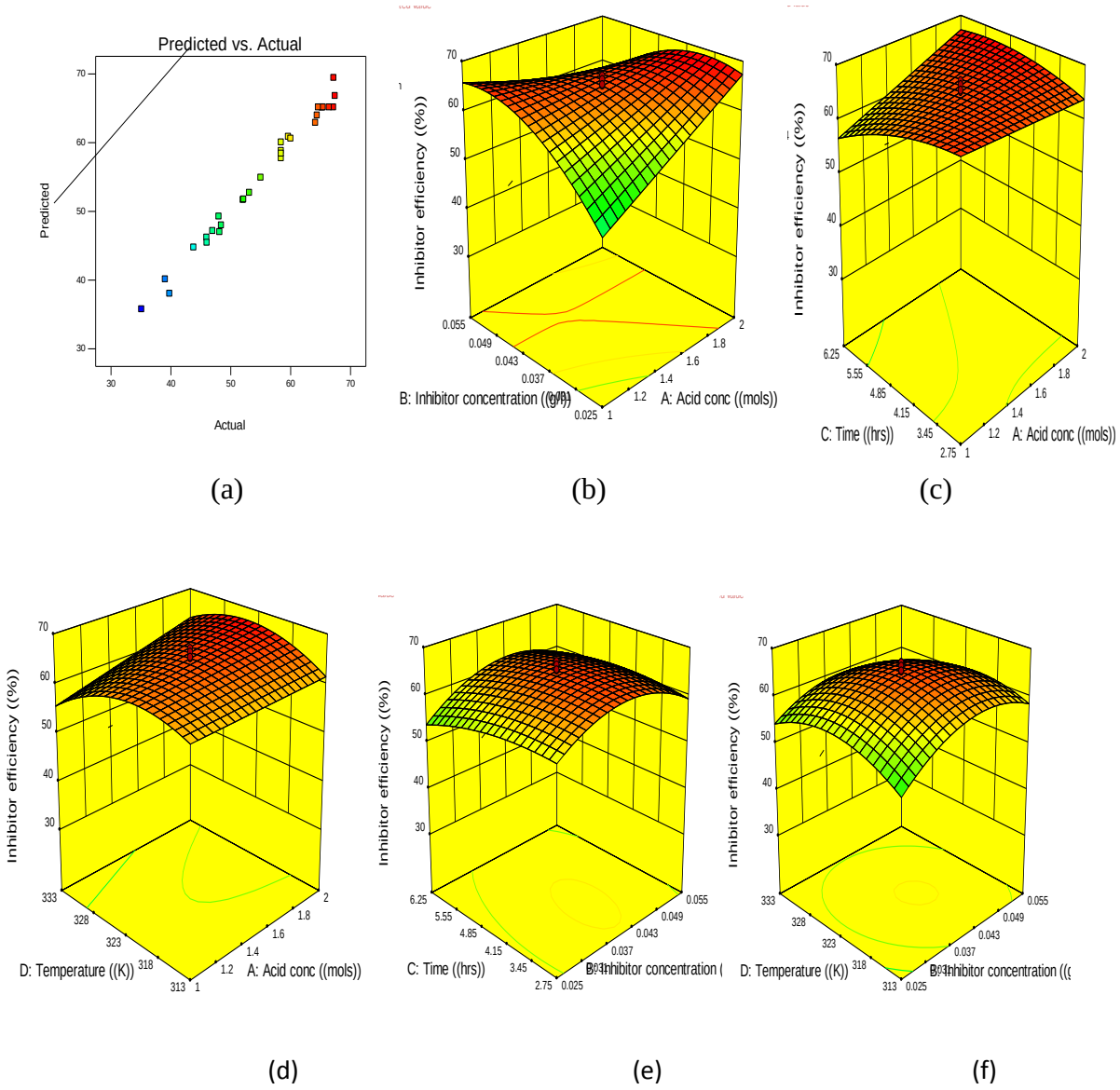

(a) (b) (c)

(d) (e) (f)

Fig 4.13(a-f): IE (%) of *Newbouldia leavis* leaves extract as corrosion inhibitor of mild steel in HCl.

a) Predicted versus Actual (b) IE (%) versus inhibitor concentration and acid concentration. (c) IE (%) versus time and acid concentration. (d) IE (%) versus temperature and acid concentration. (e) IE (%) versus time and inhibitor concentration. (f) IE (%) versus temperature and inhibitor concentration.

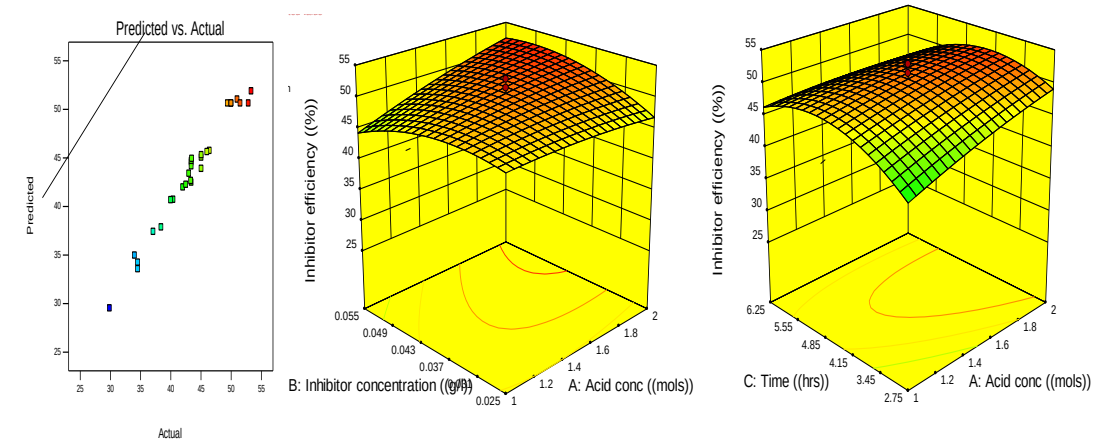

(a) (b) (c)

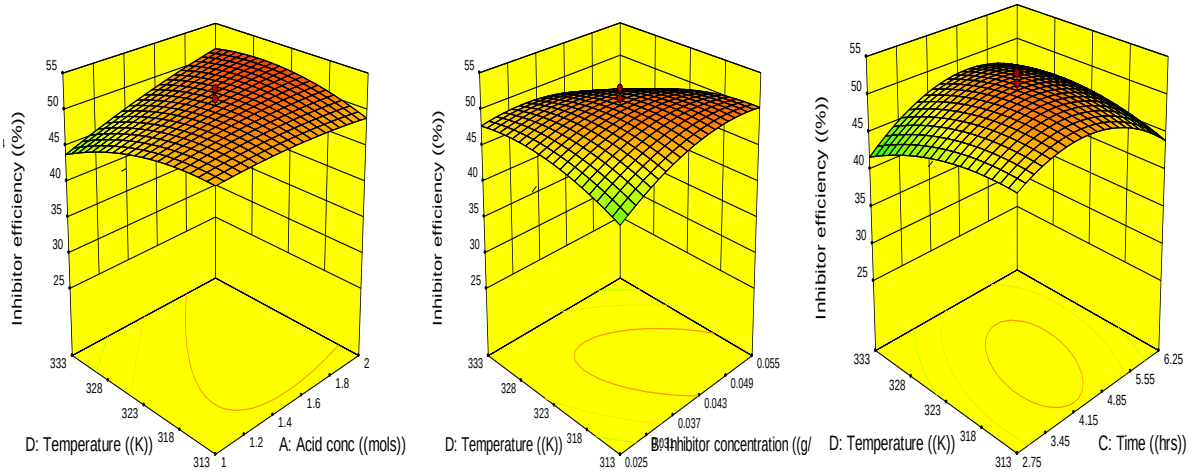

(d) (e) (f)

Fig 4.14(a-f): IE (%) of *Vitex doniana* leaves extract as corrosion inhibitor of mild steel in NaOH.

(a) Predicted versus Actual (b) IE (%) versus inhibitor concentration and acid concentration.

(c) IE (%) versus time and acid concentration. (d) IE (%) versus temperature and acid concentration. (e) IE (%) versus temperature and inhibitor concentration. (f) IE (%) versus time and temperature.

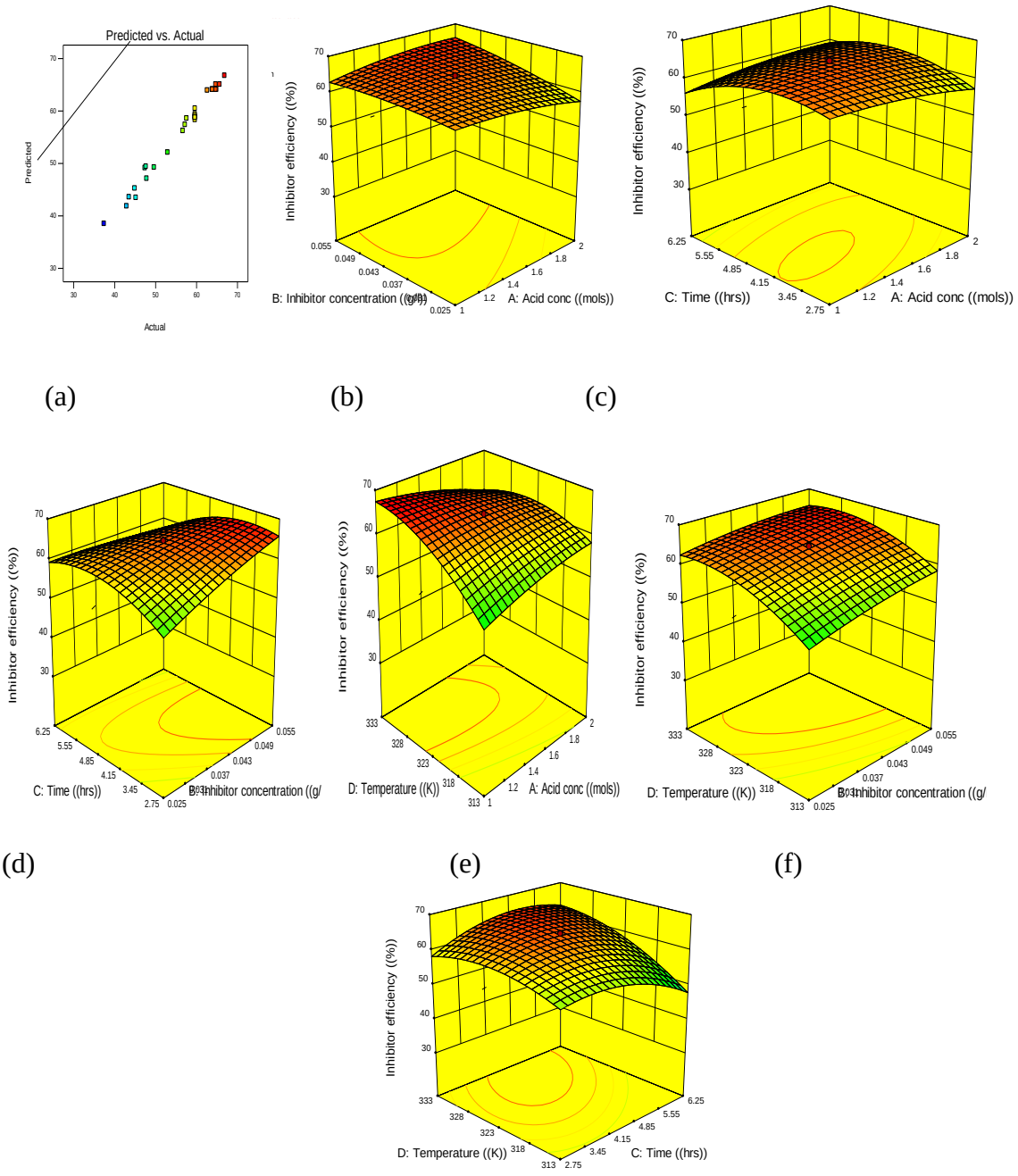

(a) (b) (c)

(d) (e) (f)

(g)

Fig 4.15(a-f): IE (%) of *Chromolena odorata* leaves extract as corrosion inhibitor of mild steel in H_2SO_4

(a) Predicted versus Actual (b) IE (%) versus inhibitor concentration and acid concentration. (c) IE (%) versus time and acid concentration. (d) IE (%) versus time and inhibitor concentration. (e) IE (%) versus temperature and acid concentration. (f) IE (%) versus temperature and inhibitor concentration. (g) IE (%) versus time and temperature.

4.5.5 Optimum conditions for the corrosion inhibition of metals

The Tables 4.87 and 4.88 display the optimum inhibitor concentration, optimum temperature, optimum time and optimum inhibition efficiency for each metal in each medium. Comparative analysis of the optimum inhibition efficiencies of various plant extracts show that *Vitex doniana* leaves extracts have the inhibition efficiency of 72.423% (with optimum inhibitor concentration of 0.055g/l, temperature of 333.00K and time of 6.250h) for the corrosion inhibition of Al in NaOH. Also, *Dennettia tripetala*, *Newbouldia leavis* and *Aspilia africana* extracts have the same inhibition efficiency of 83.67% (with optimum inhibitor concentration of 0.055g/l, temperature of 333K and time of 2.750h) for the corrosion inhibition of MS in KOH. At these optimum conditions, Dennettia tripetala, *Newbouldia leavis* and *Aspilia africana* leave extracts can be used interchangeably in H_2SO_4medium.

For aluminium in the alkaline and acid media, the optimum inhibition efficiency ranged from 42.13% to 82.93% (Table 4.88), that of mild steel ranged from 31.00% to 75.041% (Table 4.88). The optimum inhibition efficiency of the extracts of *Aspilia africana* leaf, *Chromolena odorata*,*Newbouldia leavis*, *Dennetia tripetala*, *Dialium guineeense*and *Vitex doniana* ranged from 50.07% to 83.37%, 48.22% to 78.29%, 48.820% to 82.96%, 31.00% to 85.26% and 44.20% to 78.61% (Tables 4.87 and 4.88) respectively. These high values of inhibition efficiency indicate that the plant extracts are good for surface treatment of metals in corrosion control operations.

Table 4.87 Optimum conditions for corrosion inhibition of Al in acid/base using various leaves extracts.

Media	Inhibitor (plant extract)	acid/alkaline (mols)	inhibitor conc. (g/l)	temperature (K)	time (hr)	inhibition efficiency (%)
HCl	AspiliaAfricana leaves	1.000	0.025	333.000	6.250	67.258
H_2SO_4		2.000	0.025	313.000	6.250	69.702
KOH		1.000	0.055	313.000	2.750	70.910
NaOH		2.000	0.025	313.000	2.750	73.188
HCl	*Chromolena odorata* leaves	1.000	0.055	313.000	2.750	76.405
H_2SO_4		2.000	0.025	313.000	6.250	70.201
KOH		2.000	0.055	313.000	2.750	75.344
NaOH		2.000	0.025	333.000	2.750	75.013
HCl	*Newbouldia leavis* leaves	1.000	0.055	333.000	2.750	82.926
H_2SO_4		2.000	0.055	323.000	2.750	68.496
KOH		2.000	0.025	333.000	2.750	72.830
NaOH		1.000	0.025	313.000	6.250	66.319
HCl	*Dennettia tripetala* leaves	1.491	0.025	313.000	1.502	42.13
H_2SO_4		2.000	0.055	313.000	4.500	53.223
KOH		2.000	0.055	313.000	4.500	73.184
NaOH		1.000	0.055	333.000	1.500	66.349
HCl	*Dialium guineense* leaves	2.000	0.055	313.000	2.750	74.063
H_2SO_4		1.455	0.051	323.011	4.299	62.399
KOH		1.000	0.055	333.000	2.750	70.064
NaOH		2.000	0.055	313.000	2.750	68.686
HCl	*Vitex*	1.000	0.025	333.000	6.250	77.075
H_2SO_4	*Doniana*	2.000	0.025	333.000	6.250	70.054
KOH	Leaves	2.000	0.055	313.000	6.250	73.529
NaOH		2.000	0.055	333.000	6.250	72.423

Table 4. 88 Optimum conditions for corrosion inhibition of mild steel in acid/base using various leaves extracts.

Media	Inhibitor (plant extract)	acid/alkaline (mols)	inhibitor conc. (g/l)	time (hr)	temperature (K)	Inhibition efficiency (%)
HCl	*Aspilia africana* leaves	1.000	0.055	6.250	333.000	71.608
H_2SO_4		2.000	0.055	6.250	333.000	67.984
KOH		1.000	0.025	2.750	313.000	59.271
NaOH		1.000	0.025	2.750	333.000	50.073
HCl	*Chromolena odorata* leaves	1.000	0.055	2.750	333.000	71.609
H_2SO_4		1.000	0.025	6.250	333.000	66.776
KOH		1.000	0.025	2.750	333.000	48.224
NaOH		2.000	0.025	6.250	313.000	63.069
HCl	*Newbouldia leavis* leaves	2.000	0.055	2.750	333.000	75.041
H_2SO_4		1.000	0.055	2.750	333.000	64.226
KOH		1.500	0.029	5.920	316.481	48.820
NaOH		2.000	0.025	6.250	313.000	62.683
HCl	*Dennettia tripetala* leaves	1.000	0.055	2.750	333.000	71.408
H_2SO_4		2.000	0.055	2.750	333.000	70.312
KOH		1.000	0.025	6.250	313.000	48.716
NaOH		1.000	2.000	0.025	6.250	31.00
HCl	*Dialium guineense* leaves	1.015	0.050	3.771	318.680	67.954
H_2SO_4		1.000	0.055	2.750	313.000	64.693
KOH		1.000	0.025	6.250	333.000	44.201
NaOH		1.122	0.027	5.733	314.972	50.257
HCl	Vitex Doniana Leaves	1.000	0.025	2.750	333.000	66.109
H_2SO_4		1.000	0.025	2.750	333.000	70.661
KOH		1.985	0.052	5.878	326.922	46.420
NaOH		*1.957*	*0.042*	*4.481*	*324.519*	52.140

4.5.6 Validation of results

To confirm the validity of the results, additional experiments were conducted. The chosen conditions for the concentration, temperature and time are listed in Tables 4.89 and 4.90, along with the predicted and measured inhibition efficiencies. As shown in the tables, the measured inhibition efficiencies were close to the predicted values. It shows that RSM approach was appropriate for optimizing the corrosion inhibition process.

Table 4.89 Result validation for corrosion inhibition of Al in acid/base using various leaves extracts.

Media	Inhibitor (plant extract)	Acid/alkaline (mols)	inhibitor conc. (g/l)	temperature (K)	time (hr)	Predicted inhibition efficiency (%)	Measured inhibition efficiency (%)	Percentage error (%)
HCl	*Aspilia africana* leaves	1.000	0.025	333.000	6.250	67.25	68.10	1.25
HCl		2.000	0.025	313.000	6.250	69.70	70.13	0.61
H_2SO_4		1.000	0.055	313.000	2.750	70.91	71.50	0.85
KOH		2.000	0.025	313.000	2.750	73.18	74.01	1.12
NaOH	*Chromolena odorata* leaves	1.000	0.055	313.000	2.750	76.41	77.23	1.06
HCl		2.000	0.025	313.000	6.250	70.20	70.85	0.92
H_2SO_4		2.000	0.055	313.000	2.750	75.34	76.12	1.02
KOH		2.000	0.025	333.000	2.750	75.61	76.43	1.07
NaOH	*Newbouldia leavis* leaves	1.000	0.055	333.000	2.750	82.93	84.70	2.09
HCl		2.000	0.055	323.000	2.750	68.50	69.10	0.91
H_2SO_4		2.000	0.025	333.000	2.750	72.83	72.84	0.01
KOH		1.000	0.025	313.000	6.250	66.32	67.30	1.46
NaOH	*Dennettia tripetala* leaves	1.491	0.025	313.000	1.502	42.83	43.13	0.70
HCl		2.000	0.055	313.000	4.500	53.22	54.05	1.54
H_2SO_4		2.000	0.055	313.000	4.500	73.47	74.18	1.00
KOH		1.000	0.055	333.000	1.500	66.41	67.15	1.10
NaOH	*Dialium guineense* leaves	2.000	0.055	313.000	2.750	74.76	75.03	0.36
HCl		1.455	0.051	323.011	4.299	62.80	63.51	0.01
H_2SO_4		1.000	0.055	333.000	2.750	70.06	72.15	0.04
KOH		2.000	0.055	313.000	2.750	68.69	69.11	0.61
NaOH	*Vitex doniana* leaves	1.000	0.025	333.000	6.250	77.32	79.08	0.22
HCl		2.000	0.025	333.000	6.250	70.35	71.05	0.99
H_2SO_4		2.000	0.055	313.000	6.250	73.53	73.54	0.01
KOH		2.000	0.055	333.000	6.250	72.42	73.23	0.11
NaOH		1.000	0.025	333.000	6.250	67.86	68.34	0.71

Table 4.90 Result validation for corrosion inhibition of mild steel in acid/base using various leaves extracts.

Media	Inhibitor (plant extract)	Acid/alkaline (mols)	inhibitor conc. (g/l)	temperature (K)	time (hr)	Predicted inhibition efficiency (%)	Measured inhibition efficiency (%)	Percentage error (%)
HCl	*Aspilia africana* leaves	1.000	0.055	333.000	6.250	71.61	72.15	0.75
H_2SO_4		2.000	0.055	313.000	6.250	67.98	68.42	0.64
KOH		1.000	0.025	313.000	2.750	59.27	60.13	0.14
NaOH		1.000	0.025	313.000	2.750	50.97	51.55	0.11
HCl	*Chromolena odorata* leaves	1.000	0.055	313.000	2.750	71.61	72.45	0.12
H_2SO_4		1.000	0.025	313.000	6.250	66.78	67.34	0.83
KOH		1.000	0.025	313.000	2.750	48.22	49.00	0.16
NaOH		2.000	0.025	333.000	2.750	63.87	64.24	0.56
HCl	*Newbouldia leavis* leaves	2.000	0.055	333.000	2.750	75.75	76.04	0.38
H_2SO_4		1.000	0.055	323.000	2.750	64.23	65.10	0.13
KOH		1.500	0.029	333.000	2.750	48.88	49.08	0.41
NaOH		2.000	0.025	313.000	6.250	62.68	63.19	0.81
HCl	*Dennettia tripetala* leaves	1.000	0.055	313.000	1.502	71.41	72.38	0.13
H_2SO_4		2.000	0.055	313.000	4.500	70.31	71.09	0.11
KOH		1.000	0.025	313.000	4.500	48.72	49.66	0.18
NaOH		1.000	2.000	333.000	1.500	31.00	32.01	0.32
HCl	*Dialium guineense* leaves	1.015	0.050	313.000	2.750	67.95	68.45	0.73
H_2SO_4		1.000	0.055	323.011	4.299	64.69	65.12	0.66
KOH		1.000	0.025	333.000	2.750	44.20	45.04	0.18
NaOH		1.122	0.027	313.000	2.750	50.26	51.19	0.18
HCl	*Vitex doniana* leaves	1.000	0.025	333.000	6.250	66.11	67.01	0.13
H_2SO_4		1.000	0.025	333.000	6.250	70.66	71.53	0.12
KOH		1.985	0.052	313.000	6.250	46.42	47.21	0.17
NaOH		1.957	0.042	333.000	6.250	52.08	52.14	0.12

4.6 Electrochemical Measurements

It has been established that corrosion reaction is an electrochemical process and therefore, electrochemical methods are most suitable for obtaining detailed mechanistic insights into the corrosion process. Tests to determine the inhibiting influence of the *Aspilia africana*, *Chromolena odorata*, *Newbouldia leavis*, *Dennettia tripetala*, *Dialium guineense* and *Vitex doniana* extracts on the electrochemical corrosion behavior of mild steel and aluminum in 1 M HCl, 1 M H_2SO_4, 1 M NaOH and 1 M KOH were performed using different concentrations of *Aspilia africana*, *Chromolena odorata*, *Newbouldia leavis*, *Dennettia tripetala*, *Dialium guineense* and *Vitex doniana*.

4.6.1 Potentiodynamic polarization measurements (PDP)

4.6.1.1 Potentiodynamic polarization measurements for mild steel

(a) Using *Dialium guineense* as inhibitor in the absence and presence of HCl and H_2SO_4.

Polarization measurements were performed to distinguish the effect of*Dialium guineense* (A) on the anodic and cathodic reactions. Typical potentiodynamic polarization curves for mild steel in 1M HCl and 1 M H_2SO_4 containing different concentrations of *Dialium guineense* at 30^{o}C are shown in Fig.4.16(a & b). The corresponding electrochemical parameters such as corrosion potential (E_{corr}), corrosion current densities (I_{corr}), cathodic Tafel slopes (b_c) and anodic Tafel slopes (b_a) obtained from polarization curves are presented in Table 4.91. The mild steel specimen is seen to exhibit active dissolution with no distinctive transition to passivation within the studied potential range. Careful scrutiny of the polarization curves in 1 M HCl environment (Fig. 4.16a) and 1 M H_2SO_4(Fig. 4.16b), indicates that the presence of *Dialium guineense* shifts the cathodic and anodic parts towards lower current densities in each case. The addition of *Dialium guineense* into the aggressive solutions has no significant effect on the corrosion potential (E_{corr}). If the displacement in E_{corr} is greater than 85 mV we could classify the inhibitor as anodic or cathodic and if the displacement is less than 85 mV the inhibitor may be seen as a mixed type which is in line with Chidiebere, *et al,* 2015. Results presented in Table 4.91 indicate that the maximum displacement in E_{corr} value in the studied environments was not up to 85 mV, therefore, *Dialium guineense* is regarded as a mixed-type inhibitor. Results in Table 4.91, show that the corrosion current density decreased considerably in the presence of the inhibitor

compared to the uninhibited solution and also decreased with an increase in the concentration of the extract.The inhibition efficiency was determined using the equation 3.15. In 1 M HCl the highest inhibition efficiency was 85.3% while in 1 M H_2SO_4 we have 84.2% at a concentration of 1000 mg/L at 30 ±1^{o}C.

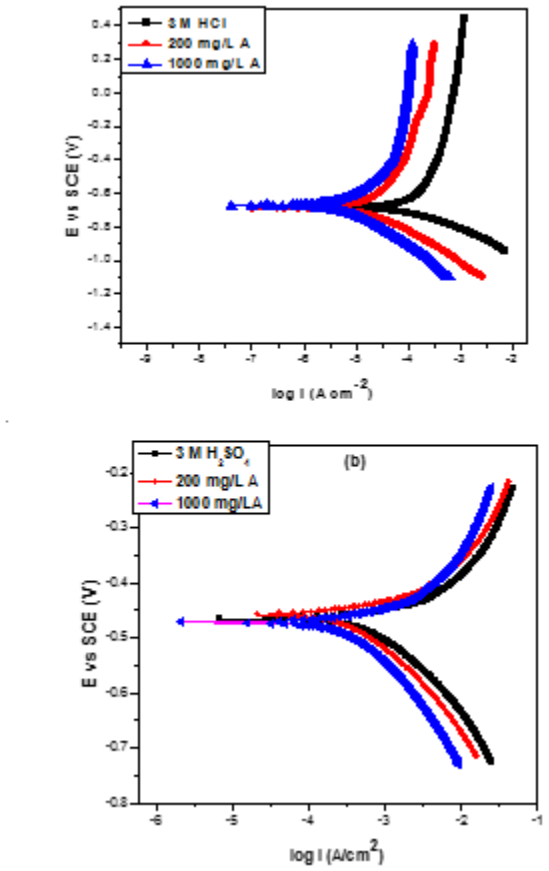

Fig 4.16**.** Potentiodynamic polarization curves for mild steel in: (a) 1 M HCl and (b) 1 M H_2SO_4 in the presence and absence of different concentrations of*Dialium guineense* extracts.

(b) Using *Dialium guineense* as inhibitor in the absence and presence of NaOH and KOH.

Polarization experiments were carried out potentiodynamically in unstirred NaOH/KOH environments in the absence and presence of*Dialium guineense*, in order to determine the effect of the inhibitor on the anodic and cathodic half reactions. From the polarization curves shown in Fig. 4.17, it is clear that the mild steel show active dissolution with no sign of transition to passivation in the aggressive solution. The electrochemical parameters, namely, the corrosion potential (E_{corr}), corrosion current densities (I_{corr}), the cathodic (b_c) and anodic (b_a) current values

obtained from polarization curves are presented in Table 4.92. Close inspection of the plot in Fig. 4.17, reveals that increase in the concentration of *Dialium guineense* retards both the anodic dissolution of metal and the cathodic hydrogen evolution reaction, the shift of cathodic curves to areas of lower corrosion current values was well pronounced. The corrosion potential E_{corr} shifts was not significant enough either to the negative or noble direction. According to literature [33] if the displacement of E_{corr} is greater than 85 mV as mentioned before we may say that the inhibitor is cathodic or anodic type, but from our results E_{corr} values ranges from 15 mV to 53 mV, therefore *Dialium guineense* can be regarded as a mixed- type inhibitor in these environments under study. This result agrees with Mistry *et al.*, 2012; Elmsellem *et al.*, 2014. Generally, the corrosion current density (I_{corr}) decreases with increase in *Dialium guineense* concentration (from 196.2 µA/cm^2 to 24.1 µA/cm^2). The values of the corrosion current density in the absence ($i_{corr,bl}$) and presence of the inhibitor ($i_{corr,inh}$) were used to estimate the inhibition efficiency from polarization data (IE %) as presented in equation 3.15.The obtained values are presented in Table 4.92. The maximum inhibition efficiency obtained for *Dialium guineense* in 1 M NaOH and 1 M KOH are 87.7% at 1000 mg/L *Dialium guineense* and 86.6% at 1000 mg/L*Dialium guineense*.

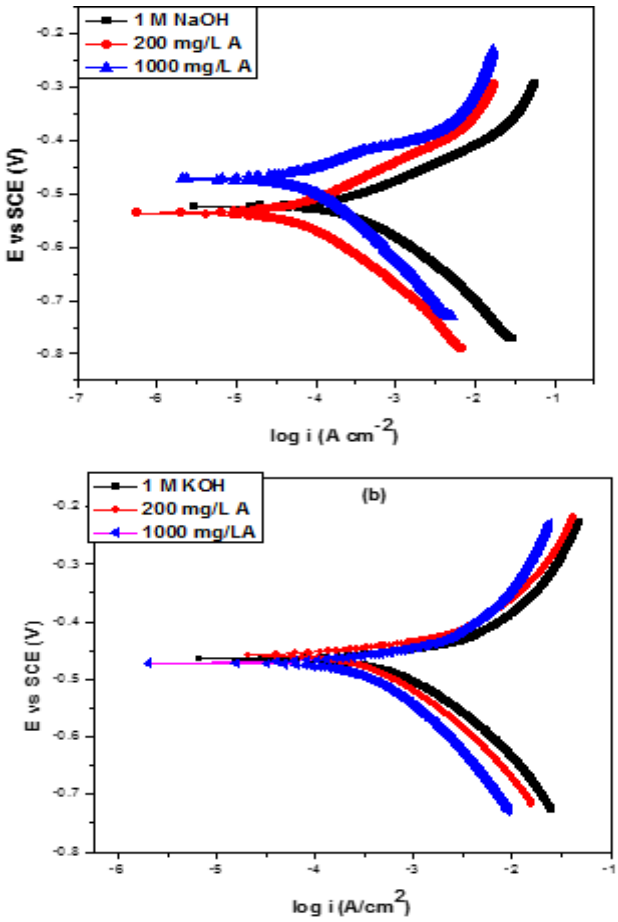

Fig. 4.17: Potentiodynamic polarization curves of mild steel in: (a) 1 M NaOH and (b) 1 M KOH in the absence and presence*Dialium guineense*.

© *Vitex doniana* (B) in the absence and presence ofHCl and M H_2SO_4

Polarization experiments were carried out to investigate the influence of *Vitex doniana* (B) on the anodic and cathodic half reactions of the corrosion process.Parts a and b of Fig 4.18show typical polarization curves for mild steel specimens in 1 M HCl and 1 M H_2SO_4, in the absence and presence of*Vitex doniana*. Accordingly, the mild steel specimen in both acidic environments shows active dissolution with no distinctive transition to passivation within the studied potential range. The obtained electrochemical parameters, namely, corrosion potential (E_{corr}), and corrosion current density (I_{corr}) were obtained and their values are presented in Table 4.91. The data presented therein reveals that in both acidic environments the I_{corr} decreases in the presence of the inhibitor compared to the uninhibited solution and the trend continues with an increase in the concentration of the inhibitor. In 1 M HCl and 1 M the polarization curves in presence of *Vitex doniana* (Fig. 4.18a and 4.19b) show evidence of inhibition. It is obvious that *Vitex doniana* has no significant effect on E_{corr} in each case, howeverH_2SO_4, a shift of both the

cathodic and anodic curves to lower corrosion current densities was observed and this effect becomes more significant with increasing *Vitex doniana* concentration in the studied environments and in line wth El Maghraby, 2009; Alinno and Ejikeme, 2012; Ghulamullah, *et al.,* 2015. The results obtained show that the rate of mild steel dissolution in 1 M HCl is higher than that in 1 M H_2SO_4.The observed differences in the polarization profiles in 1 M HCl and 1 M H_2SO_4solutions possibly suggest that the acid anions influenced the processes in different ways. The values of the corrosion current density in the absence and presence of *Vitex doniana* were used to determine the inhibition efficiency from polarization data using the formula stated earlier in equation 3.15. The values obtained are presented in Table 4.91. The observed reduction in anodic and cathodic corrosion current densities shows that the inhibitor reduced the mechanism of H_2 gas evolution reaction agrees with Ashassi-Sorkhabi *et al*, 2008 and also the anodic dissolution of mild steel. From our result, *Vitex doniana* is classed as a mixed-type inhibitor.

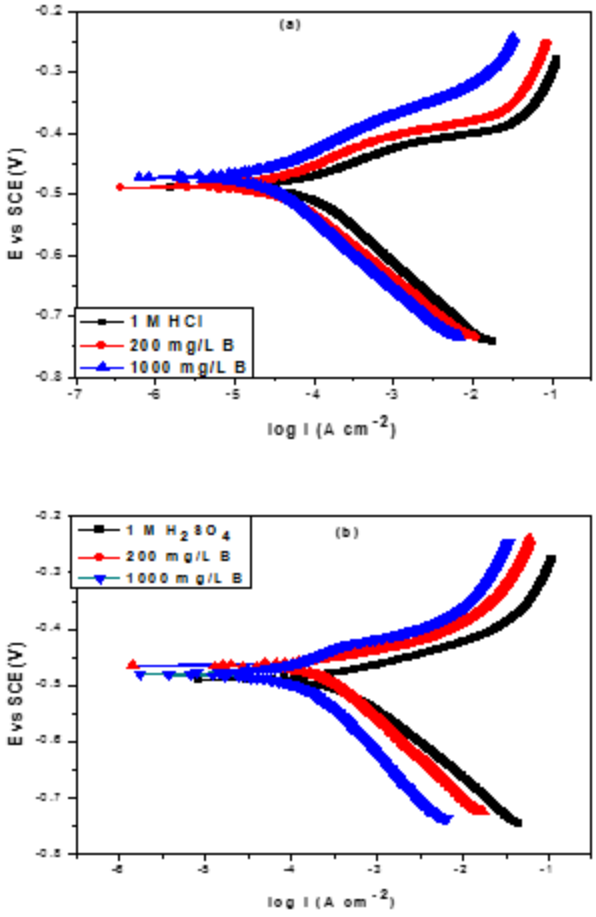

Fig 4.18. Potentiodynamic polarization curves for mild steel in: (a) 1 M HCl and (b) 1 M H_2SO_4 in the presence and absence of different concentrations of *Vitex doniana* extracts.

(d) *Vitex doniana*(B) in the absence and presence of KOH and NaOH

Fig 4.19shows a clear picture of a typical potentiodynamic polarization curves for mild steel specimens in the studied environments, in the absence and presence of *Vitex doniana*in the alkaline environments. The mild steel specimen displayed active dissolution with no distinctive transition to passivation within the studied potential range. This is in accordance with Ghulamullah, *et al.*, 2015. The corresponding electrochemical parameters, namely, corrosion potential (E_{corr}), corrosion current density (I_{corr}), anodic (b_a) and cathodic (b_c) Tafel slopes were obtained and their values are shown in Table 4.92. The data presented therein reveals that the I_{corr} decreased in the presence of *Vitex doniana* compared to the uninhibited solution and the trend

continued with an increase in the concentration of the inhibitor. Accordingly, the addition of *Vitex doniana* retarded the anodic metal dissolution process and cathodic H^+ ion reduction in this environment. This result conforms with Umoren, 2009; Chidiebere, 2012, but shows little or no effect on the E_{corr} values. Our obtained results reveal that *Vitex doniana* behaved as a mixed type inhibitor. The values of the corrosion current density in the absence and presence of the inhibitor were used to calculate the inhibition efficiency from polarization using equation 3.15. The obtained values presented in Table 4.92 reveal that efficiency of inhibition increased with an increase in *Vitex doniana* concentration.

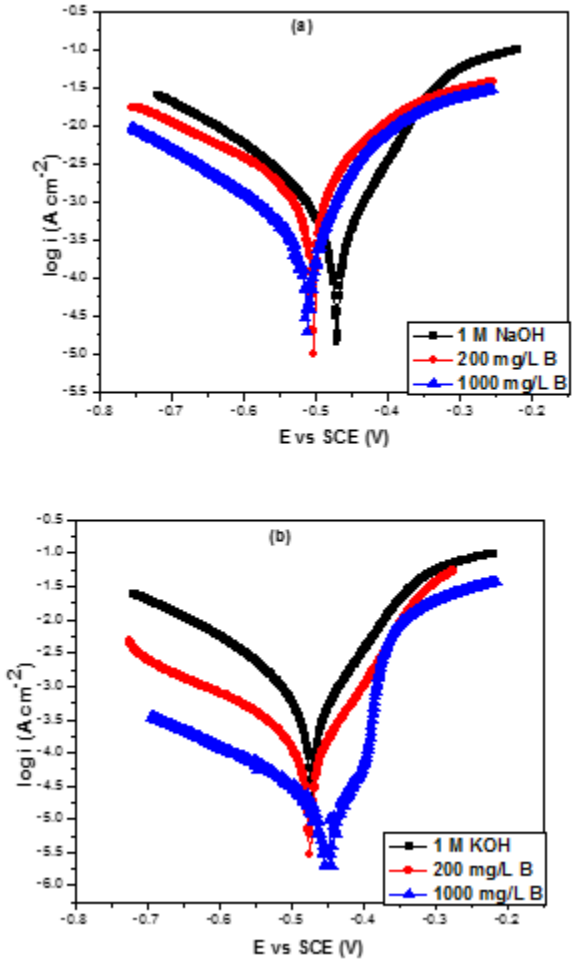

Fig 4.19**:** Potentiodynamic polarization curves of mild steel in: (a) 1 M NaOH and (b) 1 M KOH in the absence and presence *Vitex doniana*.

(e)*Newbouldia leavis*(C) in the absence and presence ofHCL and H_2SO_4

Tafel measurements were done to differentiate the influence of*Newbouldia leavis* (C) on the anodic and cathodic reactions. Typical Tafel plots for mild steel in 1 M HCl and 1 M H2SO4 comprising different concentrations of *Newbouldia leavis* at 30 ^{o}C are shown in Fig. 4.20. The equivalent electrochemical parameters such as corrosion potential (E_{corr}), corrosion current densities (I_{corr}), cathodic Tafel slopes (b_c) and anodic Tafel slopes (b_a) obtained from polarization curves are presented in Table 4.91. The mild steel specimen is seen to display active dissolution with no specific transition to passivation within the studied potential range. On careful examination of the polarization curves in 1 M HCl environment (Fig. 4.20a) and 1 M H_2SO_4(Fig. 4.20b), indicates that the presence of *Newbouldia leavis* shifts the cathodic and anodic parts towards lower current densities in each case. The addition of *Newbouldia leavis* into the aggressive solutions has no significant effect on the corrosion potential (E_{corr}). If the displacement in E_{corr} is greater than 85 mV we could classify the inhibitor as anodic or cathodic and if the displacement is less than 85 mV the inhibitor may be seen as a mixed type which is in line Chidiebere, *et al,* 2015; Refat and Ishaq 2013. Results presented in Table 4,91 indicate that the maximum displacement in E_{corr} value was not up to 85 mV, therefore, *Newbouldia leavis* is regarded as a mixed-type inhibitor.

Again, Table 4.91, show that the corrosion current density decreased significantly in the presence of the inhibitors when compared with free solutions. This can be attributed to an increase in the concentration of the extract which in line with Kotz and Treichel, 1996.The inhibition efficiency was determined using equation 3.15. In 1 M HCl the highest inhibition efficiency was 85.3% while in 1 M H_2SO_4 gave 84.2% at a concentration of 1000 mg/L at 30 ±1^{o}C.

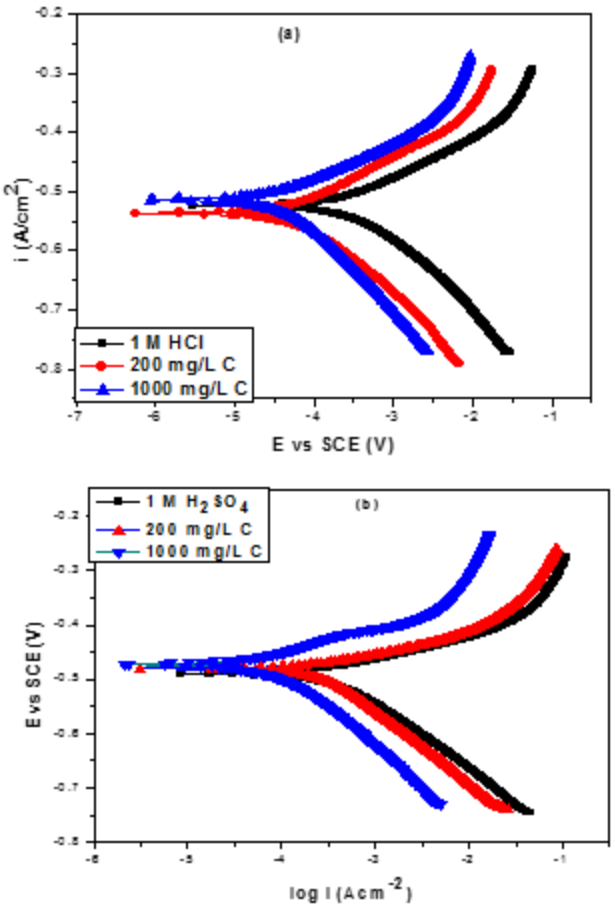

Fig 4.20: Potentiodynamic polarization for mild steel in: (a) 1 M HCl and (b) 1 M H_2SO_4 in the absence and presence of different concentration of*Newbouldia leavis*extract.

(f) *Newbouldia leavis* (C) in the absence and presence of KOH and NaOH

Fig. 4.21 shows typical anodic and cathodic potentiodynamic polarization curves of mild steel in 1 M NaOH and 1 M KOH in the absence and presence of *Newbouldia leavis*. As can be seen, both specimens exhibit a significant transition to passivation within the potential range investigated. Considering the similarity of the polarization curves for mild steel, one would expect similar corrosion mechanism for both specimens. Based on the electrochemical parameters presented in Table 4.92, it is clear that the mild steel specimen was more susceptible to corrosive attack in the uninhibited environment compared to inhibited one. This result is in line with (El Maghraby, 2009). This was evidenced by higher corrosion current (I_{corr}) values presented in the Table 4.90, showing that the anodic reaction increased and the cathodic hydrogen evolution reaction was slightly shifted to higher values. However, introduction of *Newbouldia leavis* reduced the corrosion current values in both aggressive environments. The

afore mentioned observations point towards the mild steel higher dissolution kinetics in the uninhibited solution compared to the inhibited environment. The polarization curves indicates that the anodic dissolution reaction was predominantly affected compared to the cathodic reaction which was less perturbed, similar results having been reported by Rethinnagiri, 2012. The increased number of active sites could be responsible for the observed increase in the kinetics of both partial reactions via formation of several electrochemical corrosion cells.

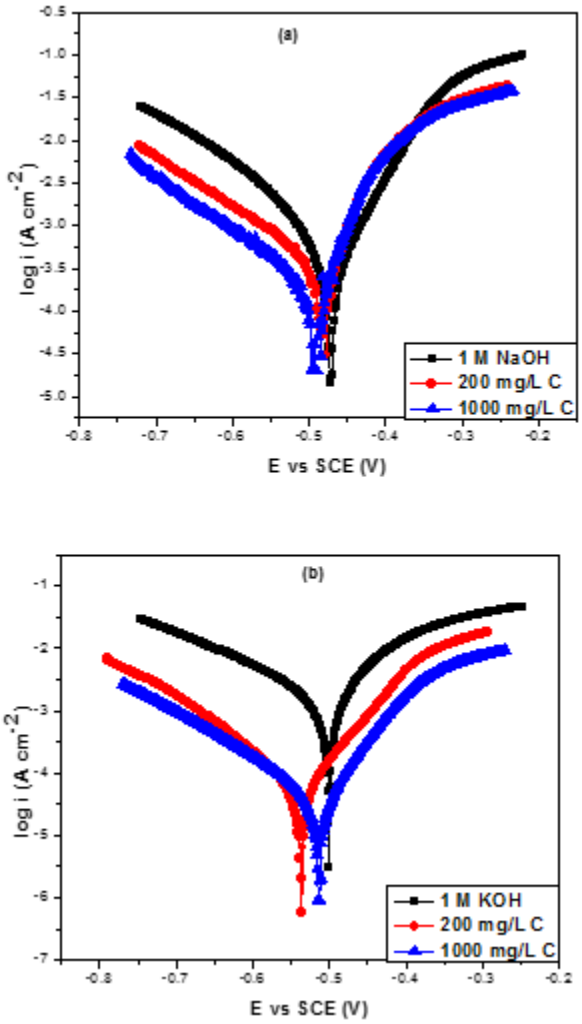

Fig 4.21: Potentiodynamic polarization curves of mild steel in: (a) 1 M NaOH and (b) 1 M KOH in the absence and presence *Newbouldia leavis*.

(g) *Aspilia africana*(D) in the absence and presence ofHCl and H_2SO_4

Potentiodynamic polarization experiments were performed to find out the effect of *Aspilia africana* on the anodic dissolution reaction of mild steel and cathodic hydrogen ion reduction. Typical potentiodynamic polarization plots for mild steel corrosion in (a) 1 M HCl and (b) 1 M

H_2SO_4in the absence and presence of *Aspilia africana* are given in Fig. 4.22, while the potentiodynamic polarization parameters derived from the polarization curves are shown in Table 4.91. The results show that *Aspilia africana* modified both the anodic and cathodic reactions, and displaced the corrosion potential (E_{corr}) slightly though not significant, towards cathodic values in 1 M HCl and slightly towards the anodic values in 1 M H_2SO_4 while reducing both the cathodic and anodic current densities as well as the reaction current density (i_{corr}), *Aspilia africana* thus functioned as a mixed-type corrosion inhibitor in both 1 M HCl and 1 M H_2SO_4. The inhibition efficiency (IE) from the potentiodynamic polarization experiments was quantified using the equation stated in 3.19 as can be seen in Nagm *et al.*, 2012a. From Table 4.91, *Aspilia africana* reduced the i_{corr} values from 336.9 µA/cm^2 in 1 M HCl to 48.5 µA/cm^2 on addition of 1000 mg/L of *Aspilia africana* ethanol extract. Also, the i_{corr} values reduced from 163.7 µA/cm² in 1 M H_2SO_4 to 10.6 µA/cm² on adding 1000 mg/L*Aspilia africana* ethanol extract indicating that the extract effectively reduced mild steel corrosion in both acid solutions. The results are in good agreement with that reported by Oguzie *et al*, 2012.

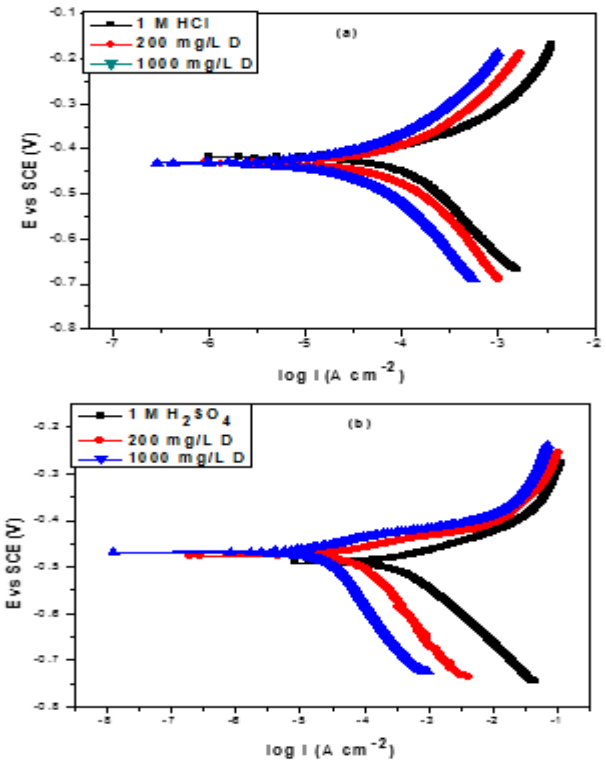

Fig 4.22: Potentiodynamic polarization for mild steel in: (a) 1 M HCl and (b) 1 M H_2SO_4 in the presence and absence of different concentration of *Aspilia africana* extracts.

(h) *Aspilia africana*(D) in the absence and presence ofKOH and NaOH

Comprehensive polarization studies were performed to provide an insight on the efficacy of *Aspilia africana* (D) on the anodic and cathodic half reactions. The potentiodynamic polarization curves for mild steel in 1 M NaOH and 1 M KOH containing different concentrations of *Aspilia africana* at 303 K are shown in Fig. 4.23a and 4.23b. The resulting electrochemical parameters viz corrosion potential (E_{corr}), corrosion current densities (I_{corr}), cathodic Tafel slopes (b_c) and anodic Tafel slopes (b_a) obtained from polarization curves are presented in Table 4.92. The substrate is seen to exhibit rapid dissolution with no sign of transition to passivation within the potential range studied. Careful scrutiny of the polarization curves in 1 M NaOH environment and 1 M KOH, indicates that the introduction of*Aspilia africana* moves the cathodic and anodic parts towards lower current densities in each case as reported by Siaka *et al.,*2012. The addition of *Aspilia africana* into the test solutions has no significant effect on the corrosion potential (E_{corr}). The results presented in Table 4.90 indicate that the highest displacement in E_{corr} value in the investigated environments was not up to 85 mV, for this reason,*Aspilia africana* is regarded as a mixed-type inhibitor.Furthermore, it was observed that the corrosion current density decreased considerably in the presence of *Aspilia africana* compared to the uninhibited solution The inhibition efficiency was determined using the equation in 3.15 as reported by Prathibha *et al.,*2012; Omotioma *et al* 2014.

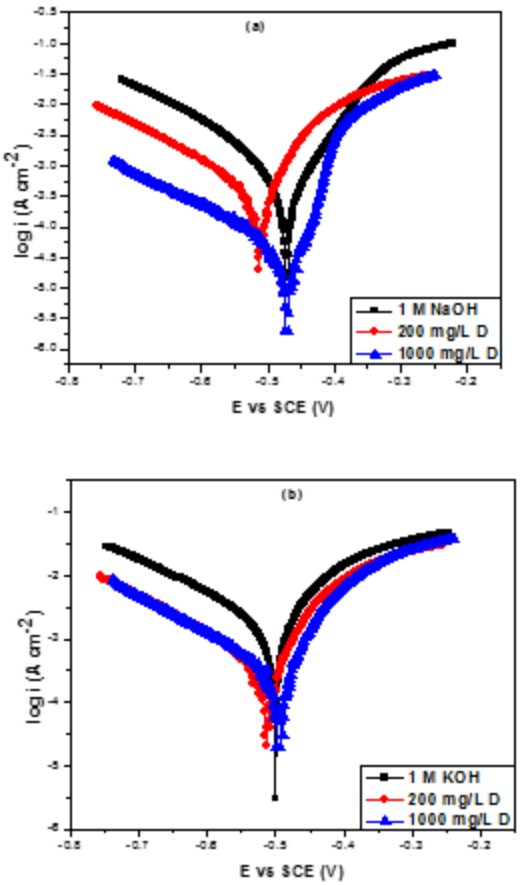

Fig 4.23: Potentiodynamic polarization curves of mild steel in: (a) 1 M NaOH and (b) 1 M KOH in the absence and presence Aspilia africana.

(i) *Dennettia tripetala*(E) in the absence and presence ofHCl and H_2SO_4

Investigation of the effect of Dennettia tripetala (E) on the anodic and cathodic partial reactions of the corrosion process was carried out. Fig 4.24 (a & b)indicate typical Tafel curves for mild steel specimens in 1 M HCl and 1 M H_2SO_4, in the absence and presence of *Dennettia tripetala*. The mild steel specimen in both acidic environments showed active dissolution with no sign of transition to passivation within the chosen potential range is in line with Omotioma *et al* 2014; Ambrish *et al.*, 2010. The corresponding electrochemical parameters, namely, corrosion potential (E_{corr}), corrosion current density (I_{corr}), anodic (b_a) and cathodic (b) Tafel slopes were obtained and their values are shown in Table 4.91. The data presented therein show that the I_{corr} decreased in the presence of *Dennettia tripetala* compared to the blank/uninhibited solution and the trend continued with an increase in the concentration of the inhibitor is similar to that reported by

Rajam *et al.*, 2012; Hany *et al* 2012. Showing that the inhibition is concentration dependent. Introduction of *Dennettia tripetala* into 1 M HCl environment slightly shifts E_{corr} values towards the anodic direction and the effect increases with an increase in the concentration of *Dennettia tripetala*, the same observation holds in 1 M H_2SO_4, E_{corr} shift towards the positive direction was quite negligible.

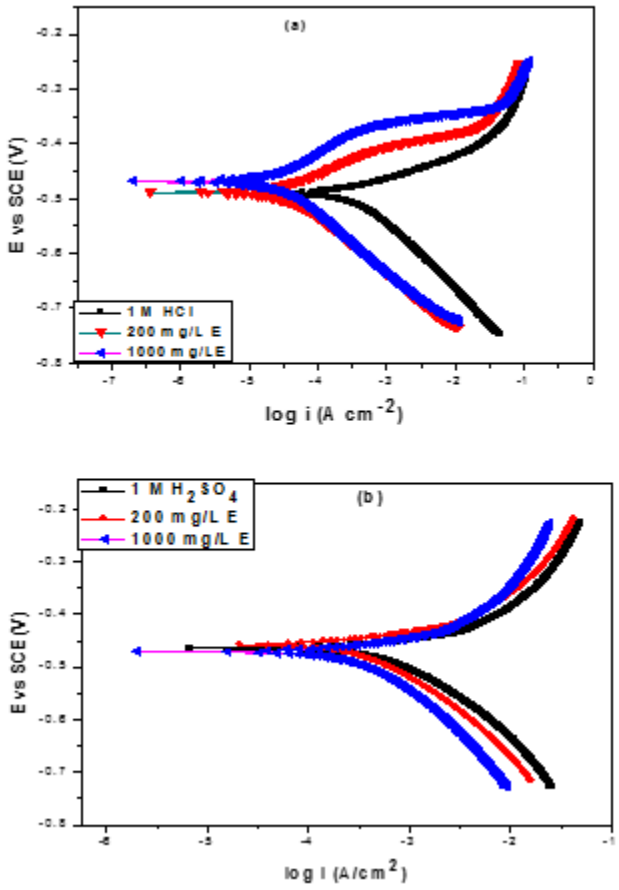

Fig 4.24**:** Potentiodynamic polarization for mild steel in: (a) 1 M HCl and (b) 1 M H_2SO_4 in the presence and absence of different concentration of *Dennettia tripetala* extracts.

(j) *Dennettia tripetala* (E) in the absence and presence of KOH and NaOH

Dennettia tripetala extracts was used to distinguish the anodic dissolution of mild steel and cathodic hydrogen ion reduction. Typical potentiodynamic polarization curves for mild steel in the absence and presence of *Dennettia tripetala* at different concentrations are presented in Fig. 4.25. The values of associated electrochemical parameters, i.e., corrosion potential (E_{corr}), corrosion current density (I_{corr}) and percentage inhibition efficiency IE (%) values were

calculated from polarization curves and listed in Table 4.92. The inhibition efficiency IE (%) was calculated from polarization measurements according to the relation given in equation 3.16. They are determined by extrapolation of potentiodynamic polarization lines to the respective corrosion potentials. Generally with increasing inhibitor concentration the corrosion current density and corrosion rate decreased. This is similar with the report of Buchweishaija, 2009. This shows that the level of adsorption to metal surface increases and protects mild steel from corrosion with increase in concentration of the *Dennettia tripetala*. The anodic curves in Fig. 4.25 (a&b) indicate that mild steel was in an active state at the corrosion potential. At higher concentration of *Dennettia tripetala*, we observed a pronounced decreased in the corrosion current. In the presence of higher concentration of *Dennettia tripetala* more of itsspecies will be available, this also accounts for its higher inhibition efficiency. This agrees with Varvara *et al.*, 2010 and Rani and Basu, 2012. It is clear from potentiodynamic experiment that *Dennettia tripetala* is very effective as a corrosion inhibitor for mild steel in the various alkaline solutions.

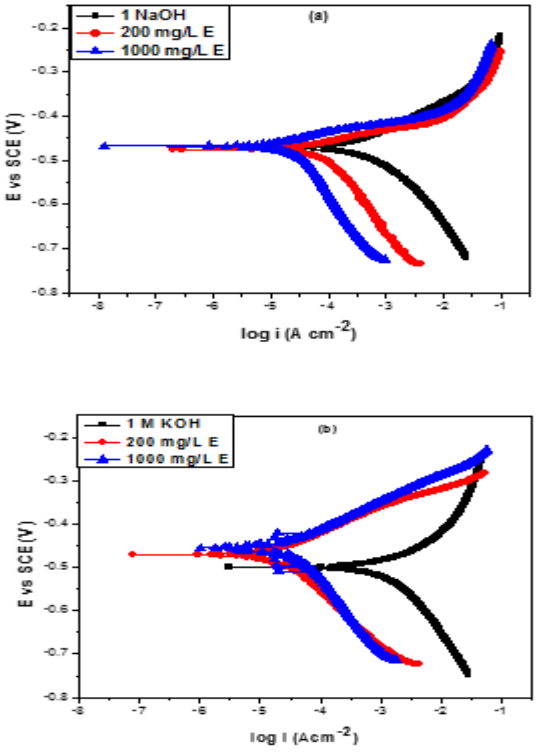

Fig 4.25: Potentiodynamic polarization curves of mild steel in: (a) 1 M NaOH and (b) 1 M KOH in the absence and presence *Dennettia tripetala*.

(k) *Chromolena odorata*(F) in the absence and presence ofHCL and H_2SO_4

Polarization measurements were carried out to investigate the effect of *Chromolena odorata* (F) on the anodic and cathodic partial reactions of the corrosion process. Fig. 4.26show typical potentiodynamic polarization curves for mild steel specimens in 1 M HCl and 1 M H_2SO_4, in the absence and presence of *Chromolena odorata*. The mild steel specimen in both acidic environments displayed rapid dissolution with no distinctive transition to passivation within the studied potential range is line with Znini,*et al,* 2010. The corresponding electrochemical parameters, namely, corrosion potential (E_{corr}) and corrosion current density (I_{corr}) were obtained and their values are shown in Table 4.91. The data presented therein shows that the I_{corr} decreases in the presence of *Chromolena odorata*compared to the blank solution and the trend continues with an increase in the concentration of the inhibitor. This result agrees with Rosaline-Vimela,*et al,* (2012). Close scrutiny of the polarization curves in Fig. 4.26(a and b) reveals that within the potential range studied; cathodic polarization curves are more linear compared to anodic Tafel curves especially in 1 M HCl environment. This may be attributed to the deposition of corrosion products on the metal surface. The values of the corrosion current density in the absence and presence of the inhibitor were used to calculate the inhibition efficiency from polarization data using equation 3.19.The values obtained are presented in Table 4.91. From the table, it is evident that the introduction of *Chromolena odorata* into 1 M HCl environment slightly shifts E_{corr} values towards the cathodic direction and the effect increases with an increase in the concentration of *Chromolena odorata*, similar result was observed in 1 M $H_2SO_4$and in line with El Quariachi *et al* 2010. E_{corr} shift was quite negligible. Accordingly, *Chromolena odorata* retarded the anodic and cathodic corrosion current densities in both acidic solutions. This shows that the inhibitor reduced the mechanism of H_2 gas evolution reaction and also the anodic dissolution of mild steel.

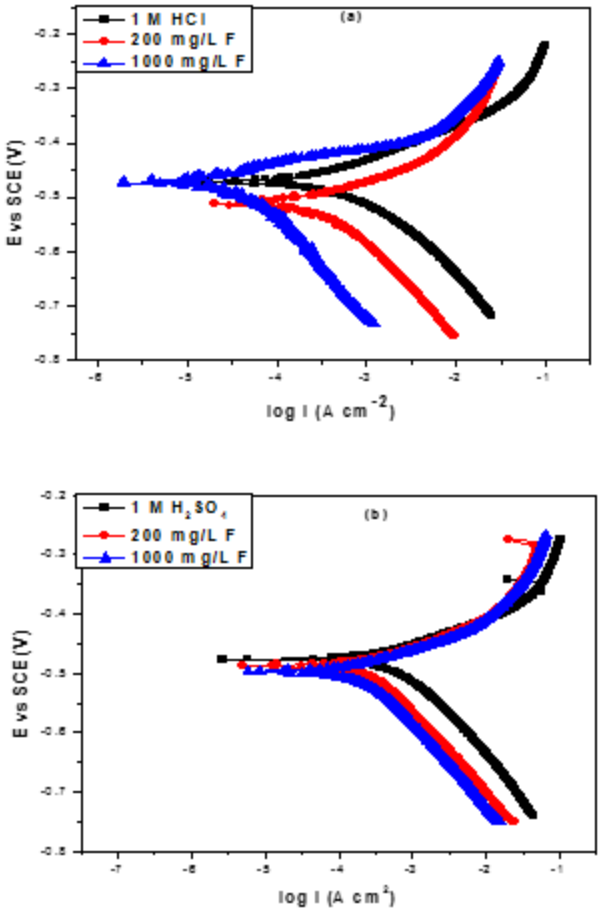

Fig 4.26: Potentiodynamic polarization for mild steel in: (a) 1 M HCl and (b) 1 M H_2SO_4 in the presence and absence of different concentration of *Chromolena odorata* extracts.

(l) *Chromolena odorata*(F) in the absence and presence of KOH and NaOH

The anodic dissolution of mild steel in alkaline solutions has been studied, the electrode process are shown to involve two one–electron stages. Polarization experiments were undertaken to determine some mechanistic insight on the effect of the solutions on the anodic and cathodic reactions of mild steel agrees with Yuce and Kardas, 2012. The polarization curves for the mild steel samples, after immersion in the different concentrations of 1 M NaOH and 1 M KOH solutions are presented in Figs 4.27 (a & b), respectively.The corrosion potential (E_{corr}) and corrosion current densities (i_{corr}), estimated from polarization curves are presented in Table 4.92. The obtained values were extrapolated from the respective axis in the potential–current polarization curve, at the intersections of the cathodic β_c, and anodic, β_a, Tafel slopeswhich is in line with Rani and Basu, 2012.

The corrosion current density is a measure of the corrosion rate of the sample in the electrolyte solutions, while the corrosion potential is a measure of the tendency of the sample to become dissoluble in the solutions. Careful examination of the figures shows that the mild steel specimen in both solutions underwent rapid dissolution in the presence and absence of the inhibitor. The figures show that the mild steel metal in KOH could effectively transit from active dissolution to a stable passivation, which signifies the formation of corrosion protective film layer on the surface of the mild steel metal when the potential was made more positive, similar result was reported by Mistry,*et al*, (2012). The Figures show active dissolution to stable passivation at higher concentration while at lower concentration a slight break of the film layer was observed. However, the corrosion current (I_{corr}) values decreased in the presence of *Chromolena odorata*. E_{corr} values shifted to more negative potentials. The E_{corr} values in this environment became more negative as the concentration increased, this observation was not significant at all in 1 M KOH environment and in line with Sulaiman *et al.*, 2012.

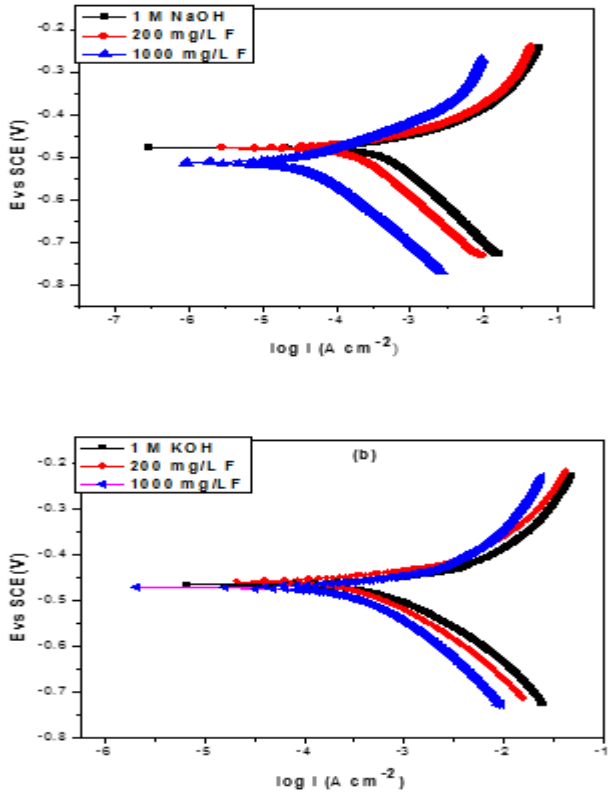

Fig 4.27: Potentiodynamic polarization curves of mild steel in: (a) 1 M NaOH and (b) 1 M KOH in the absence and presence *Chromolena odorata*.

4.6.1.2: Potentiodynamic polarization measurements for aluminum

(a) *Dialium guineense* (A) in the absence and presence ofHCl and H_2SO_4

The potentiodynamic polarization curves of Al in the absence and presence of Dialium guineense are shown in Fig. 4.28, for the samples in 1 M HCl and 1 M H_2SO_4 solutions. The values of the polarization parameters are provided in Table 4.93 where E_{corr} and i_{corr} are, respectively the corrosion potential and current density. Both were obtained from the extrapolation of the anodic and cathodic Tafel slopes with respect to the E_{corr} values. The values in Table 4.93reveal that in the presence of *Dialium guineense* and at higher concentration of 1000 mg/L Al displayed lower i_{corr} and more positive E_{corr} values in studied environment. In 1 M HCl environment, (Fig. 4.28a), the corrosion potential, E_{corr}, and the corresponding i_{corr} of Al in the absence and presence of *Dialium guineense* are presented in Table 4.93. The result shows that the introduction of *Dialium guineense* reduces both the cathodic and the anodic corrosion current densities, thus implying that the corrosion rate of Al sample in the presence of the inhibitor was reduced when compared to the uninhibited Al. Also, the E_{corr} of the inhibited Al is more positive (anodic) than the uninhibited Al. This shows that in the absence of *Dialium guineense*, Al have a higher susceptibility to corrosion in this environment than the uninhibited Al sample. In 1 M H_2SO_4solution (Fig. 4.28b), the corrosion potential E_{corr} for Al in the absence and presence of A Al are slightly more negative than the corrosion potential E_{corr} of the Al sample in 1 M HCl solution. The corresponding current densities are shown in Table 4.93. It is evident that the *Dialium guineense*shifts both the anodic and cathodic curves to lower values of current densities. The polarization curves for the Al samples in both environments exhibit passivation behavior and do not differ in nature of transition from active to passive states. This agrees with Abdurahman *et al.,* 2011. The similarity of the polarization curves of both the uninhibited and inhibited Al samples indicates that the mechanism of the corrosion of Al in the absence of the inhibitor did not change even when *Dialium guineense* was introduced into the aggressive solutions.

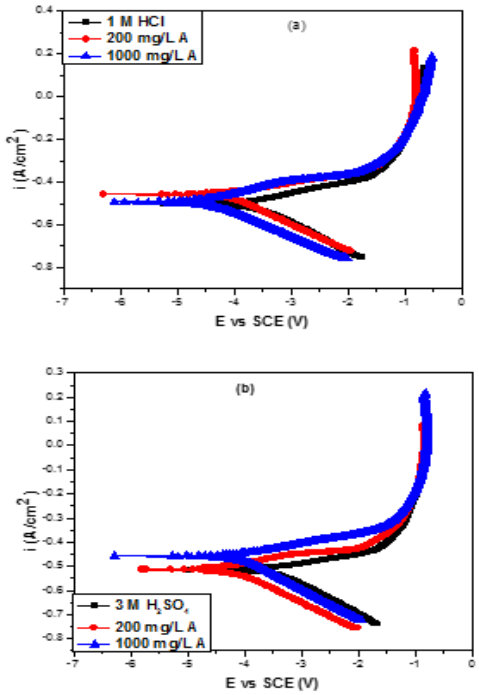

Fig. 4.28**:** Potentiodynamic polarization curves of Al in: (a) 1 M HCl and (b) 1 M H_2SO_4 in the absence and presence *Dialium guineense*.

(b) *Dialium guineense* (A) in the absence and presence of KOH and NaOH

Polarization experiments were carried out potentiodynamically in unstirred NaOH/KOH environments in the absence and presence of *Dialium guineense* (A), in order to determine the effect of the inhibitor on the anodic and cathodic half reactions. From the polarization curves shown in Fig. 4.29, it is clear that the mild steel show active dissolution with no sign of transition to passivation in the aggressive solution. The electrochemical parameters, namely, the corrosion potential (E_{corr}), corrosion current densities (I_{corr}), the cathodic (b_c) and anodic (b_a) current values obtained from polarization curves are presented in Table 4.92. Inspection of the plot in Fig. 4.29, reveals that increase in the concentration of *Dialium guineense* retards both the anodic dissolution of metal and the cathodic hydrogen evolution reaction, the shift of cathodic curves to areas of lower corrosion current values was well pronounced. Similar result was obtained by Varvara, *et al.*, 2010; Taleb, *et al.*, 2011; Negm, *et al.*, 2012b. The corrosion potential E_{corr} shifts was not significant enough either to the negative or noble direction. According to literatureif the displacement of E_{corr} is greater than 85 mV as mentioned before we may say that the inhibitor is cathodic or anodic type, but from our results E_{corr} values ranges from 15 mV to 53 mV, therefore

Dialium guineense can be regarded as a mixed- type inhibitor in these environments under study. Generally, the corrosion current density (I_{corr}) decreases with increase in *Dialium guineense* concentration (from 196.2 µA/cm^2 to 24.1 µA/cm^2). This is in agreement with Okoli, *et al.*, 2007. The values of the corrosion current density in the absence ($i_{corr,bl}$) and presence of the inhibitor ($i_{corr,inh}$) were used to estimate the inhibition efficiency from polarization data (IE %) as presented in equation 3.15.The obtained values are presented in Table 4.94. The maximum inhibition efficiency obtained for *Dialium guineense* in 1 M NaOH and 1 M KOH are 87.7% at 1000 mg/L *Dialium guineense* and 86.6% at 1000 mg/L *Dialium guineense*.

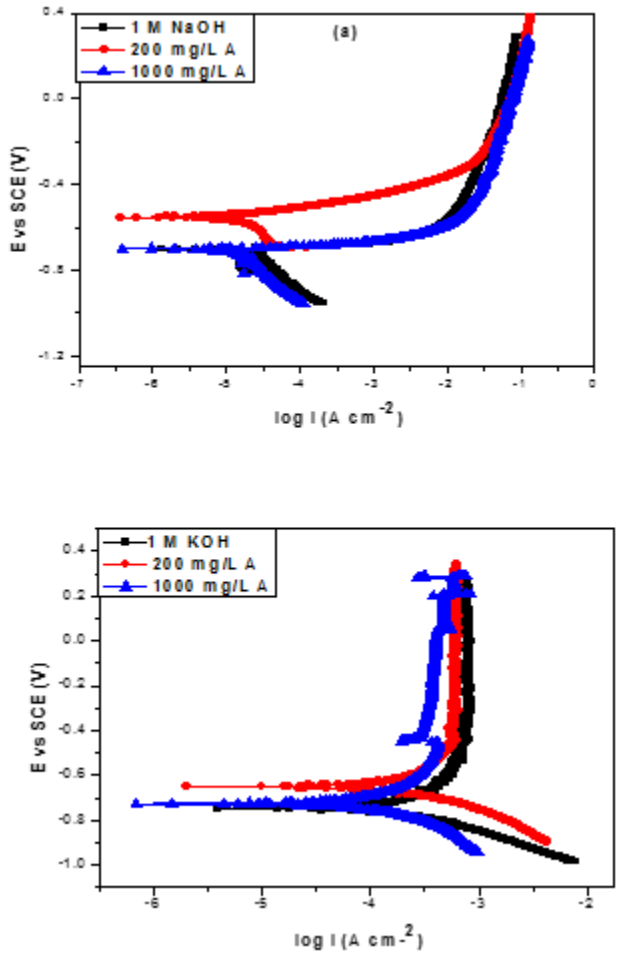

Fig. 4.29: Potentiodynamic polarization curves of Al in: (a) 1 M NaOH and (b) 1 M KOH in the absence and presence *Dialium guineense*.

(c) *Vitex doniana*(B) in the absence and presence ofHCL and H_2SO_4

To ascertain the effects for *Vitex doniana*on aluminium corrosion, we used the lowest and the most effective concentration of *Vitex doniana*as determined i.e. 200 and 1000 mg/L*Vitex doniana*. The polarization curves for the Al sample in 1 M HCl without and with different concentrations of *Vitex doniana* presented in Fig.4.30(a & b) show some features of active–passive transition at sufficiently positive potentials, though the passive region is not well defined. Addition of *Vitex doniana*does not notably affect the corrosion potential (E_{corr}) in 1 M HCl environment but in 1 M H_2SO_4 solution a slight shift towards the lower direction was observed. In 1 M HCl solution *Vitex doniana*exerts a significant effect on the cathodic hydrogen ion reduction decreasing the current density at all potentials within the cathodic region. This is in line with Gade*et al.*,2017.

The effect on the anodic reaction is not pronounced to any large extent, to what is obtainable in 1 M H_2SO_4 environment. These findings all shows that *Vitex doniana* functioned as a good inhibitor and mainly as a mixed-type inhibitor. The obtained results are presented in Table 4.93.

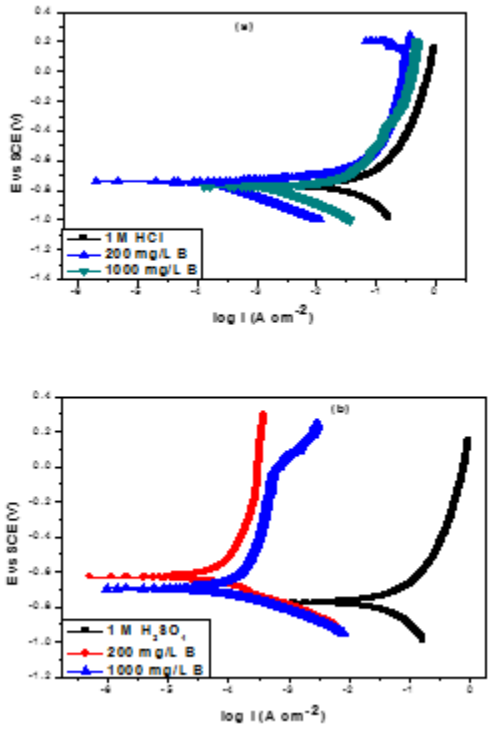

Fig. 4.30: Potentiodynamic polarization curves for Al in: (a) 1 M HCl and (b) 1 M H_2SO_4 in the presence and absence of different concentration of *Vitex doniana* extracts.

(d) *Vitex doniana*(B) in the absence and presence ofNaOH and KOH

Fig. 4.31 shows typical potentiodynamic polarization curves of aluminum metal in the two alkaline (1 M NaOH and 1 M KOH) environments. The extrapolated polarization parameters are clearly presented in Table 4.94. As can be seen in both environments, the metal exhibited transition to passivation within the potential range studied, characteristics of aluminum metal. The shapes of the polarization curves for Al in both alkaline solutions are closely similar, suggesting comparable corrosion mechanisms. However, Al displays a more positive corrosion potential in 1 M KOH solution. The observed variation in corrosion susceptibility results from the nature of the corrodents. Addition of *Vitex doniana* into the 1 M KOH solution reflected a pronounced shift of $E_{corr,}$ towards the lower direction, also, a reduction in the current densities of both the cathodic and anodic process was observed. In 1 M NaOH environment similar trend was observed in the presence *Vitex doniana* and in line with Cushnie *et al.*, 2014 and Qiu *et al.*, 2014. All of the results indicate that *Vitex doniana* functioned as an anodic inhibitor. The mean values of the corresponding electrochemical parameters such as corrosion potential (E_{corr}), corrosion current density (I_{corr}), cathodic Tafel slopes (b_c) and anodic Tafel slopes (b_a) estimated by extrapolating the Tafel lines are presented in Table 4.94. The IE% values presented in Table 4.94 show maximum values of 94.6% and 89.9.5%, for aluminum in 1 M KOH and 1 M NaOH, respectively.

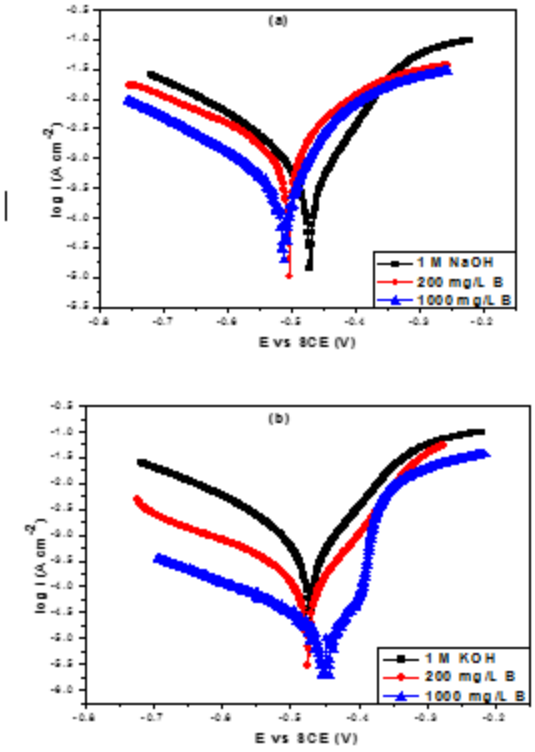

Fig. 4.31**:** Potentiodynamic polarization curves of Al in: (a) 1 M NaOH and (b) 1 M KOH in the absence and presence of *vitex doniana*.

(e) *Newbouldia leavis*(C) in the absence and presence of HCl and H_2SO_4

The effect of an increase in the concentration of *Newbouldia leavis* (C) on the anodic and cathodic polarization curves of aluminum electrode in 1 M HCl and 1 M H2SO4 solution was studied. The obtained polarization curves are presented in Fig. 4.32 (a and b). The corrosion parameters of Al such as $E_{corr.}$, andi_{corr} were calculated and listed in Table 4.91. A steady potential was readily attained, corresponding to the free corrosion potential, E_{corr}, of the metal. By the inspection of the table, it is clear that the values of E_{corr} are changed by increasing the concentration of the inhibitor. This agrees with the work of Mishra and Tiwari, 2011; Amorati and Valgimigli, 2012. In the presence of *Newbouldia leavis* the values of $E_{corr.}$ are shifted to a more positive potential, this effect occurred in both acid solutions indicating that the *Newbouldia leavis* acted predominantly as an anodic inhibitor for Al. When the additive concentrations were

increased the values of i_{corr} decreased considerably. This indicates that the resistance of mild steel to corrosion starts to increase.

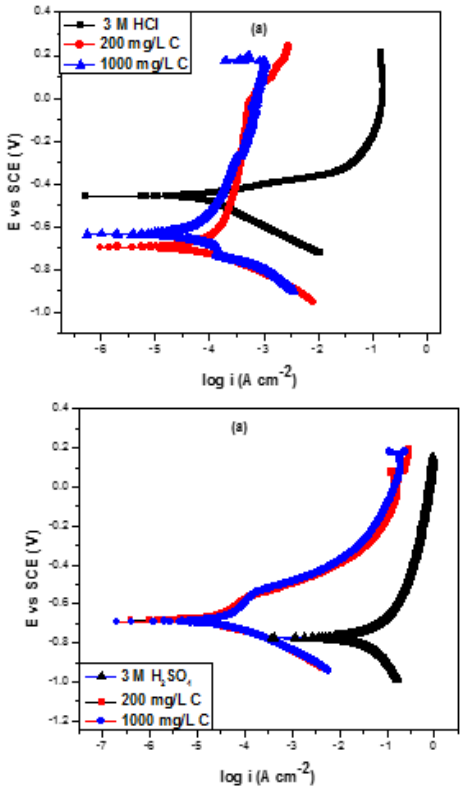

Fig. 4.32: Potentiodynamic polarization for Al in: (a) 1 M HCl and (b) 1 M H_2SO_4 in the presence and absence of different concentration of *Newbouldia leavis* extract.

(f) *Newbouldia leavis*(C) in the absence and presence ofNaOH and KOH

The polarization curves for the Al sample in 1 M NaOH and 1 M KOH without and with *Newbouldia leavis*all exhibit active dissolution with evidence of distinctive transition to passivation as seen in Fig. 4.33. *Newbouldia leavis* can be seen to shift E_{corr} in the anodic direction especially in NaOH environment, the anodic polarization was more pronounced than the cathodic polarization, indicating that the corrosion process was under anodic control. This result was observed at both low and high *Newbouldia leavis* concentrations. The effect of *Newbouldia leavis* on the anodic dissolution process is noticeably dependent on the amount of *Newbouldia leavis* present in the solution. *Newbouldia leavis* is observed to exert a slight depolarizing action on the anodic process at potentials more negative than E_{corr} in the blank acid is similar to Anees et al (2009). This effect persisted for a wider potential range at low

Newbouldia leavis concentration, beyond which the inhibitor ceased to affect the anodic reaction. High concentration of *Newbouldia leavis* abridged the depolarization region and subsequently retards the anodic dissolution reaction. In other words a high concentration of *Newbouldia leavis* is required to inhibit the anodic dissolution of Al in 1 M NaOH agrees with Anthony and Susai, (2012).

The potentiodynamic polarization behaviour of the Al specimen in 1 M KOH shows distinct features of passive transition. At high *Newbouldia leavis* concentration the metal shows tendency to passivate after the critical current has been attained, rather the anodic current remains almost steady at this critical value. Similar result was obtained by Nadia,*et al*, (2011). Nonetheless, *Newbouldia leavis* reduced the current densities in the cathodic and active anodic regions (mixed inhibition) as well as the critical and passive current densities, the resuls are presented in Table 4.94.

On the whole, it appears that the Al specimen initially passivates to some extent. Addition of *Newbouldia leavis* at low concentration promotes passivation, increases the stability of the passive film and improves resistance to pitting corrosion.

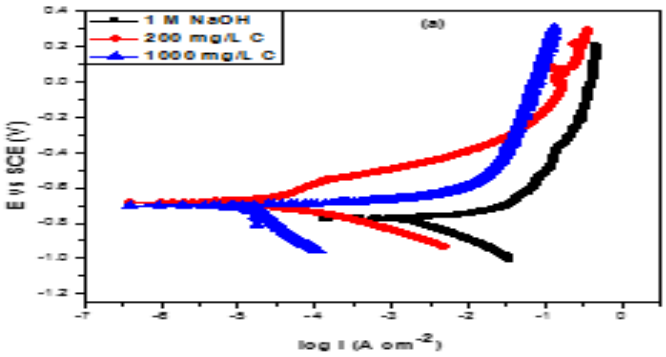

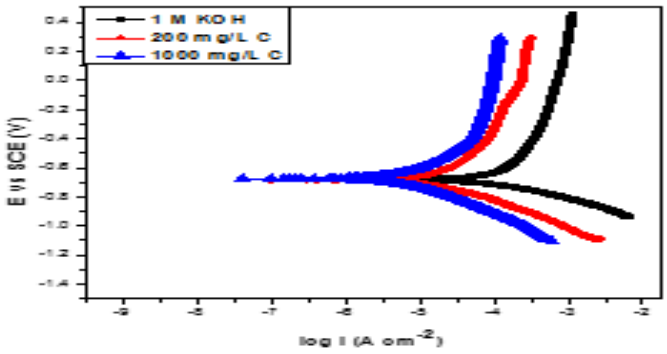

Fig. 4.33: Potentiodynamic polarization curves of Al in: (a) 1 M NaOH and (b) 1 M KOH in the absence and presence *Newbouldia leavis*.

(g) *Aspilia africana*(D) in the absence and presence ofHCl and H_2SO_4

Fig. 4.34 is a typical potentiodynamic polarization curves of aluminum in 1 M HCl and 1 M H_2SO4. The corresponding polarization parameters are given in Table 4.93. As expected, both specimens exhibited transition to passivation within the potential range investigated. The shapes of the polarization curves for Al in both acidic solutions are closely similar, suggesting comparable corrosion mechanisms as suggested before now. Nonetheless, Al displays a more positive corrosion potential in both acidic solutions. To assess the effect of *Aspilia africana* extract on the polarization behaviour of Al in 1 M HCl and 1 M H_2SO_4, tests were conducted in inhibited solutions containing 200 and 1000 mg/L *Aspilia africana*. The corresponding polarization plots are presented in Fig. 4.34a and b respectively. For Al in 1 M HCl, addition of *Aspilia africana*reflected a pronounced shift of $E_{corr,}$ towards the nobel direction, also, a reduction in the current densities of both the cathodic and anodic process was observed. In 1 M H_2SO_4 environment similar trend was observed in the presence *Aspilia africana*. All of the results indicate that *Aspilia africana* functioned as an anodic inhibitor agrees with Loto and Poppoola, (2012). The mean values of the corresponding electrochemical parameters such as corrosion potential (E_{corr}), corrosion current density (I_{corr}), cathodic Tafel slopes (b_c) and anodic Tafel slopes (b_a) estimated by extrapolating the Tafel lines are presented in Table 4.93. The IE% values presented in Table 4.93 show maximum values of 94.6% and 89.9.5%, 93.5% and 78.9% for aluminum and mild steel in 1 M HCl and 1 M $H_2SO_{4,}$ respectively.

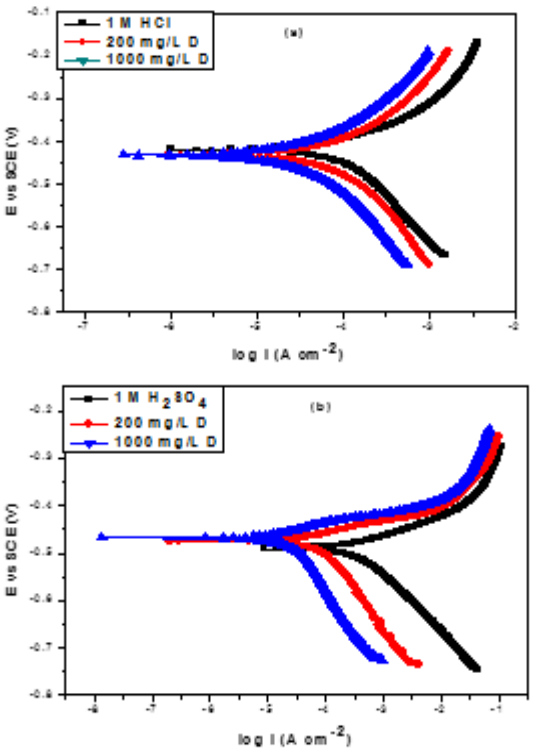

Fig. 4.34: Potentiodynamic polarization for Al in: (a) 1 M HCl and (b) 1 M H_2SO_4 in the presence and absence of different concentration of *Aspilia africana* extracts.

(h) *Aspilia africana*(D) in the absence and presence ofNaOH and KOH

The polarization curves of Al in the absence and presence of *Aspilia africana* are presented in Fig. 4.35, for the substrates in 1 M NaOH and 1 M KOH solutions. The values of the polarization parameters are provided in Table 4.94 where E_{corr} and i_{corr} are, represents the corrosion potential and current density which is in line with Lebe,*et al.*, (2013). Both were obtained from the extrapolation of the anodic and cathodic Tafel slopes with respect to the E_{corr}values. The values in Table 4.94 reveal that in the presence of *Aspilia africana*and at higher concentration of 1000 mg/L of *Aspilia africana* displayed lower i_{corr} and more positive E_{corr} values in studied environments especially in 1 M KOH solution. In 1 M NaOH environment, (Fig. 4.35a), the corrosion potential, E_{corr}, and the corresponding i_{corr} of Al in the absence and presence of *Aspilia africana* are presented in Table 4.94. The result shows that the introduction of *Aspilia africana* reduces both the cathodic and the anodic corrosion current densities, thus implying that the corrosion rate of Al sample in the presence of the inhibitor was reduced when compared to the

uninhibited Al. Also, the E_{corr} of the inhibited Al is more negative (cathodic) than the uninhibited Al was equally reported by Patel *et al*, (2013). In 1 M KOH solution (Fig. 4.35b), the corrosion potential E_{corr} for Al in the absence and presence of *Aspilia africana* is slightly more positive than the corrosion potential E_{corr} of the Al sample in 1 M KOH solution. The corresponding current densities have been given in Table 4.94. It is evident that the *Aspilia africana*shifts both the anodic and cathodic curves to lower values of current densities. The polarization curves for the Al samples in both environments exhibit Passivation behavior, characteristics of Al, and do not differ in nature of transition from active to passive states. The similarity of the polarization curves of both the uninhibited and inhibited Al samples indicates that the mechanism of the corrosion of Al in the absence of the inhibitor did not changed even when *Aspilia africana* was introduced into the aggressive solutions was reported by Elmsellem,*et al*, (2014).

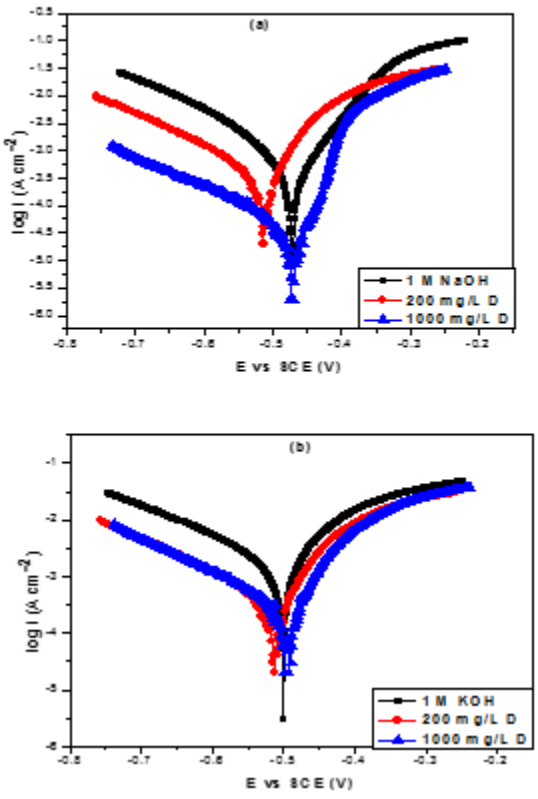

Fig. 4.35: Potentiodynamic polarization for Al in: (a) 1 M KOH and (b) 1 M NaOHin the presence and absence of different concentration of *Aspilia africana* extracts.

(i) *Dennettia tripetala*(E) in the absence and presence of HCl and H_2SO_4

Fig. 4.36 shows the experimental results from the polarization curves of Al 1 M HCl and 1 M H_2SO_4 without and with the addition of different concentrations of *Dennettia tripetala*in at 30°C. Corrosion parameters were calculated on the basis of cathodic and anodic potential versus current density characteristics in the Tafel potential region. The values of the corrosion current density (I_{corr}) for the investigated metal without and with the inhibitor, respectively, were carefully determined by the extrapolation of the cathodic and anodic Tafel lines to the corrosion potential (E_{corr}). It can be seen that the presence of *Dennettia tripetala* results a marked shift in both cathodic and anodic branches of the polarization curves towards lower current densities. This means that, the inhibitor affects both the cathodic and anodic reactions. A positive shift in the corrosion potential (E_{corr}) is observed. The results showed that the inhibiting action of *Dennettia tripetala* on the both cathodic and anodic processes seems to be approximately equal. The inhibitor may decrease the corrosion through the reduction of Al reactivity. We observed passivation within the studied potential range which could be due to the aluminum oxide film formed on the surface of Al even in the absence of the inhibitor. Accordingly to this mechanism, a reduction of either the anodic or the cathodic reaction or both arises from the adsorption of the inhibitor on the corresponding active sites.

The data in Table 4.93 exhibited that the corrosion current density (I_{corr}) decreases and the inhibition efficiency increases as an increase in the concentration of *Dennettia tripetala*.

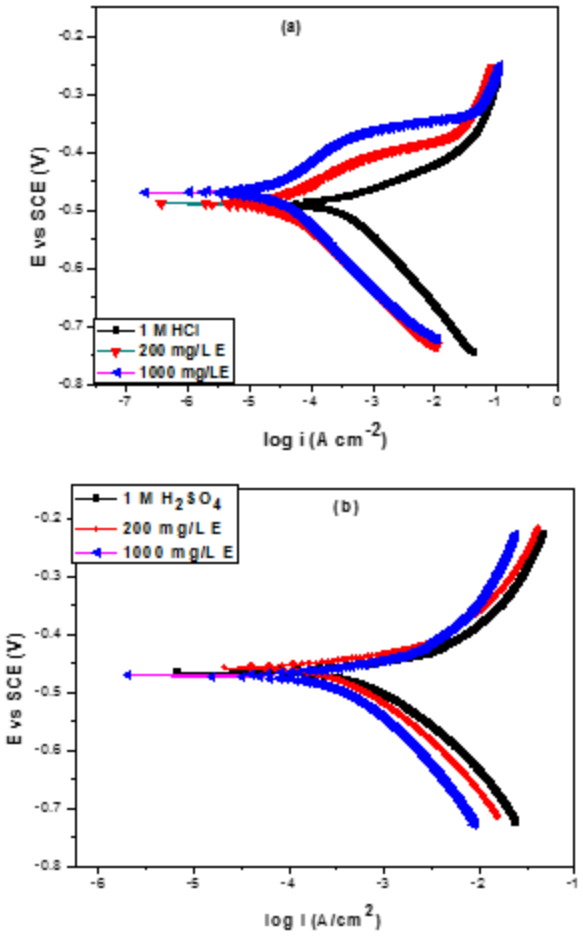

Fig. 4.36: Potentiodynamic polarization for Al in: (a) 1 M HCl and (b) 1 M H_2SO_4 in the presence and absence of different concentration of *Dennettia tripetala* extract.

(j) *Dennettia tripetala* (E) in the absence and presence of KOH and NaOH

It can be seen from the Tafel plot presented in Fig 4.37, that increase in the concentration of *Dennettia tripetala* extract causes decrease on the corrosion current in the absence and presence of 3 M KOH and 1 M NaOH. The corresponding electrochemical parameters such as corrosion potential (E_{corr}) and corrosion current densities (I_{corr}) obtained from polarization curves are presented in Table 4.94. The aluminum specimen is seen to exhibit active dissolution with no distinctive transition to passivation within the studied potential range. The kinetic parameters shown in Table 4.94, shows that E_{corr} is shifted slightly to the anodic region, also a shift of the polarization curves towards areas of low corrosion current was observed. The corrosion current

generally decrease as the concentration of the extract is increased implying reduction in corrosion rate and increasing inhibition efficiency. Results presented in Table 4.94 indicate that the maximum displacement in E_{corr} value is less than - 85 mV, therefore the observed behaviour shows that *Dennettia tripetala* is a mixed type inhibitor, with predominant anodic effect.

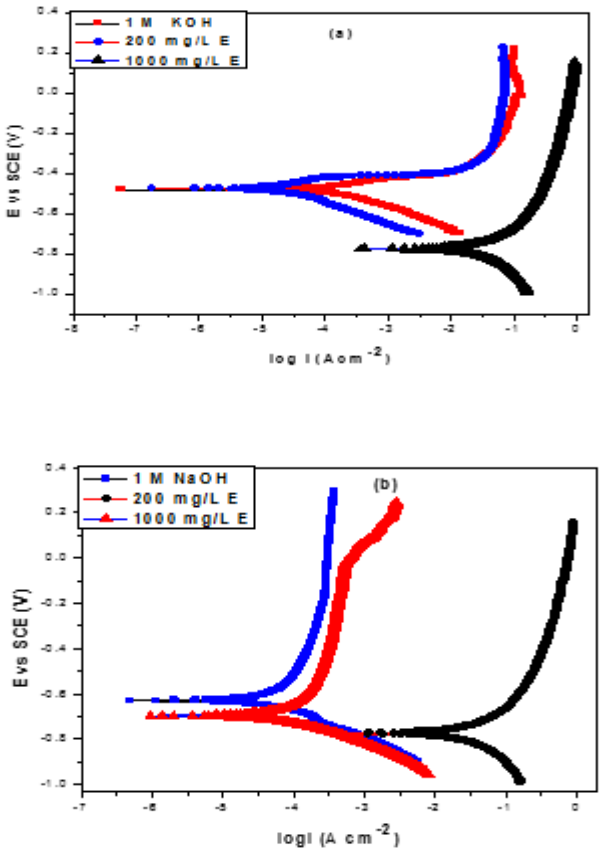

Fig. 4.37:Potentiodynamic polarization for Al in: (a) 1 M NaOH& (b) 1 M KOHsolution in the absence and presence of*Dennettia tripetala* extract.

(k) *Chromolena odorata*(F) in the absence and presence ofHCl and H_2SO_4

This method helps to explain the inhibiting effect of*Chromolena odorata*(F) on the metal dissolution reaction and hydrogen evolution reaction. Fig. 4.38 presents the polarization curves for Al in 1 M HCl and 1 M H_2SO_4 solution. In the two aggressive environments rapid dissolution was observed in the absence of *Chromolena odorata* (F). The corrosion potential (E_{corr}) and corrosion current densities (i_{corr}), estimated from polarization curves are presented in Table 4.93. In the presence of *Chromolena odorata*, the anodic and cathodic current values decreased, compared to the uninhibited solution. This indicates that *Chromolena odorata* retarded the anodic dissolution of steel and cathodic hydrogen evolution. Accordingly, a transition to

passivation within the studied potential range was observed. This behaviour increased with increased concentration of the inhibitor. The corrosion potential E_{corr} in 1 M HCl and 1 M H_2SO_4 solution shifts significantly towards the nobel direction, though this was more pronounced in 1 M HCl environment. In each case E_{corr} was more than 85 mV therefore *Chromolena odorata* is classified as an anodic inhibitor. The values of corrosion current density in the absence ($i_{corr,bl}$) and presence of *Chromolena odorata* ($i_{corr,inh}$) were used to estimate the inhibition efficiency (IE %).

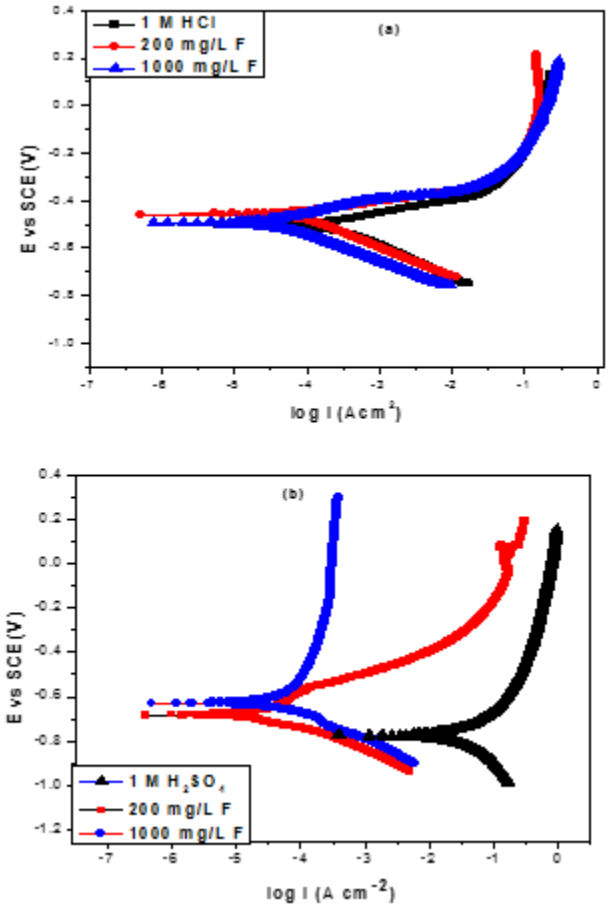

Fig. 4.38: Potentiodynamic polarization curves of Al in 1 M HCl and 1 M H_2SO_4 solution in the absence and presence of *Chromolena odorata*.

(l) *Chromolena odorata*(F) in the absence and presence ofNaOH and KOH

The anodic dissolution of Al in alkaline solutions has been studied, the electrode process are shown to involve two one–electron stages. Polarization experiments were undertaken to determine some mechanistic insight on the effect of the solutions on the anodic and cathodic

reactions of Al. The polarization curves for the Al samples, after immersion in the different concentrations of 1 M NaOH and 1 M KOH solutions are presented in Figs 4.39, respectively. The corrosion potential (E_{corr}) and corrosion current densities (i_{corr}), estimated from polarization curves are presented in Table 4.94. The obtained values were extrapolated from the respective axis in the potential–current polarization curve, at the intersections of the cathodic β_c, and anodic, β_a, Tafel slopes. The corrosion current density is a measure of the corrosion rate of the sample in the electrolyte solutions, while the corrosion potential is a measure of the tendency of the sample to become dissoluble in the solutions. Careful examination of the figures shows that the Al specimen in both (without and with *Chromolena odorata)* solutions underwent rapid dissolution in the presence and absence of the inhibitor. The figures show that the Al metal in KOH could effectively transit from active dissolution to a stable passivation, which signifies the formation of corrosion protective film layer on the surface of the Al metal when the potential was made more positive. The Figures show active dissolution to stable passivation at higher concentration while at lower concentration a slight break of the film layer was observed. However, the corrosion current (I_{corr}) values decreased in the presence of *Chromolena odorata*. E_{corr} values shifted to more negative potentials. The E_{corr} values in this environment became more negative as the concentration increased, this observation was not significant at all in 1 M KOH environment.

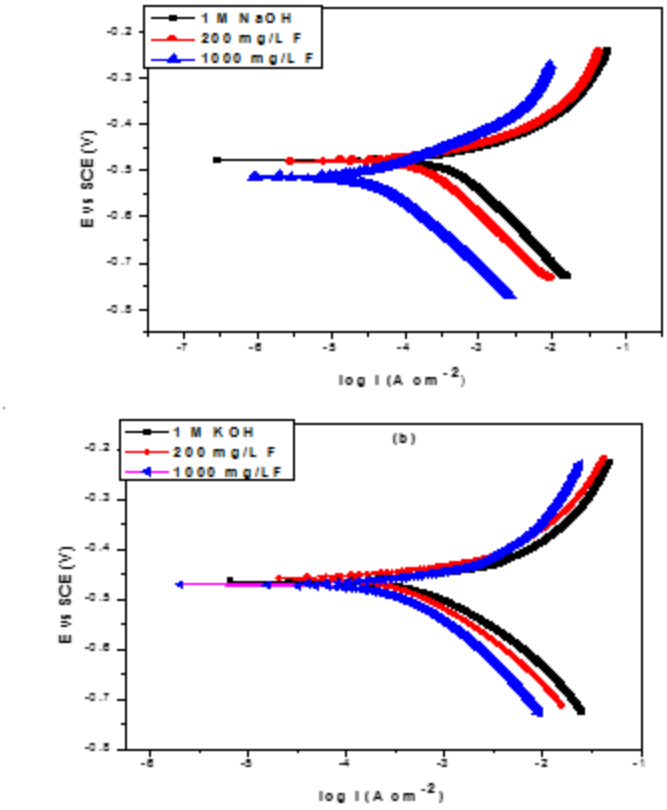

Fig. 4.39: Potentiodynamic polarization curves of Al in: (a) 1 M NaOH and (b) 1 M KOH in the absence and presence *Chromolena odorata*.

Table 4.91: Polarization parameters for mild steel in 1 M HCl and 1 M H_2SO_4 in the absence and presence of various plants extracts.

System	*Dialium guineense*			*Vitex doniana*			*Newbouldia leavis*			*Aspilia africana*			*Dennettia tripetala*			*Chromolena odorata*	
	E_{corr} (mV vs SCE)	I_{corr} (µA/cm^2)	IE%	E_{corr} (mV vs SCE)	I_{corr} (µA/m^2)	IE%	E_{corr} (mV vs SCE)	I_{corr} (µA/m^2)	IE%	E_{corr} (mV vs SCE)	I_{corr} (µA/m^2)	IE%	E_{corr} (mV vs SCE)	I_{corr} (µA/m^2)	**IE%**	E_{corr} (mV vs SCE)	I_{corr} (µA/cm^2)
1 M HCl	-500.2	192		-500.2	192		-500.2	192		-500.2	192		-500.2	192		-500.2	192
200mg/L	-464.8	41.3	78.4	-488.3	40.8	78.8	-467.3	51.1	73.4	-440.4	68.4	62.6	-464.8	52.7	72.5	-464.8	32.3
1000mg/L	-468.5	28.2	85.3	-470.8	20.6	89.3	-513.7	34.7	81.9	-443.7	38.5	78.9	-468.5	21.5	88.8	-468.5	16.6
1MH_2SO_4	-509.7	168.5		-509.7	168.5		-509.7	168.5		-509.7	168.5		-478.7	168.5		-509.7	168.5
200 mg/L	-502.4	82.8	50.8	-488.9	20.3	87.9	-480.9	12.2	92.8	-483.2	16.9	89.7	-489.2	54.2	67.8	-502.4	34.1
1000mg/L	-544.6	26.7	84.2	-463.7	4.6	97.3	-457.7	4.6	97.3	-478.5	10.6	93.5	-498.3	9.3	94.4	-544.6	23.2

Table 4.92: Polarization parameters for mild steel in 1 M KOH and 1 M NaOH in the absence and presence of various plants extracts.

System	*Dialium guineense*			*Vitex doniana*			*Newbouldia leavis*			*Aspilia africana*			*Dennettia tripetala*			*Chromolena odorata*		
	E_{corr} (mV vs SCE)	I_{corr} (µA/m^2)	IE %	E_{corr} (mV vs SCE)	I_{corr} (µA/cm^2)	IE %	E_{corr} (mV vs SCE)	I_{corr} (µA/m^2)	IE %	E_{corr} (mV vs SCE)	I_{corr} (µA/m^2)	IE %	E_{corr} (mV vs SCE)	I_{corr} (µA/m^2)	IE%	E_{corr} (mV vs SCE)	I_{corr} (µA/m^2)	IE%
1 M HCl	- 529	196.2		- 529	196.2		- 529	196.2		- 529	196.2		- 497.6	196.2		- 529	196.2	
200mg/L	- 536	57.6	70.6	- 536	78.6	59.9	- 536	57.6	70.6	- 536	47.6	75.7	- 498.2	76.4	61.1	- 536	43.6	77.8
1000mg/L	- 476	24.1	87.7	- 476	37.2	81	- 476	24.1	87.7	- 476	22.2	88.7	- 489.9	52.8	73.1	- 476	16.2	91.7
1MH_2SO_4	- 452	288.6		- 452	288.6		- 452	288.6		- 452	299.5	72.4	- 502.2	288.5	91.7	- 452	288.5	
200 mg/L	- 450	108.7	62.3	- 450	118.7	58.9	- 450	108.7	62.3	- 450	82.7	88.1	-458.2	24.9	92.9	- 450	118.7	58.9
1000mg/L	- 467	38.8	86.6	- 467	28.8	90	- 467	38.8	86.6	- 467	35.6		-456.7	21.3		- 467	10.4	96.4

Table 4.93: Polarization parameters for aluminum in 1 M HCl and 1 M H_2SO_4 in the absence and presence of various plants extracts.

System	*Dialium guineense*			*Vitex doniana*			*Newbouldia leavis*			*Aspilia africana*			*Dennettia tripetala*			*Chromolena odorata*		
	E_{corr} (mV vs SCE)	I_{corr} (µA/cm^2)	IE%	E_{corr} (mV vs SCE)	I_{corr} (µA/cm^2)	IE%	E_{corr} (mV vs SCE)	I_{corr} (µA/cm^2)	IE%	E_{corr} (mV vs SCE)	I_{corr} (µA/cm^2)	IE%	E_{corr} (mV vs SCE)	I_{corr} (µA/cm^2)	IE%	E_{corr} (mV vs SCE)	I_{corr} (µA/cm^2)	IE%
1 M HCl	- 512	207.2		- 512	207.2		- 512	207.2		- 512	207.2		- 512	207.2		- 512	207.2	
200mg/L	- 508	72.8	64.9	- 506	92.5	55.4	- 506	32.5	82.6	- 511	70.5	65.2	- 504.4	83.4	59.7	- 508	50.2	75.8
1000mg/L	-499	24.7	88.1	- 498	43.4	79.1	- 498	20.2	89.2	- 496	22.4	79.9	- 512.4	30.4	85.3	- 499	24.7	88.1
1MH_2SO_4	- 524	258.9		- 524	258.9		- 524	258.9		- 524	258.9		- 524	258.9		- 524	258.9	
200 mg/L	- 517	82.5	68.1	- 516	81.2	68.6	- 516	81.2	68.6	- 519	97.8	62.2	- 600.2	112.6	56.5	- 517	56.4	78.2
1000mg/L	- 455	12.4	95.2	- 458	10.3	96.2	- 458	10.3	96.2	- 453	34.4	86.7	- 608.5	24.7	90.5	- 455	17.2	93.4

Table 4.94: Polarization parameters for aluminum in 1 M KOH and 1 M NaOH in the absence and presence of various plants extracts.

System	*Dialium guineense*			*Vitex doniana*			*Newbouldia leavis*			*Aspilia africana*			*Dennettia tripetala*			*Chromolena odorata*		
	E_{corr} (mV vs SCE)	I_{corr} (µA/cm^2)	IE%	E_{corr} (mV vs SCE)	I_{corr} (µA/cm^2)	IE%	E_{corr} (mV vs SCE)	I_{corr} (µA/cm^2)	IE%	E_{corr} (mV vs SCE)	I_{corr} (µA/cm^2)	IE%	E_{corr} (mV vs SCE)	I_{corr} (µA/cm^2)	IE%	E_{corr} (mV vs SCE)	I_{corr} (µA/cm^2)	IE%
1 M HCl	- 636	182.6		- 636	182.6		- 636	182.6		- 636	182.6		- 529	196.2		- 636	182.6	
200mg/L	- 572	63.4	65.3	- 572	78.6	57	- 572	73.2	59.9	- 629	98.4	53.9	- 536	52.6	73.2	- 514	123.4	32.4
1000mg/L	- 624	28.1	84.6	- 624	37.2	79.6	- 624	38.5	78.9	- 638	16.7	90.9	- 476	22.5	88.5	- 599	48.2	73.6
1MH_2SO_4	- 765	265.9		- 765	265.9		- 765	265.9		- 765	265.9		- 452	288.6		- 765	265.9	
200 mg/L	- 692	98.7	62.9	- 692	118.7	53.4	- 692	20.8	92.1	- 658	74.2	72.1	- 450	26.4	90.9	- 692	90.7	65.9
1000mg/L	- 756	12.5	95.3	- 568	28.8	89.2	- 756	7.4	97.2	- 742	14.6	94.5	- 467	20.4	92.9	- 756	29.8	83.6

4.6.2 Electrochemical impedance spectroscopy studies.

Electrochemical impedance spectroscopy measurements were performed in order to understand the characteristics and kinetics of the electrochemical processes taking place at the metal/solution interface, and how they were modified by *Aspilia africana, Chromolena odorata, Newbouldia leavis, Dennettia tripetala, Dialium guineense*and *Vitex doniana* extracts.

4.6.2.1 Electrochemical impedance spectroscopy measurements for mild steel.

(a) *Dialium guineense*(A) in the absence and presence of HCL and H_2SO_4

Figures 4.40(a-c) and 4.41(a-c) represent the Nyquist, Bode modulus and Bode phase angle plots of the impedance response of mild steel in the absence and presence of various concentrations of *Dialium guineense*extract. The obtained plots generally comprise of only one depressed capacitive semicircle in the high-frequency region, which is attributed to one time constant in the Bode plots. The observed depression of the Nyquist semicircle with center under the real axis is typical for solid metal electrodes that show frequency dispersion of the impedance data. It occurs due to roughness and inhomogeneity of the metal surfaces was equally reported by Abdel – Gaber *et al.,* 2009). The transfer function can be represented by a solution resistance R_s, shorted by a capacitor C that is placed in parallel to the charge transfer resistance R_{ct}:

$$Z_{(w)} = R_s + \left(\frac{1}{R_{ct}} + jwc\right)^{-1} \qquad (4.1)$$

This transfer function is applicable, however, only for homogeneous systems with one time constant when the center of the semicircle lies on the abscissa and cannot account for the depression of the capacitive semicircle. When a non-ideal frequency response is present, the capacitor is replaced by a constant phase element (CPE).The application of such a CPE accounts for the deviations from ideal dielectric behavior and is related to surface in homogeneities. The impedance, Z, of the CPE is:

$$Z_{CPE} = Q^{-1}(j\omega)^{-n} \qquad (4.2)$$

where Q and n depicts the CPE constant and exponent, respectively, $j^2 = -1$ is an imaginary

number, and ω is the angular frequency in rad s^{-1} (ω = 2πf when f is the frequency in Hz), CPE can represent resistance (Z_{CPE} = R, n = 0), capacitance (Z_{CPE} = C, n =1). To determine the values of the corresponding impedance parameters shown in Table 4.95(a &b), the obtained impedance spectra were analyzed using an equivalent circuit model (Fig. 4.42) which has been employed previously to model the metal/acid interface is in line with (Oguzie *et al.,* 2010; Chidiebere *et al.,* 2015). The diameter of the Nyquist semicircle is related to charge transfer resistance (R_{ct}). Addition of *Dialium guineense*extract to 1 M HCl(Fig. 4.40) and 1 M H_2SO_4 (Fig. 4.41) solution led to an increase in the size of the Nyquist semicircle in each case which indicates inhibition of the corrosion process. Increasing the concentration ofDialium guineense extract enhanced the magnitude of the impedance response, but did not affect the mechanism of the process. Conversely, the C_{dl} reduced in the presence of the extract and decreased consistently with *Dialium guineense*concentration. Such decrease normally results from a reduction in the local dielectric constant and/or an increase in the double layer thickness. The behaviour may be ascribed to the adsorption of *Dialium guineense* species on the metal/solution interface. This is in line with the Helmholtz model, given by the equation

$$C_{dl} = \frac{\varepsilon \varepsilon_o A}{\delta} \tag{4.3}$$

where ε_o is the vacuum permittivity and ε the relative permittivity of the film. Accordingly, the trend of C_{dl} means that the observed increase in R_{ct} resulted from the formation of an adsorbed layer of *Dialium guineense*extract on the metal/solution interface, which protects the metal surface from corrosion.The inhibition efficiency (*IE %*) for different inhibitor concentrations were calculated from Nyquist plots using the equation:

$$IE\% = \left(\frac{R_{ct(inh)} - R_{ct}}{R_{ct(inh)}}\right) x\ 100 \tag{4.4}$$

Where R_{ct} and $R_{ct\ (inh)}$ denotes charge transfer resistance in the absence and presence of the inhibitor. The EIS result follows the same trend with the PDP data.

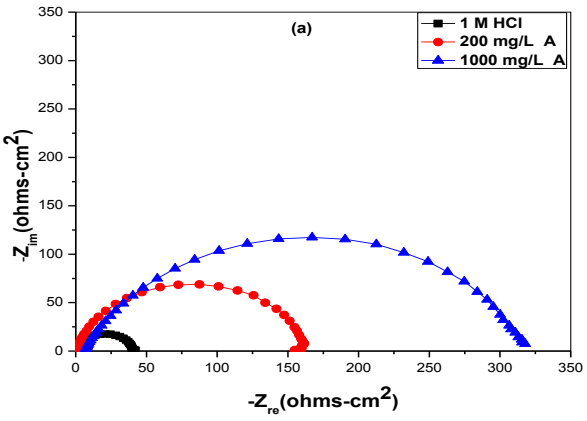

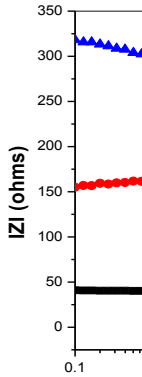

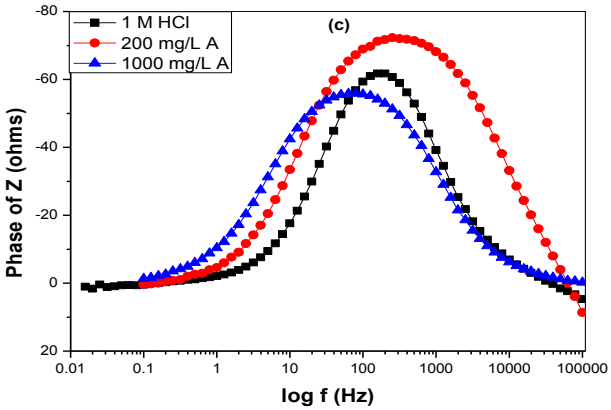

Fig. 4.40: Electrochemical impedance spectra for mild steel in 1 M HCl in the presence and absence of different concentrations of *Dialium guineense* extract: (a) Nyquist, (b) Bode modulus and (c) Bode phase angle plots.

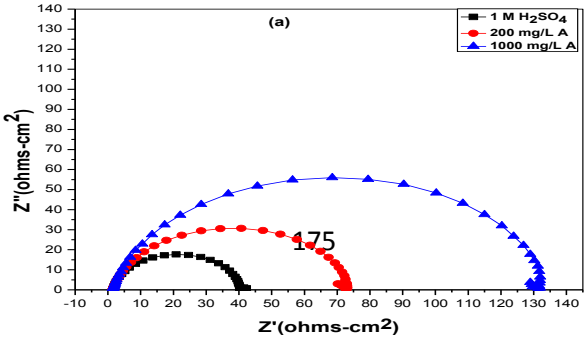

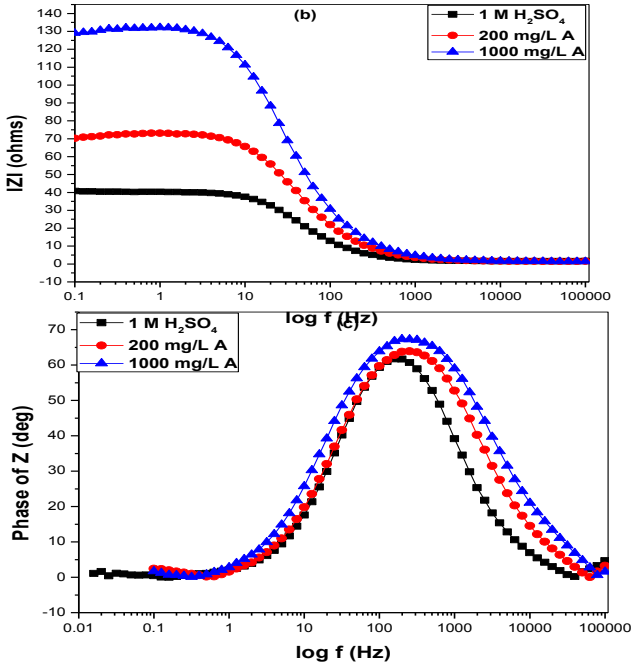

Fig. 4.41: Electrochemical impedance spectra for mild steel in 1.5 M H_2SO_4in the presence and absence of different concentrations of *Dialium guineense* extract: (a) Nyquist, (b) Bode modulusand (c) Bode phase angle plots.

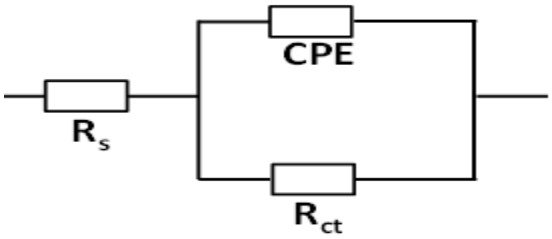

Fig. 4.42: Equivalent circuit model for mild steel with the accompanying experimental fit

(b) *Dialium guineense* (A) in the absence and presence of NaOH and KOH

Measurements were carefully undertaken to investigate the interactions of aluminum/electrolyte interface in the absence and presence of *Dialium guineense*. The calculated impedance data are listed in Table 4.96(a&b). Figures 4.43(a-c) and 4.44(a-c) shows the different impedance plots for mild steel in the absence and presence of *Dialium guineense*, respectively. The Nyquist plots show single depressed capacitive loop over the frequency range investigated, which corresponds to one time constant in the Bode plots. Addition of *Dialium guineense* increases the size of the semicircle (increase in charge transfer resistance) in Figures 4.43a and 4.44a, in the impedance of the interface in Figures 4.43b and 4.44b and also in the maximum phase angle in Figures 4.43c and 4.44c, respectively. The observation shows that inhibition of corrosion process is taking place at the mild steel/interface, and the level of charge transfer resistance is seen to increase with an increase in the concentration of *Dialium guineense* indicating the presence of a thin film layer formed/adsorbed on the mild steel surface. The high frequency intercept with the real axis in the Nyquist plots is assigned to the solution resistance (R_s) and the low frequency intercept with the real axis is ascribed to the charge transfer resistance (R_{ct}). To obtain the numerical values of the various impedance parameters presented in Table 4.96(a&b) the impedance spectra were analyzed by fitting to the equivalent circuit model R_s ($Q_{dl}R_{ct}$), which has been used previously to adequately model the mild steel/acid interface. Table 4.96(a&b) clearly shows that *Dialium guineense* enhanced the R_{ct} at all concentrations in both solutions which corresponds to an increase in the diameter of the Nyquist semicircle and in the magnitude of the impedance modulus in the Bode plots, confirming the corrosion inhibiting effect. The Inhibition efficiency from the impedance data (IE%) was estimated by comparing the values of the charge transfer resistance in the absence ($R_{ct,bl}$) and presence of the inhibitor ($R_{ct,inh}$) using equation 4.4.The values of the double-layer capacitance (C_{dl}) shown in Table 4.6 were obtained at the frequency at which the imaginary component of the impedance is a maximum ($Z_{im(max)}$) using the equation:

$$f(Z_{im(max)}) = \frac{1}{2\pi C_{dl} R_{ct}} \qquad (4)$$

The parameter C_{dl} was modified in the presence of A yielding a lower value than observed in the uninhibited corrodent. Lower C_{dl} values correspond to reduced interfacial capacitance, which, according to the Helmholtz model, results from a decrease in the dielectric constant (ε) or an increase in the double-layer thickness (δ) due to species adsorption at the double layer C_{dl} =

$\varepsilon\varepsilon_o A/\delta$, ε is the dielectric constant of the medium, ε_o is the vacuum permittivity, A is the electrode area, and δ is the thickness of the interfacial layer. The reduction in C_{dl} value calculated from our EIS measurements provides experimentalevidence of adsorption of the inhibitor on the corroding mild steel surface. The reduction in interfacial capacitance could be due to replacement of water molecules on mild steel surface by the organic compound which has smaller dielectric constants compared to water. Secondly, an increase in the thickness of the double layer due to adsorption of the inhibitor on the steel surface also contributes to reduction of interfacial capacitance.The increase in resistance at certain inhibitor concentration suggests the enhancement of adsorption of organic molecules on the mild steel surface and blocking of the steel surface efficiently. Our results show that, the inhibitor under investigation is efficient for inhibiting mild steel corrosion in 1 M NaOH and 1 M KOH the solutions.

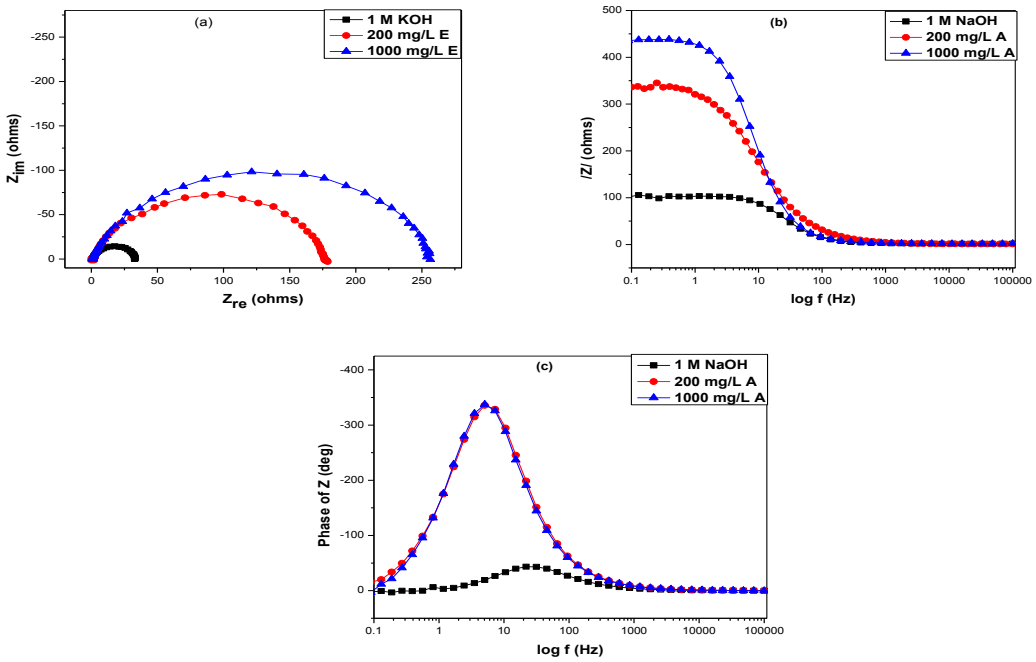

Fig. 4.43: Electrochemical impedance spectra of mild steel in 1 M NaOH solution in the absence and presence of*Dialium guineense* extract:(a) Nyquist, (b) Bode phase angle and (c) Bode modulus.

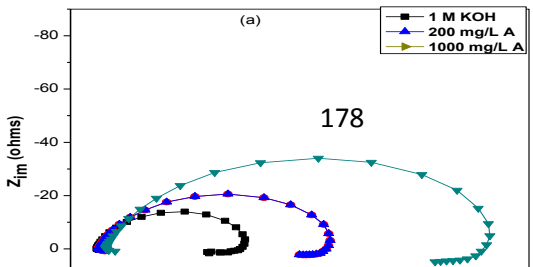

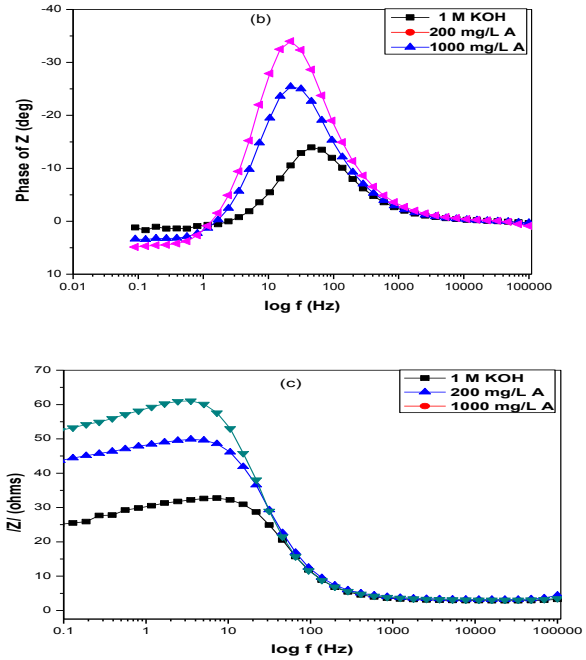

Fig 4.44: Electrochemical impedance spectra of mild steel in 1 M KOHsolution in the absence and presence of*Dialium guineense* extract: (a) Nyquist, (b) Bode phase angle and (c) Bode modulus.

(c) *Vitex doniana* (B) in the absence and presence of HCl and H_2SO_4

Figures 4.45(a-c) and 4.46(a-c) represent the impedance plots for mild steel in 1 M HCl and 1.5 M H_2SO_4 in the absence and presence of different concentrations of *Vitex doniana*. The

experiment was carried at the open circuit potential. In a 1.5 M H_2SO_4 solution, the Nyquist plots in the presence of *Vitex doniana* are characterized by a capacitive loop at high-to-medium frequency. The capacitive loop at high frequencies shows the phenomenon associated with the double electric layer. This arises from the time constant of the electrical double layer and charge transfer in the corrosion process. In 1 M HCl environment, the corresponding Nyquist plots show single semicircles for all systems over the frequency range studied, relating to one time constant in the Bode plots. The high frequency intercept with the real axis in the Nyquist plots is assigned to the solution resistance (R_s) and the low frequency intercept with the real axis is ascribed to the charge transfer resistance (R_{ct}). It is evident in Figures 4.45 and 4.46 that introduction of *Vitex doniana* to the acidic environments result to an increase in the charge transfer resistance which points towards inhibition of the corrosion process. In order to determine the numerical values of the various impedance parameters presented in Table 4.95(a&b), the impedance spectra were analyzed by fitting to the equivalent circuit model presented earlier. From the data presented in Table 4.95(a&b), it is clear that introduction of *Vitex doniana* leads to an increase in the R_{ct} values at all concentrations in 1 M HCl and 1.5M H_2SO_4. Due to a modification on introduction of *Vitex doniana*, the values of C_{dl} decrease more than observed in the absence of the inhibitor is in line with (Umoren, *et al*, 2013). Charge transfer resistance and double layer capacitance also show the opposite trend, according to Helmholtz model.The decrease in C_{dl} value which occurs due to a decrease in the dielectric constant and/or an increase in the double layer thickness can be related to the adsorption of *Vitex doniana* species on a corroding metal surface. An increase in resistance with inhibitor concentration, suggests enhanced adsorption of *Vitex doniana* species on a steel surface and efficient blocking of the steel surface was equally reported by (Saviour *et al*, 2010). Also, the inhibition efficiency (*IE %*) from EIS data was determined by comparing the values of the charge transfer resistance in the absence and presence of *Vitex doniana*.The obtained inhibition efficiency values are shown in Table 4.95 (a&b)**.** Though the result follows the same trend, however, a slight variation in the computed corrosion rate and inhibition efficiency values was observed from polarization and impedance measurements. This could be ascribed to the processes associated with the different techniques. For example, the mild steel surfaces were held close to the equilibrium corrosion potential for impedance measurements, but taken far away from the equilibrium potential during polarization measurements, which should

influence the measured values from both techniques. This is in agreement with (Chidiebere *et al*, 2015).

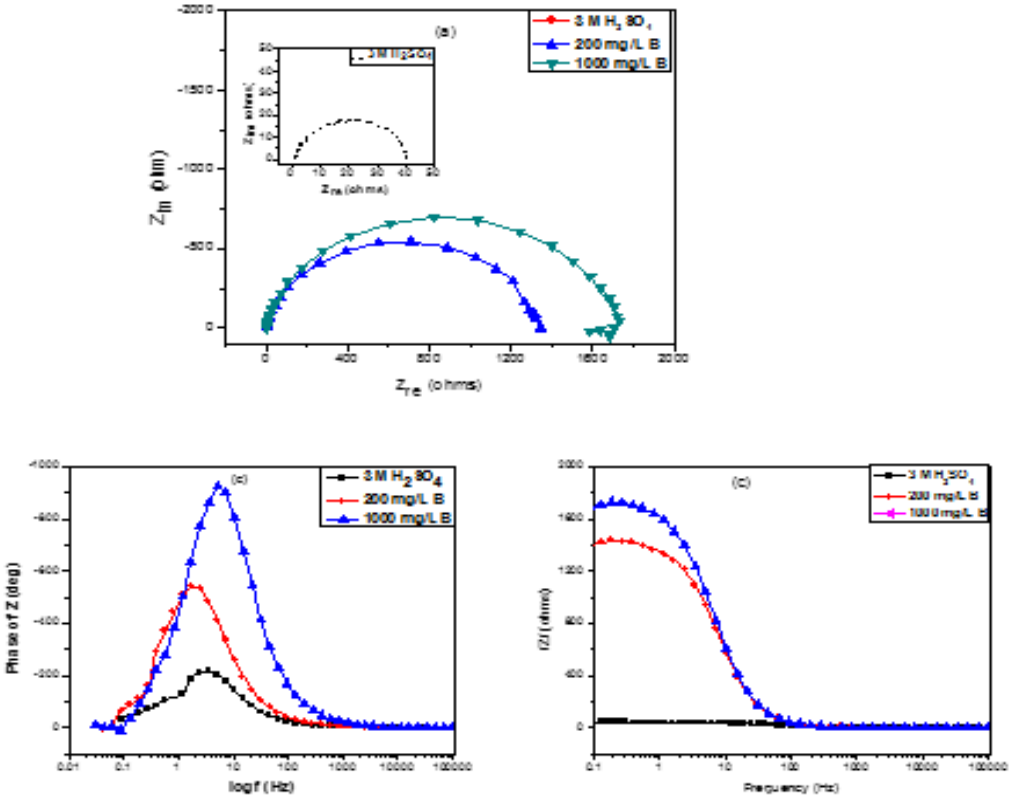

Fig.4.45: Electrochemical impedance spectra of mild steel in 1 M H_2SO_4 solution in the absenceand presence of*vitex doniana* extract:(a) Nyquist and (b) Bode phase angle and (c) Bode modulus

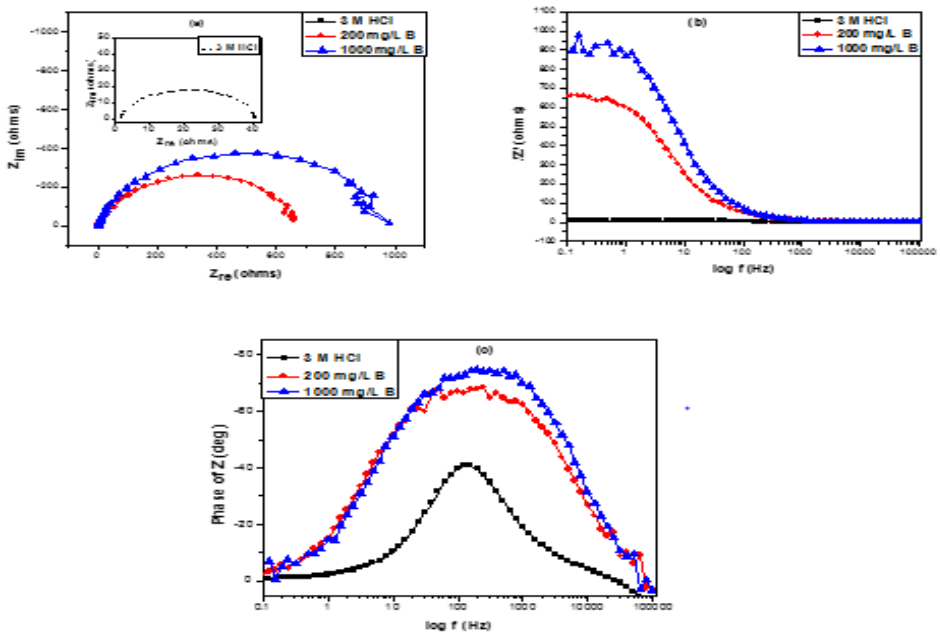

Fig.4.46: Electrochemical impedance spectra of mild steel in 1 M HClsolution in the absence and presence of*Vitex doniana*:(a) Nyquist and (b) Bode modulus (c) Bode phase angle.

(d) *Vitex doniana* (B) in the absence and presence of NaOH and KOH

It has been established that this method provide insight on the characteristics and kinetics of the electrochemical processes taking place at the metal/solution interface. Figures 4.47 and 4.48 represent the impedance plots for mild steel in 1 M NaOH and 1 M KOH in the absence and presence of different concentrations of *Vitex doniana*. The Nyquist plots show single semicircles over the frequency range studied, relating to one time constant in the Bode plots. The high frequency intercept with the real axis in the Nyquist plots is assigned to the solution resistance (R_s) and the low frequency intercept with the real axis is ascribed to the charge transfer resistance (R_{ct}). It is evident in Figures 4.47 and 4.48, that the introduction of *Vitex doniana* result in an increase in the size of the Nyquist semicircle (charge transfer resistance), which all shows inhibition of the corrosion process. The numerical values of the various impedance parameters presented in Table 4.96(a&b),were analyzed by fitting to the equivalent circuit models R_s ($Q_{dl}R_{ct}$), which have been used previously to model the mild steel/acid interface agrees with (Oguzie *et al*, 2012; Chidiebere *et al*, 2012 2010 and Kissi *et al*, 2006). A CPE is used in place of a capacitor to compensate for deviations from ideal dielectric behavior arising from the inhomogeneous nature of the electrode surfaces. The impedanceof the CPE is given by the

equation in 4.3. Considering the data presented in Table 4.96(a&b), it is clear that *Vitex doniana* increased the R_{ct} values at all concentrations compared with the uninhibited solution. Modification of the interface by adsorbed inhibitor lowered the values of C_{dl}, according to Helmholtz model. The observed decrease in C_{dl} value thus results from a decrease in the dielectric constant and/or an increase in the double layer thickness, due to the adsorption of *Vitex doniana* on the corroding steel surface. This involves the replacement of water molecules by the inhibitor species which has smaller dielectric constants. The increase in resistance with B concentration, suggests enhanced adsorption of *Vitex doniana* molecules on the mild steel surface and efficient blocking of the steel surface. This in line with (Moretti *et al,* 2004).The inhibition efficiency (*IE %*) from impedance data was calculated by comparing the values of the charge transfer resistance in the absence and presence of *Vitex doniana* using equation 4.2.The obtained inhibition efficiency values are presented in Table 4.96(a&b). The obtained data is in line with the polarization results.

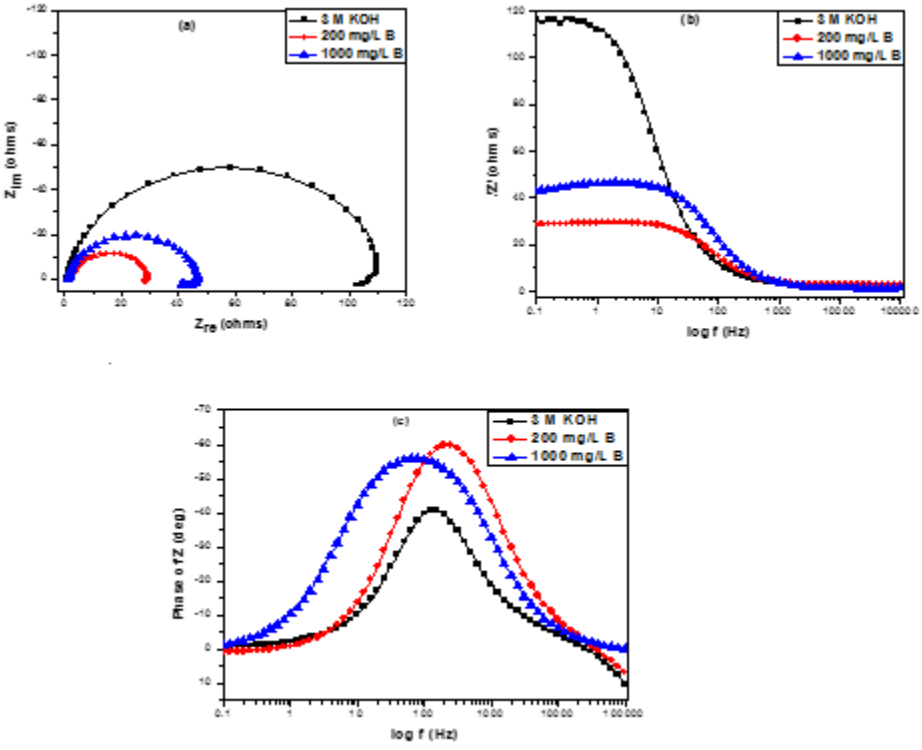

Fig.4.47: Electrochemical impedance spectra of mild steel in 1 M KOHsolution in the absence and presence of*Vitex doniana*: (a) Nyquist, (b) Bode phase angle and (c) Bode modulus.

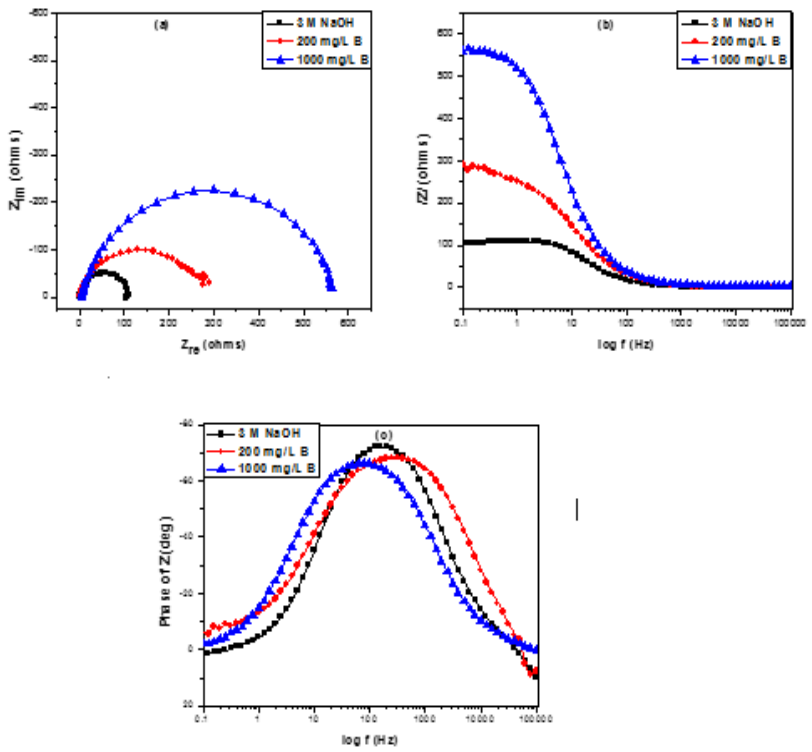

Fig. 4.48: Electrochemical impedance spectra of mild steel in 1 M NaOHsolution in the absence and presence of*Vitex doniana*: (a) Nyquist, (b) Bode phase angle and (c) Bode modulus.

(e) *Newbouldia leavis* (C) in the absence and presence of HCl and H_2SO_4

It has been established that this method provide insight on the characteristics and kinetics of the electrochemical processes taking place at the metal/solution interface. Figures 4.49 and 4.50 represent the impedance plots for mild steel in 1 M HCl and 1 M H_2SO_4 in the absence and presence of different concentrations of *Newbouldia leavis*. Accordingly, the Nyquist plots show single semicircles over the frequency range studied, relating to one time constant in the Bode plots. The high frequency intercept with the real axis in the Nyquist plots is assigned to the solution resistance (R_s) and the low frequency intercept with the real axis is ascribed to the charge transfer resistance (R_{ct}) as stated earlier. It is evident in Figures 4.49 and 4.50, that introduction of *Newbouldia leavis* result in an increase in the size of the Nyquist semicircle (charge transfer resistance), which all shows inhibition of the corrosion process. The numerical values of the various impedance parameters presented in Table 4.95(a&b),were analyzed by fitting to the equivalent circuit models $R_s(Q_{dl}R_{ct})$, which have been used previously to model the mild steel/acid interface. The result is similar to that reported by(Oguzie *et al*, 2012; Chidiebere

et al, 2012; Kissi et al, 2006). A CPE is used in place of a capacitor to compensate for deviations from ideal dielectric behavior arising from the inhomogeneous nature of the electrode surfaces. Considering the data presented in Table 4.95(a&b), it is clear that *Newbouldia leavis* increased the R_{ct} values at all concentrations compared with the uninhibited solution, this shows that *Newbouldia leavis* is a good inhibitor. Modification of the interface by adsorbed inhibitor lowered the values of C_{dl}, according to Helmholtz model. The observed decrease in C_{dl} value thus results from a decrease in the dielectric constant and/or an increase in the double layer thickness, due to the adsorption of *Newbouldia leavis* on the corroding steel surface. This involves the replacement of water molecules by the inhibitor species which has smaller dielectric constants. The increase in resistance with *Newbouldia leavis* concentration, suggests enhanced adsorption of *Newbouldia leavis* molecules on the mild steel surface and efficient blocking of the steel surface is in agreement witth (Moretti *et al*, 2004).The inhibition efficiency (*IE %*) from impedance data was calculated by comparing the values of the charge transfer resistance in the absence and presence of *Newbouldia leavis* using equation 4.2.The obtained inhibition efficiency values are presented in Table 4.95(a&b). The obtained data is in line with the polarization results.

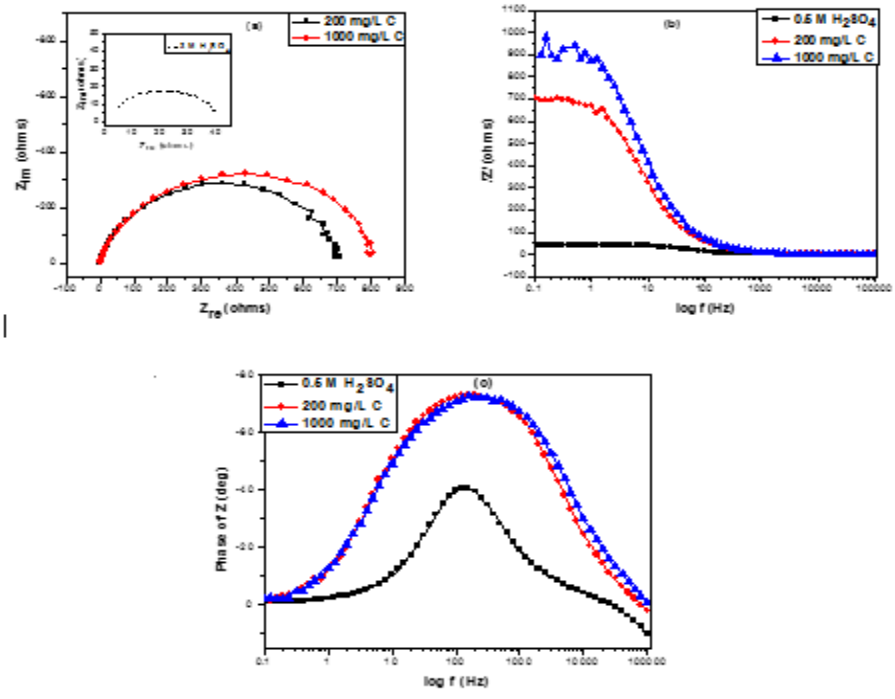

Fig. 4.49: Impedance spectra for mild steel in 1 M H_2SO_4 in the presence and absence of different concentration of *Newbouldia leavis* extract: (a) Nyquist and (b) Bode modulus (c) Bode phase angle.

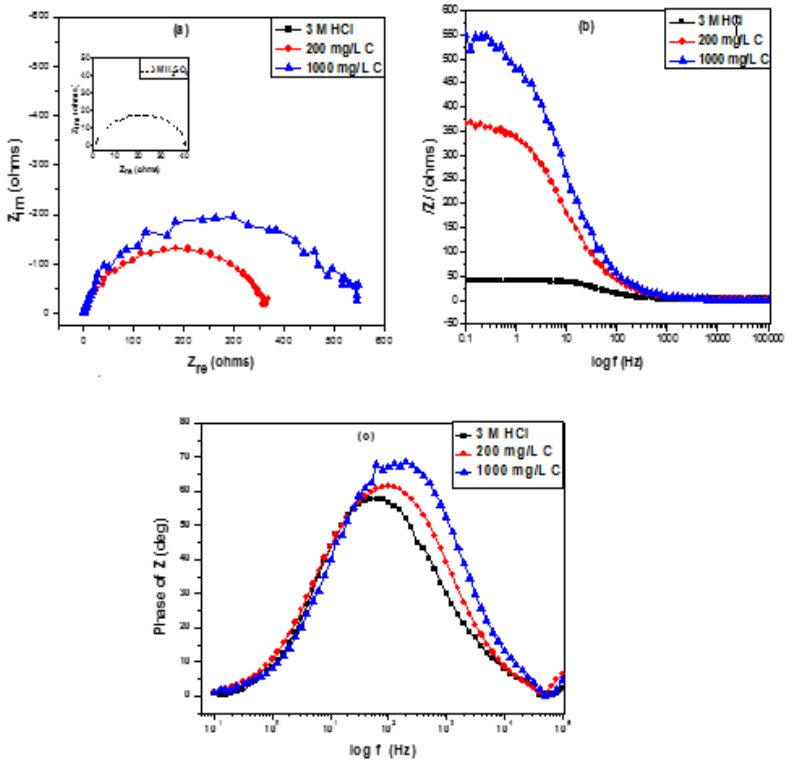

Fig 4.50. Electrochemical impedance spectroscopy for mild steel in 1 M HCl in the presence and absence of different concentration of*Newbouldia leavis*extract:(a) Nyquist and (b) Bode modulus (c) Bode phase angle.

(e) *Newbouldia leavis* (C) in the absence and presence of NaOH and KOH

Figures 4.51 and 4.52 shows the impedance spectra plots for mild steel in 1 M NaOH and 1 M KOH in the uninhibited and inhibited solutions. Table 4.96 (a&b) lists the corresponding impedance parameters. The plots show single depressed capacitive semicircles over the frequency range studied. The appearance of the capacitive loop is attributable to charge transfer processes across the metal/solution interface and its diameter is related to the interfacial charge transfer resistance (R_{ct}). The plots for mild steel in the two alkaline solutions are similar, indicating similar corrosion mechanisms. However, the smaller size of the semicircle for mild steel in the uninhibited solutions of 1 M NaOH and 1 M KOHsuggests lower charge transfer resistance Table 4.96 (a&b), hence higher susceptibility to corrosion. Addition of *Newbouldia leavis* increased the impedance of mild steel in 1 M NaOH and 1 M KOH, hence*Newbouldia leavis* in the absence and presence of NaOH and KOHinhibited the corrosion reaction without

modifying the mechanism of the corrosion process in either system. The impedance spectra were analyzed by fitting to the equivalent circuit model R_s ($Q_{dl}R_{ct}$), used frequently to model the steel/acid interface. From the data presented in Table 4.96(a&b), it is clear that R_{ct} for both systems increased with *Newbouldia leavis* concentration, implying that the electrode surfaces get more protection. The values of double-layer capacitance (C_{dl}) were determined using the relation given earlier. The double-layer capacitance (C_{dl}) for mild steel in both solutions decreased with increase in inhibitor concentration, the Helmholtz equation provides sufficient experimental evidence of inhibitor adsorption. In other words, the lower C_{dl} values result from a decrease in the dielectric constant and/or an increase in the double layer thicknessdue to adsorption of organic constituents of *Newbouldia leavis* (with lower dielectric constant than the displaced water molecules) on the metal/solution interface. Thus higher R_{ct} values at higher *Newbouldia leavis* concentrations indicate enhanced adsorption of the extracts on the mild steel surface, thereby retarding the attack of the aggressive environment during corrosion reaction process. A quantitative measure of the protective effect was obtained by the difference in values of R_{ct} in the absence and presence of the inhibitor.The obtained inhibition efficiency values are presented in Table 4.96(a&b). The slight disparities in the computed inhibition efficiency values from i_{corr} and R_{ct} values are attributable to the inherent differences in the features of either technique. For instance, the impedance measurements are carried out on unperturbed metal surfaces (at E_{corr} and minimal current transfer).

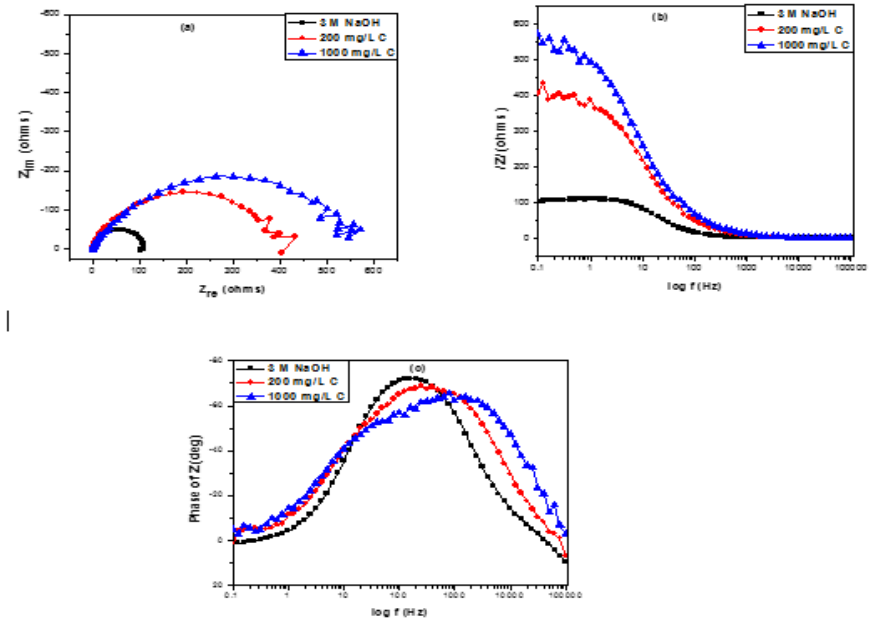

Fig. 4.51: Electrochemical impedance spectra of mild steel in 1 M NaOHsolution in the absence and presence of*Newbouldia leavis*: (a) Nyquist, (b) Bode modulus and (c) Bode phase angle plots.

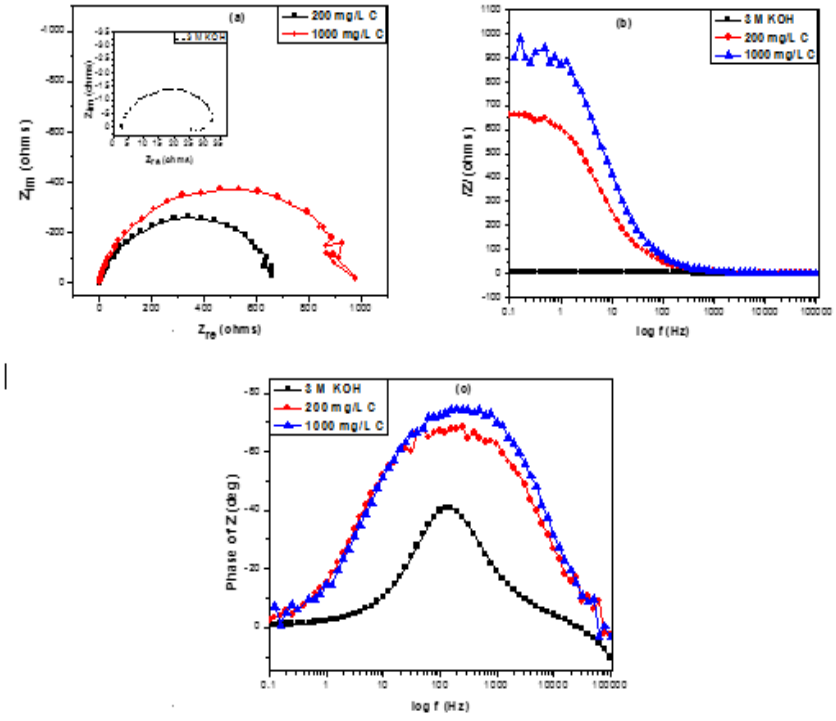

Fig. 4.52: Electrochemical impedance spectra of mild steel in 1 M KOHsolution in the absence

and presence of*Newbouldia leavis*: (a) Nyquist, (b) Bode phase angle and (c) Bode modulus.

(g) *Aspilia africana* (D) in the absence and presence of HCl and H_2SO_4

Fig. 4.53 gives the various impedance plots for mild steel corrosion in 1 M HCl without and with *Aspilia africana* and Fig. 4.54 gives the corresponding plots in 1 M H_2SO_4 environment. The electrochemical parameters derived from the impedance responses are given in Table 4.93(a&b). Again, the Nyquist plots in both solutions show single capacitive semi-circles in the high frequency region, corresponding to just one time constant. The high frequency intercept with the real axis is called the solution resistance (Rs) while the corresponding low frequency intercept with the real axis is the charge transfer resistance (Rct). The impedance data given in Table 4.95(a&b) were gotten by fitting into an equivalent circuit model $Rs(Q_{dl}R_{ct})$ shown earlier, which has been used by other researchers to model the impedance response for the mild steel/acid system. The inhibition efficiency calculated from the impedance data (IE%) was quantified by the usual formular. Addition of *Aspilia africana* improved the R_{ct} values but decreased the C_{dl} values. The former effect describes the anticorrosion action of *Aspilia africana*, whereas the latter effect points towards adsorption of some organic constituents of the extract onto the metal/solution interface. Reduction in C_{dl} values could result from either an increase in the interfacial thickness or a reduction in dielectric constant). Reduction in C_{dl} values indicates that some adsorbed water molecules have been replaced by organic species, which have lower dielectric constants than water. Either way, it is reasonable to assume that lower C_{dl} values in the presence of *Aspilia africana* implies that some organic constituents of *Aspilia africana* have been adsorbed on the corroding metal surface.

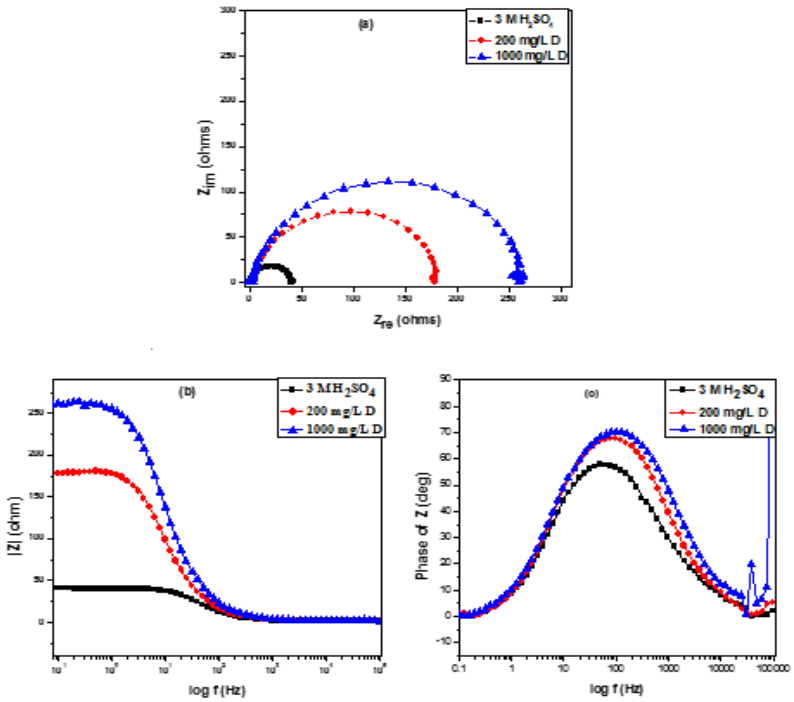

Fig.4.53: Electrochemical impedance spectra of mild steel in 1 M H_2SO_4solution in the absence and presence of*Aspilia africana*: (a) Nyquist, (b) Bode modulus and (c) Bode phase angle.

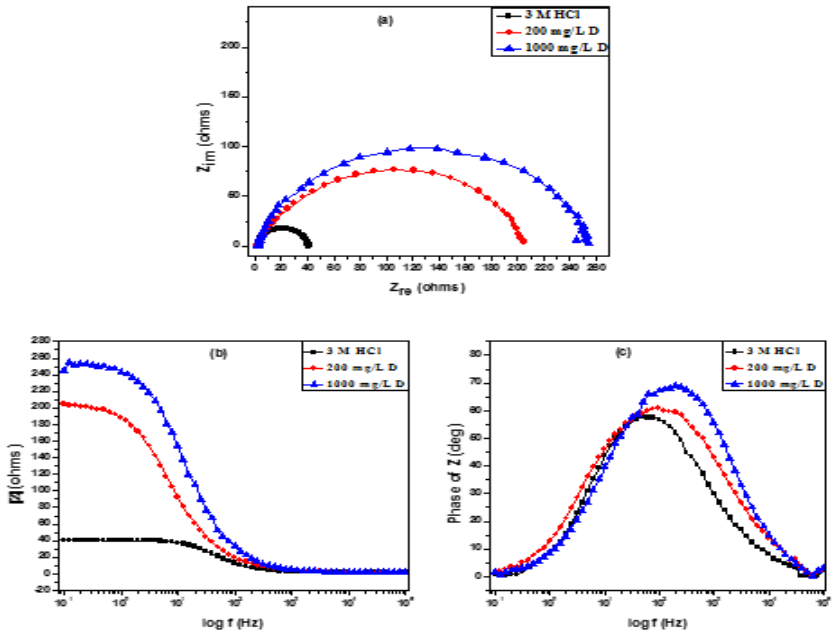

Fig. 4.54: Electrochemical impedance spectra of mild steel in 1 M HClsolution in the absence and presence of*Aspilia africana*: (a) Nyquist, (b) Bode modulus and (c) Bode phase angle.

(h) *Aspilia africana* (D) in the absence and presence of NaOH and KOH

Figures 4.55 and 4.56 represent the impedance plots for mild steel in 1 M NaOH and 1 M KOH in the absence and presence of different concentrations of *Aspilia africana*. In 1 M NaOH environment, the corresponding Nyquist plots as expected, show single semicircles for all systems over the frequency range studied, relating to one time constant in the Bode plots. It is evident in Figures 4.55 and 4.56 that addition of *Aspilia africana* to both alkaline solutions result in an increase in the size of the Nyquist semicircle (charge transfer resistance) and the impedance of the interface, which all points towards inhibition of the corrosion process. In order to determine the numerical values of the various impedance parameters presented in Table 4.96(a&b), the impedance spectra were analyzed by fitting to the equivalent circuit model R_s ($Q_{dl}R_{ct}$) which has been used previously to model the mild steel/acid interface. From the data presented in the Table,4.98(a&b) it is observed that *Aspilia africana* increased the R_{ct} values at all concentrations in 1 M NaOH and 1 M KOH, respectively. The values of double-layer capacitance (C_{dl}) were determined at the frequency at which imaginary component of the impedance is a maximum ($Z_{im\ (max)}$)using the relation $f\left(Z_{im(\max)}\right) = \frac{1}{2\pi C_{dl} R_{ct}}$. Due to a modification in the presence of the inhibitor, the values of C_{dl} decrease more than observed in the absence of the inhibitor. Charge transfer resistance and double layer capacitance show the opposite trend, according to Helmholtz model. The decrease in C_{dl} value which occurs due to a decrease in the dielectric constant and/or an increase in the double layer thickness can be ascribed to the adsorption of *Aspilia africana* on the corroding steel surface. The increase in resistance with inhibitor concentration, suggests enhanced adsorption of *Aspilia africana* molecules on the mild steel surface and efficient blocking of the steel surface.

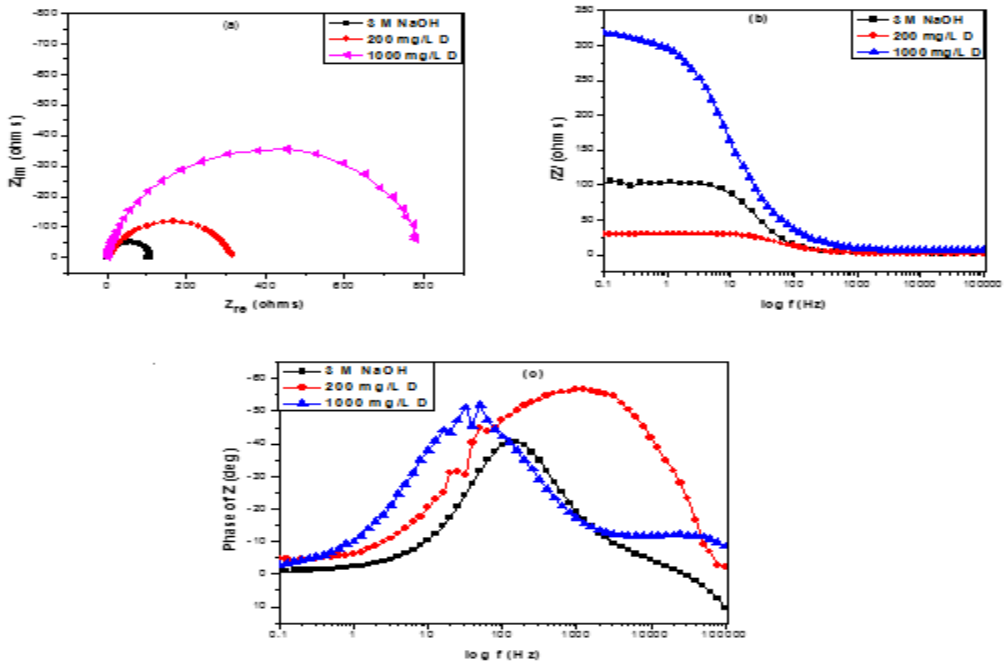

Fig 4.55: Impedance spectra for mild steel in 1 M NaOH in the presence and absence of different concentration of *Aspilia africana* extract:(a) Nyquist and (b) Bode modulus (c) Bode phase angle.

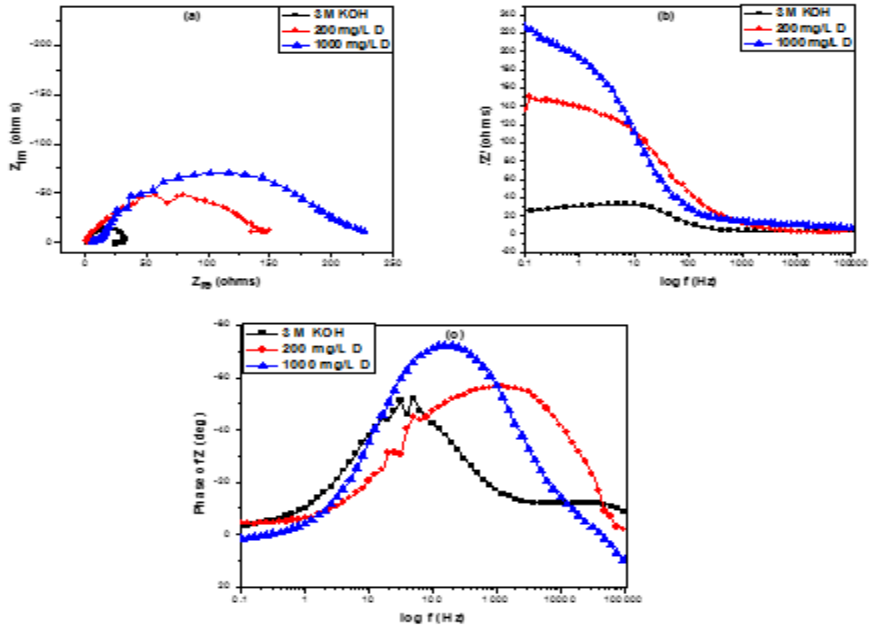

Fig 4.56: Electrochemical impedance spectroscopy for mild steel in 1 M KOH in the presence and absence of different concentration of *Aspilia africana* extract:(a) Nyquist and (b) Bode modulus (c) Bode phase angle.

(i) *Dennettia tripetala*(E) in the absence and presence of HCl and H_2SO_4

Figures 4.57 and 4.58 shows the impedance spectra for mild steel in 1 M HCl and 1 M H_2SO_4 in the uninhibited and inhibited solutions. Table 4.95(a&b) lists the corresponding impedance parameters. The plots show single depressed capacitive semicircles over the frequency range studied. The plots for mild steel in the two acid solutions are similar, indicating similar corrosion mechanisms. However, the smaller size of the semicircle for mild steel in the uninhibited solutions of 1 M HCl and 1 M H_2SO_4suggests lower charge transfer resistance Table 4.95(a&b), hence higher susceptibility to corrosion. Addition of *Dennettia tripetala* increased the impedance of mild steel in 1 M HCl and 1 M H_2SO_4, hence inhibited the corrosion reaction without modifying the mechanism of the corrosion process in either system. The impedance spectra were analyzed by fitting to the equivalent circuit model R_s ($Q_{dl}R_{ct}$), used frequently to model the steel/acid interface. From the data presented in Table 4.95(a&b), it is clear that R_{ct} for both systems increased with *Dennettia tripetala* concentration, implying that the electrode surfaces get more protection. The values of double-layer capacitance (C_{dl}) were determined using the relation given earlier. The double-layer capacitance (C_{dl}) for mild steel in both solutions decreased with *Dennettia tripetala* addition, which, alongside the Helmholtz equation provides sufficient experimental evidence of inhibitor adsorption. In other words, the lower C_{dl} values result from a decrease in the dielectric constant and/or an increase in the double layer thicknessdue to adsorption of the constituents of Dennettia tripetala (with lower dielectric constant than the displaced water molecules) on the metal/solution interface. Thus higher R_{ct} values at higher *Dennettia tripetala* concentrations indicate enhanced adsorption of the Dennettia tripetala constituents on the steel surface, which hinders the corrosion reaction. A quantitative measure of the protective effect obtained by comparing the values of R_{ct} in the absence and presence of the inhibitor using the equation given in equation 4.5.The obtained inhibition efficiency values are presented in Table 4.95(a&b). A slight disparities in the computed inhibition efficiency values from i_{corr} and R_{ct} values, and it is attributable to the inherent differences in the features of either technique. For instance, the impedance measurements are carried out on unperturbed metal surfaces (at E_{corr} and minimal current transfer), whereas polarization measurements are accompanied by considerable deformation of the metal surface (with potential scans positive and negative of E_{corr} and considerable current transfer).

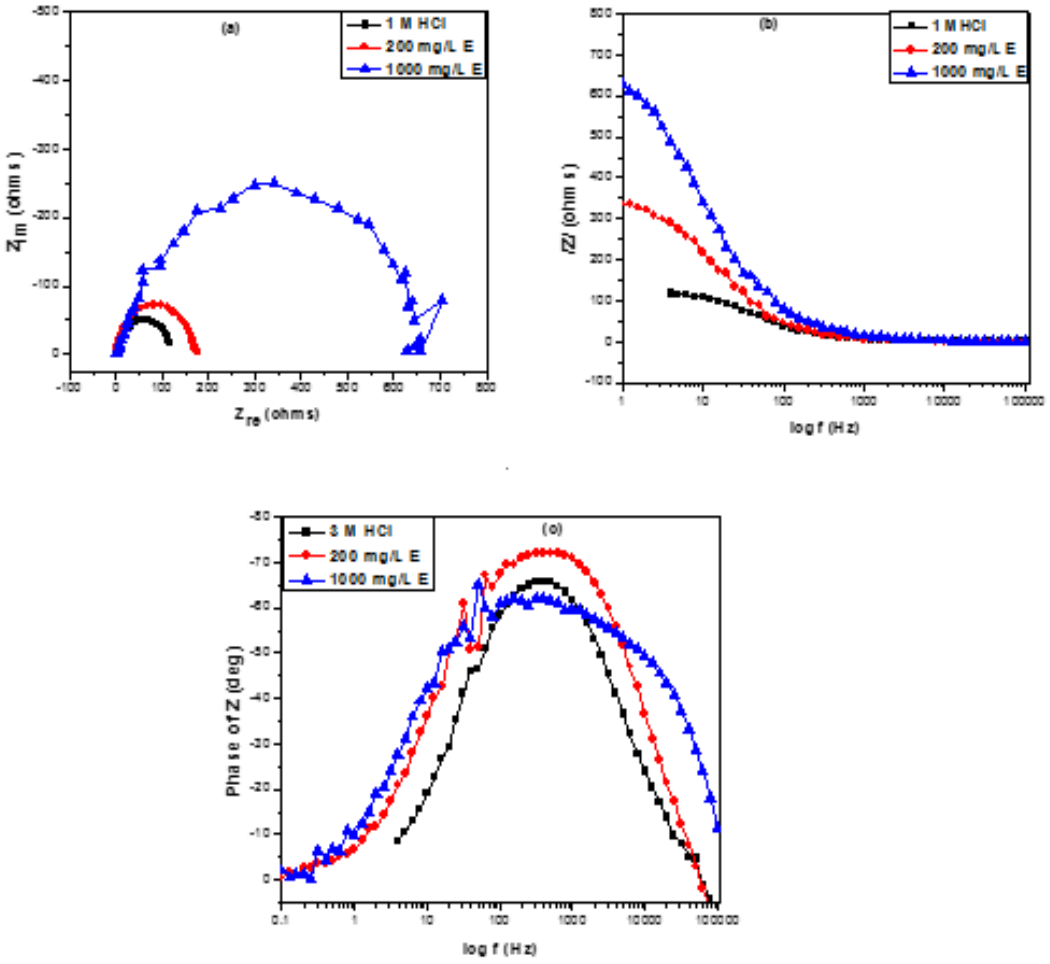

Fig. 4.57: Electrochemical impedance spectroscopy for mild steel in 1 M HCl in the presence and absence of different concentration of *Dennettia tripetala* extract :(a) Nyquist and (b) Bode modulus (c) Bode phase angle.

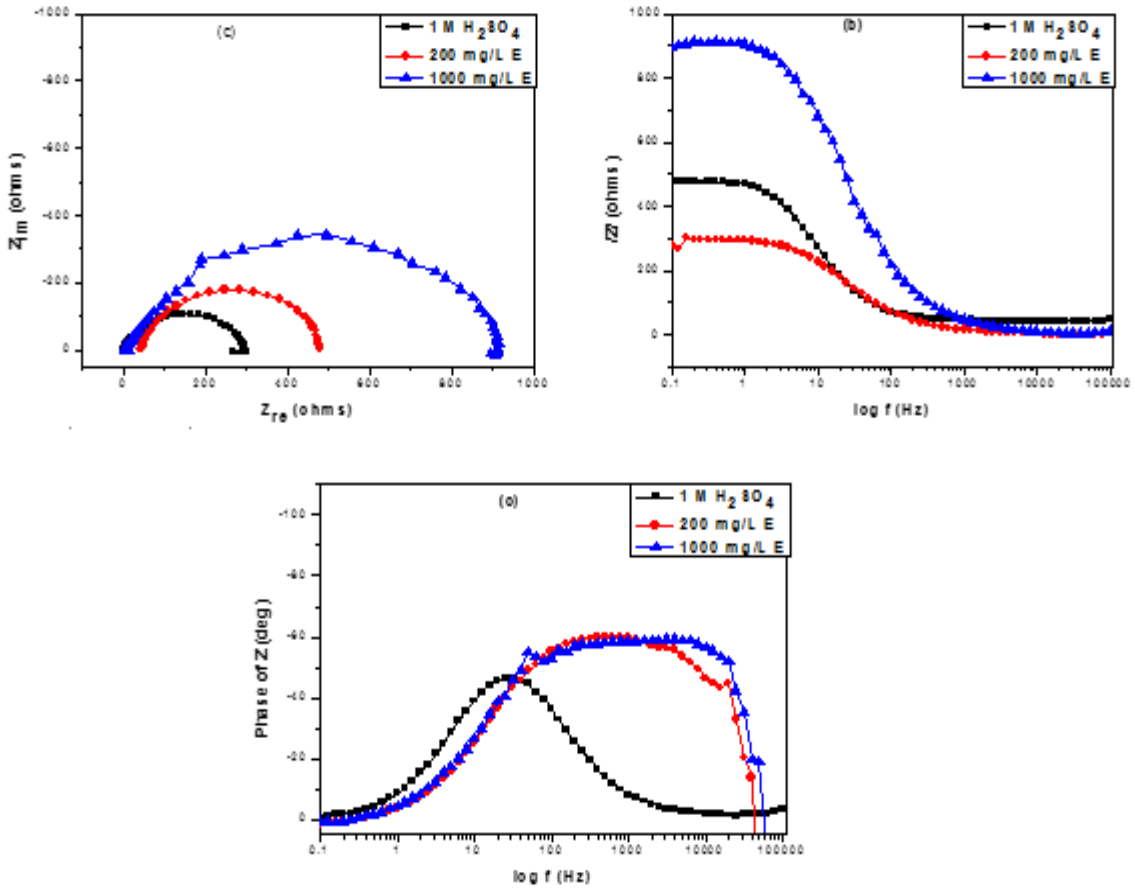

Fig. 4.58: Electrochemical impedance spectroscopy for mild steel in 1 M H_2SO_4 in the presence and absence of different concentration of *Dennettia tripetala* extract:(a) Nyquist and (b) Bode modulus (c) Bode phase angle.

(j) *Dennettia tripetala* (E) in the absence and presence of NaOH and KOH

Nyquist, Bode modulus and Bode phase plots for mild steel corrosion in 1 M NaOH and 1 M KOH in the presence and absence of *Dennettia tripetala* at different concentrations are shown in Figures 4.59 and 4.60 respectively. From our nyquist plots a single semicircle was observed. Data's for the electrochemical parameters are presented in Table 4.96(a&b). In the case of EIS studies, the inhibition efficiency (IE%) was calculated using the charge transfer resistance as shown earlier. It is clear from the nyquist plot that charge transfer resistances increased with increase in the concentration of *Dennettia tripetala*. The increase in R_{ct} values in the inhibited systems, which corresponds to an increase in the diameter of the Nyquist semicircle and in the magnitude of phase angles in our Bode plots, confirms the corrosion inhibiting effect of

Dennettia tripetala. A decrease in the dielectric constant and/or an increase in the double layer thickness lead to decrease in C_{dl}, which can be attributed to the adsorption of the organic matter onto the metal/electrolyte interface. The above is achieved by gradual removal of water molecules by *Dennettia tripetala* molecules on the electrode surface and consequently leads to decrease in the number of active sites necessary for the corrosion reaction. Results shown in Table 4.96 for mild steel in alkaline solutions are in line with potentiodynamic polarization results obtained.

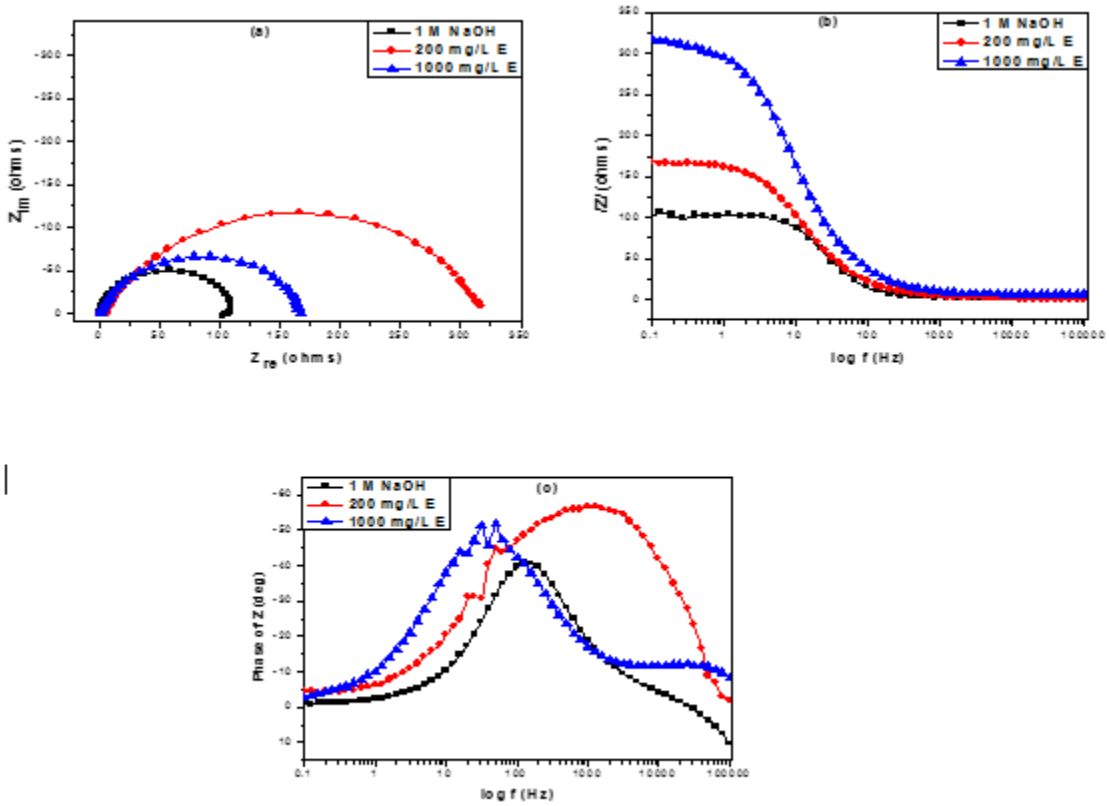

Fig. 4.59: Electrochemical impedance spectroscopyfor mild steel in 1 M NaOH in the absence and presence *Dennettia tripetala*: (a) Nyquist and (b) Bode modulus (c) Bode phase angle.

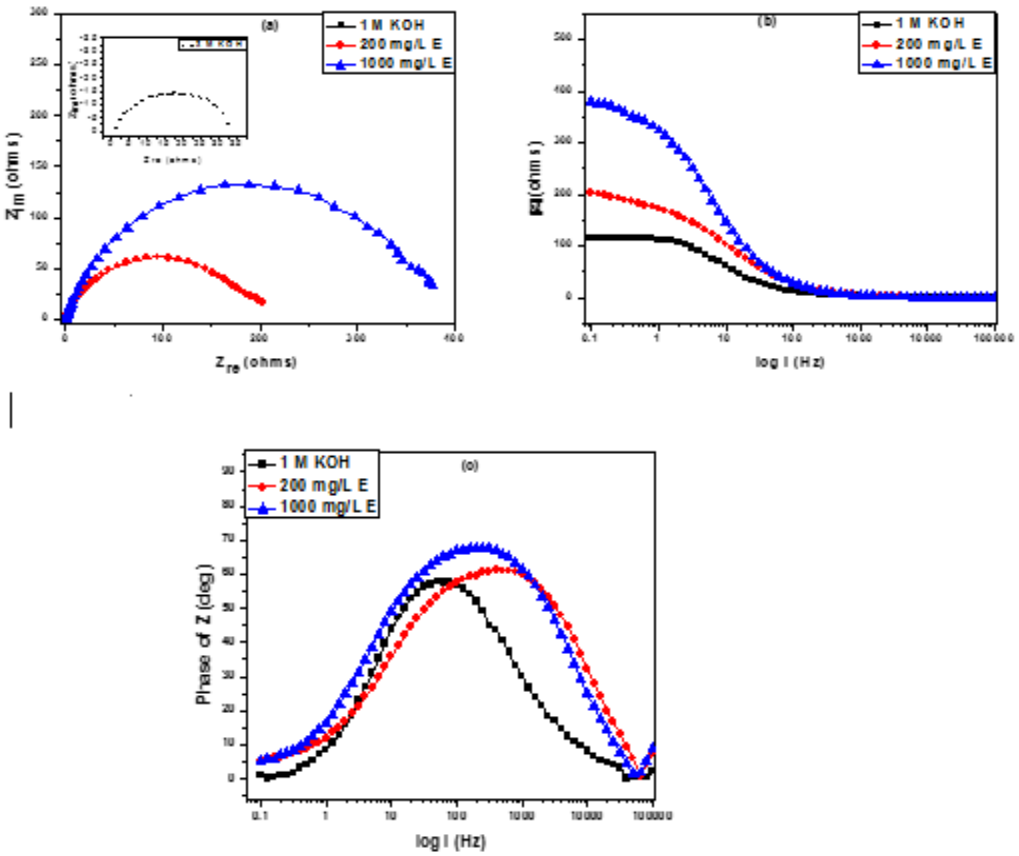

Fig. 4.60: Electrochemical impedance spectroscopy for mild steel in 1 M KOH in the absence and presence *Dennettia tripetala*:(a) Nyquist and (b) Bode modulus (c) Bode phase angle.

(k) *Chromolena odorata* in the absence and presence of M HCl and H_2SO_4

Figures 4.61 and 4.62 represent the Nyquist plots for mild steel in 1 M HCl and 1 M H_2SO_4 in the absence and presence of different concentrations of *Chromolena odorata* (F). In 1 M HCl environment, the corresponding Nyquist plots show single semicircles for all systems over the frequency range studied, relating to one time constant in the Bode plots. The high frequency intercept with the real axis in the Nyquist plots is assigned to the solution resistance (R_s) and the low frequency intercept with the real axis is ascribed to the charge transfer resistance (R_{ct}). In a 1 M H_2SO_4 environment, the Nyquist plots in the presence of *Chromolena odorata* are characterized by a large capacitive loop at high-to-medium frequency. The capacitive loop at high frequencies shows the phenomenon correlated with the double electric layer. This arises from the time constant of the electrical double layer and charge transfer in the corrosion process. It is evident in the Figures that the addition of *Chromolena odorata* to both acidic solutions result

in an increase in the size of the Nyquist semicircle (charge transfer resistance) which points towards inhibition of the corrosion process. From the data presented in Table 4.95(a&b), it is clear that *Chromolena odorata* increased the R_{ct} values at all concentrations in 1 M HCl and 1 M H_2SO_4, respectively. The values of double-layer capacitance (C_{dl}) were determined at the frequency at which imaginary component of the impedance is a maximum ($Z_{im\ (max)}$)using the equation stated earlier, because of a modification in the presence of the inhibitor, the values of C_{dl} decrease more than observed in the absence of the inhibitor. The decrease in C_{dl} value which occurs due to a decrease in the dielectric constant and/or an increase in the double layer thickness can be ascribed to the adsorption of *Chromolena odorata* on the corroding steel surface. This involves the replacement of water molecules by the *Chromolena odorata* species which has smaller dielectric constants. The increase in resistance with inhibitor concentration, suggests enhanced adsorption of *Chromolena odorata* molecules on the mild steel surface and efficient blocking of the steel surface.

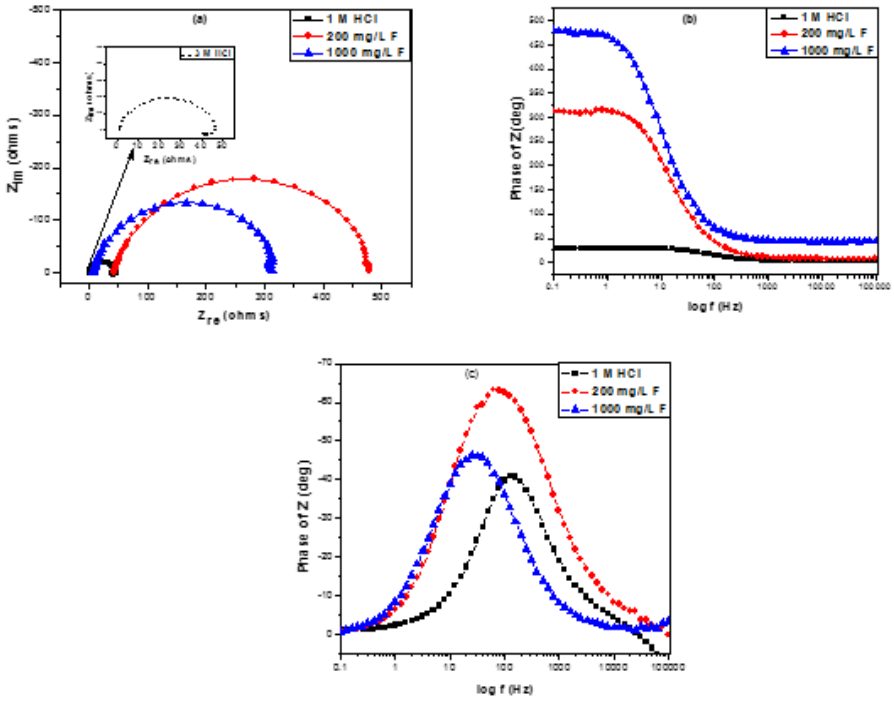

Fig. 4.61: Electrochemical impedance spectroscopy for mild steel in 1 M HCl in the presence and absence of different concentration of *Chromolena odorata* extract:(a) Nyquist and (b) Bode modulus (c) Bode phase angle.

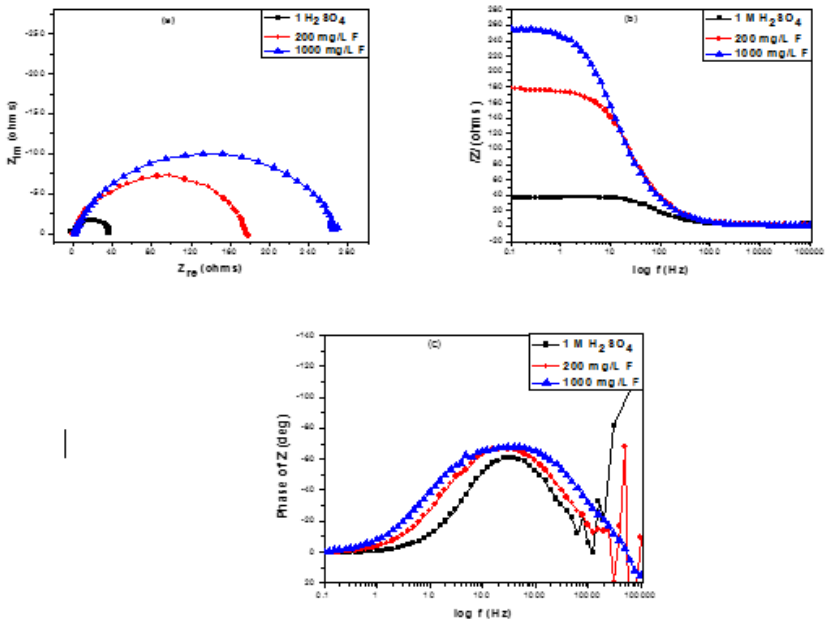

Fig. 4.62: Electrochemical impedance spectroscopy for mild steel in 1 M H_2SO_4 in the presence and absence of different concentration of *Chromolena odorata* extract:(a) Nyquist and (b) Bode modulus (c) Bode phase angle.

(l) *Chromolena odorata* (F) in the absence and presence of NaOH and KOH

It has been established that this method provide insight on the characteristics and kinetics of the electrochemical processes taking place at the metal/solution interface. Figuress 4.63 and 4.64 represent the impedance plots for mild steel in 1 M NaOH and 1 M KOH in the absence and presence of different concentrations of *Chromolena odorata*. The Nyquist plots show single semicircles over the frequency range studied, relating to one time constant in the Bode plots. The high frequency intercept with the real axis in the Nyquist plots is assigned to the solution resistance (R_s) and the low frequency intercept with the real axis is ascribed to the charge transfer resistance (R_{ct}). It is evident in Figures 4.63 and 4.64, that the introduction of *Chromolena odorata* result in an increase in the size of the Nyquist semicircle (charge transfer resistance), which all shows inhibition of the corrosion process. The numerical values of the various impedance parameters presented in Table 4.94(a&b),were analyzed by fitting to the equivalent circuit models R_s ($Q_{dl}R_{ct}$), which have been used previously to model the mild

steel/acid interface is in line with (Oguzie *et al,* 2012; Chidiebere *et al,* 2012; 2010; Kissi *et al,* 2006). A CPE is used in place of a capacitor to compensate for deviations from ideal dielectric behavior arising from the inhomogeneous nature of the electrode surfaces. The impedanceof the CPE is given by the equation in 4.3. Considering the data presented in Table 4.96(a&b), it is clear that *Chromolena odorata* increased the R_{ct} values at all concentrations compared with the uninhibited solution. Modification of the interface by adsorbed inhibitor lowered the values of C_{dl}, according to Helmholtz model. The observed decrease in C_{dl} value thus results from a decrease in the dielectric constant and/or an increase in the double layer thickness, due to the adsorption of *Chromolena odorata* on the corroding steel surface. This involves the replacement of water molecules by the inhibitor species which has smaller dielectric constants. The increase in resistance with *Chromolena odorata* concentration, suggests enhanced adsorption of *Chromolena odorata* molecules on the mild steel surface and efficient blocking of the steel surface agrees with (Moretti *et al,* 2004).The inhibition efficiency (*IE %*) from impedance data was calculated by comparing the values of the charge transfer resistance in the absence and presence of *Chromolena odorata* using equation 4.2.The obtained inhibition efficiency values are presented in Table 4.96(a&b). The obtained data is in line with the polarization results.

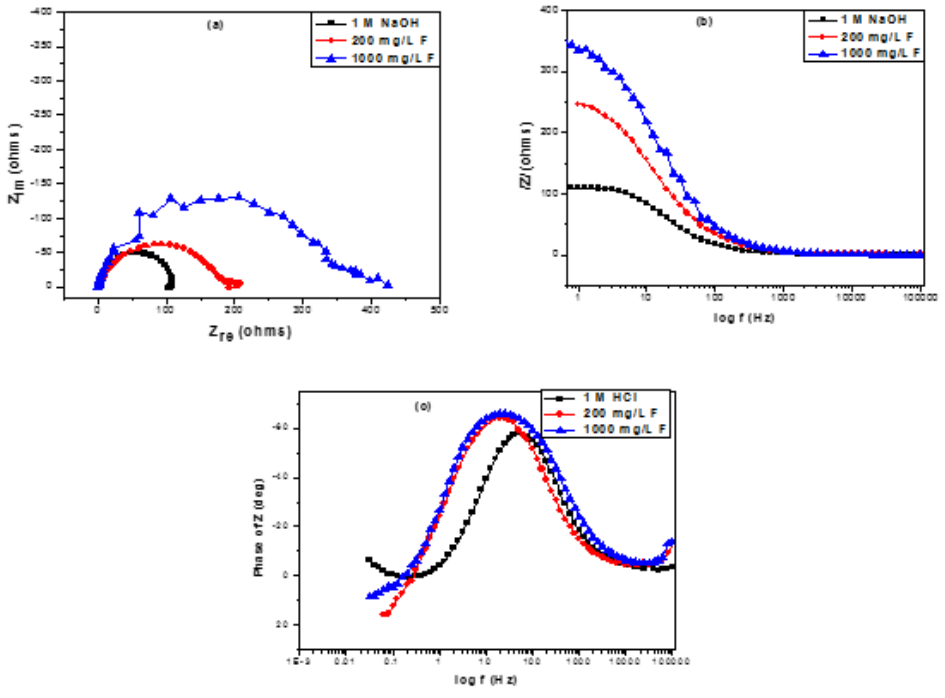

Fig. 4.63: Impedance spectra of mild steel in 1 M NaOH solution in the absence and presence of*Chromolena odorata*:(a) Nyquist, (b) Bode modulus and (c) Bode phase angle plots.

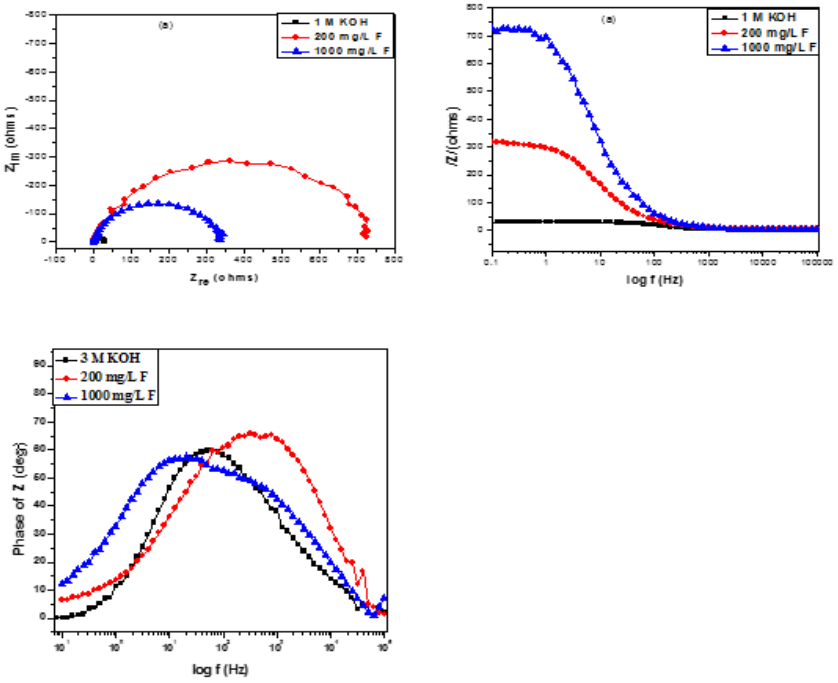

Fig. 4.64: Electrochemical impedance spectra of mild steel in 1 M KOHsolution in the absence and presence of*Chromolena odorata*: (a) Nyquist, (b) Bode modulus and (c) Bode phase angle.

4.6.2.2 Electrochemical impedance spectroscopy measurements for aluminum.

(a) *Dialium guineense* (A) in the absence and presence of HCl and H_2SO_4

The Nyquist plots showed a capacitive loop followed by an inductive loop for the Al samples in 1 M HCl and 1 M H_2SO_4 solution as shown in Figures 4.66 and 4.67. The diameter of the semi circles are related to charge transfer resistance. The size of the capacitive loops was greater in the presence of *Dialium guineense*, compared to that in the absence of the inhibitor; an indication of a higher corrosion resistance for Al in the presence of *Dialium guineense*. The occurrence of an inductive loop in both inhibibited and uninhibited aggressive solutions may indicate certain non – faradaic processes, such as adsorption and desorption of corrosion products, occurring at the sample/electrolyte interface. The equivalent circuit model shown in Fig 4.65 was used to model the impedance results in Table 4.97(a&b) obtained for Al in both solutions, after fitting with Zsimpwin software. The R_s is the solution resistance, Q_{dl} show the values of capacitance of charge and the resistance of the charge layer to penetration of the electrolyte solution. On the other hand, the inductance, L, and charge transfer resistance, (R_{ct}) characterize the processes

beneath the store of charges and is in line with Kissi, et al, 2009). It is obvious that introduction of *Dialium guineense* can modify the electrochemistry of the Al sample by reducing the penetrations of electrolyte into the substrate–electrolyte interface, thus, decreasing the rate of the corrosion in the acid solutions. This can also be evidenced by the higher value of R_{ct}, for Al in the presence of the inhibitor than the value obtained in the absence of *Dialium guineense*. It is well known that Al surfaces can form a protective layer of Al_2O_3 when in contact with aqueous solutions and is in line with (Meyer 1992; Sastri *et al*, 2007). This layer can characteristically lower the rate of the electrochemical corrosion on the Al surface. However, in the presence of *Dialium guineense*, its species adsorbs on the surface of Al, this creates a strong barrier between the Al surface and the electrolyte solutions. In this way, the corrosion potential of the Al sample shifts to more positive regions (noble values) implying a decreased surface area available for which is in agreement with the electrochemical processes. Furthermore, addition of the inhibitor also reduces the rate of penetration of the electrolyte, hence, the rate of the electrochemical processes in the Al/electrolyte interface. From the present result, the introduction of *Dialium guineense* in both solutions seem to reduce the susceptibility of the Al substrate to dissolution and to the electrochemical processes occurring at the substrate / electrolyte interface. This was made evident by the shift of E_{corr} to more positive potentials, the reduction of current densities in the inhibited environment and the increased size of the diameter of the Nyquist plots. It can be deduce that the adsorption of *Dialium guineense* species serve as a barrier blocking the contact between the Al substrate and the electrolyte solutions agrees with (Kissi,*et al*, 2006).

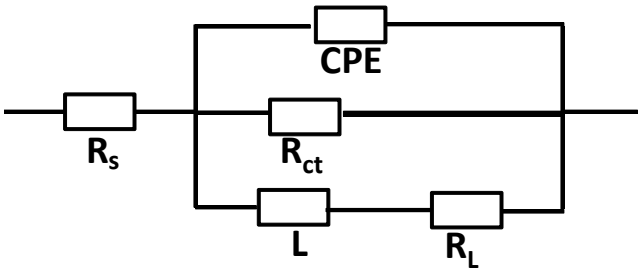

Fig. 4.65: Equivalent circuit model for Al sample.

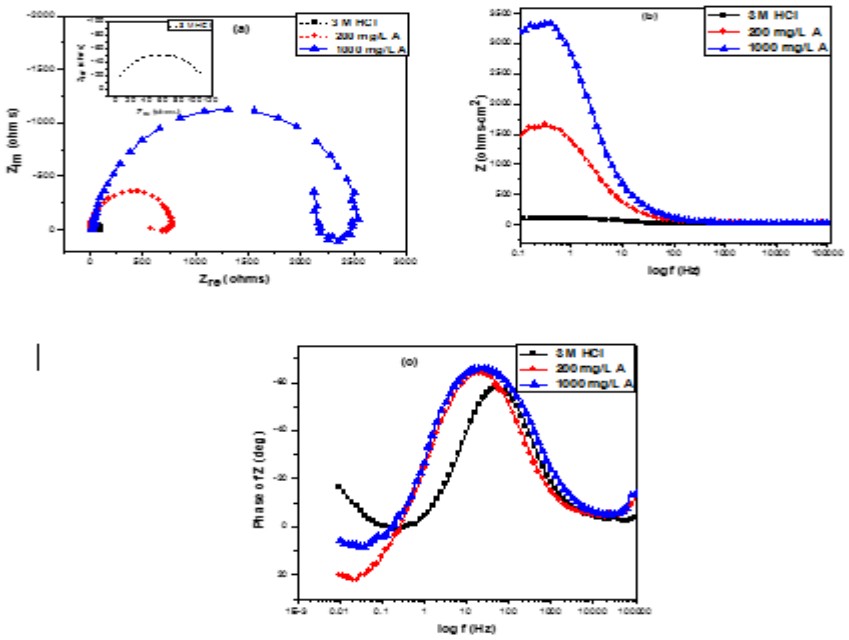

Fig 4.66: Electrochemical impedance spectroscopy for aluminum in 1 M HClin the presence and absence of different concentrations of *Dialium guineense* extract: (a) Nyquist, (b) Bode modulus and (c) Bode phase plots.

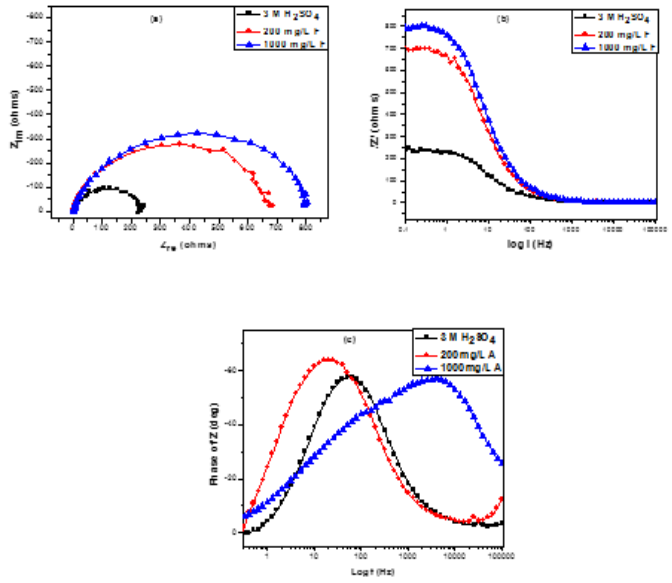

Fig 4.67: Impedance spectra for aluminum in 1 M H_2SO_4in the presence and absence of different concentrations of *Dialium guineense* extract: (a) Nyquist, (b) Bode modulus and (c) Bode phase angle plots.

(b) *Dialium guineense* (A) in the absence and presence of NaOH and KOH

The Nyquist plots showed a capacitive loop followed by an inductive loop for the Al samples in 1 M NaOH and 1 M KOH solutions as shown in Figures 4.68 and Fig 4.69. The diameter of the semi circles are related to charge transfer resistance. The size of the capacitive loops was greater in the presence of *Dialium guineense*, compared to that in the absence of the inhibitor; an indication of a higher corrosion resistance for Al in the presence of *Dialium guineense*. The occurrence of an inductive loop *Dialium guineense* in 1 M KOH solution solutions may indicate certain non – faradaic processes, such as adsorption and desorption of corrosion products, occurring at the sample / electrolyte interface. The equivalent circuit model shown in Figure 4.65 was used to model the impedance results obtained for Al in 1 M KOH environment, after fitting with Zsimpwin software. The inductance, L, and charge transfer resistance, (R_{ct}) characterize the processes beneath the store of charges. The result in Table 100(a&b) shows that the C_{dl} value was lower in the inhibited environment compared to the uninhibited solution. Similarly, the value of inductance was greater for the inhibited Al sample than for the uninhibited. It may indicate that introduction of *Dialium guineense* can modify the electrochemistry of the Al sample by reducing the penetrations of electrolyte into the substrate–electrolyte interface, thus, decreasing the rate of the corrosion in the acid solutions. This can also be evidenced by the higher value of R_{ct}, for Al in the presence of the inhibitor than the value obtained in the absence of *Dialium guineense*.It has been stated earlier that Al surfaces can form a protective layer of Al_2O_3 when in contact with aqueous solutions, this layer in question can characteristically lower the rate of the electrochemical corrosion on the Al surface. However, in the presence of A, its species adsorbs on the surface of Al, this creates a strong barrier between the Al surface and the electrolyte solutions. Again, addition of *Dialium guineense* also reduces the rate of penetration of the electrolyte. The presented result see Table 4.98(a&b)) shows clearly that the introduction of *Dialium guineense* in both environments seem to reduce the susceptibility of the Al substrate to dissolution and to the electrochemical processes occurring at the substrate/electrolyte interface. Finally one may conclude that the adsorption of *Dialium guineense* species serve as a barrier blocking the contact between the Al surface and the aggressive solutions.

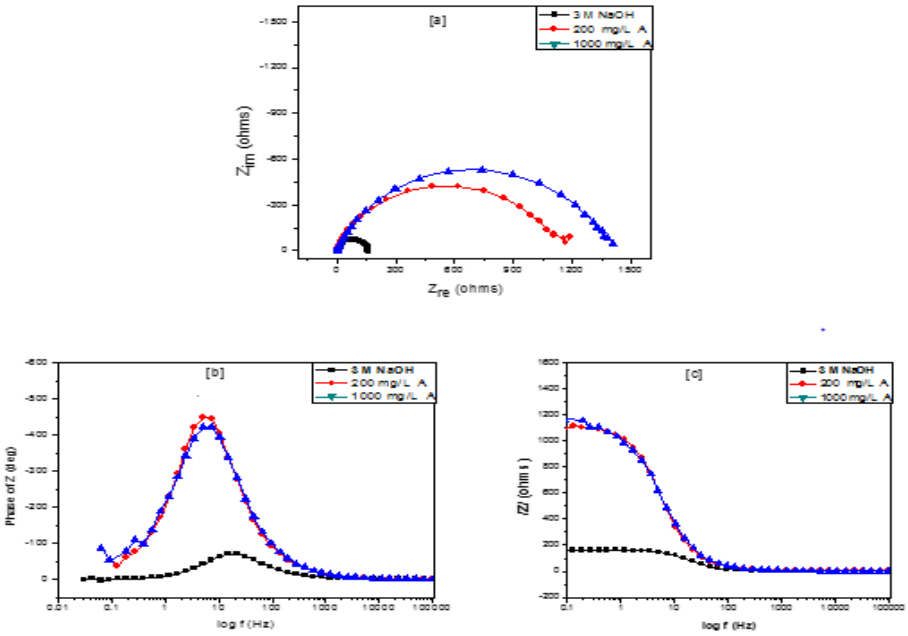

Fig 4.68: Impedance spectra of aluminum in 1 M NaOH solution in the absence and presence of *Dialium guineense*: (a) Nyquist, (b) Bode phase angle and (c) Bode modulus plots.

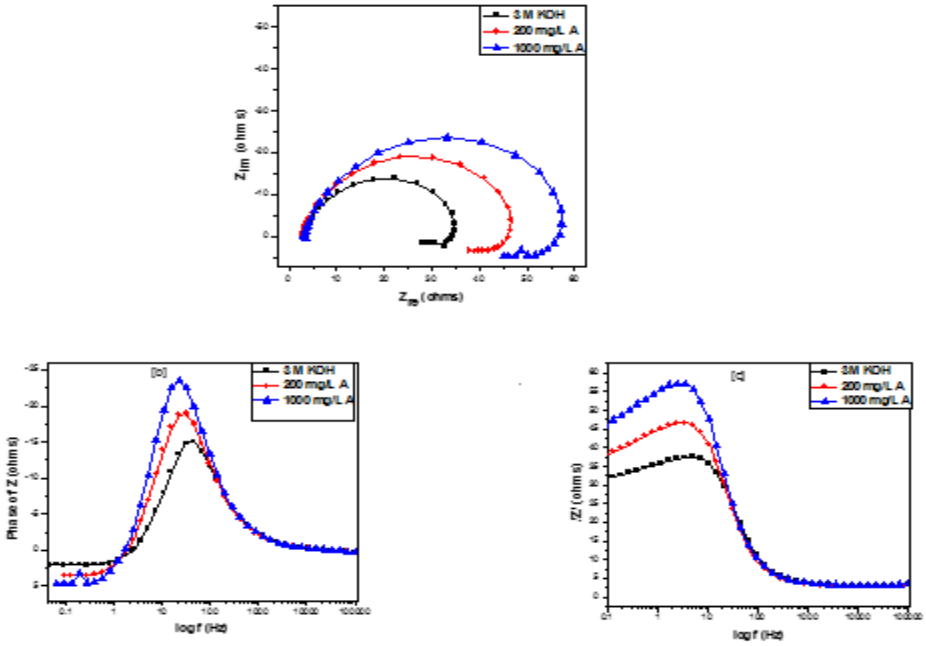

Fig 4.69: Impedance spectra ofaluminum in 1 M KOH solution in the absence and presence of *Dialium guineense*: (a) Nyquist, (b) Bode phase angle and(c) Bode modulus, plots.

(c) *Vitex doniana* (B) in the absence and presence of HCl and H_2SO_4

Electrochemical impedance spectroscopy experiment was carried out in 1 M HCl and 1 M H_2SO_4 with and without extract. Nyquist plots were recorded after 1800 s at the respective open circuit potential (OCP). The results show that the introduction of the inhibitor has a significant influence on the EIS data. Nyquist, plots for Aluminum in 1 M HCl and 1 M H_2SO_4 with and without *Vitex doniana* extract are presented in Figures 4.70 and 4.71. The Nyquist plots generally comprise one large depressed capacitve loop at high frequency and a low frequency inductive loop. The high frequency capacitive is usually related to the charge transfer process of the corrosion reaction, including formation of an oxide film whereas the low frequency inductive may be attributed to bulk or surface relaxation processes due to the adsorption of intermediate product on the oxide film covering the electrode surface and is in line with (Ihebrodike *et al* 2011). Another possible explanation for the origin of the capacitive loop at high frequency as put forward by Umoren S.A et al 2010, is the reactions involved in the formation of the oxide layer. They suggested that at the metal/oxide interface aluminum is oxidized to Al^+ intermediates. The Al^+ will subsequently be oxidized to Al^{3+} at the oxide / solution interface while 0^{2-} and H^+ ions are formed. This results in a local acidification at the oxide/electrolyte interface. Thus, the electrode impedance in this case was determined by the metal/oxide interface, the oxide film, and the oxide/solution interface. The ionic conductivity and the dielectric properties of oxide film means that it can be represented as a parallel circuit of a resistor and a capacitor. The observed depression of the Nyquist semicircle with center under the real axis is typical for solid metal electrodes that show frequency dispersion and is in line with (Ihebrodike *et al* 2011). When such a non-idea frequency response is present the capacitance of the oxide film is replaced by a constant phase element (CPE). The use of such a CPE accounts for the deviations from ideal dielectric behaviour and is related to surface inhomogeneties. Using the Zsimpwin software the Nyquist plot for Al in uninhibited 1 M HCl and 1 M H_2SO_4 was analysed by fitting to the equivalent circuit model R (QR) while the plot for the *Vitex doniana* inhibited system was analysed using a similar circuit but with one inductive element R (QR (LR)) as presented earlier.

The electrochemical parameters derived from the Nyquist plots are given in Table 4.97(a&b) and reveal that the introduction of *Vitex doniana* into the acid corrodents caused the charge transfer resistance to increase whilst reducing the double layer capacitance at any time which is a clear evidence of corrosion inhibition. It is observed from the plots that the introduction of *Vitex*

doniana extract to the corrodent led to an increase in the size of the semicircle (or diameter) which all indicate inhibition of the corrosion process. The increase in the semicircles, and decrease in double layer capacitance observed in the two environments is attributed to the formation of barrier (oxide film). This barrier also enhances the charge transfer resistance. In 1 M HCl, this barrier could arise from the change in the chemical composition of the surface film due to incorporation of Cl^- ions into the film especially through defect sites with low ionic resistance and is in line with (Abdel A.M *et al*, 2007). Abdel *et al* 2007, proposed a mechanism for the incorporated Cl^- ions on the aluminum metal oxide film to form transition compounds such as; Al $(OH)_2Cl$, Al $(OH)Cl_2$ and $AlCl_3$ in alkaline medium. If aluminum hydroxide could be formed from the interaction of its ion with dissolved oxygen and the water from the diluted acid, then, incorporation of Cl^- ions from the HCl could produce a similar transitory compounds proposed.Since the anodic reaction rate (which determines the capacitive semicircle size) is determined by the movement of ions through the surface of film, it can be said that the formation of resistory transitory compounds in the film is responsible for the increase in the charge transfer resistance and decrease in the double layer capacitance.

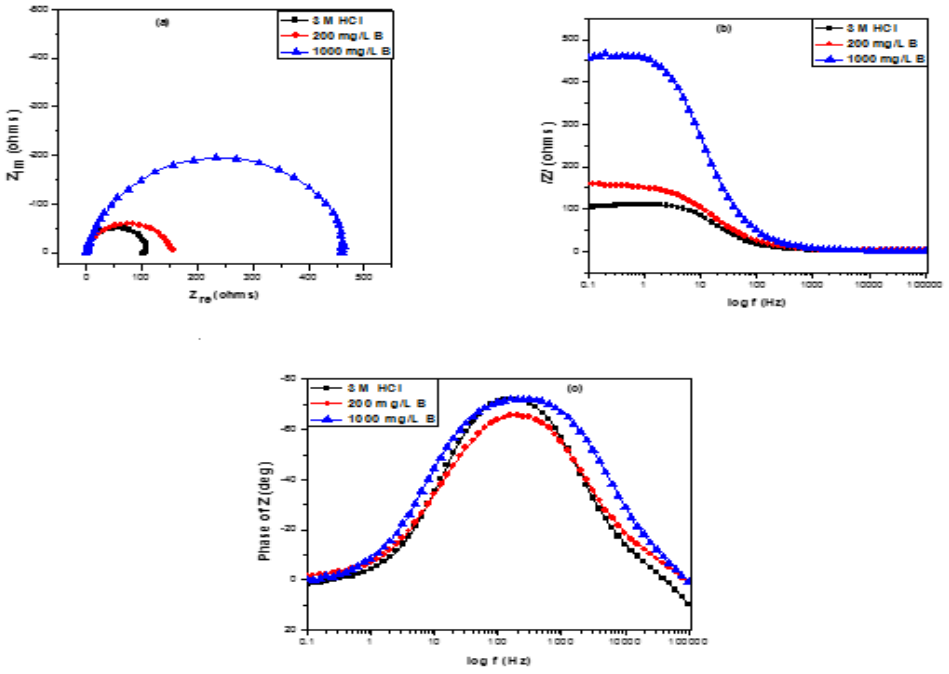

Fig 4.70: Electrochemical impedance spectroscopy for aluminum in 1 M HCl in the presence and absence of different concentration of *Vitex doniana* extracts:(a) Nyquist and (b) Bode modulus (c) Bode phase angle.

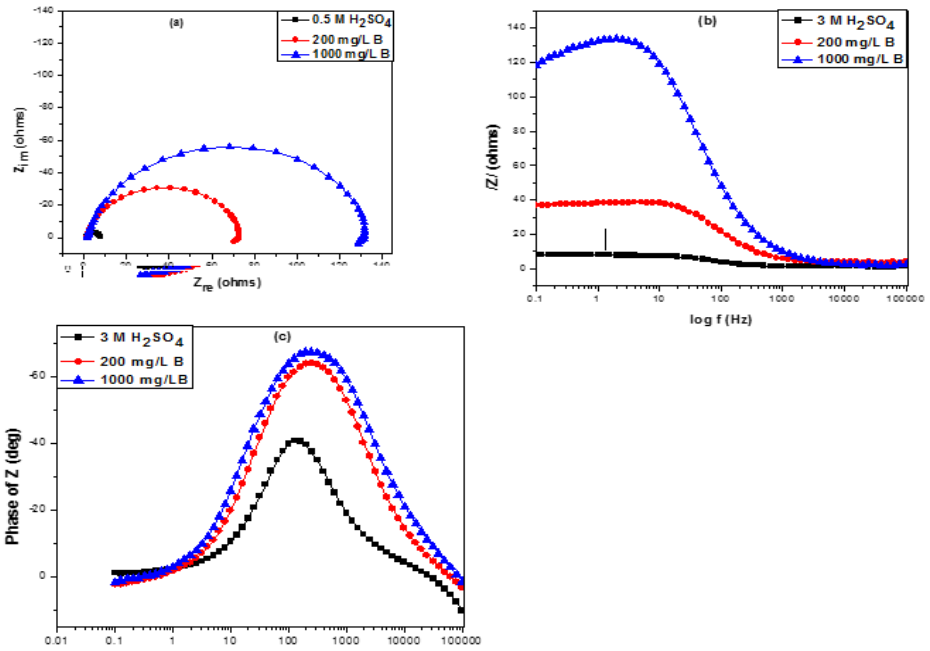

Fig 4.71: Impedance spectra for aluminum in 1 M H2SO4 in the presence and absence of different concentration of *Vitex doniana* extracts: (a) Nyquist and (b) Bode modulus (c) Bode phase angle.

(d) *Vitex doniana* extracts(B) in the absence and presence of NaOH and KOH

Nyquist, Bode modulus and Bode phase plots for aluminumcorrosion in 1 M NaOH and 1 M KOH in the presence and absence of *Vitex doniana* extracts at different concentrations are shown in Figures 4.72 and 4.73 respectively. From our nyquist plots a single semicircle was observed. Data's for the electrochemical parameters are presented in Table 4.96(a&b). In the case of EIS studies, the inhibition efficiency (IE%) was calculated using the charge transfer resistance as shown earlier. It is clear from the nyquist plot that charge transfer resistances increased with increase in the concentration of*Vitex doniana* extracts. The increase in R_{ct} values in the inhibited systems, which corresponds to an increase in the diameter of the Nyquist semicircle and in the magnitude of phase angles in our Bode plots, confirms the corrosion inhibiting effect of*Vitex doniana* extracts. A decrease in the dielectric constant and/or an increase in the double layer thickness lead to decrease in C_{dl}, which can be attributed to the adsorption of the organic matter onto the metal/electrolyte interface. The above is achieved by gradual removal of water molecules by *Vitex doniana* extracts molecules on the electrode surface and consequently leads to decrease in the number of active sites necessary for the corrosion reaction. Our results shown in Table 4.98(a&b) is in agreement with our potentiodynamic polarization results.

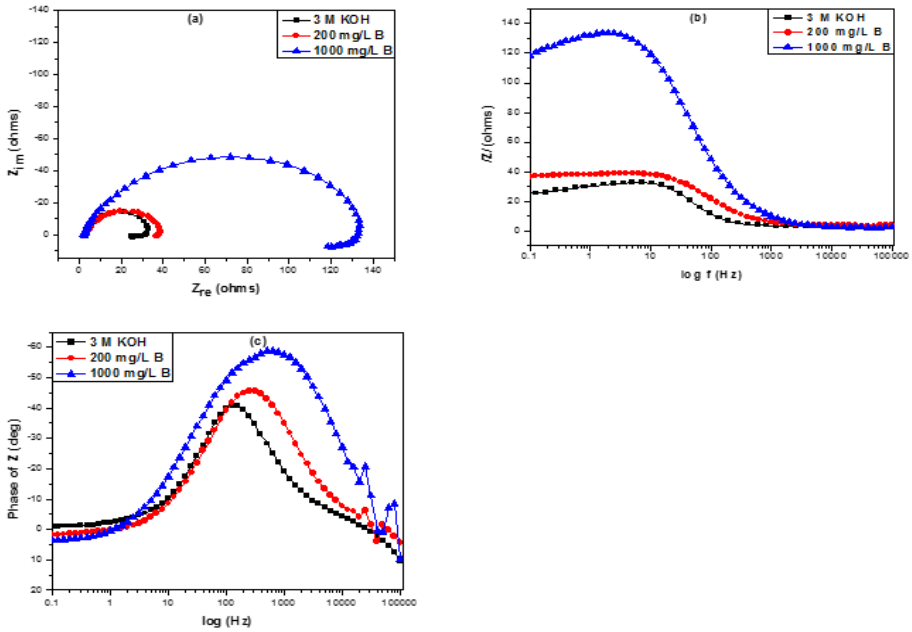

Fig 4.72: Impedance spectra for aluminum in 1 M KOH in the absence and presence of *Vitex doniana*:(a) Nyquist and (b) Bode modulus (c) Bode phase angle.

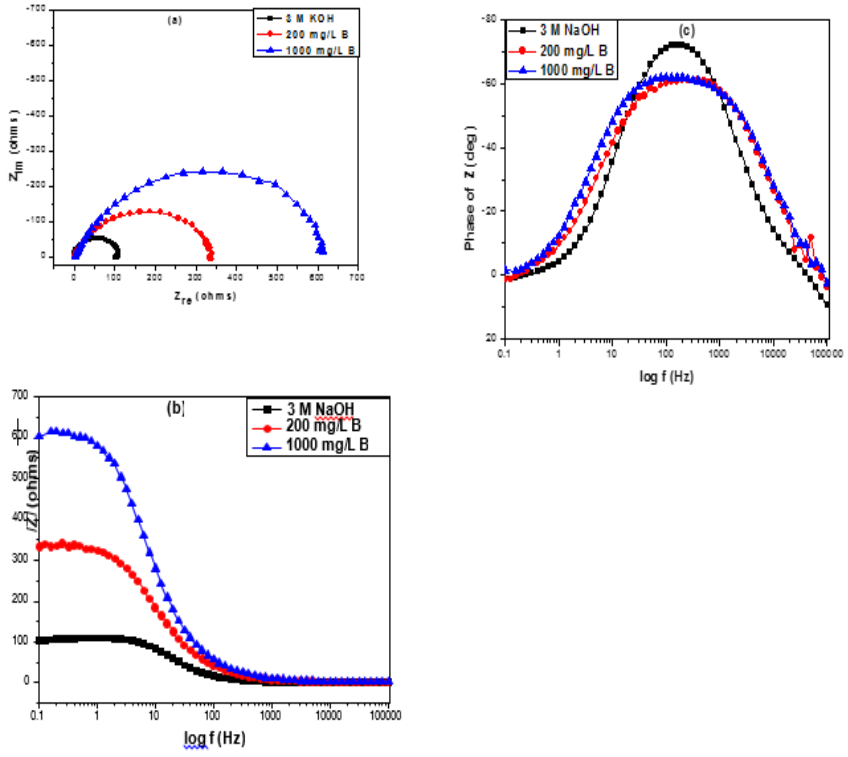

Fig 4.73: Impedance spectra for aluminum in 1 M NaOH in the absence and presence of *Vitex doniana*:(a) Nyquist and (b) Bode modulus (c) Bode phase angle.

(e) *Newbouldia leavis* (C) in the absence and presence of HCl and H_2SO_4

In the presence of *Newbouldia leavis* the Nyquist plots showed a capacitive loop followed by an inductive loop for the Al samples immersed in 1 M HCl and 1 M H_2SO_4 solution as shown in Figures 4.74 and 4.75. The diameter of the Nyquist plots are related to charge transfer resistance as mentioed before now. As expected, the size of the capacitive loops was greater in the presence of *Newbouldia leavis*, compared to that in the uninhibited solution; aprove of higher corrosion resistance for this metal in the presence of the inhibitor. Accordingly, addition of *Newbouldia leavis* modified the electrochemistry of the Al sample by reducing the penetrations of electrolyte into the substrate–electrolyte interface, thus, reducing the rate of the corrosion in the acid solutions. Further prove can be seen via the higher values of R_{ct}, for Al in the presence of the inhibitor than the value obtained in the absence of *Newbouldia leavis*. The electrochemical impedance parameters of Al were calculated and listed in Table 4.97(a&b).Furthermore, addition of the inhibitor also reduces the rate of penetration of the electrolyte, hence, the rate of the electrochemical processes in the Al/electrolyte interface. The presence of *Newbouldia leavis* in both solutions reduced the susceptibility of the Al substrate to dissolution and to the electrochemical processes occurring at the substrate/electrolyte interface. One may say that the adsorption of *Newbouldia leavis* species serve as a barrier hindering the contact between the Al surface and the electrolyte solutions.

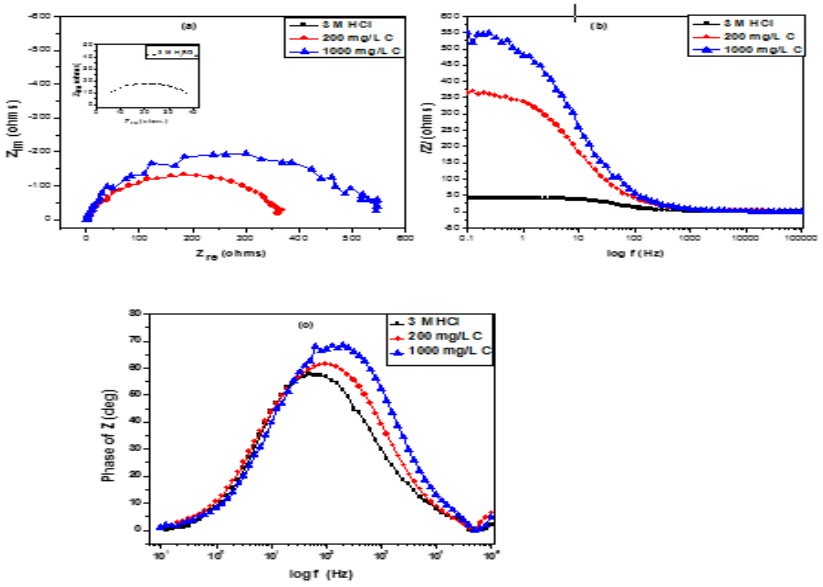

Fig 4.74. Impedance spectra for aluminum in 1 M HCl in the presence and absence of different concentration of *Newbouldia leavis* extract: (a) Nyquist and (b) Bode modulus (c) Bode phase angle.

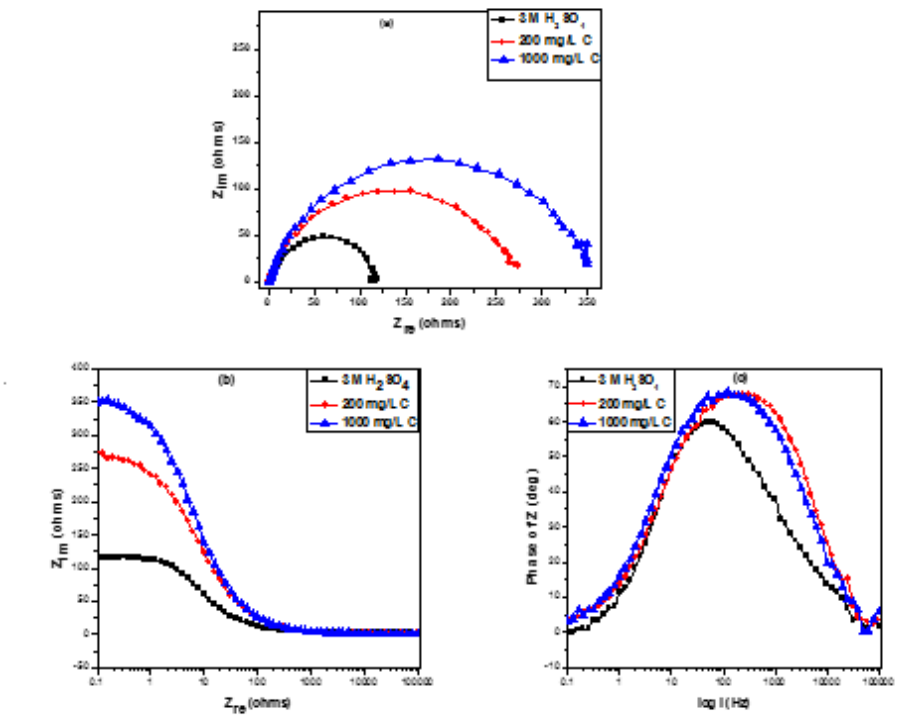

Fig 4.75. Electrochemical impedance spectroscopy for aluminum in 1 M H_2SO_4 in the presence and absence of different concentration of *Newbouldia leavis*extract:(a) Nyquist and (b) Bode modulus (c) Bode phase angle.

(f) *Newbouldia leavis* (C) in the absence and presence of NaOH and KOH

Figures 4.76 and 4.77 shows the impedance spectra plots for mild steel in 1 M NaOH and 1 M KOH in the uninhibited and inhibited *Newbouldia leavis* solutions. Table 4.98(a&b) lists the corresponding impedance parameters. The plots show single depressed capacitive semicircles over the frequency range studied. The appearance of the capacitive loop is attributable to charge transfer processes across the metal/solution interface and its diameter is related to the interfacial charge transfer resistance (R_{ct}). The plots for mild steel in the two alkaline solutions are similar, indicating similar corrosion mechanisms. However, the smaller size of the semicircle for mild steel in the uninhibited solutions of 1 M NaOH and 1 M KOHsuggests lower charge transfer resistance (Table 4.98(a&b)), hence higher susceptibility to corrosion. Addition of *Newbouldia leavis* increased the impedance of mild steel in 1 M NaOH and 1 M KOH, hence inhibited the corrosion reaction without modifying the mechanism of the corrosion process in either system. The impedance spectra were analyzed by fitting to the equivalent circuit model R_s ($Q_{dl}R_{ct}$), used

frequently to model the steel/acid interface.

From the data presented in Table 4.98(a&b), it is clear that R_{ct} for both systems increased with *Newbouldia leavis* concentration, implying that the electrode surfaces get more protection. The values of double-layer capacitance (C_{dl}) were determined using the relation given earlier.

The double-layer capacitance (C_{dl}) for mild steel in both solutions decreased with *Newbouldia leavis* addition, which, alongside the Helmholtz equation provides sufficient experimental evidence of inhibitor adsorptionand is in line withNwabanne and Okafor, 2011; Alinnor and Ejikeme, 2012; Nnanna,*et al.,* 2013. In other words, the lower C_{dl} values result from a decrease in the dielectric constant and/or an increase in the double layer thicknessdue to adsorption of organic constituents of *Newbouldia leavis* (with lower dielectric constant than the displaced water molecules) on the metal/solution interface. Thus higher R_{ct} values at higher *Newbouldia leavis* concentrations indicate enhanced adsorption of the extract constituents on the steel surface, which hinders the corrosion reactionand is in line withEbadi,*et al.,* 2012; Fouda, *et al.,* 2014 and Ashassi-Sorkhabi, *et al.,* 2015. A quantitative measure of the protective effect obtained by comparing the values of R_{ct} in the absence and presence of the inhibitor.The obtained inhibition efficiency values are presented in Table 4.98(a&b). The slight disparities in the computed inhibition efficiency values from i_{corr} and R_{ct} values is attributable to the inherent differences in the features of either technique. For instance, the impedance measurements are carried out on unperturbed metal surfaces (at E_{corr} and minimal current transfer), whereas polarization measurements are accompanied by considerable deformation of the metal surface (with potential scans positive and negative of E_{corr} and considerable current transfer). Accordingly, the measured responses from both systems are not exactly comparable as can seen from Okeoma (2015).

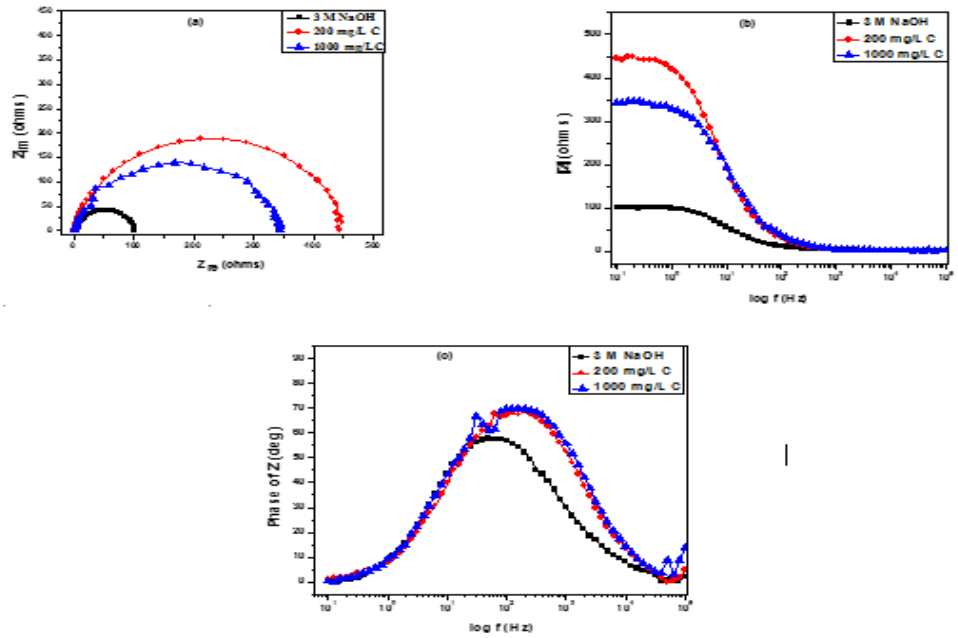

Fig 4.76 Electrochemical impedance spectra of aluminum in 1 M NaOHsolution in the absence and presence of*Newbouldia leavis*: (a) Nyquist, (b) Bode modulus and (c) Bode phase angle

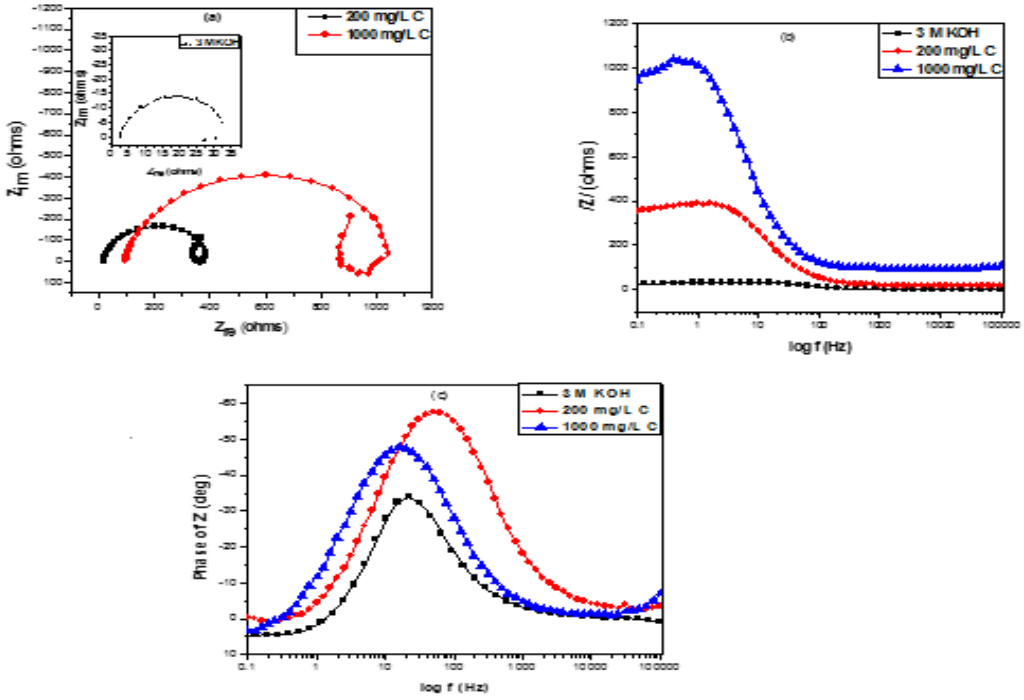

plots.

Fig 4.77 Electrochemical impedance spectra of aluminum in 1 M KOHsolution in the absence

and presence of*Newbouldia leavis*: (a) Nyquist, (b) Bode phase angle and (c) Bode modulus.

(g) *Aspilia Africana* (D) in the absence and presence of HCl and H_2SO_4

The Nyquist plots showed a capacitive loop for the Al samples in 1 M HCl and 1 M H_2SO_4 acid solution as shown in Figures 4.78 and 4.79. The diameter of the semi circle was greater for the inhibited Al sample, than the uninhibited; an indication of a higher corrosion resistance for Al in the presence of the inhibitor (*Aspilia Africana*). The correct equivalent circuit model was used to model the impedance results obtained for the inhibited and uninhibited Al samples in 1 M HCl and 1 M H_2SO_4 solution, after fitting with Zsimpwin software. We observed that the value of the charge transfer resistance was greater for the inhibited Al sample than for the uninhibited sample. It may indicate that the adsorption of the *Aspilia Africana* species can modify the electrochemistry of the Al sample by retarding the penetrations of electrolyte into the substrate–electrolyte interface, thus, decreasing the rate of the corrosion in the acid solutions and is in line with (Ebadi,*et al.*, 2012; Fouda, *et al.*, 2014 and Ashassi-Sorkhabi, *et al.*, 2015). This can also be evidenced by the reduction in the double layer capacitance for the inhibited Al samples in the two aggressive environments. The obtained values are presented in Table 4.97(a&b). The trend is in line with the potentiodynamic polarization results.

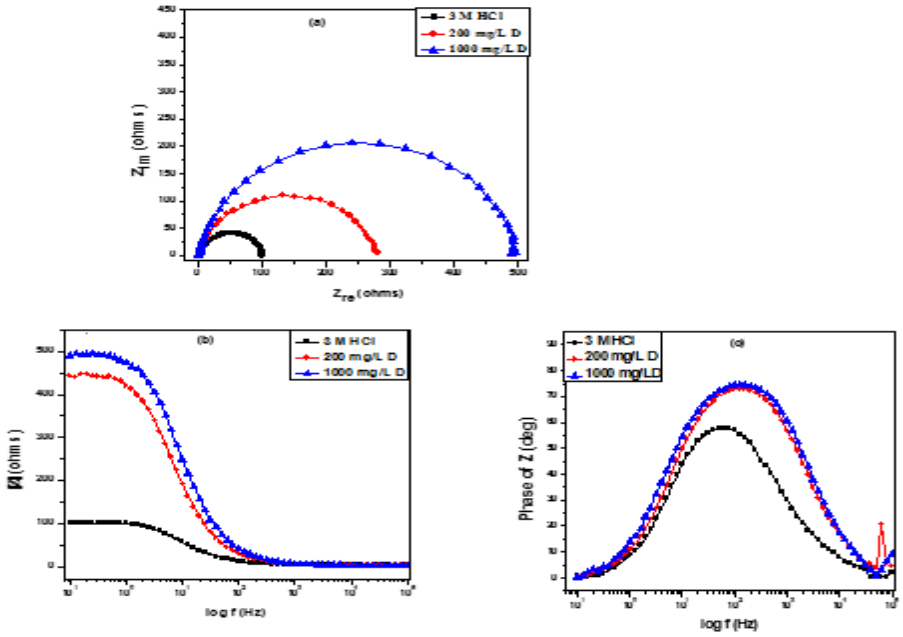

Fig 4.78: Electrochemical impedance spectroscopy for Aluminum in 1 M HCl in the presence and absence of different concentration of *Aspilia Africana* extract:(a) Nyquist and (b) Bode modulus (c) Bode phase angle.

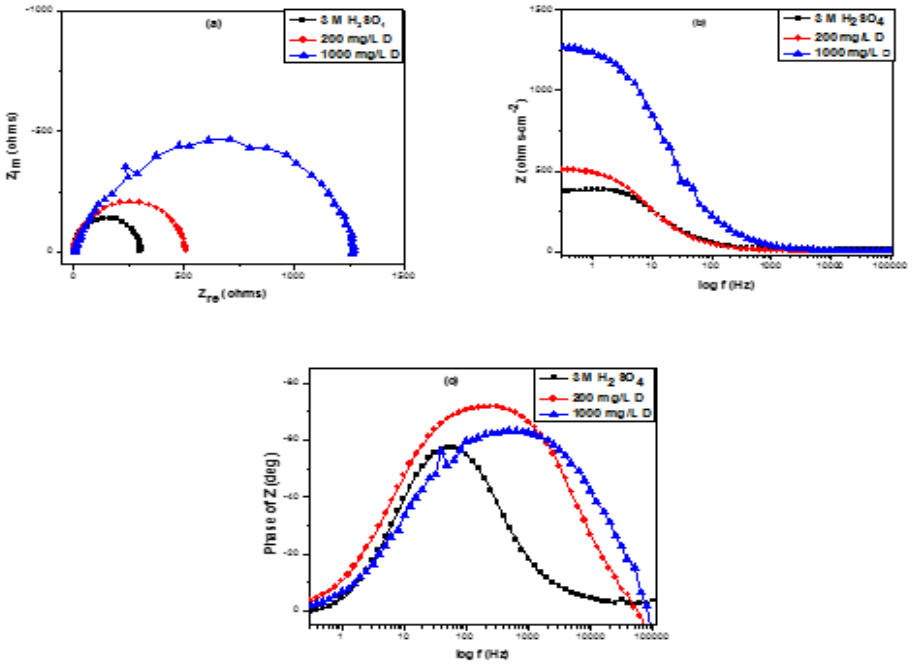

Fig 4.79**:** Electrochemical impedance spectroscopy for aluminum in 1 M H_2SO_4 in the presence and absence of different concentration of *Aspilia Africana* extract:(a) Nyquist and (b) Bode modulus (c) Bode phase angle.

(h) *Aspilia Africana* (D) in the absence and presence of NaOH and KOH

The inhibitor *Aspilia Africana* was tested whether it will give good inhibition efficiency. The corrosion of Al in 1 M NaOH and 1 M KOH in the presence of *Aspilia Africana*was investigated by EIS at 30^{o}C after an exposure period of 1800 s. Nyquist, Bode modulus and Bode phase plots for Al obtained at the interface in the absence and presence of *Aspilia Africana* at different concentrations is given in Figures 4.80 and 4.81. The impedance diagram obtained shows only one capacitive loop. An increase in the diameter of Nyquist plots was observed on increasing the *Aspilia Africana* concentration, and it is related to the charge transfer resistance R_{ct}. This proves that the *Aspilia Africana* decreases corrosion rate. Only one semicircle was also observed, From Tables 4.100(a&b), capacitance (C_{dl}) values decreased on increasing the *Aspilia Africana*

concentration indicating reduction of charges accumulated in the double layer due to formation of *Aspilia Africana* layer.

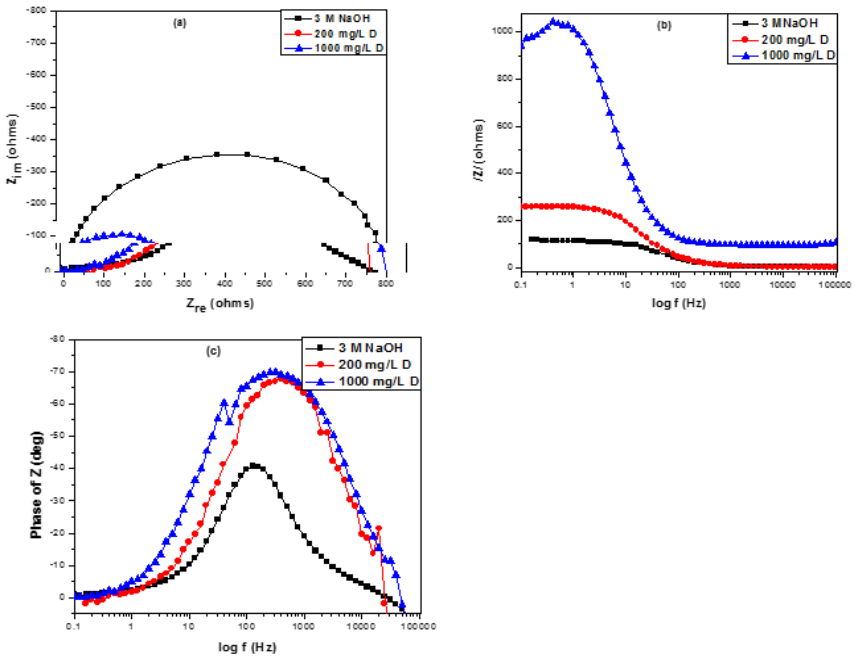

Fig 4.80: Electrochemical impedance spectroscopy for aluminum in 1 M NaOH in the presence and absence of different concentration of *Aspilia Africana* extract: (a) Nyquist and (b) Bode modulus (c) Bode phase angle.

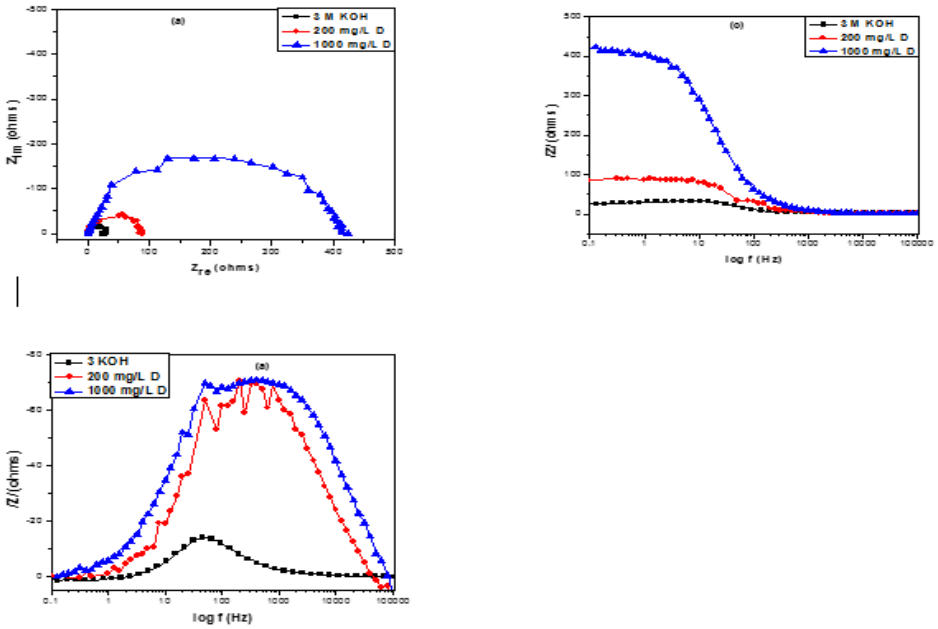

Fig 4.81: Electrochemical impedance spectroscopy for aluminum in 1 M KOH in the presence and absence of different concentration of *Aspilia Africana* extract: (a) Nyquist and (b) Bode modulus (c) Bode phase angle.

(i) *Dennettia tripetala*(E) in the absence and presence of HCl and 1 M H_2SO_4

EIS experiments were performed for Al in 1 M HCl and 1 M H_2SO_4 with and without *Dennettia tripetala* and the result presented in Figures 4.82 and 4.83. The Nyquist plots were recorded after 1800s at the respective open circuit potential (OCP). The Nyquist plots generally comprise one large depressed capacitive loop at high frequency and a low frequency inductive loop and is in line with (Gade*et al.*,2017). The results were analyzed using the Zsimpwin software, the Nyguist plots for aluminum in uninhibited and in the inhibited systems where analysed by fitting to the equivalent circuit model. The electrochemical parameter obtained from the Nyquist plots are given in Table 4.97(a&b) and show that the addition of *Dennettia tripetala* into the acid corrodent caused the charge transfer resistance to increase while a reduction in the double layer capacitance values at any time provides evidence of corrosion inhibition and is in line with John,*et al*, (2013). The values of charge transfer resistance (R_{ct}) which increases with inhibitor addition gives an indication for the system resistivity towards corrosion and has been observed to be inversely proportional to the corrosion rate. The increase in the diameter of the semicircles all indicate inhibition of the corrosion process.Also there is evidence of passivation or self protection, and was observed in both the inhibited and uninhibited systems. This is probably because of the formation of a passive oxide film. Since the anodic reaction rate, is said to be determined, by the movement of ions through the surface films, the formed passivation oxide transitory layer, could be responsible for the observed increase in charge transfer resistance (R_{ct}), decrease in double layer capacitance (C_{dl}), and increase in inhibition efficiency of the plots and is in line with Singh and Mukherjee, 2010; Negm,*et al.*, 2012b):. These results are in agreement with the results obtained in the presence of other inhibitors. A reasonable inhibition efficiency values were obtained as well.

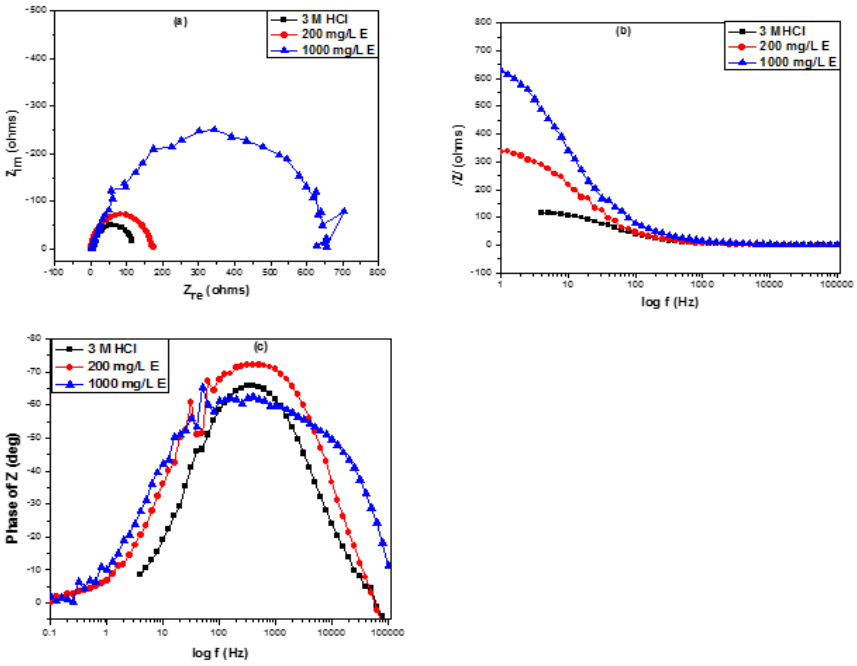

Fig 4.82: Electrochemical impedance spectroscopy for alumium in 1 M HCl in the presence and absence of different concentration of *Dennettia tripetala* extract:(a) Nyquist and (b) Bode modulus (c) Bode phase angle.

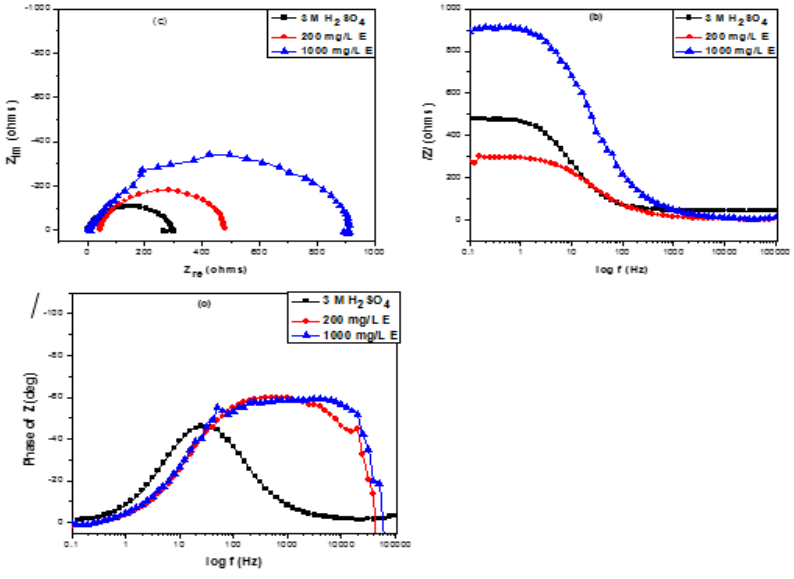

Fig 4.83: Impedance spectra for alumium in 1 M H2SO4 in the presence and absence of different concentration of *Dennettia tripetala* extract:(a) Nyquist and (b) Bode modulus (c) Bode phase angle.

(j) *Dennettia tripetala* (E) in the absence and presence of KOHandNaOH

Figures 4.84 and 4.85 shows the Nyquist plot, Bode modulus and the Bode phase angle plots obtained from impedance measurements for aluminum in 3 M KOHand1 M NaOH in the absence and presence of*Dennettia tripetala* (E) . The semi circles in Figures 4.83 and 4.84 increases as the concentration of *Dennettia tripetala* increases and this leads to an increase in the inhibition efficiency values. The shape of the semi circle in the presence and absence of the *Dennettia tripetala* remains the same showing the presence of similar mechanism which operates throughout the different concentrations and is in line with Mistry,*et al*,2012. The parameters obtained from the Nyquist and Bode plots are shown in Table 4.98(a&b). From this one can see that the solution resistance does not change much as the concentration is increased but the charge transfer resistance increases appreciably as the concentration is increasing and the double layer capacity decreases thus implying increasing inhibition efficiency as the concentration of *Dennettia tripetala* is increased and is in line with Singh and Mukherjee, 2010; Negm,*et al.*, 2012b. The formular for calculating the efficiency using impedance measurements is also given in equation 3.16.

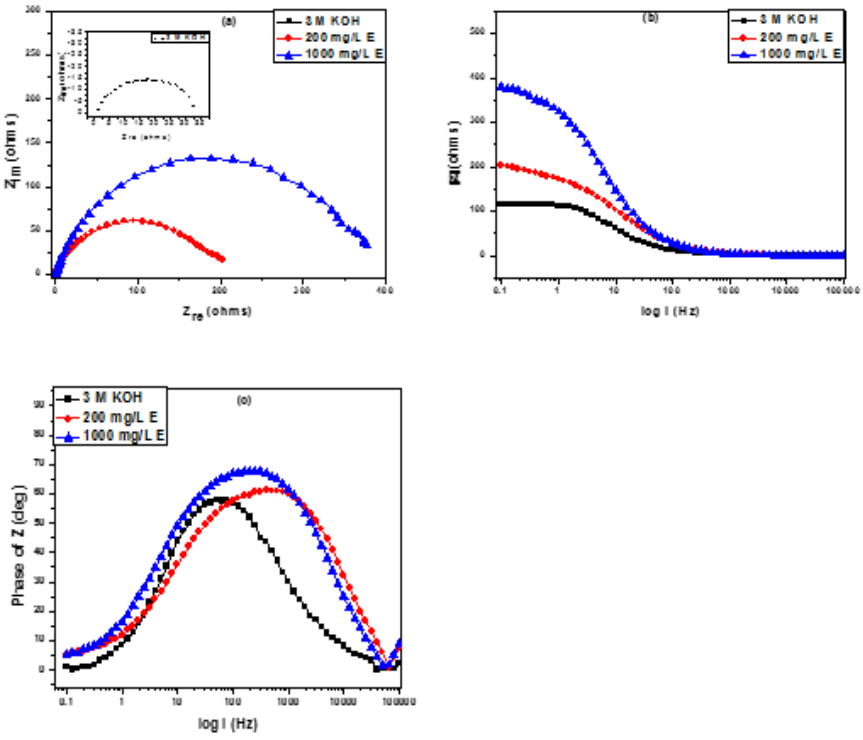

Fig 4.84: Impedance spectra for alumium in 1 M KOH in the presence and absence of different concentration of *Dennettia tripetala* extract:(a) Nyquist and (b) Bode modulus (c) Bode phase angle.

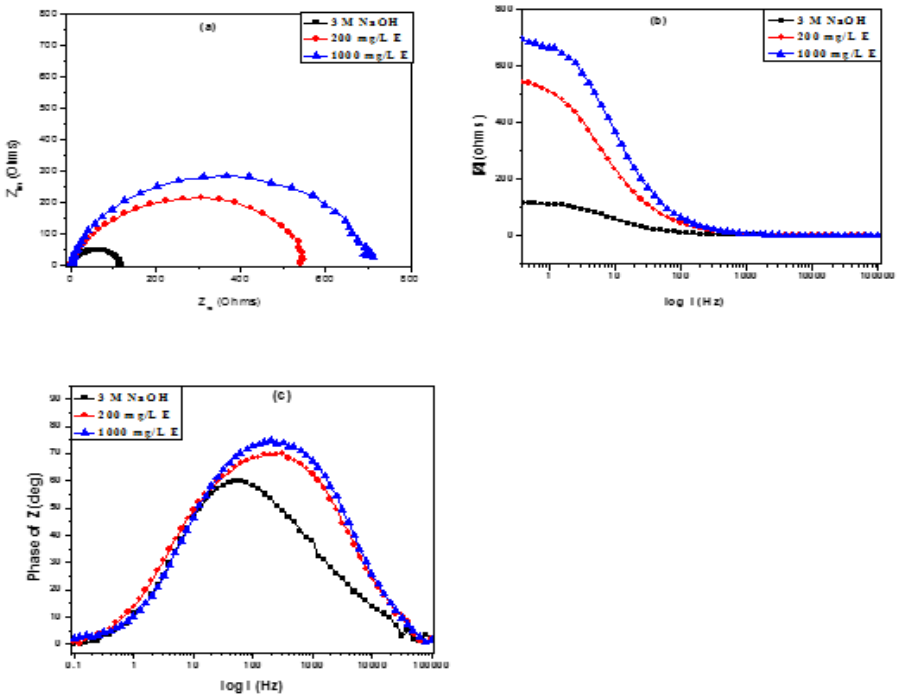

Fig 4.85: Impedance spectra for alumium in 1 M NaOH in the presence and absence of different concentration of *Dennettia tripetala* extract:(a) Nyquist and (b) Bode modulus (c) Bode phase angle.

(k) *Chromolena odorata* (F) in the absence and presence of HCl and H_2SO_4

The Nyquist plots in the presence of *Chromolena odorata* showed a capacitive loop followed for the Al samples immersed in 1 M HCl and 1 M H_2SO_4 environments as presented in Figures 4.86 and 4.87. The diameter of the Nyquist plots are related to charge transfer resistance as mentioned earlier. As one would expect, the size of the capacitive loops was more in the presence of *Chromolena odorata*, compared to that in the absence of the inhibitor; a prove of higher corrosion resistance for Aluminum in the presence of the inhibitor and is in line with Nesrin,*et al.*, 2008; Udhayakala,*et al.*, 2012. Accordingly, the result reveals that R_{ct} was greater for the inhibited Al sample than for the uninhibited, showing that introduction of *Chromolena odorata* can modify the electrochemistry of the Al sample by resisting the penetrations of the acid species

into the substrate–electrolyte interface, thus, decreasing the rate of the corrosion in the acid environments. The electrochemical impedance parameters of Al were calculated and listed in Table 4.97(a&b). The presence of *Chromolena odorata* in both solutions reduced the susceptibility of the Al substrate to dissolution and to the electrochemical processes occurring at the substrate/electrolyte interface. We therefore suggest, that the adsorption of *Chromolena odorata* species serve as a barrier blocking the contact between the Al substrate and the electrolyte solutions and is in line with Kang *et al.*, 2012.

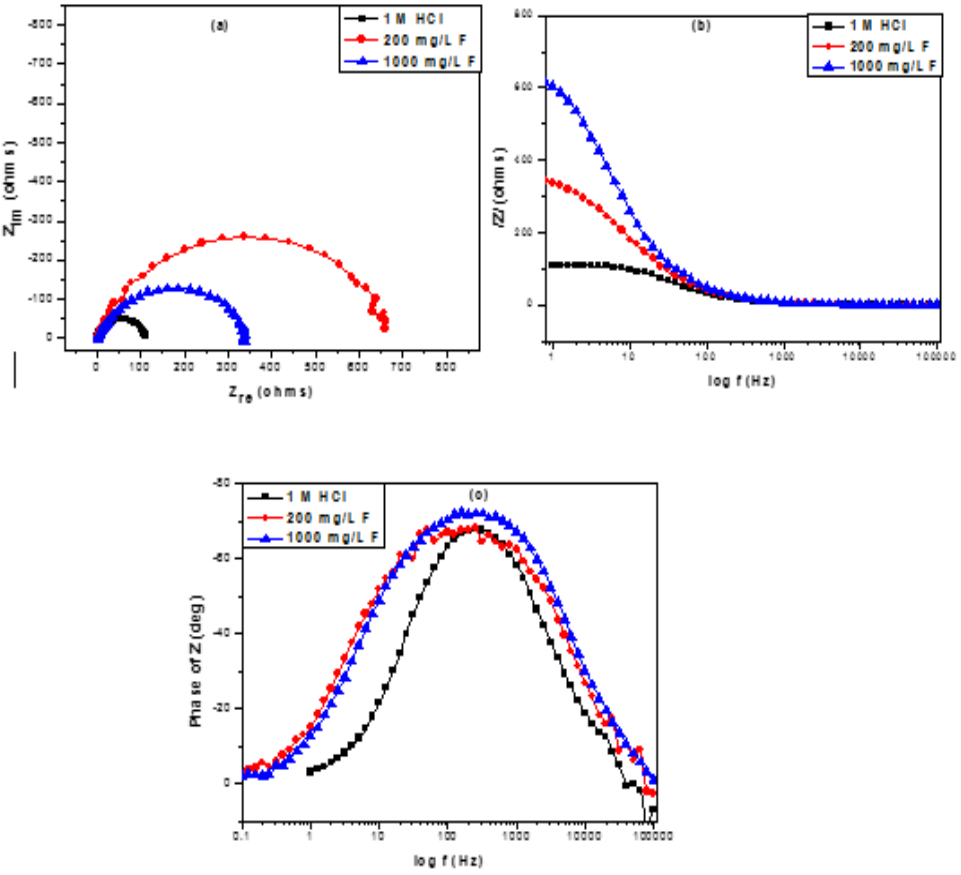

Fig 4.86: Impedance spectra of Aluminum in 1 M HCl solution in the absence and presence of *Chromolena odorata* extract: (a) Nyquist and (b) Bode modulus (c) Bode phase angle.

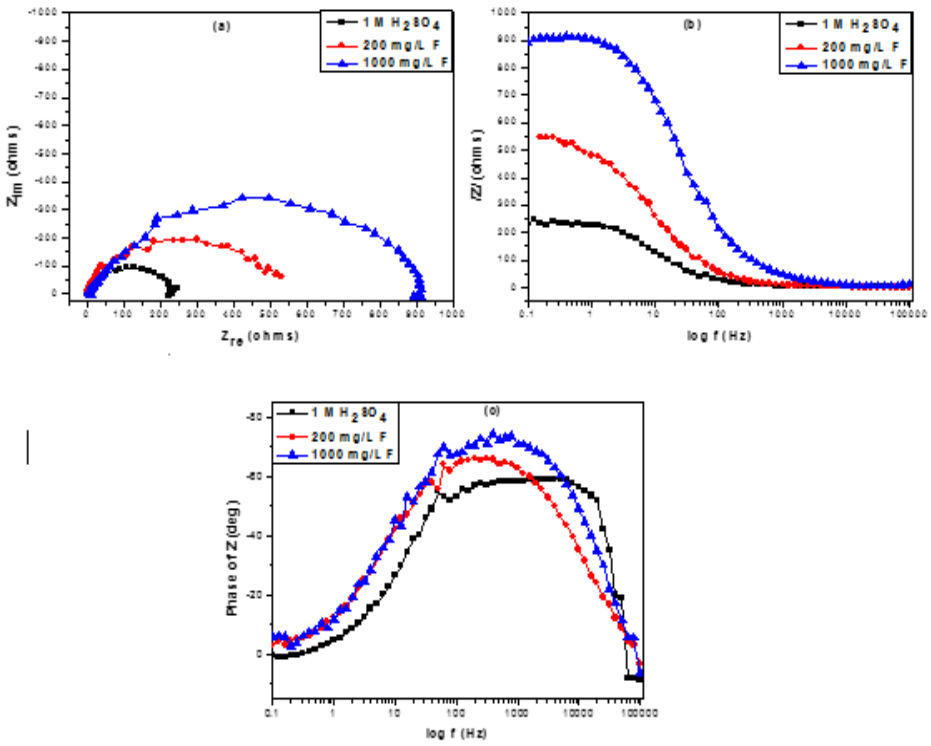

Fig 4.87: Impedance spectra of Aluminum in 3 M H_2S0_4 solution in the absence and presence of *Chromolena odorata* extract: (a) Nyquist and (b) Bode modulus (c) Bode phase angle.

(l) *Chromolena odorata* (F) in the absence and presence of KOH and NaOH

Figures 4.88 and 4.89 shows the impedance spectra for Al in the inhibited and uninhibited alkaline environments utilizing *Chromolena odorata*. Table 4.98(a&b) lists the corresponding impedance parameters. The plots show single depressed capacitive semicircles over the frequency range studied. Just like the plots obtained in the case Dialium guineense, *vitex doniana, Newbouldia leavis, Aspilia Africana* and Dennettia tripetala. The plots for the specimen is similar, implying similar corrosion mechanisms which agrees with Udhayakala,*et al*, (2012). However, the smaller size of the semicircle in the uninhibited environment suggests lower charge transfer resistance, hence higher susceptibility to corrosion. Addition of *Chromolena odorata* increased the impedance Al, hence inhibited the corrosion reaction without modifying the mechanism of the corrosion process in either system. This is is similar to Nesrin,*et al*, (2008). The impedance spectra were as well analyzed by fitting to the equivalent circuit model R_s ($Q_{dl}R_{ct}$), used earlier to model the steel/acid interface. From the data presented in Table

4.96(a&b), it is clear that R_{ct} for Al increased with *Chromolena odorata* concentration, implying that the electrode surfaces get more protection. The double-layer capacitance (C_{dl}) for the specimen decreased with *Chromolena odorata* addition.

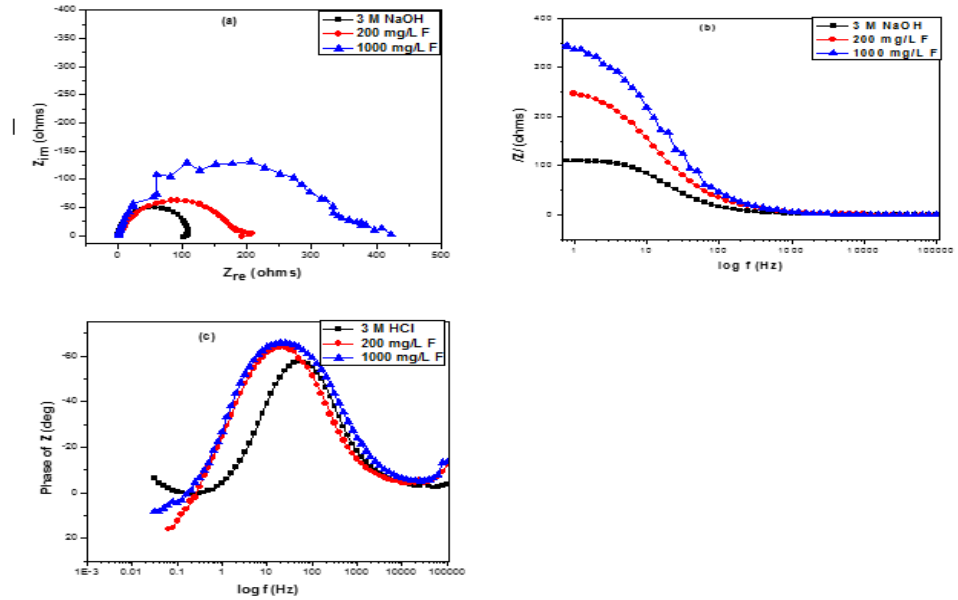

Fig 4.88: Impedance spectra of aluminum in 1 M NaOHsolution in the absence and presence of*Chromolena odorata extract*: (a) Nyquist, (b) Bode phase angle and (c) Bode modulus.

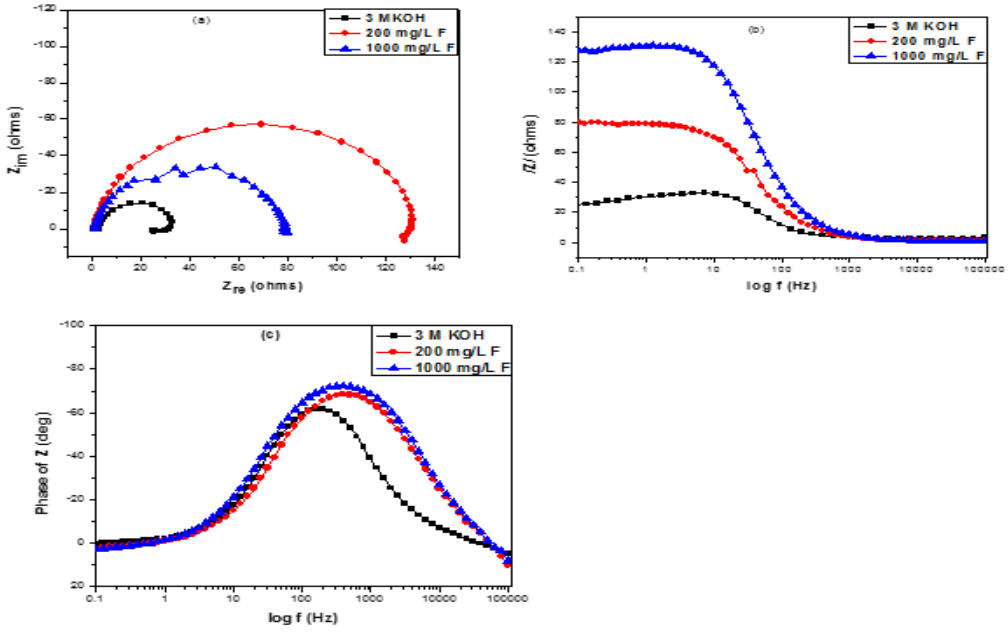

Fig 4.89: Impedance spectra of aluminum in 1 M NaOH&1 M KOHsolution in the absence and presence of*Chromolena odorata extract*: (a) Nyquist, (b) Bode phase angle and (c) Bode modulus

Table 4.95 (a): Electrochemical impedance parameters for mild steel in 1 M HCl and 1 M H_2SO_4 in the absence and presence of various plants extracts.

		Dialium guineense				*Vitex doniana*				*Newbouldia leavis*			
System	N	R_{ct} (Ω cm^2)	Rs (Ωcm^2)	C_{dl} (μF cm^{-2})	IE%	Rs (Ωcm^2)	R_{ct} (Ω cm^2)	C_{dl} (μF cm^{-2})	IE%	Rs (Ωcm^2)	R_{ct} (Ω cm^2)	C_{dl} (μF cm^{-2})	IE%
1 M HCl	0.87	1.77	45.6	87.2		2.92	38.2	153.3		1.77	45.6	87.2	
200 mg/L	0.89	1.80	162.3	34.8	71.9	3.53	1206.4	56.4	96.8	1.80	361.4	28.8	87.4
1000 mg/L	0.89	1.84	320	26.4	85.8	3.4	1609.3	36.3	97.6	1.84	542	26.9	91.6
1 M	0.86	2.92	38.2	153.3		1.77	45.6	87.2		2.92	38.2	153.3	
H2SO4	0.89	3.32	72.4	62.6	47.2	2.13	644.3	54.3	92.9	3.32	698.6	60.2	94.5
200 mg/L	0.89	3.52	132.7	47.7	71.2	3.03	905	47.2	95	3.52	797.2	45.3	95.2
1000 mg/L													

Table 4.95(b): Electrochemical impedance parameters for mild steel in 1 M HCl and 1 M H_2SO_4 in the absence and presence of various plants extracts.

		Aspilia africana				*Dennettia tripetala*				*Chromolena odorata*			
System	N	R_{ct} (Ω cm^2)	Rs (Ωcm^2)	C_{dl} (μF cm^{-2})	IE%	Rs (Ωcm^2)	R_{ct} (Ω cm^2)	C_{dl} (μF cm^{-2})	IE%	Rs (Ωcm^2)	R_{ct} (Ω cm^2)	C_{dl} (μF cm^{-2})	IE%
1 M HCl	0.87	1.77	45.6	87.2		1.77	45.6	87.2		1.77	45.6	87.2	
200 mg/L	0.89	1.84	202	41.7	77.4	1.83	131.6	33.2	65.4	1.80	308.5	34.8	85.2
1000 mg/L	0.89	1.80	256	30.6	82.2	1.86	354	28.5	87.1	1.84	470	26.4	90.3
1 M	0.86	2.92	38.2	153.3		2.92	38.2	153.3		2.92	38.2	153.3	
H2SO4	0.89	3.37	172.6	98.3	77.9	3.32	104.8	60.9	63.5	3.32	179.2	62.6	78.7
200 mg/L	0.89	3.62	264	50.1	85.5	3.52	453.5	45.2	91.6	3.52	272.9	47.7	86
1000 mg/L													

Table 4.96(a):Electrochemical parameters for mild steel in uninhibited and inhibited 1 M NaOH and 1 M KOH of various plants extracts.

System		*Dialium guineense*				*Vitex doniana*				*Newbouldia leavis*			
	R_{L1} (Ωcm^2)	Rs (Ωcm^2)	R_{ct} (Ω cm^2)	C_{dl} (μF cm^{-2})	IE%	Rs (Ωcm^2)	R_{ct} (Ω cm^2)	C_{dl} (μF cm^{-2})	IE%	Rs (Ωcm^2)	R_{ct} (Ω cm^2)	C_{dl} (μF cm^{-2})	IE%
1 M HCl	6.2	2.13	98.7	3.12		2.13	3.12	98.7		2.13	98.7	3.12	
200 mg/L	412	3.23	342.2	1.54	71.2	3.23	1.55	287.4	65.7	3.23	400.2	1.54	71.2
1000 mg/L	1988	3.67	812.5	1.02	87.9	3.67	1.07	559.4	82.4	3.67	512.5	1.02	87.9
1 M H2SO4	7.6	2.06	27.5	3.62	44.8	2.06	3.62	27.5		2.06	27.5	3.62	
200 mg/L	187	2.66	48.4	3.15	65.2	2.64	3.14	49.7	44.7	2.73	622	3.27	95.6
1000 mg/L	1124	3.12	79.1	2.84		3.19	2.83	108.6	74.7	3.33	932.3	2.99	97.1

Table 4.96(b):Electrochemical parameters for mild steel in uninhibited and inhibited 1 M NaOH and 1 M KOHof various plants extracts.

System		*Aspilia africana*				*Dennettia tripetala*				*Chromolena odorata*			
	R_{L1} (Ωcm^2)	Rs (Ωcm^2)	R_{ct} (Ω cm^2)	C_{dl} (μF cm^{-2})	IE%	Rs (Ωcm^2)	R_{ct} (Ω cm^2)	C_{dl} (μF cm^{-2})	IE%	Rs (Ωcm^2)	R_{ct} (Ω cm^2)	C_{dl} (μF cm^{-2})	IE%
1 M HCl	6.2	2.13	98.7	3.12		2.13	98.7	3.12		2.13	98.7	3.12	
200 mg/L	412	3.25	313.7	1.52	68.5	3.23	164.5	1.54	40	3.23	417.3	1.54	76.3
1000 mg/L	1988	3.66	794.6	1.09	87.6	3.67	328.2	1.02	70.2	3.67	1113.9	1.02	91.2
1 M H2SO4	7.6	2.06	27.5	3.62		2.06	27.5	3.62		2.06	27.5	3.62	
200 mg/L	187	2.64	128.4	3.11	78.6	2.66	176.2	3.15	84.4	2.66	312.8	3.15	44.8
1000 mg/L	1124	3.12	219.6	2.82	87.5	3.12	252.4	2.84	89.1	3.12	718.6	2.84	96.2

Table 4.97(a): Electrochemical impedance parameters for Al in 1 M HCl and 1 M H_2SO_4 in the absence and presence of various plants extracts.

System		*Aspilia africana*				*Dennettia tripetala*				*Chromolena odorata*			
	N	R_{ct} (Ω cm^2)	Rs (Ωcm^2)	C_{dl} (μF/cm	IE%	Rs (Ωcm^2)	R_{ct} (Ω cm^2)	C_{dl} (μF/cm	IE%	Rs (Ωcm^2)	R_{ct} (Ω cm^2)	C_{dl} (μF cm)	IE%
1 M HCl	0.87	2.38	108	2.39		2.36	100	2.39		2.38	108	a	
200 mg/L	0.89	4.03	287	3.33	65.2	4.92	197.4	2.13	49.3	3.53	329	2.93	67.2
1000 mg/L	0.89	5.42	498	1.22	79.9	6.02	652	1.01	84.7	3.88	642	2.05	83.2
1 M H2SO4	0.86	1.98	251.2	3.40		1.96	251.2	3.42		1.98	251.2	3.40	
200 mg/L	0.89	3.92	502	3.15	50	4.93	439.5	3.09	42.8	3.32	537.8	3.28	53.3
1000 mg/L	0.89	4.00	1196.3	2.78	79	6.87	902	0.99	72.2	4.18	900	2.97	72.1

Table 4.97(b): Electrochemical impedance parameters for Al in 1 M HCl and 1 M H_2SO_4 in the absence and presence of various plants extracts.

System		*Dialium guineense*				*Vitex doniana*				*Newbouldia leavis*			
	R_{L1} (Ωcm^2)	Rs (Ωcm^2)	R_{ct} (Ω cm^2)	C_{dl} (μF cm^{-2})	IE%	Rs (Ωcm^2)	R_{ct} (Ω cm^2)	C_{dl} (μF cm^{-2})	IE%	Rs (Ωcm^2)	R_{ct} (Ω cm^2)	C_{dl} (μF cm^{-2})	IE%
1 M HCl	6.2	2.38	108	2.41		2.38	108	2.41		2.38	108	2.41	
200 mg/L	716	5.53	735	2.33	85.3	6.23	161.7	3.21	33.2	6.44	341.4	3.43	68.4
1000 mg/L	1240	6.88	2452	2.05	95.6	6.98	452	1.42	76.1	6.88	492.5	1.73	78.1
1 M H2SO4	7.7	1.98	251.2	3.40		1.98	251.2	3.40	76.7	1.98	125	3.40	
200 mg/L	645	3.67	739	3.13	66	3.79	755	3.10	91.6	3.71	268	3.17	53.4
1000 mg/L	3192	5.09	3402	2.94	92.6	4.07	3007	2.98		4.04	351	2.92	64.4

Table 4.98(a):Electrochemical parameters for Al in uninhibited and inhibited 1 M NaOH and 1 M KOH of various plants extracts.

System	*Dialium guineense*					*Vitex doniana*				Newbouldia leavis			
	R_{L1} (Ωcm^2)	Rs (Ωcm^2)	R_{ct} (Ω cm^2)	C_{dl} (μF cm^{-2})	IE%	Rs (Ωcm^2)	R_{ct} (Ω cm^2)	C_{dl} (μF cm^{-2})	IE%	Rs (Ωcm^2)	R_{ct} (Ω cm^2)	C_{dl} (μF cm^{-2})	IE%
1 M HCl	6.2	2.13	145.8	3.12		2.13	145.8	3.12		2.13	145.8	3.12	
200 mg/L	532	3.72	1050.7	2.53	86.1	3.72	350	2.53	58.3	3.89	349.7	2.58	58.3
1000 mg/L	1879	3.98	1418.2	2.12	89.7	3.98	625	2.12	76.7	3.23	438.9	2.16	66.8
1 M H2SO4	7.6	2.06	30.2	3.62		2.06	30.2	3.62		2.06	30.2	3.62	
200 mg/L	32	2.67	47.4	3.64	36.3	2.67	44.6	3.64	32.3	2.11	377.8	3.23	92
1000 mg/L	68	3.22	59.5	2.93	50.2	3.22	132.8	2.93	77.3	2.04	959.6	2.71	96.9

Table 4.98(b):Electrochemical parameters for Al in uninhibited and inhibited 1 M NaOH and 1 M KOH of variousplants extracts.

System	*Aspilia africana*					*Dennettia tripetala*				*Chromolena odorata*			
	R_{L1} (Ωcm^2)	Rs (Ωcm^2)	R_{ct} (Ω cm^2)	C_{dl} (μF cm^{-2})	IE%	Rs (Ωcm^2)	R_{ct} (Ω cm^2)	C_{dl} (μF cm^{-2})	IE%	Rs (Ωcm^2)	R_{ct} (Ω cm^2)	C_{dl} (μF cm^{-2})	IE%
1 M HCl	6.2	2.13	145.8	3.12		2.13	145.8	3.12		2.13	145.8	3.12	
200 mg/L	230	3.71	262	2.55	44.4	3.42	528	2.59	72.4	3.72	206.4	2.53	29.4
1000 mg/L	369	3.99	802	2.18	81.8	3.87	679.7	2.23	78.5	3.98	413.9	2.12	64.8
1 M H2SO4	7.6	2.06	30.2	3.62		2.06	30.2	3.62	85.4	2.06	30.2	3.62	
200 mg/L	246	2.61	96.4	3.62	68.8	2.73	206.9	3.66	92.2	2.67	81.3	3.64	62.9
1000 mg/L	562	3.29	412.2	2.91	92.7	3.24	387.5	2.92		3.22	132.5	2.93	77.2

In summary, the results obtained from this work indicate that ethanol extracts of *Dialium guineense*, *vitex doniana, Newbouldia leavis, Aspilia Africana* and *Dennettia tripetala* and *Chromolena odorata*on mild steel and aluminum corrosion in 1 M HCl and 1 M H_2SO_4 solution and also in 1 M NaOH and 1 M KOH are good corrosion inhibitors. They six ethanol extracts actually inhibited the metals (aluminum and mild steel) from corrosion in the studied environments (KOH, NaOH, HCl and H_2SO_4) in a concentration dependent manner. The extracts functioned by adsorption of the organic constituents on the metal surface as revealed by the electrochemical impedance measurements, and inhibited both the cathodic and anodic reactions as shown in the potentiodynamic polarization examination carried out. The extracts gave excellent inhibition efficiencies.

4.7 Quantum Chemical Study

It is obvious that our experimental results so far suggest that the corrosion inhibiting performance of the selected active constituents [aspartic acid (AA), 2-hydroxymethylcyclopentano (HMCP), polygalitol (PGT), undecanoic acid (UCA), malic acid (MA), N-methyl-3,4 methylenedioxy phenylpropan-3-amine (NMPA), propanamide (PNM), carbamodithioic acid (CDA), morpholine, 4-methyl-4-oxide (MMO), octanal, 3-dodecanol, 3,7,11-trimethyl (ODT) and 9-oxononanoic acid (OAA)] of *Dialium guineense*, *vitex doniana, Newbouldia leavis, Aspilia Africana* and*Dennettia tripetala* and *Chromolena odorata* results from adsorption of these inhibitor constituents on the mild steel surface. To further validate our findings, density functional theory (DFT) has been employed to precisely calculate information regarding molecular geometries and electron distributions. Due to its accuracy and smaller time required for the computation, the DFT method was used to give some insight into the inhibitory mechanism of these active constituents on the mild steel surface. Quantum chemical parameters such as E_{HOMO}, E_{LUMO}, the energy gap ΔE ($E_{LUMO} - E_{HOMO}$) and adsorption energy were obtained for*Dialium guineense, vitex doniana, Newbouldia leavis, Aspilia Africana* and *Dennettia tripetala* and *Chromolena odorata* active constituents in order to predict its activity toward a mild steel surface.

$$\Delta E = (E_{LUMO} - E_{HUMO}) \quad (4.5)$$

These parameters were generated after geometric optimization with respect to all nuclear coordinates. Frontier molecular orbital theory is very useful in predicting the adsorption centers

in these molecules, which are responsible for interaction with the metal surface. Figures 4.90 – 4.100(a - e), show the total electron density, the Fukui functions for electrophilic (F^-) and nucleophilic (F^+), the highest occupied molecular orbital (HOMO) and lowest unoccupied molecular orbital (LUMO). The HOMO and LUMO energy orbitals are mostly occupied on the heteroatoms present in the molecules under study. The Mulliken charge analysis was used to estimate the adsorption centers of the inhibitors. Negatively charged atoms have high ability to adsorb on the mild steel surface. The adsorption of inhibitor molecules on the metal surface is due to the donor−acceptor interaction between inhibitor molecules and the metal surface. The electron donating ability of the molecule is associated with the E_{HOMO}. High values of E_{HOMO} indicate the tendency of inhibitor molecules to donate electrons to the acceptor molecules with empty molecular orbitals. The ability of a molecule to accept the electrons is related to E_{LUMO}. The lower value of E_{LUMO} indicates the easier acceptance of electrons from the metal surface and may lead to higher inhibition efficiency, though this has not been well established. The energy gap between the LUMO and HOMO energy levels, that is, ΔE of the molecule, is another important factor to determine the inhibition efficiency. The molecules with low ΔE values give better inhibition efficiencies because the excitation energy gap is more polarizable and is generally associated with chemical reactivity. Table 4.99 provides some quantum chemical parameters (HOMO, LUMO, energy gap, molecular surface area and adsorption energy) related to the molecular electronic structures of the most stable conformations. We really expect a flat – lying adsorption orientation as shown in Figures 4.90 – 4.100 (f & g), because the electron density is spread all around the molecule of each represented inhibitor. Forcite molecular dynamics was employed to calculate different low energy adsorption configurations of HMCP, PGT, UCA, MA, NMPA, PNM, OAA, MMO, ODT and CDA molecule on Fe surface.The Fe surface was cleaved along the (110) plane because it has a density packed surface and the most stabilization at this position. Calculations were carried out in a 12 x 10 supercell using the COMPASS (Condensed phase opitimzed molecular potentials for atomistic simulation studies) force field and the smart algorithm with NVE (microanonical) ensemble, a time step of 1 fs, and simulation time 5 psand is in line with Udhayakala,*et al*, (2012). The temperature was fixed at 350 K. Simulation was done using the optimized structure of the selected active constituents and Fe. The system was quenched every 250 steps.Figures 4.90 – 4.100 (f & g) show the optimized (lowest energy) adsorption structures for the selected active constituents in each case on the Fe

(110) surface from our simulation. As proposed earlier, due to delocalization of the electron density all around the chosen molecules a flat – lying adsorption orientation was observed. This orientation increases contact and this result to an increase in the degree of surface coverage. However, the properties calculated by quantum chemical approach, give information about reactivity of these molecules but the reactivity cannot directly be translated to corrosion inhibition efficiency, which involves more processes such as competitive adsorption, film formation, etc. Therefore the correlations generated were not enough for optimizing the inhibitor structure. The adsorption energy (E_{ads}) which is important in characterizing the adsorption of these molecules onto the Fe surface was estimated using the equation:

$$E_{ads} = E_{total} - \left(E_{inhibitor} - E_{surface}\right) \quad (4.6)$$

where $E_{inhibitor}$, $E_{surface}$, and E_{total} represents the energy of a single molecule of these selected active components, the Fe slab without adsorption, and the total energy of the system containing a molecule and Fe surface, respectively. The order of the calculated adsorption energy for the selected active constituents of the inhibitors are presented in Table 4.99.

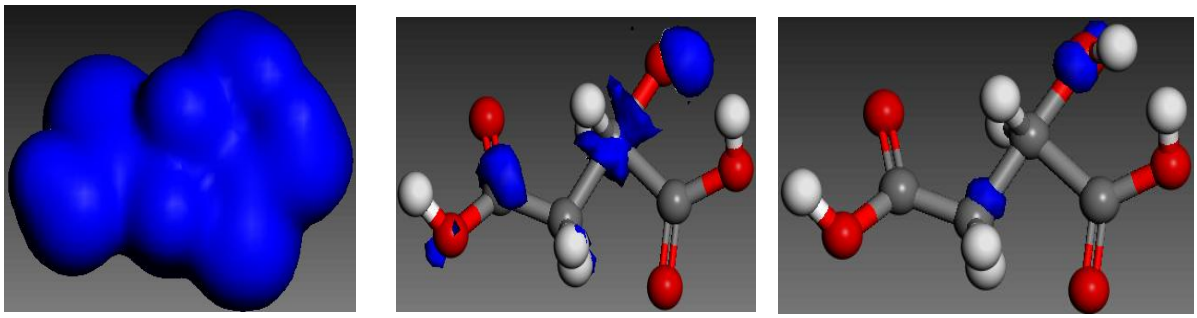

(a) Electron density (b) Electrophilic F(-) (c) Nucleophilic F(+)

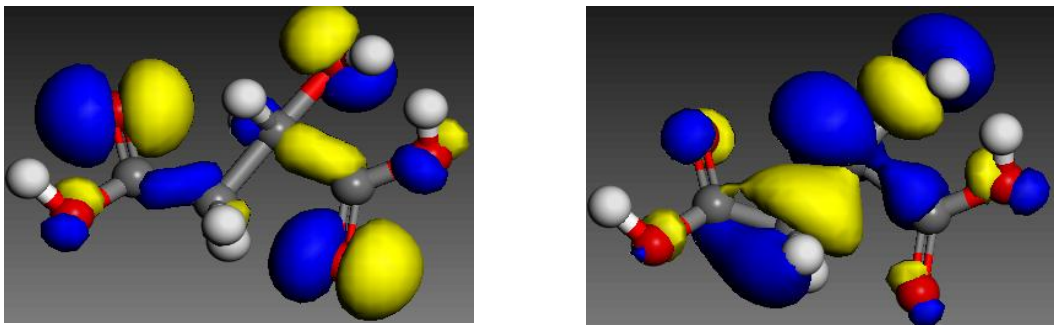

(d) HOMO (e) LUMO

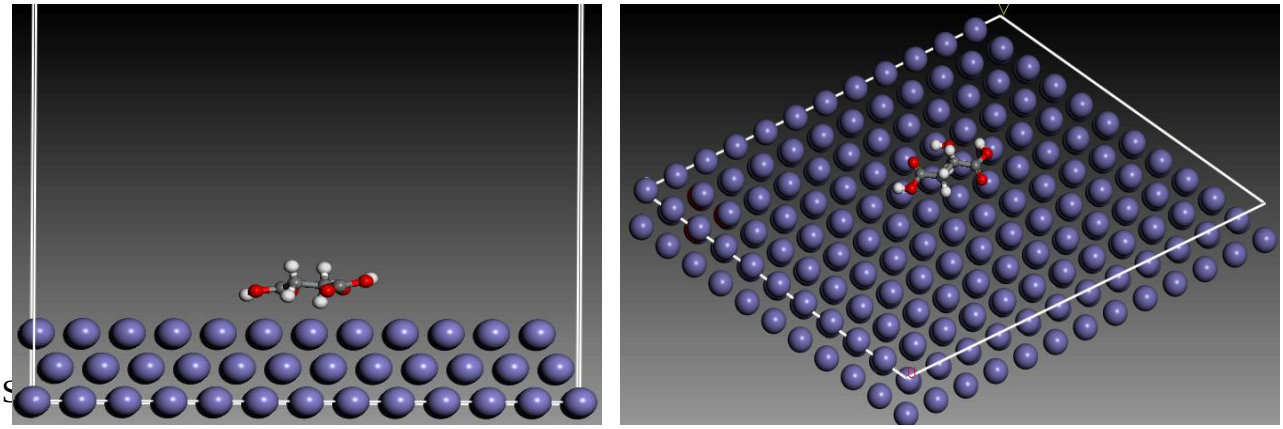

(f) S

Fig4.90: Electronic properties of malic acid (a) electron density, (b) electrophilic f (-), (c) nucleophilic f (+), (d) HOMO, (e) LUMO (f) side view of the snapshot for malic acid from molecular dynamics model. (g) Top view of the snapshot for malic acid from molecular dynamics model. Atom legend: white = H; gray = C; red = O. The blue and yellow isosurfaces depict the electron density difference: the blue regions show electron accumulation while the yellow regions show electron loss.

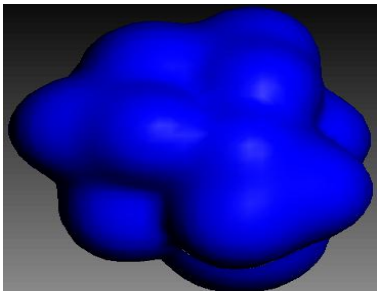

(a) Electron density

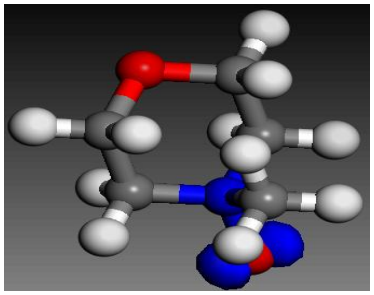

(b) Electrophilic F(-)

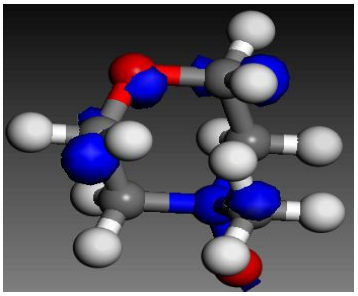

(c) Nucleophilic F (+)

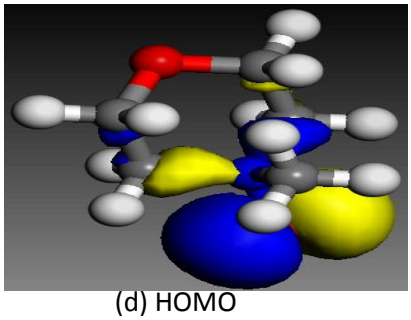

(d) HOMO

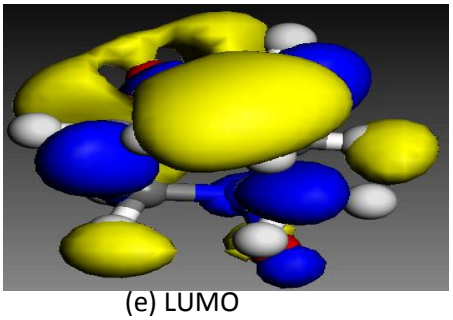

(e) LUMO

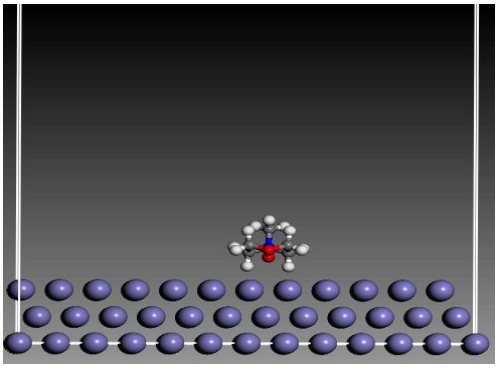

(f) Side view

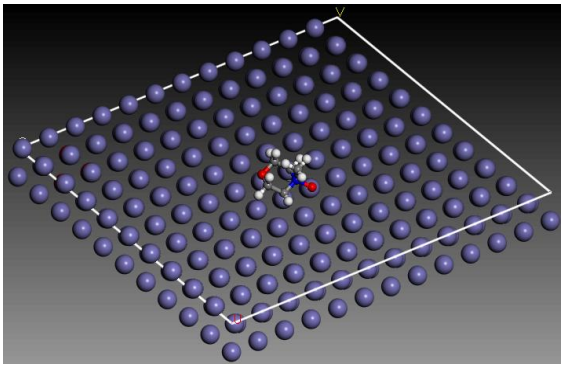

(g) Top view

Fig 4.91: Electronic properties of morpholine (a) electron density, (b) electrophilic f (-), (c) nucleophilic f (+), (d) HOMO, (e) LUMO (f) side view of the snapshot for morpholine from molecular dynamics model. (g) top view of the snapshot for morpholine from molecular dynamics model. Atom legend: white = H; gray = C; red = O; blue = nitrogen. The blue and yellow isosurfaces depict the electron density difference: the blue regions show electron accumulation while the yellow regions show electron loss.

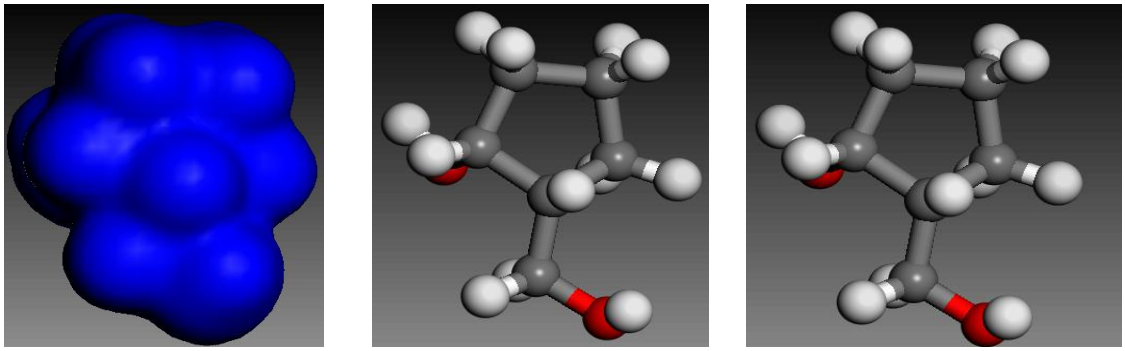

(a) Electron density (b) Electrophilic F(-) (c) Nucleophilic F (+)

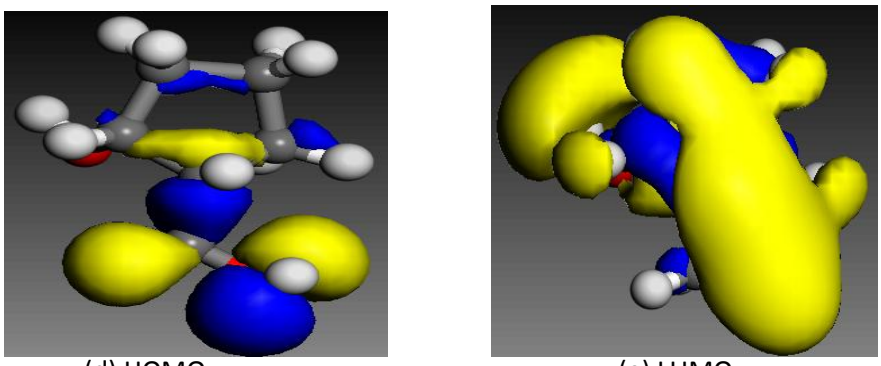

(d) HOMO (e) LUMO

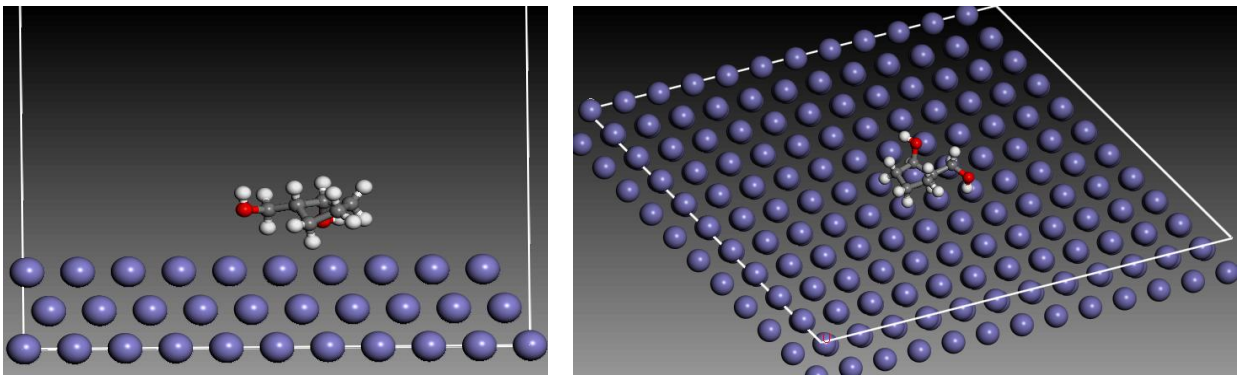

(f) Side view (g) Top view

Fig 4.92: Electronic properties of 2-hydroxymethylcyclopentano (a) electron density, (b) electrophilic f (-), (c) nucleophilic f (+), (d) HOMO, (e) LUMO (f) side view of the snapshot for 2-hydroxymethylcyclopentano from molecular dynamics model. (g) top view of the Snapshot for 2-hydroxymethylcyclo pentano from molecular dynamics model. Atom legend: white = H; gray = C; red = O. The blue and yellow isosurfaces depict the electron density difference: the blue regions show electron accumulation while the yellow regions show electron loss.

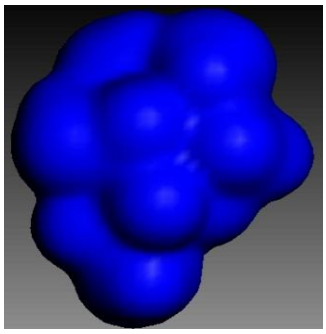

(a) Electron density

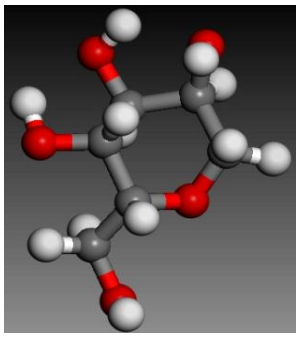

(b) Electrophilic F(-)

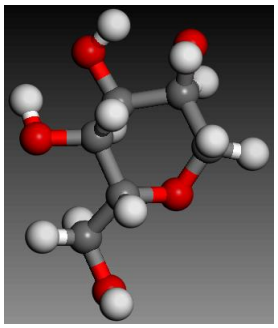

(c) Nucleophilic (+)

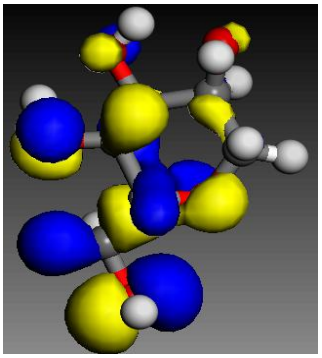

(d) HOMO

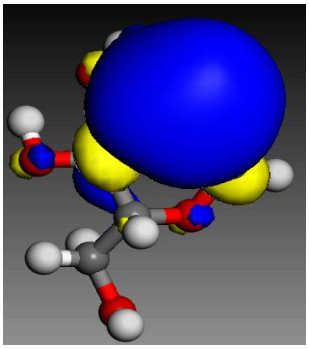

(e) LUMO

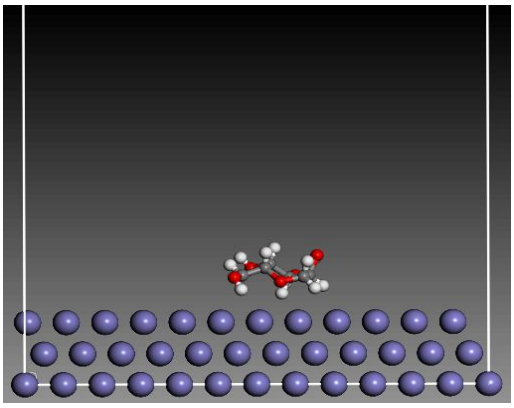

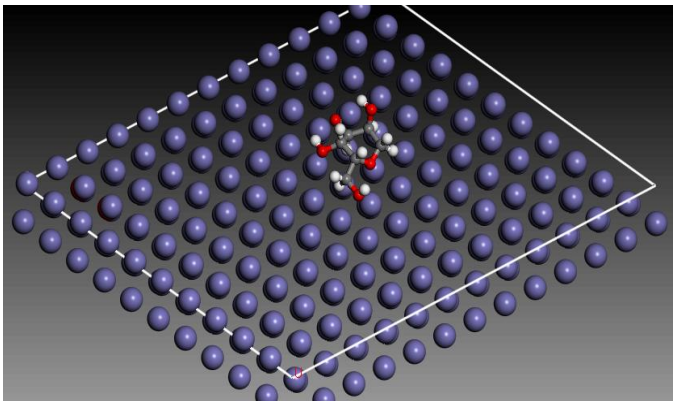

(f) Side view (g) Top view

Fig 4.93: Electronic properties of poligalytol(a) electron density, (b) electrophilic f (-), (c) nucleophilic f (+), (d) HOMO, (e) LUMO (f) Side view of the Snapshot for poligalytol from molecular dynamics model. (g) top view of the snapshot for poligalytol from molecular dynamics model. Atom legend: white = H; gray = C; red = O. The blue and yellow isosurfaces depict the electron density difference: the blue regions show electron accumulation while the yellow regions show electron loss.

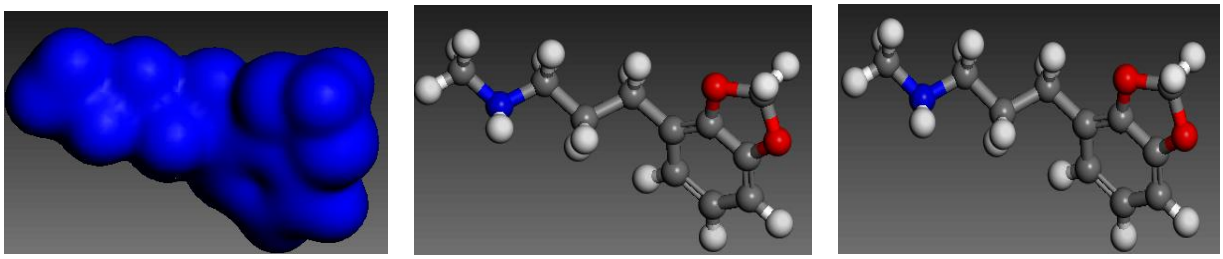

(a) Electron density (b) Electrophilic F(-) (c) Nucleophilic F(+)

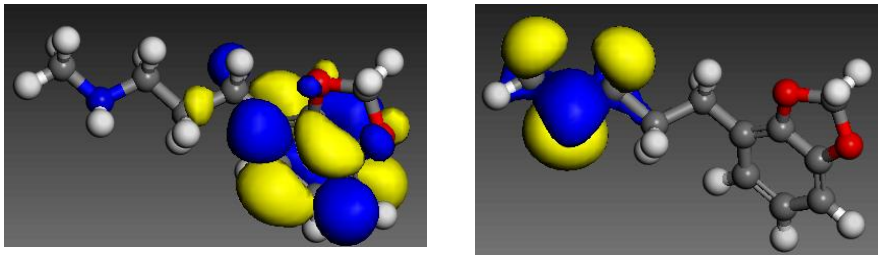

(d) HOMO (e) LUMO

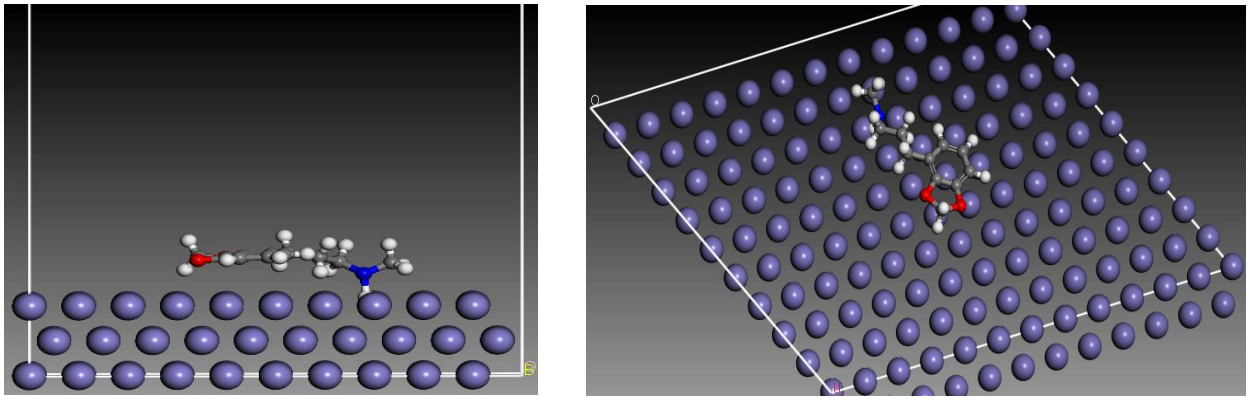

Fig 4.94: Electronic properties of N-methyl-3,4 methylenediOxy phenylpropan-3-amine

(a) Electron density, (b) electrophilic f (-), (c) nucleophilic f (+), (d) HOMO, (e) LUMO (f) side view of the snapshot for N-methyl-3,4 methylenedioxy phenylpropan-3-amine from molecular dynamics model. (g) top view of the Snapshot for N-methyl-3,4 methylenedioxy phenylpropan-3-amine from molecular dynamics model. Atom legend: white = H; gray = C; red = O. The blue and yellow isosurfaces depict the electron density difference: the blue regions show electron accumulation while the yellow regions show electron loss.

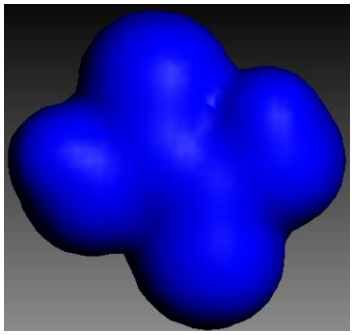

(a) Electro density

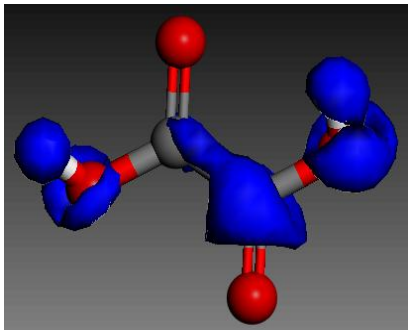

(b) Electrophilic F(-)

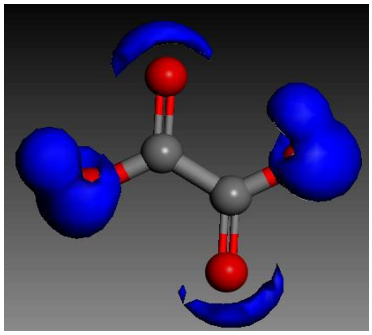

(c) Nucleophilic F(+)

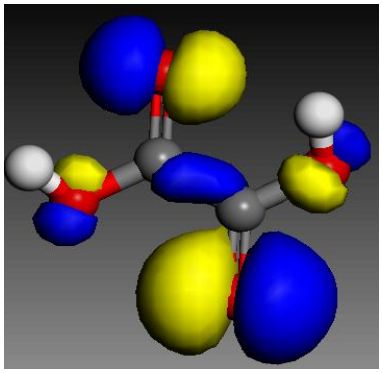

(d) HOMO

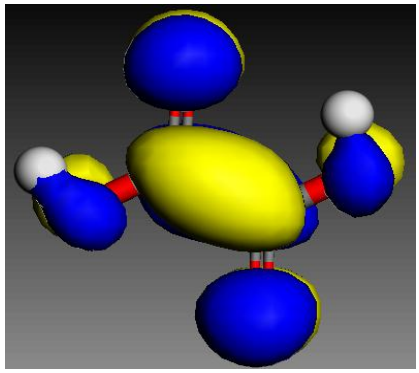

(e) LUMO

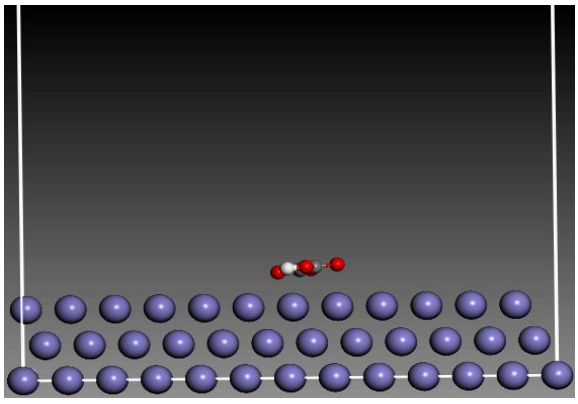

(f) Side view

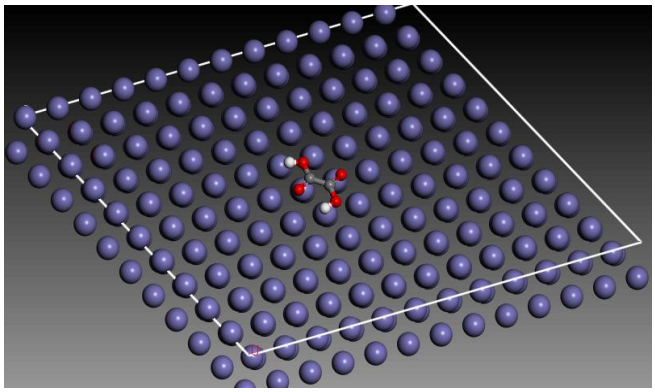

(g) Top view

Fig 4.95: Electronic properties of aspartic (a) electron density, (b) electrophilic f (-), (c) nucleophilic f (+), (d) HOMO, (e) LUMO (f) side view of the snapshot for aspartic from molecular dynamics model. (g) top view of the Snapshot for aspartic from molecular dynamics model. Atom legend: white = H; gray = C; red = O. The blue and yellow isosurfaces depict the electron density difference: the blue regions show electron accumulation while the yellow regions show electron loss

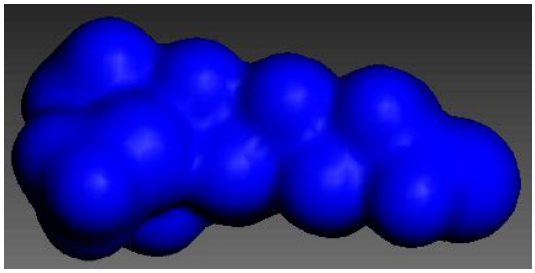

(a) Electron density

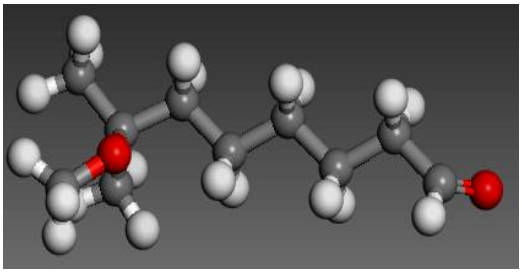

(b) Electrophilic F(-)

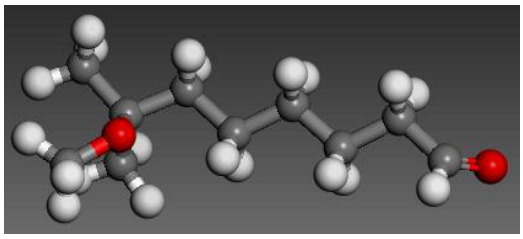

(c) Nucleophilic F(+)

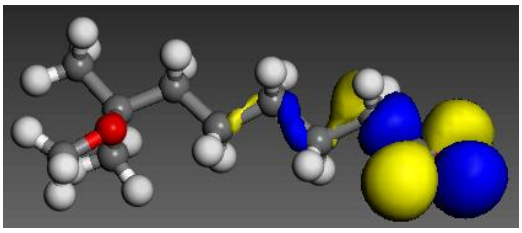

(d) HOMO

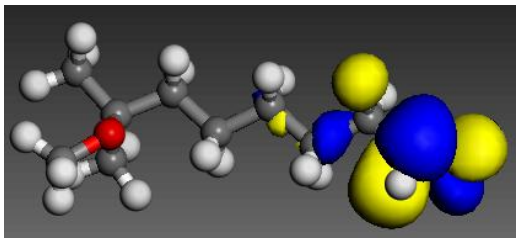

(e) LUMO

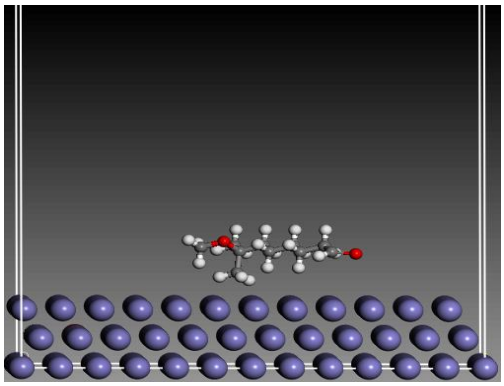

(f) Side view

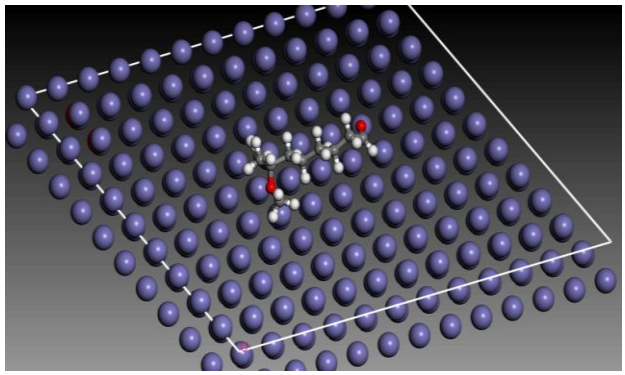

(g) Top view

Fig 4.96: Electronic properties of Propanamide (a) Electron density, (b) Electrophilic f (-), (c) Nucleophilic f (+), (d) HOMO, (e) LUMO (f) Side view of the Snapshot for Propanamide from molecular dynamics model. (g) Top view of the Snapshot for Propanamide from molecular dynamics model. Atom legend: white = H; gray = C; red = O. The blue and yellow isosurfaces depict the electron density difference: the blue regions show electron accumulation while the yellow regions show electron loss.

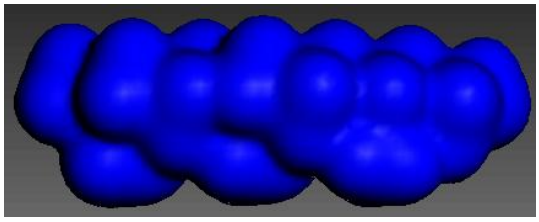

(a) Electron density

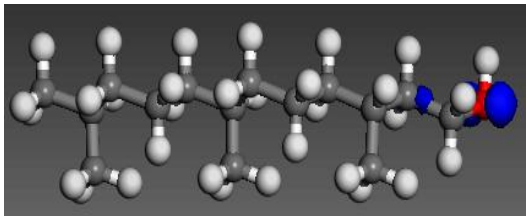

(b) Electrophilic F(-)

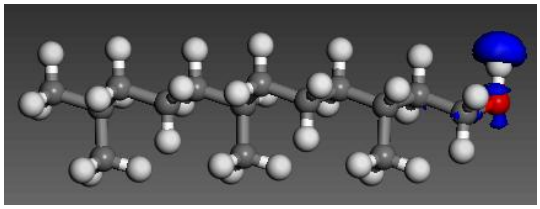

(c) Nucleophilic F(+)

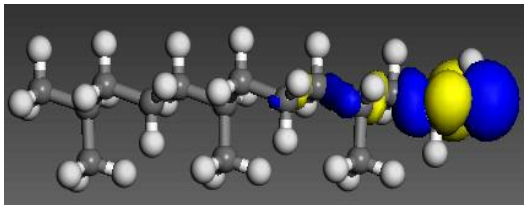

(d) HOMO

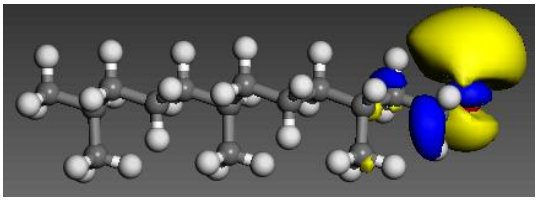

(e) LUMO

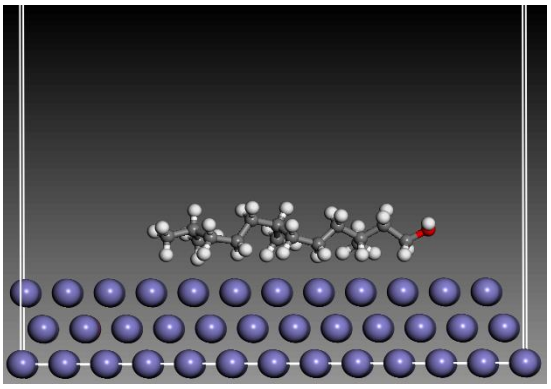

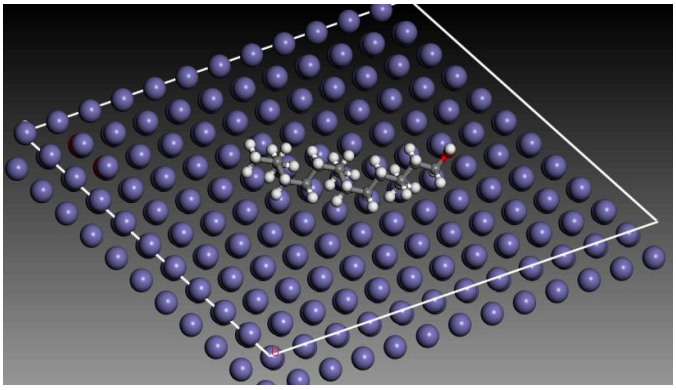

Fig 4.97: Electronic properties of octanal,3-dodecanol, 3,7,11-trimethyl (a) electron density, (b) electrophilic f (-), (c) nucleophilic f (+), (d) HOMO, (e) LUMO (f) side view ofthe snapshot for octanal,3-dodecanol, 3,7,11-trimethyl from molecular dynamics model. (g) top view of the snapshot for octanal,3-dodecanol, 3,7,11-trimethyl from molecular dynamics model. Atom legend: white = H; gray = C; red = O. The blue and yellow isosurfaces depict the electron density difference: the blue regions show electron accumulation while the yellow regions show electron loss.

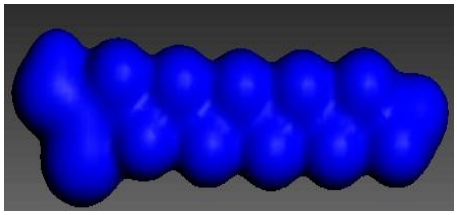

(a) Electron density

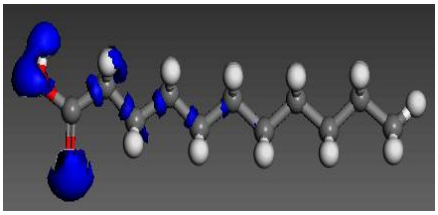

(b) Electrophilic F(-)

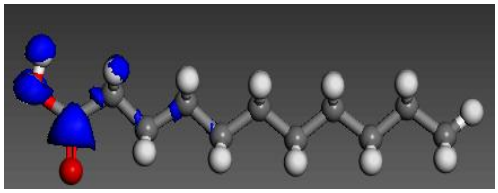

(c) Nucleophilic F(+)

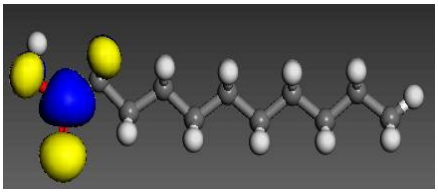

(d) HOMO

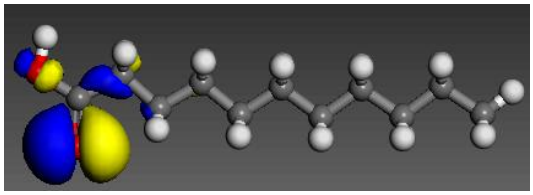

(e) LUMO

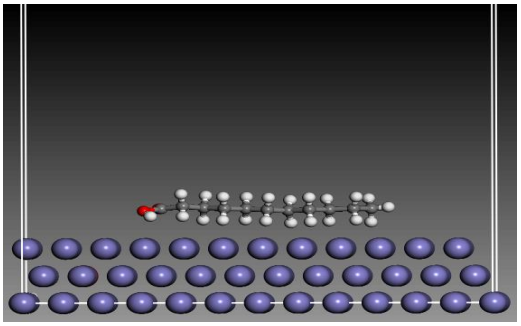

(f) Side view

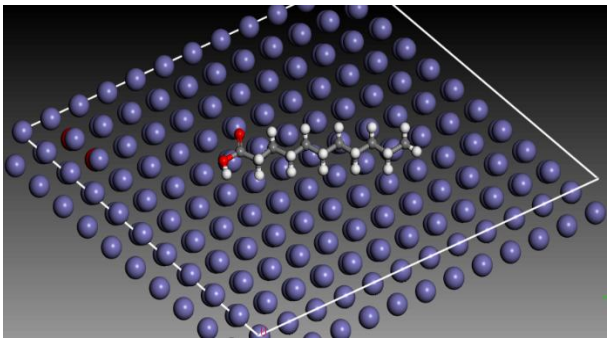

(g) Top view

Fig 4.98: Electronic properties of Undecanoic acid (a) Electron density, (b) Electrophilic f (-), (c) Nucleophilic f (+), (d) HOMO, (e) LUMO (f) Side view ofthe Snapshot for Undecanoic acid from molecular dynamics model. (g) Top view of the Snapshot for Undecanoic acid from molecular dynamics model. Atom legend: white = H; gray = C; red = O. The blue and yellow isosurfaces depict the electron density difference: the blue regions show electron accumulation while the yellow regions show electron loss.

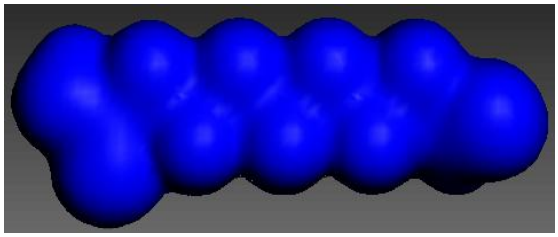

(a) Electron density

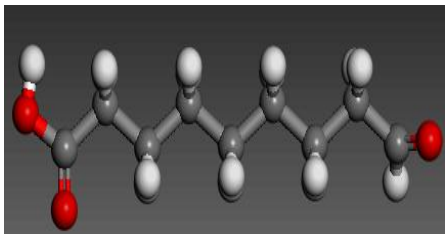

(b) Electrophilic F(-)

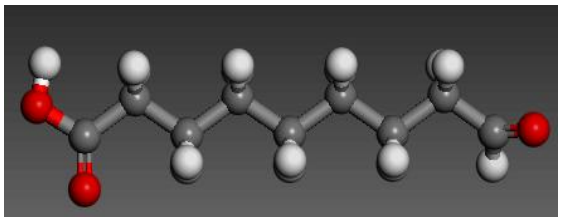

(c) Nucleohilic F(+)

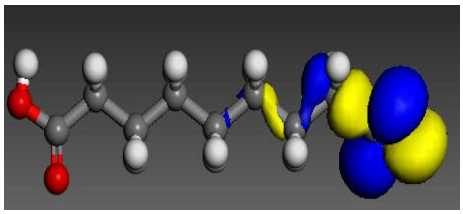

(d) HOMO

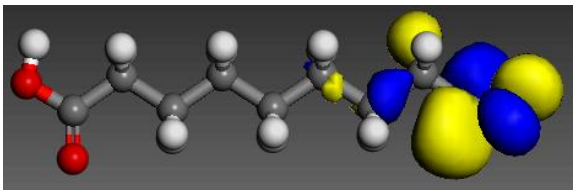

(e) LUMO

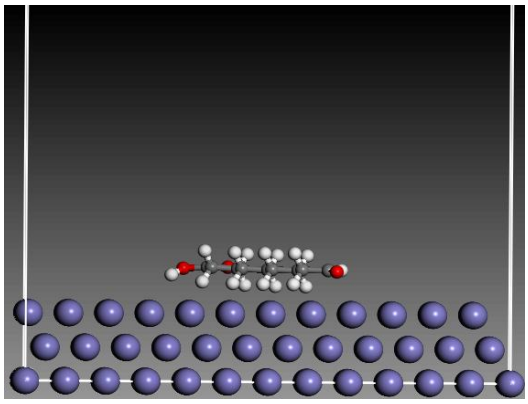

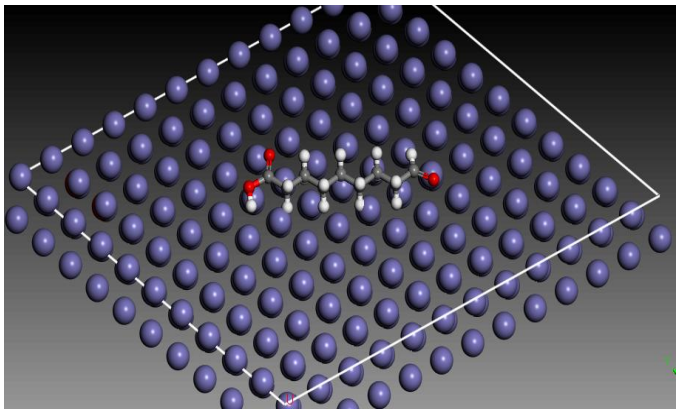

Fig 4.99: Electronic properties of 9-oxononanoic acid (a) electron density, (b) electrophilic f (-), (c) nucleophilic f (+), (d) HOMO, (e) LUMO (f) side view ofthe snapshot for 9-oxononanoic acid from molecular dynamics model. (g) top view of the snapshot for 9-oxononanoic acid from molecular dynamics model. Atom legend: white = H; gray = C; red = O. The blue and yellow isosurfaces depict the electron density difference: the blue regions show electron accumulation while the yellow regions show electron loss.

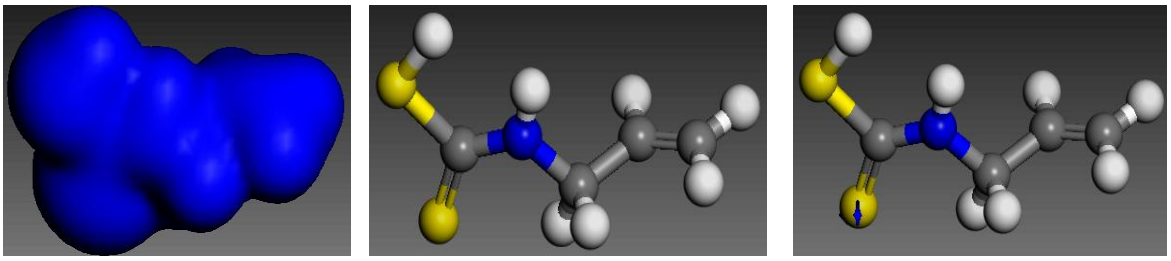

(a) Electron density (b) Electrophilic F(-) (c) Nucleophilic F(+)

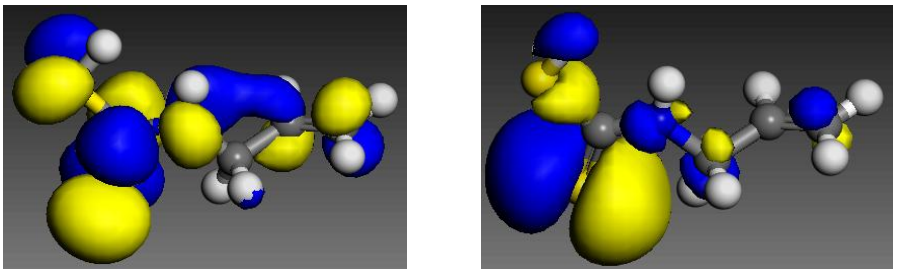

(d) HOMO (e) LUMO

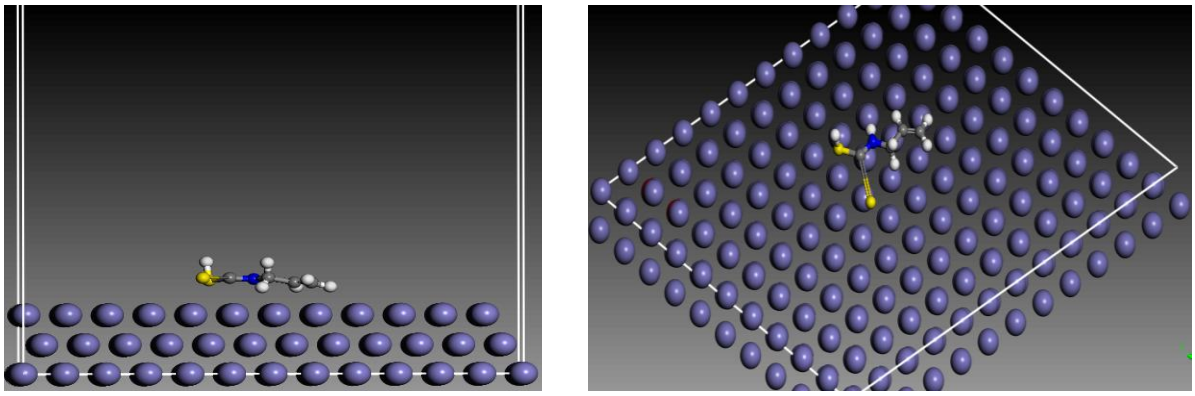

(f) Side view (g) Top view

Fig 4.100: Electronic properties of carbamodithioic acid (a) electron density, (b) electrophilic f (-), (c) nucleophilic f (+), (d) HOMO, (e) LUMO (f) side view ofthe snapshot for carbamodithioic acid from molecular dynamics model. (g) top view of the snapshot for carbamodithioic acid from molecular dynamics model. Atom legend: white = H; gray = C; red = O. The blue and yellow isosurfaces depict the electron density difference: the blue regions show electron accumulation while the yellow regions show electron loss.

Table 4.99: Calculated quantum chemical properties for the most stable conformation of the selected active constituents of the inhibitors.

Molecule	E_{HOMO} (eV)	E_{LUMO} (eV)	ΔE	Adsorption Energy (Kcal/mol	Molecular Surface Area (Å)
9-Oxononanoic acid	-6.612	-2.782	6.533	- 203.7	251.1
Aspartic acid	-6.304	-5.109	5.778	- 7.79	108.9
Polygalitol	-5.950	-0.256	5.694	- 0.55	188.5
2-Hydroxymethylcyclopentano	-5.884	0.649	4.66	- 91.7	164.1
Malic acid	-5.726	-5.199	4.114	- 39.8	164.6
N-methyl-3,4 methylenedi Oxy phenylpropan-3-amine	-5.363	-1.249	3.83	- 53.6	252.1
Octanal,3-Dodecanol, 3,7,11-trimethyl-	-5.070	0.708	3.328	- 177.6	341.9
Undecanoic acid	-5.054	-2.191	3.032	- 245.3	291.5
Carbamodithioic acid	-5.028	-1.700	2.863	- 128.1	177.1
Morpholine, 4-methyl-, 4-oxide	-4.825	-0.165	1.195	- 131.1	150.1
Propanamide	-4.451	-1.419	0.527	- 154	117.2

CHAPTER FIVE

CONCLUSIONS AND RECOMMENDATIONS

5.1 Conclusions

The conclusions drawn from this work are as follows:

1. The six leaf extracts examined were found to be effective inhibitors for the corrosion of aluminum and mild steel in alkaline and acid solutions.
2. The inhibition efficiency of all the leaf extracts increased with increase in extractconcentrations in the order *Dialium guineense>Dennettia tripetala>Newbouldia leavis>Aspilia africana>Chromolena odorata>Vitex doniana* and decreased with increase temperature.
3. The extracts (*Aspilia africana*, *Chromolena odorata*, *Newbouldia leavis*, *Dialium guineense*, *Dennettia tripetala*and *Vitex doniana*) exert their inhibitive properties by being adsorbed spontaneously on the surface of aluminum and mild steel.
4. The adsorption characteristics of the compounds have been found to obey physical adsorption mechanism and follow Temkin,Flory-Huggins, Langmuir and Frumkin adsorption isotherm models but only the Temkin isotherm yielded adsorption free energy values consistent with the experimental findings which deters the endothermic monoatomic dissolution of aluminum, mild steel in the solutions.
5. The values of free energy of adsorption and heat of adsorptionindicate that the corrosion inhibition is attributed to physical adsorption of the phytochemical components of the extractson the surface of the aluminum and mild steel. The negative signs of ΔG_{ads} and $\triangle$H indicate that the adsorption process is spontaneous and exothermic.
6. SEM examinations showed surfaces of transformation on addition of *Aspilia africana*, *Chromolena odorata*, *Newbouldia leavis*, *Dialium guineense*, *Dennettia tripetala* and *Vitex doniana* extracts respectively.
7. Potentiodynamic polarization studies showed that the inhibitors act as mixed-type inhibitors in HCl, H_2SO_4, KOH and NaOH solutions respectively and their inhibition mechanism is adorption-assissted by hydrogen bond.

8. Impedance results showed thatthe values ofconstant phase elements(CPE) exponent, i.e, phase shift (*n*) tend to decrease with increasing inhibitor concentration due to increase in the electrical double layer.
9. Both polarization resistance and inhibition efficiency IE% tend to increase with increasing inhibitor concentrations as a result of increase in the surface coverage of the inhibitors, i.e the decrease of electrochemical active surface area.
10. DFT-based quantum chemical calculations of parameters associated molecular electronic structures ofactive constituents of the extracts confirmed their inhibiting potential and established their individual contributions to the observed inhibiting effect.

5.2 Recommendations

1. Further work on quantum mechanical approach should be carried out to determine the molecular structures.
2. Leaves of other plants should be explored as corrosion inhibitors of metals in acid and alkaline solutions.
3. Researchers should explore the use of metals like stainless steel and its alloy in corrosion study.
4. The use of polymeric materials as corrosion inhibitors should be investigated.

5.3 Contribution to Knowledge

1. This work have successfully used other methods (potentiodynamic polarization, electrochemical impedance spectroscopy and quantum chemical study) of corrosion test to achieve the set objectives.
2. The work inhibition of plant leaf extracts on Aluminum and mild steel in alkaline and acidic media using different corrosion techniques has added to the existing literature a new ideal on corrosion study.

REFERENCES

Abdallah, M., (2004). Guar gum as corrosion inhibitor for carbon steel in sulpfuric acid solutions. Protugaliae Electrochemical Acta, 22, 161 – 175.

Abdel-Gaber, M., Abd-El-Nabey, B. A., Sidahmed, I. M., El-Zayaday, A. M. & Saa, M., (2006). Inhibitive action of some plant extracts on the corrosion of steel in acidic media. Corrosion Sci., 48, 2765-2779

Abdulraman, A. S., Mohammad, I. & Mohammad, S. H. (2011). Corrosion inhibitors for steel reinforcement in concrete: A review. Scientific Research and Essays, 6 (20), 4152- 4162.

Abdulwahab, M., Kasim, A., Bello, K. A. and Gaminana, J. O. (2012). Corrosion inhibition of multi-component aluminium alloy in hydrochloric acid solution by aqueous extract of bitter Leaf (*Verninia amygdalina*) powder. Advanced Materials Research, 367, 319-325.

Acha, U. Ezeoke, Olalere, G. Adeyemi, Opeyemi A. Akerele, Nelson O. Obi-Egbedi, (2012), Computational and experimental studies of 4-aminoantipyrine as corrosion inhibitor for mild steel in sulphuric acid solution, International Journal of Electrochemical Science, 7, 534-553.

Aggarwal, O. P. (2010). Engineering Chemistry, Kahanna Publishers, New Delhi, 3rd Ed., 718 - 797.

Alinnor, I. J. & Ejikeme, P. M. (2012). Corrosion inhibition of aluminum in acidic medium by different extracts of *Osmium gratissium*. American Chemical Science Journal 2(4), 122 - 135.

Ambrish, S., Ashish, K. S. & Quraishi, M. A., (2010). Dapsone: A novel corrosion inhibitor for mild steel in acid media. The Open Electrochemistry Journal. 2, 45 - 51.

Amorati, R. & Valgimigli, L., (2012). Modulation of the antioxidant activity of phenols by non-covalent interactions. Org Biomol Chem.10 (21), 4147-58.

Anees, A. K., Aprael S. Y., Abdul, A. H. K., Ahmed, S. A. & Ahmed, Y. M., (2009). The effect of temperature and acid concentration on corrosion of low carbon steel in hydrochloric acid media. American Journal of Applied Sciences, 6(7), 1403 - 1409.

Anthony, S. S. R. & Susai, R. (2012), Inhibition of corrosion of carbon steel well water by arginine-Zn^{2+} System. J. Electrochem. Sc. Eng., 2, 91 - 104.

Aounti, A., Khaled, K.F. & Hammouti, B., (2013), Correlation between inhibition efficiency and chemical structure of some aminoacids on the corrosion of Armco iron in molar HCL. INT. J. Electrochem. Sci., 8.

Aprael S. Yaro, Anees A. Khadom &Rafal K. Wael., (2013). Apricot juice as green corrosion inhibitor of mild steel in phosphoric acid. Alexandria Engineering Journal (52), 129–135.

Ashassi-Sorkhabi H. and Es'haghi M., 2009, Corrosion inhibition of mild steel in acidic media by [BMIm]Br Ionic liquid, Materials Chemistry and Physics 114, 267–271

Ayssar Nahle, Ideisan Abu-Abdioun, Ibrahim Abdel-Rahman &Maysoon Alkhayat, (2010). UAE Neem extract as a corrosion inhibition for carbon steel in HCL solution. International journal of corrosion, Article ID 460154, doi:1155/2010/460154.

Barbara A. Shaw & Robert G. Kelly, (2006), Interface, The electrochemical society, Spring.

Buchwesihaija, J. (2009). Photochemical as Green corrosion inhibitors in various corrosive media, A review. Tanz. J. Sci., 35. 77 – 91.

Chidiebere M. A., Ogukwe C. E., Oguzie K. L., Eneh C. N., Oguzie E. E., (2012).Corrosion inhibition and adsorption behavior of Punica granatum extract on mild steel in acidic environments: experimental and theoretical studies. Ind. Eng. Chem. Res. 51: 668 - 677.

Chidiebere, Maduabuchi A.,Emeka E. Oguzie, Li Liu, Ying Li, Fuhui Wang (2015). Adsorption and corrosion inhibiting effect of riboflavin on Q235 mild steel corrosion in acidic environments. Materials Chemistry and Physics, 156, 95-104

Okoli, C.O., Akah P.A. & Okoli, A.S., (2007).Potentials of leaves of *Aspilia africana* (compositae) in wound care: an experimental evaluation, BMC complementary and alternative medicine

Cushnie, T. P., Cushnie, B. & Lamb, A. J., (2014). Alkaloids: An overview of their antibacterial, antibiotic-enhancing and antivirulence activities. Int. J. Antimicrob Agents. 44 (5), 377–386.

Dara, S.S.; 2000. A textbook of Engineering Chemistry, S.C hand &Company Ltd, Ram Nagar New Delhi, pg 193-232.

Davis, G. D, Fraunhofer, J. A., Rebs, L. A. & Dacres, C. M., (2001). The use of tobacco extracts as corrosion inhibitor. Corrosion, 58

Dubey, A. K. & Singh, G. (2007). Corrosion inhibition of mild steel in sulphuric acid solution by using polyethylene glycol methyl ether (PEGME). Portugaliae Electrochemical Acta, 25, 221 – 235.

Ebenso, E.E., Hailemicheal Alemu, Umoren,S.A. & Obot, I. B., (2008), Inhibition of mild steel corrosion in sulphuric acid using alizarin yellow GG dye and synergistic iodide additive. Int. J. Electrochem. Sci, 1325-1339.

Ebenso, E. E. & Ekpe, U. J., (1996). Kinetic study of corrosion and corrosion inhibition of mild steel in H_2SO_4 using *Carica Papaya* leaves extract. W. Afri. J. Biol. Applied Chem., 41, 21 – 27.

Ebenso, E. E., Ibok, U. J., Ekpe, U. J., Umoren, S., Jackson, E., Abiola, O. K., Oforka, N. C. & Martine, Z. (2004). Corrosion inhibition studies of some plant extracts on aluminium in acidic medium. Trans of SAEST 39(4), 117 -123.

Ebenso,E.E., Eddy, N.O., and Odiongenyi, A.O., (2008), Corrosion of inhibitive properties and adsorptionbehaviour of ethanol of piper guinensis as a green corrosion inhibitor for mild steel in H_2SO_4. African Journal of Pure and Applied Chemistry; vol: 2(11), pg 107 -115.

Eddy N.O. & Ebenso E.E., (2008), Adsorption and inhibitive properties and of ethanol extract of Musa Sapientum peels as a green corrosion inhibitor for mild steel in H_2SO_4. Afri. J. Appl. Chem, 2(6), 1 –9.

Eddy, N. O., Ita, B. I., Dodo, S. N. & Paul, E. D. (2012). Inhibitive and adsorption properties of ethanol extract of *Hibiscus sabdariffa Calyx* for the corrosion of mild steel in 0.1M HCl. Green Chemistry Letters and Reviews, 5 (1), 43 – 53.

El Maghraby, A. A. (2009). Corrosion inhibition of aluminum in hydrochloric acid solution using potassium iodate inhibitor. The Open Corrosion Journal, 2, 189 – 196.

El Ouariachi, E., Paolini, J., Bouklah, M., Elidrissi, A., Bouyanzer, A., Hammouti, B., Desjobert, J. M. and Costa, J. (2010). Adsorption properties of *Rosmarinus of ficinalis* oil as green corrosion inhibitors on C38 steel in 0.5M H_2SO_4. Acta Metal. Sin. (Engl. Lett.), 23 (1), 13 – 20.

Elmsellem H., Aouniti A., Khoutoul M., Chetouani A., Hammouti B., Benchat N., Touzani R.& Elazzouzi M., (2014). Theoretical approach to the corrosion inhibition efficiency of some pyrimidine derivatives using DFT method of mild steel in HCl solution. Journal of Chemical and Pharmaceutical Research, 6(4), 1216-1224.

Farooqi, H. I., Quraishi, M. A. &Saini, P. A. (1997). Natural compounds as corrosion inhibitors for mild steel in industrial cooling systems. Proceedings from European Federation of corrosion (EUROCORR. 97), Trondheim, 1, 186 – 194.

Foo K. Y. & Hameed B. H., (2010). Insights into modeling of adsorption isotherm systems. Chemical Engineering Journal, 156 (1), 2-10.

Fouda,A.S., Shalabi, K &Mohamed, N.H., (2014), Corrosion inhibition of aluminium in hydrochloric acid Solutions using some chalcone derivatives. International Journal of Innovative Research in Science, Engineering and Technology, (3)3, 9861-9875.

Gade S., Rajamanikyam M., Vadlapudi V., Nukala, K.M., Aluvala, R., Giddigari, C., Karanam, N.J., Barua, N.C., Pandey, R, Upadhyayula, V.S., Sripadi, P., Amanchy, R., Upadhyayula, S.M., (2017). Acetylcholinesterase inhibitory activity of stigmasterol &

hexacosanol is responsible for larvicidal and repellent properties of *Chromolena odorata*, Biochim Biophys Acta, 1861(3):541-550.

Ghulamullah, Khan, Kaxi, Md. Salim, Newaz, Wan, Jefrey Basirun, Hapipah, Mohd. Ali, Fadhil, Lafta Faraj, Ghulam, Mustafa Khan, (2015). Application of natural products as green corrosion inhibitors for metals and alloys in acid pickling processes. A review, International Journal of Electrochemical Science, (10), 6120-6134.

Gopal, J., Sudhish, K. S., Priyanka, D., Shanthi, S., Ebenson, E. E., Rajiv, P. (2012). *Parthenium hysterophorus* plant extract as an efficient green corrosion inhibitor for mild steel acidic environment. Int. J. Electrochem. Sci., 7, 9933 – 9945.

Green, D. W. & Perry, R. H., (2008). Perry's Chemical Engineers' Handbook, 8th edition, Mc Graw-Hill Company Inc., USA, Sections 25 and 28.

Guangling, S., Andrej, A. & David, St. J. (2001). Hydrogen evolution method for the estimation of the corrosion rate of magnesium alloys. Magnesium Technology, Ed. John N. Hryn, TMS, 255-262.

Habib Ashassi-Sorkhabi, Shoja Mirzaee, Taghi Rostamikia, and Robabeh Bagheri, (2015), Pomegrante (Punica granatum) Peel Extract as a Green Corrosion Inhibitor for Mild Steel in Hydrochloric Acid Solution, International Journal of Corrosion, Article ID 197587, 48,

Hany, M. A., Aliyeva, L. I., Abbasov, V. M., Ismayilov, T. I., (2012). Corrosion inhibition of low carbon steel in CO_2 – Saturated solution using anionic surfactant. Advances in Applied Science Research, 3(2): 1185 – 1201.

http://www.fruitsinfo.com/velvet-tamarind.php July 2018

http://www.worldagroforestry.org/treedb2/AFTPDFS/Vitex_doniana.PDF, July 2018

https://en.wikipedia.org/wiki/Aspilia, July 2018

https://en.wikipedia.org/wiki/Chromolaena_odorata, July 2018

https://globalfoodbook.com/18-wondrous-benefits-of-pepper-fruit-dennettia-tripetala, July 2018

https://globalfoodbook.com/incredible-benefits-of-newbouldia-laevis-ogilisi, July 2018

I.B. Obot, S.A. Umoren, Z.M. Gasem, Rami Suleiman and Bassam, El-Ali, (2015), Theoretical prediction and electrochemical evaluation of vinylimidazole and allylimidazole as corrosion inhibitors for mild steel in 1M HCL. Journal of Industrial and Engineering chemistry, 21, 1328-1339.

Ihebrodike, M.M., Nwandu, M.C., Okeoma, K.B., Nnanna, L.A., Chidiere, M.A., Eze, F.C., & Oguzie, E.E., (2012). Experimental and theoretical assessment of the inhibiting action of

Aspilia africana extract on corrosion of Aluminum alloy AA 3003 in hydrochloric acid. J.Mat.Sci, 47, 2559-2572, DOI 10.1007/s 10853-011-6079-2.

Ikpi, M.E., Udoh,I.I., Okafor, P.C., Ekpe, U.J. & Ebenso, E.E., (2012), Inhibition and adsorption behaviour of extracts from piper guineensis on mild steel corrosion in acidic media, Int. J. of Electrochem. Sci., 7, 12193-12206.

John, L., Gennady, Y. G., Alexander, V. N. (2013). Density functional theory methods for characterization of porous materials, ELSEVIER, Colloids and Surfaces A: Physicochemical and Engineering Aspects, 437, 3-32.

Kang, W. T., Mohd, J. K., Chuan, W. O. (2012). Possible Improvement of Catching as Corrosion Inhibitor in Acidic Medium. Corrosion Science 65, 152 – 162.

Khaled, K.F., 2010. Studies of iron corrosion inhibition using chemical, electrochemical and computer simulation techniques, Electrochimica Acta, 55: 6523-6532.

Khaled, K.F. & Al-Mobarak, N. A., (2012).A Predictive Model for corrosion inhibition of mild steel by thiophene and its derivatives using artificial neural network.Int. J.Electrochem. Sci., *(*7)1045 – 1059

Khamis, A., Saleh, M.M.&Awad,M.I., (2013). Synergistic inhibitor effect of cetylpyridinium chloride and other halides on the corrosion of mild steel in 0.5M H_2SO_4. Corrosion science, 66, 343-349.

Kliskic, M. Radosevic,& Gudics J. Katalinic, V. (2000). Aqueous extract of Rosmarinus officinalis L. as inhibitor of Al - Mg alloy Corrosion in Chloride solution. J. Appl. Electrochem, 30(7), 823 – 830.

Kissi, M., Bouklah, M., Hammouti, B., Benkaddour M., (2006). Establishment of equivalent circuits from electrochemical impedance spectroscopy study of corrosion inhibition of steel by pyrazine in sulphuric acidic solution. Appl. Surf. Sci. 252: 4190 - 4197.

Koch, G. H., Brongers, M. P. H., Thompson, N. G. Virmani, U. P., Payer, J. H. (2002). Corrosion costs and Preventive Strategies in the United Stats. NACE Intt PHWA - RD

Kotz, J. C. & Treichel, P. (1996). Chemistry and Chemical Reativity, 3rd edition, Harcourt Brace Col. Publishers, New York.

Kumar, M. D., Kumar, U. R. & Chaturvedi, A. (2010). Study of corrosion inhibition efficiency of some Schiff's bases on aluminum trichloroacetic acid solution. Rev. Roum. Chim. 55(4) 227 – 232.

Lame A, Kokalari E, Jano A., (2013). Use of green inhibitors for concrete Armor protection against H_2SO_4 Corrosion. Asian journal of chemistry, 25(7): 4017 4021.

Latifa K. & Abdelilah C. (2007). Corrosion Inhibitor of Titanium in Artificial Saliva Containing Fluoride. Leonardo Journal of Sciences, 11, 33 - 40.

Lebe, A. N., Israel, O. O., Onyinyechi, C. N., Nneka, D. E., Wisdom, J. O. (2013). Adsorption and corrosion inhibition of *Gnetum Africana* leaves extract on carbon steel. International Journal of Materials and Chemistry. 3(1) 10 - 16.

Li, X. & Deng, S. (2012). Inhibition effect of *Dendrocalamus brandissi* leaves extracts on aluminum in HCl, H_3PO_4, Solutions. Corrosion Science 65, 299 - 308.

Loto, C. A. & Popoola, A. P. I. (2012). Plant extracts corrosion inhibition of Aluminum alloy in H_2SO_4. Canadian Journal of Pure and Applied Sciences. 6, (2), 1973 – 1980

Manoj Acharya, Jinendra Singh Chouhan, Anita Dixit, D. K. Gupta (2013), Green Inhibitors for Prevention of Metal and Alloys Corrosion: An OverviewChemistry and Materials Research, 3 (6).

Mehdi Ebadi, Wan Jeffrey Basirun, Hamid Khaledi, & Hapipah Mohd Ali, (2012), Corrosion inhibition properties of Pyrazolylindolenine compounds on copper surface in acidic media, Chemistry Central Journal (6)163: 1-10.

Moretti G., Guidi F., Grion G., (2004). Tryptamine as a green iron corrosion inhibitor in 0.5 M deaerated sulphuric acid. Corros. Sci, 46, 387- 403.

Mishra, B. B. & Tiwari, V. K. (2011). Natural products: an evolving role in future drug discovery. Eur J Med Chem.46 (10), 4769–807.

Mistry, B. M., Patel, N. S., Sahoo, S. and Jauhari, S. (2012). Experimental and quantum chemical studies on corrosion inhibition performance of quinoline derivatives for MS in 1N HCl. Bull. Mater. Sci., 35. (3), 459 – 469.

Nadia, H., Hacene C., Gildas, G., Kamel, B. (2011). The Corrosion Protection Behaviour of Zincs Rich Epoxy paint in 3% NaCl solution. Advances in Chemical Engineering and Science. 1, 51 – 60.

Nagm, A. N., Badr, E. A., Aiad, I. A., Zaki, M. F., Said, M. M. (2012a). Investigation of the inhibitory action of novel diquaternary Schiff dibases on the acid dissolution of carbon steel in 1m hydrochloric acid solution. Corrosion Science, 65, 77 – 86.

Nagm, A. N., Kandile, N. G., Badr, E. A. and Mohammed, M. A. (2012b). Gravimetric and electrochemical evaluation of environmentally friendly nonionic corrosion inhibitors for carbon steel in 1 M HCl. Corrosion Science 65, 94-103.

Ndibe, O. M., Menkiti, M. C., Ijomah, M. N. C. & Onukwuli, O. D. (2011). Corrosion inhibition of mild steel by acid extraction of *Vernonia amygdalina* in HCl and HNO_3. EJEAFChe, 10(9), 2847 – 2860.

Nesrin, T., Zeynel, S., Cemil, O. & Nermin, E. (2008). Quantum chemical studies on the structures of some heterocyclic azo disperse dyes. ARKIVOC (xv) 9-20

Nnanna, L. A., Owate, I. O., Nwadiuko, O. C., Ekekwe, N. D. and Oji, W. J. (2013). Adsorption and corrosion inhibition of *Gnetum Africana* leaves extract on carbon steel. International Journal of Materials and Chemistry, 3(1), 10-16.

Nnanna,L.A., Obasi,V.U., Nwadiuko,O.C., Mejeh, K.I.,Ekekwe, N.D., Udensi,S.C. (2012). Inhibition of *Newbouldia leavis* Leaf Extract of the Corrosion of Aluminium in HCL and H_2S0_4 Solutions. Scholars Research Library, 4(1): 207-217.

Nwabanne, J. T. and Okafor, V. N. (2011). Inhibition of the corrosion of mild steel in acidic medium by *Vernonia amygdalina*: Adsorption and Thermodynamic study. Journal of Emerging Trends in Engineering and Applied Science (JETEAS) 2(4): 619 - 625.

Nwajo, H. U. (2005). Efficacy of aqueous leaf extract of *Vernonia amygdalina* on plasma lipoproteins and oxidative status in diabetic rat model. Nig. J. Physiol. Sci., 20: 39 - 42.

Obot, IB, Ebenso EE, Gasem ZM, (2012), Eco-friendly corrosion inhibitors: Adsorption and inhibitive action of ethanol extracts of *Chromolena odorata* leaves for corrosion of mild steel in H2SO4 Solutions. Journal of Electrochemical Sciences, 7(3): 1997-2008.

Obot, I.B., Obi-Egbedi, N.O., (2010a). Adsorption properties and inhibition of mild steel in sulphuric acid solution by ketoconazole: experimental and theoretical investigation. Corros. Sci. 52: 198 - 204.

Obot, I.B., Obi-Egbedi, N.O., (2010b), An interesting and efficient green corrosion inhibitor for aluminium from extracts of *Chromolena odorata* leaves in acidic solution. Journal of applied Electrochemistry, 40(11): 1977-1984.

Octave, L., (2003). Chemical Reaction Engineering, Third Edition, John Wily and Sons, New York.

Oguzie, E. E., Enenebeaku, C. K., Akalezi, C. O., Okoro, S. C., Ayuk, A. A., Ejike E. N., (2010). Adsorption and corrosion-inhibiting effect of *Dacryodis edulis* extract on low-carbon-steel corrosion in acidic media. Journal of Colloid and Interface Science 349 283-292.

Oguzie E. E., Adindu C. B., Enenebeaku C. K., Ogukwe C. E., Chidiebere M. A., Oguzie K. L., (2012). Natural products for materials protection: mechanism of corrosion inhibition of mild steel by acid extracts of piper guineense. J.phys. Chem. 116: 13603 - 13615.

Ojezele, M. O. and Agunbiade, S. (2013). Phytochemical constituents & medicinal properties of different extracts of anacardium occidentale and *psidium guajava*. Asian journal of Biomedical and Pharmaceutical Science, 3 (16), 1-5.

Okeoma Kelechukwu B., (2015), Computational and Experimentalstudies on the inhibitive effects of Newbouldia laevis extract and magnetic fields on copper corrosion in aqueous acidic media. International letter of Chemistry, Physics and Astronomy, 54, 135-142.

Omotioma, M., Egbuna, S. O., Obiora-Okafo, I. A., Okafor, C. E. and Deigh, S. S. (2014). Comparative analysis of the inhibitive effects of sodium chromate on mild steel in natural and oil polluted seawater. Journal of Science and Technology, 20, 1-9.

Papavinasam, S. (2000). Corrosion Inhibitors, Uhlig's corrosion handbook (Jn. F. Winston Reversed Ed.) Second Edition. John Wiley & Sons. Inc. Canada, 1089 - 1105.

Patel, N. S., Jauhariand, S., Mehta, G. N., Al-Deyeb, S. S., Warad, I. &Hammouti, B. (2013). Mild steel corrosion inhibition by various plants extracts in 0.5M sulphuric acid. Int. J. Electrochem. Sc., 8, 2635 – 2655.

Prathibha, B. S., Kotteeswaran, P., Bheema, V. R., (2012). Study on the inhibition of Mild steel corrosion by cationic surfactant in HCl medium. IOSR Journal of applied chemistry (IOSR JAC), 2 (1), 45-53.

Punita Mourya, Sitashree Banerjee, & Singh, M.M., (2014), Corrosion inhibition of mild steel in acidic solution by Tagetes erecta (Marigold flower) extracts as a green inhibitor, corrosion Science, 85, 352-363.

Qiu, S., Sun, H., Zhang, A. H., Xu, H. Y., Yan, G. L., Han, Y. (2014). Natural alkaloids: basic aspects, biological roles, and future perspectives. Chin J Nat Med12 (6): 401- 406.

Quraishi, M. A., Ambrish, S., Vinod, K. S., Dileep, K. Y. and Ashish, K. S., (2010). Green approach to corrosion inhibition of mild steel in hydrochloric acid and sulphuric acid solutions by the extract of *Murraya koenigii* leaves, Materials Chemistry and Physics, 122; 114-122.

Rajam, K., Rajendram, S., Manivannan, M. & Saranya, R. (2012). Corrosion inhibition by *Alium sativum* (garlic) extract. Journal of Chemical, Biological and Physical Sciences, 2 (3), 1223 – 1233.

Rajendran, S., Sri, V.G., Arockaselvi, J., Amalraj, A;J;, (2005), Corrosion inhibition by plant extracts- an overview, Bulletin of Electrochemistry, 21(8): 367-377.

Ralston, K. D., Chrisanti, S., Young, T. L. and Buchheit, R. G. (2008). Corrosion inhibition of aluminum alloy 2024 - T3 by aqueous vanadium species. Journal of the Electrochemical Society. 155 (7) 350 – 359.

Rani, B. E. A. & Basu, B. B. J. (2012). Green inhibitors for corrosion protection of metals and alloys: An overview, International Journal of Corrosion, 2012, 15.

Refat, M. H. & Ishaq, A. Z., (2013). Kinetics of corrosion inhibition of aluminium in acidic media by water - soluble natural polymeric pectates as aniomic polyelectrolyte inhibitors. Materials 6, 2430 – 2451.

Rethinnagiri, V., Jeyaprakash, P., Arunkumar, M., Maheswaran, V., & Madhiyalagan, A., (2012). Investigation and inhibition of aluminum corrosion in hydrochloric acid solutions by organic compound. Advances in Applied Science Research 3(3), 1718 - 1726.

Rosaline-Vimela, J., Leema, R. A. & Raja, S. (2012). A Study on the phytochemical analysis and corrosion inhibition on mild steal by *Annona Muricata* L. leaves extract in 1N hydrochloric acid. Der Chemica Sinica, 3(3), 582-588.

Sanjay, K. Sharma, Ackmez Muhdoo, Gargi Jain & Jyoti Sharma, (2010), Corrosion and adsorption properties of Azadirachta indica mature leaves extract as green inhibitor for mild steel in HNO_3, Green chemistry letters and Review, 3(1): 7-15.

Saviour, Umoren A., Zuhair M. G., Obot I. B., (2013). Natural products for material protection: Inhibition of mild steel corrosion by date palm seed extracts in acidic media Ind. Eng. Chem. Res. 52: 14855 - 14865.

Shanthi T & Rajendran S., (2013). Corrosion resistance of mild simulate concrete pore solution in presence of carboxy methyl cellulose, Journal of Chemical, Biological and Physical Science**s,** 3(4); 2550-2556

Sharma, K. K, & Sharma, L. K., (1999). A textbook of Physical Chemistry, 9th edition, Viska Publishers, New Delhi.

Shreir, L. L, Jarman, R. A., & Burstein, G. T. (2000). Metal/Environment Reactions in Corrosion, 3rd ed., Butterworth Heinemann, Great Britain.

Siaka, A. A., Eddy, N. O., Idris, S. O., Muhammed, A., Elinge, C. M. and Atiku, F. A., (2012). FTIR spectroscopic information on the corrosion inhibition potential of ampicillin in HCl solution. Innovations in Science and Engineering, 2, 41 - 48.

Sikandar, K. S., Tasveer, Z. B., Kanwal, N., Syed, A. G. & Shahana U. K., (2013). Qualitative phytochemical screening and antifungal activity of *Carica papaya* leaf extract against human and plant pathogenic fungi. Int. J. Pharm., 4(7), 88-86.

Singh, S. K. & Mukherijee, A. K., (2010). Kinetics of mild steel corrosion aqueous acatic acid solution. J. Mater. Sci. Technol., 26(3), 264 – 269.

Skoog, D., West, D. Holler, J. & Crouch, S. (2004). Fundamentals of Analytical Chemistry, 8th edition, India.

Suleiman, M. N. (2011). *In vitro* phytochemical investigation on five medicinal plants in Anyigba and its environs, Kogi State Nigeria. *Der Pharmacia Chemica*, 2(4), 108 - 111.

Syed, S. (2006). Atmospheric Corrosion of Materials, Emirates Journal for Engineering Research, 11 (1), 1-24

Taleb, H. I. & Mohamed, A. Z., (2011). Corrosion inhibition of mild steel using fig leaves extract in hydrochloric acid solution. Int. J. Electrochem. Sci., 6, 6442 – 6455.

Torres, V. V., Amado, R. S., Camila, F., Fernandez, T. L., Carlos A. S. R., Torres, A. G. & Elian, D. (2011). Inhibitory action of aqueous coffee ground extracts on the corrosion of carbon steel in HCl solution. Corrosion Science, 53, 2385 - 2392.

Trethewey, K. R. & Chamberlain, J. (1995). Corrosion for science and Engineering, 2nd Edition, Longman Group Limited, England.

Udhayakala P., Rajendiran, T. V. & Gunasekaran, S., (2012). Theoretical approach to the corrosion inhibition efficiency of some pyrimidine derivatives using DFT method. Journal of Computational Methods in Molecular Design, 2 (1), 1-15.

Ugwoke, C. E. C., Uzekwe, U. & Ameh, G. I. (2010). Phytochemical constituents and ethno botany of the leaf extract of bitter leaf (*Vernonia amygdalina)Del*., Journal of Pharmaceutical Allied Science, 7, 3.

Umoren, S. A, Obot, I. B., Obi-Egbedi, N. O., (2009). Raphia hookeri gum as a potential eco-friendly inhibitor for mild steel in sulfuric acid. J. Mater. Sci. 44: 274 - 279

Uppal, M. M. & Bhatia, S. C., (2009). Engineering chemistry (chemical technology), Khanna publishers, New Delhi, 7th edition, 269-308.

Uwah,I.E., Okafor,P.C., Ebiekpe,V.E. (2013).Inhibitive action of ethanol extracts from Nauclea latifolia on the corrosion of mild steel in H2SO4 solutions and their adsorption characteristics, Arabian Journal of Chemistry, (6), 285–293.

Varvara, S., Rotarum, I., Popa, M., Bostan, R., Glevitzky, M. & Muresan, L. (2010). Environmentally – safe corrosion inhibitors for the protection of Bronzes against corrosion in acidic media. Chem. Bull Polytechnic Univ., 55 (69).

Vasudha, V. G. & Shanmuga, P. K. (2013). Polyalthia longitolia as a corrosion inhibitor for mild steel in HCl solution. Research Journal of Chemical Sciences, 3(1), 21 - 26.

Wang, H. B., Shi, H., Hong, T., Kang, C. & Jepson, W. P., (2001). Characterization of inhibitor and corrosion product film using electrochemical impedance spectroscopy (EIS). Corrosion. NACE International. Paper no 01023.

Yuce, A. O. & Kardas, G. (2012). Adsorption and Inhibition effect of 2 – thiohydantoin on mild steel corrosion in 0.1M HCl. Corrosion Science 58, 86 – 94.

Znini, M., Majidi, L., Bouyanzer, A., Paolini, J., Desjobert, J. M., Costa, J., Hmmonti, B. (2012). Essnetials oil of *salvia aucheri mesatlantica* as a green inhibitor for the corrosion of steel in 0.5m H_2SO_4. Arabian Journal of Chemistry, 5, 467 – 474.

APPENDICES

APPENDIX A

FTIR spectra of different pure plant extracts and scratched oxide film

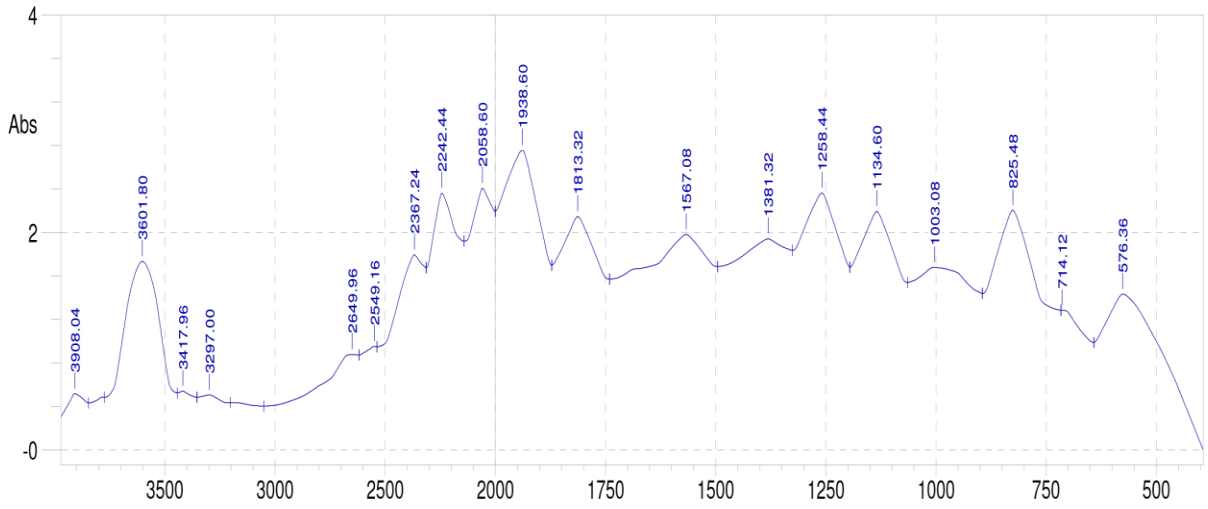

Appendix A1: FTIR Spectrum for *Dennettia tripetala*Ethanol Extract

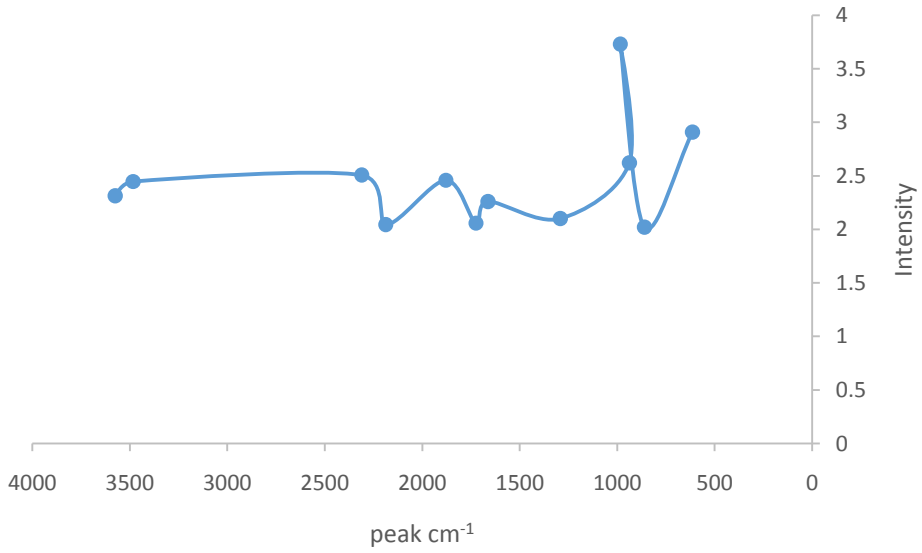

Appendix. A2: FTIR Spectrum for *Dennettia tripetala*scratched oxide film

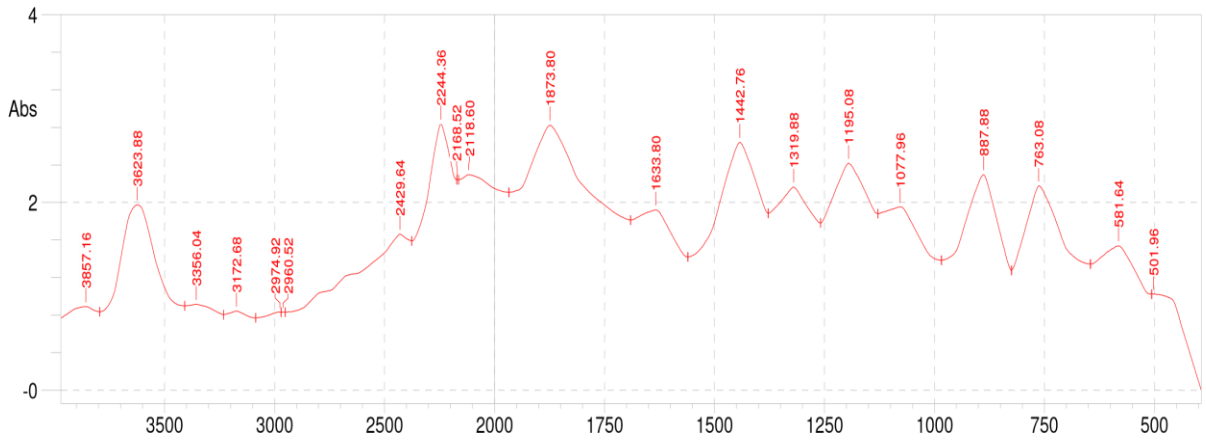

AppendixA3: FTIR Spectrum for *Dialium guineense* Ethanol Extract

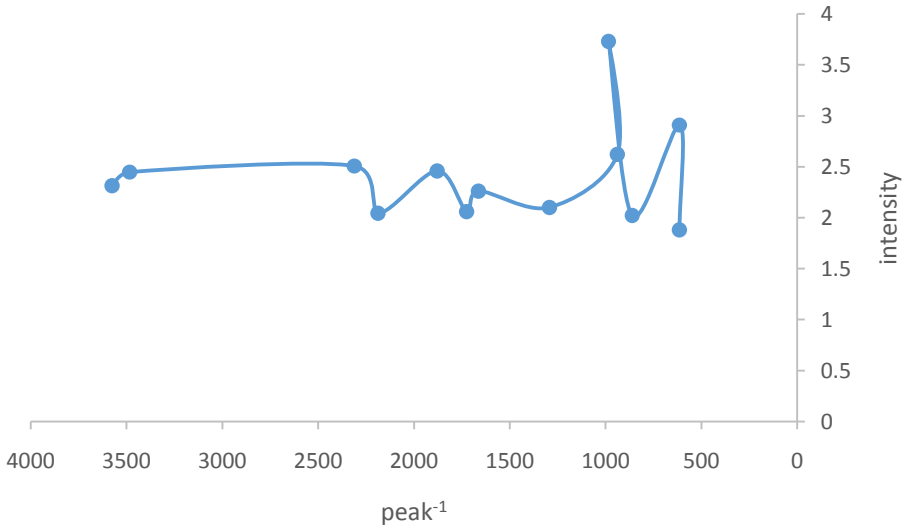

Appendix A4: FTIR Spectrum for*Dialium guineense* of scratched Al oxide film in NaOH

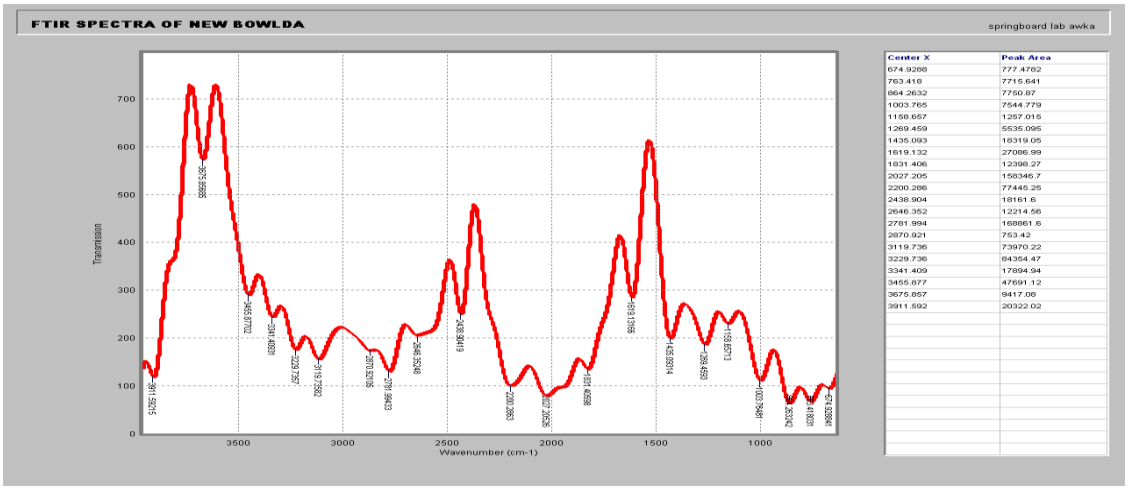

Appendix A5: FTIR Spectrum for *Newbouldia laevis*Ethanol Extract

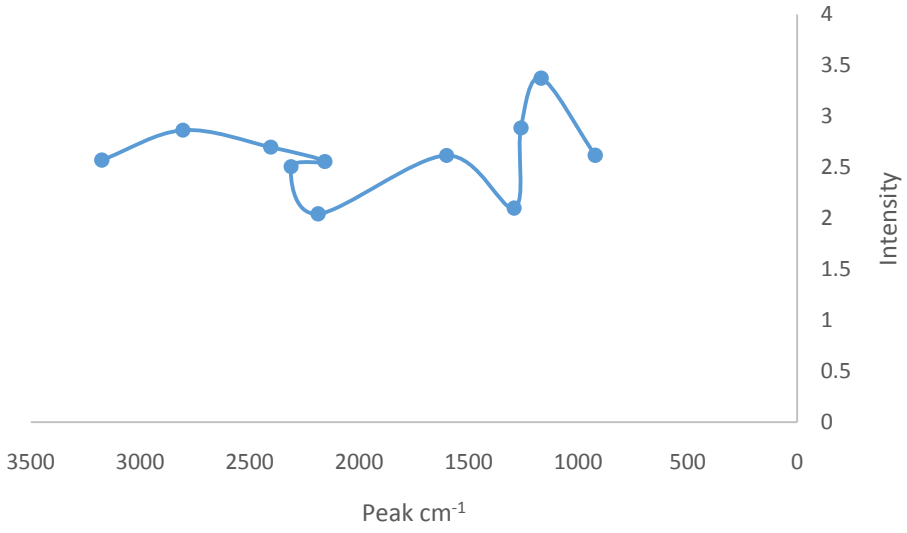

Appendix A6: *Newbouldia leavis*extract of scratched mild steel oxide film using KOH.

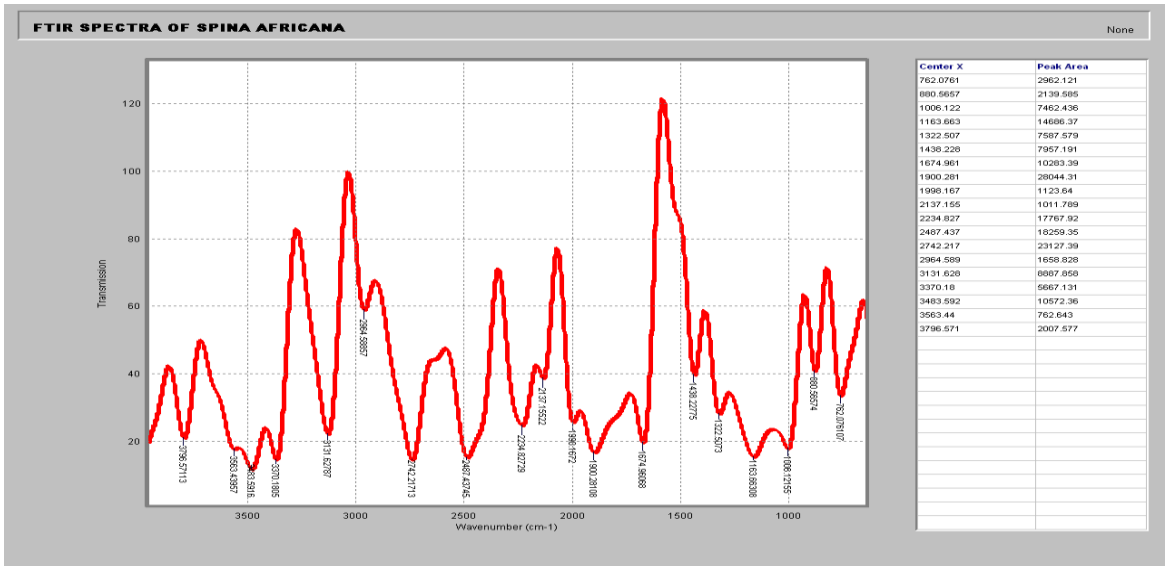

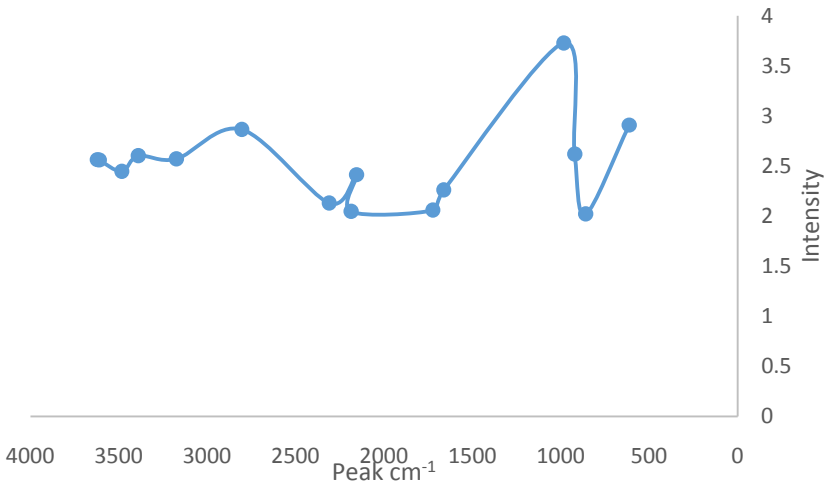

Appendix A8: *Aspilia africana* extract and scratched mild steel oxide film using HCL.

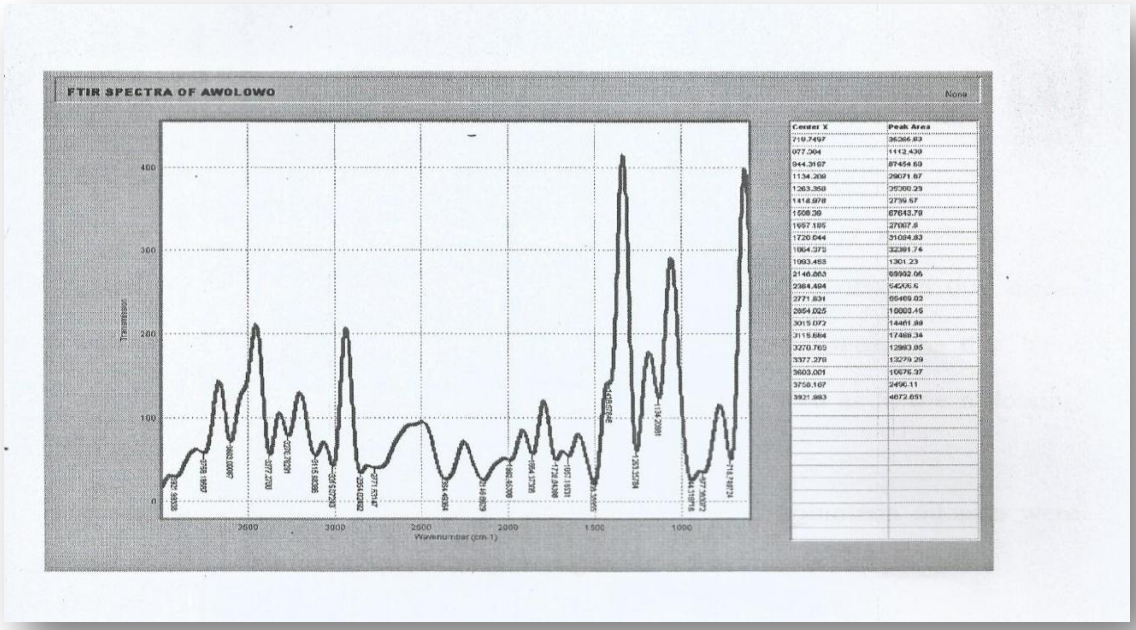

Appendix A9: FTIR Spectrum for *Chromolena odorata*Ethanol Extract

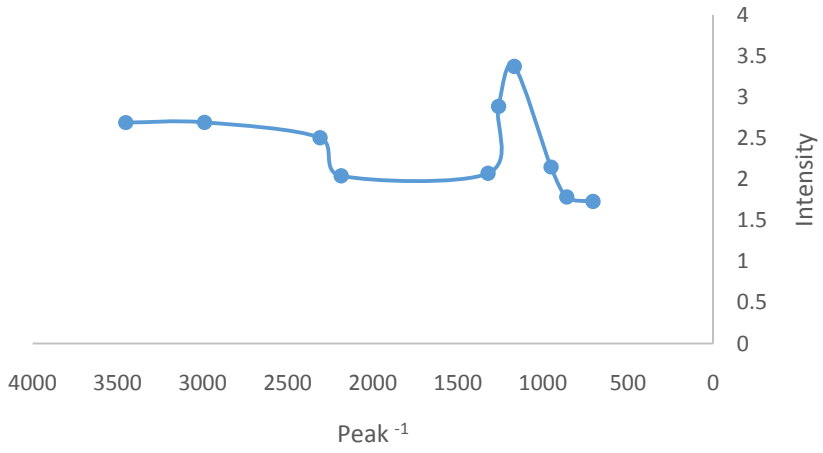

Appendix A10: FTIR analysis of *Chromolena odorata* extract and scratched mild steel oxide film using H_2S0_4

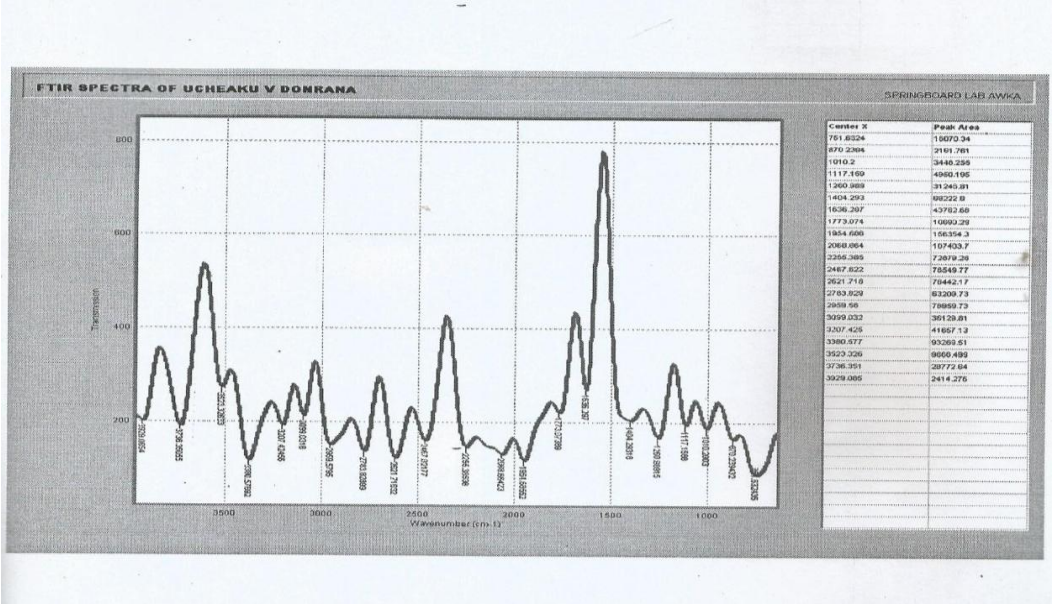

Appendix A11: FTIR Spectrum for *Vitex doniana*Ethanol Extract

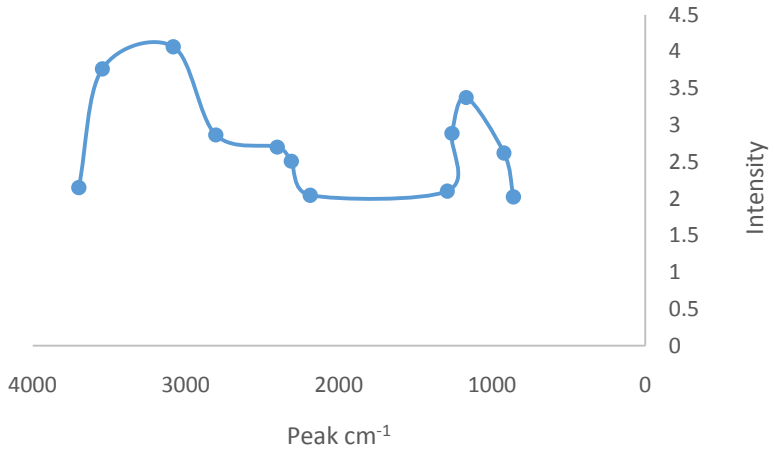

Appendix A12: *Vitex doniana* extract and scratched mild steel oxide film using NaOH .

APPENDIX B:

WEIGHT LOSS, CORROSION RATE AND INHIBITION EFFICIENCY

The data of the weight loss, corrosion rate (CR) and inhibition efficiency (IE) are presented in Appendixs B1 –B48.

B1: Data of corrosion inhibition of Al in NaOH with *Aspilia africana* leaves extract.

Parameter	303K						323K						343K					
Inhibitor conc. g/l	0.0	0.2	0.4	0.6	0.8	1.0	0.0	0.2	0.4	0.6	0.8	1.0	0.0	0.2	0.4	0.6	0.8	1.0
Weight loss (g)	0.68	0.36	0.33	0.25	0.16	0.15	0.81	0.48	0.41	0.37	0.35	0.32	1.7	1.07	0.9	0.84	0.76	0.71
CR (mg/cm^2hr)	51	27	24.75	18.75	12	11.25	60.75	36	30.75	27.75	26.25	24	127.5	80.25	67.5	63	57	53.3
IE (%)		47.06	51.47	63.24	76.47	77.94		40.74	49.38	54.32	56.79	60.49		37.06	47.06	50.59	55.29	58.2

Appendix B2: Data of corrosion inhibition of Al in NaOH *Chromolena odorata* leaves extract.

Parameter	303K						323K						343K					
Inhibitor conc. g/l	0.0	0.2	0.4	0.6	0.8	1.0	0.0	0.2	0.4	0.6	0.8	1.0	0.0	0.2	0.4	0.6	0.8	1.0
Weight loss (g)	0.29	0.17	0.13	0.11	0.1	0.1	0.36	0.23	0.177	0.16	0.153	0.15	0.73	0.48	0.43	0.42	0.41	0.38
CR (mg/cm^2hr)	43.5	25.5	19.5	16.5	15	15	54.01	34.5	26.55	24	22.95	22.5	109.5	72.01	64.51	63.01	61.51	57.01
IE (%)		41.38	55.17	62.07	65.52	65.52		36.11	50.83	55.56	57.5	58.33		34.25	41.1	42.47	43.84	47.95

Appendix B3: Data of corrosion inhibition of Al in NaOH with *Newbouldia leavis* leaves extract.

Parameter	303K						323K						343K					
Inhibitor conc. g/l	0.0	0.2	0.4	0.6	0.8	1.0	0.0	0.2	0.4	0.6	0.8	1.0	0.0	0.2	0.4	0.6	0.8	1.0
Weight loss (g)	0.860	0.427	0.340	0.180	0.170	0.157	1.060	0.547	0.440	0.400	0.390	0.350	2.150	1.180	0.920	0.900	0.840	0.833
CR (mg/cm^2hr)	43.00	21.35	17.00	9.00	8.50	7.85	53.00	27.35	22.00	20.00	19.50	17.50	107.5	59.00	46.00	45.00	42.00	41.65
IE (%)		50.35	60.47	79.07	80.23	81.74		48.4	58.49	62.26	63.21	66.98		45.12	57.21	58.14	60.93	61.26

Appendix B4: Data of corrosion inhibition of Al in NaOH with Dennettia tripetala leaves extract.

Parameter	303K						323K						343K					
Inhibitor conc. g/l	0.0	0.2	0.4	0.6	0.8	1.0	0.0	0.2	0.4	0.6	0.8	1.0	0.0	0.2	0.4	0.6	0.8	1.0
Weight loss (g)	0.29	0.17	0.13	0.11	0.1	0.097	0.36	0.23	0.177	0.16	0.153	0.147	0.73	0.48	0.43	0.42	0.41	0.38
CR (mg/cm^2hr)	43.5	25.5	19.5	16.5	15	14.55	54.01	34.5	26.55	24	22.95	22.05	109.5	72.01	64.51	63.01	61.51	57.01
IE (%)		49.19	60.47	66.28	76.74	77.91		47.17	58.21	60.66	62.26	64.15		44.65	56.74	57.81	60.47	60.60

Appendix B5: Data of corrosion inhibition of Al in NaOH with Dialium guineense leaves extract.

Parameter	303K						323K						343K					
Inhibitor conc. g/l	0.0	0.2	0.4	0.6	0.8	1.0	0.0	0.2	0.4	0.6	0.8	1.0	0.0	0.2	0.4	0.6	0.8	1.0
Weight loss (g)	0.68	0.36	0.33	0.25	0.18	0.18	0.81	0.48	0.41	0.37	0.35	0.33	1.7	1.07	0.9	0.84	0.76	0.72
CR (mg/cm^2hr)	43.5	25.5	19.5	16.5	15	14.55	54.01	34.5	26.55	24	22.95	22.05	109.5	72.01	64.51	63.01	61.51	57.01
IE (%)		47.06	51.47	63.24	73.53	73.53		40.74	49.38	54.52	56.79	59.26		37.06	47.06	50.59	55.29	57.65

AppendixB 6: Data of corrosion inhibition of Al in NaOH with *Vitex doniana* leaves extract.

Parameter	303K						323K						343K					
Inhibitor conc. g/l	0.0	0.2	0.4	0.6	0.8	1.0	0.0	0.2	0.4	0.6	0.8	1.0	0.0	0.2	0.4	0.6	0.8	1.0
Weight loss (g)	0.29	0.17	0.13	0.11	0.1	0.097	0.36	0.23	0.177	0.16	0.153	0.147	0.73	0.48	0.43	0.42	0.41	0.38
CR (mg/cm^2hr)	43.5	25.5	19.5	16.5	15	14.55	54.01	34.5	26.55	24	22.95	22.05	109.5	72.01	64.51	63.01	61.51	57.01
IE (%)		41.38	55.17	62.07	65.52	66.55		36.11	50.83	55.56	57.5	59.17		34.25	41.1	42.47	43.84	47.95

Appendix B 7: Data of corrosion inhibition of Al in KOH with*Aspilia africana* leaves extract.

Parameter	303K						323K						343K					
Inhibitor conc. g/l	0.0	0.2	0.4	0.6	0.8	1.0	0.0	0.2	0.4	0.6	0.8	1.0	0.0	0.2	0.4	0.6	0.8	1.0
Weight loss (g)	1.100	0.630	0.510	0.330	0.300	0.25	1.180	0.690	0.600	0.410	0.380	0.350	2.163	1.300	1.180	0.860	0.830	0.820
CR (mg/cm^2hr)	73.33	42.00	34.00	22.00	20.00	16.67	78.67	46.00	40.00	27.33	25.33	23.33	144.20	86.67	78.67	57.33	55.33	54.67
IE (%)		42.73	53.64	70	72.73	77.27		41.53	49.15	65.25	67.8	70.34		39.9	45.45	60.24	61.63	62.09

Appendix B 8: Data of corrosion inhibition of Al in KOH with *Chromolena odorata* leaves extract.

Parameter	303K						323K						343K					
Inhibitor conc. g/l	0.0	0.2	0.4	0.6	0.8	1.0	0.0	0.2	0.4	0.6	0.8	1.0	0.0	0.2	0.4	0.6	0.8	1.0
Weight loss (g)	0.38	0.237	0.2	0.14	0.13	0.13	0.4	0.26	0.23	0.16	0.15	0.147	0.69	0.46	0.43	0.31	0.3	0.297
CR (mg/cm^2hr)	76	47.4	40	28	26	26	80	52	46	32	30	29.4	138	92	86	62	60	59.4
IE (%)		42.73	53.64	69.73	72.09	73.36		41.53	49.15	65	66.95	67.54		39.9	45.12	60.19	61.17	61.63

Appendix B 9: Data of corrosion inhibition of Al in KOH with Newbouldia laevis leaves extract.

Parameter	303K						323K						343K					
Inhibitor conc. g/l	0.0	0.2	0.4	0.6	0.8	1.0	0.0	0.2	0.4	0.6	0.8	1.0	0.0	0.2	0.4	0.6	0.8	1.0
Weight loss (g)	0.86	0.52	0.44	0.28	0.26	0.22	0.93	0.58	0.52	0.33	0.32	0.3	1.72	1.08	0.98	0.73	0.72	0.69
CR (mg/cm^2hr)	86	52	44	28	26	22	93	58	52	33	32	30	172	108	98	73	72	69
IE (%)		39.53	48.84	67.44	69.77	74.42		37.63	44.09	64.52	65.59	67.74		37.21	43.02	57.56	58.14	59.88

Appendix B 10: Data of corrosion inhibition of Al in KOH with Dennettia tripetala leaves extract.

Parameter	303K						323K						343K					
Inhibitor conc. g/l	0.0	0.2	0.4	0.6	0.8	1.0	0.0	0.2	0.4	0.6	0.8	1.0	0.0	0.2	0.4	0.6	0.8	1.0
Weight loss (g)	1.100	0.630	0.510	0.330	0.307	0.297	1.180	0.690	0.600	0.413	0.390	0.390	2.163	1.300	1.180	0.860	0.837	0.830
CR (mg/cm^2hr)	73.33	42.00	34.00	22.00	20.47	19.80	78.67	46.00	40.00	27.53	26.00	25.33	144.20	86.67	78.67	57.33	55.80	55.33
IE (%)		42.73	53.64	70.00	72.09	73.00		41.53	49.15	65.00	66.95	67.80		39.90	45.45	60.24	61.30	61.63

Appendix B 11: Data of corrosion inhibition of Al in KOH with Dialium guineense leaves extract.

Parameter	303K						323K						343K					
Inhibitor conc. g/l	0.0	0.2	0.4	0.6	0.8	1.0	0.0	0.2	0.4	0.6	0.8	1.0	0.0	0.2	0.4	0.6	0.8	1.0
Weight loss (g)	0.38	0.237	0.2	0.14	0.13	0.13	0.4	0.26	0.23	0.16	0.15	0.147	0.69	0.46	0.43	0.31	0.3	0.297
CR (mg/cm^2hr)	76	47.4	40	28	26	26	80	52	46	32	30	29.4	138	92	86	62	60	59.4
IE (%)		37.63	47.37	63.16	65.79	65.79		35	42.5	60	62.5	63.25		33.33	37.68	55.05	56.52	56.96

Appendix B 12: Data of corrosion inhibition of Al in KOH with *Vitex doniana* leaves extract.

Parameter	303K						323K						343K					
Inhibitor conc. g/l	0.0	0.2	0.4	0.6	0.8	1.0	0.0	0.2	0.4	0.6	0.8	1.0	0.0	0.2	0.4	0.6	0.8	1.0
Weight loss (g)	0.86	0.52	0.44	0.28	0.26	0.22	0.93	0.58	0.52	0.33	0.32	0.3	1.72	1.08	0.98	0.73	0.72	0.69
CR (mg/cm^2hr)	86	52	44	28	26	22	93	58	52	33	32	30	172	108	98	73	72	69
IE (%)		39.53	48.84	67.44	69.77	74.42		37.63	44.09	64.52	65.59	67.74		37.21	43.02	57.56	58.14	59.88

AppendixB 13: Data of corrosion inhibition of Al inHCL with *Aspilia africana* leaves extract.

Parameter	303K						323K						343K					
Inhibitor conc. g/l	0.0	0.2	0.4	0.6	0.8	1.0	0.0	0.2	0.4	0.6	0.8	1.0	0.0	0.2	0.4	0.6	0.8	1.0
Weight loss (g)	0.53	0.33	0.28	0.2	0.18	0.14	0.57	0.39	0.35	0.28	0.25	0.19	0.6	0.42	0.35	0.31	0.27	0.24
CR (mg/cm^2hr)	26.5	16.5	14	10	9	7	28.5	19.5	17.5	14	12.5	9.5	30	21	17.5	15.5	13.5	12
IE (%)		37.74	47.17	62.26	66.04	73.58		31.58	38.6	50.88	56.14	66.67		3030	41.67	48.33	55	60

Appendix B 14: Data of corrosion inhibition of Al in HCL with *Chromolena odorata* leaves extract.

Parameter	303K						323K						343K					
Inhibitor conc. g/l	0.0	0.2	0.4	0.6	0.8	1.0	0.0	0.2	0.4	0.6	0.8	1.0	0.0	0.2	0.4	0.6	0.8	1.0
Weight loss (g)	1.26	0.76	0.51	0.31	0.3	0.28	1.35	0.86	0.55	0.41	0.41	0.4	1.41	0.92	0.64	0.53	0.523	0.52
CR (mg/cm^2hr)	21	12.67	8.5	5.167	5	4.667	22.5	14.33	9.167	6.833	6.833	6.667	23.5	15.33	10.67	8.833	8.717	8.667
IE (%)		39.68	59.52	75.4	76.19	77.78		36.3	59.26	69.63	69.63	70.37		34.75	54.61	62.41	62.91	63.12

Appendix **B**15: Data of corrosion inhibition of Al in HCL with *Newbouldia leavis* leaves extract.

Parameter	303K						323K						343K					
Inhibitor conc. g/l	0.0	0.2	0.4	0.6	0.8	1.0	0.0	0.2	0.4	0.6	0.8	1.0	0.0	0.2	0.4	0.6	0.8	1.0
Weight loss (g)	1.26	0.76	0.51	0.31	0.3	0.28	1.35	0.86	0.55	0.41	0.41	0.33	1.41	0.92	0.64	0.53	0.523	0.52
CR (mg/cm^2hr)	26.5	16.5	14	10	9	7	28.5	19.5	17.5	14	12.5	9.5	30	21	17.5	15.5	13.5	12
IE (%)		39.68	59.52	75.4	76.19	77.78		36.3	59.26	69.63	69.63	75.56		34.75	54.61	62.41	62.91	63.12

Appendix **B** 16: Data of corrosion inhibition of Al in HCL with Dennettia tripetala leaves extract.

Parameter	303K						323K						343K					
Inhibitor conc. g/l	0.0	0.2	0.4	0.6	0.8	1.0	0.0	0.2	0.4	0.6	0.8	1.0	0.0	0.2	0.4	0.6	0.8	1.0
Weight loss (g)	0.53	0.33	0.28	0.2	0.18	0.14	0.57	0.39	0.35	0.28	0.25	0.21	0.6	0.42	0.35	0.31	0.27	0.24
CR (mg/cm^2hr)	26.5	16.5	14	10	9	7	28.5	19.5	17.5	14	12.5	10.5	30	21	17.5	15.5	13.5	12
IE (%)		37.74	47.17	62.26	66.04	73.58		31.58	38.6	50.88	56.14	63.16		30	41.67	48.33	55	60

Appendix **B** 17: Data of corrosion inhibition of Al in HCL with Dialium guineense leaves extract.

Parameter	303K						323K						343K					
Inhibitor conc. g/l	0.0	0.2	0.4	0.6	0.8	1.0	0.0	0.2	0.4	0.6	0.8	1.0	0.0	0.2	0.4	0.6	0.8	1.0
Weight loss (g)	1.610	0.863	0.530	0.340	0.320	0.290	1.690	0.923	0.580	0.450	0.420	0.410	1.750	0.980	0.690	0.610	0.590	0.587
CR (mg/cm^2hr)	16.10	8.63	5.30	3.40	3.20	2.90	16.90	9.23	5.80	4.50	4.20	4.10	17.50	9.80	6.90	6.10	5.90	5.87
IE (%)		46.40	67.08	78.89	80.12	81.99		45.38	65.68	73.37	75.15	75.74		44.00	60.57	65.14	66.29	66.46

Appendix **B** 18: Data of corrosion inhibition of Al in HCL with *Vitex doniana* leaves extract.

Parameter	303K						323K						343K					
Inhibitor conc. g/l	0.0	0.2	0.4	0.6	0.8	1.0	0.0	0.2	0.4	0.6	0.8	1.0	0.0	0.2	0.4	0.6	0.8	1.0
Weight loss (g)	1.26	0.76	0.51	0.31	0.3	0.28	1.35	0.86	0.55	0.41	0.41	0.4	1.41	0.92	0.64	0.53	0.523	0.52
CR (mg/cm^2hr)	21	12.67	8.5	5.167	5	4.667	22.5	14.33	9.167	6.833	6.833	6.667	23.5	15.33	10.67	8.833	8.717	8.667
IE (%)		39.68	59.52	75.4	76.19	77.78		36.3	59.26	69.63	69.63	70.37		34.75	54.61	62.41	62.91	63.12

Appendix **B** 19: Data of corrosion inhibition of Al in $H_2S0_4$with *Aspilia africana* leaves extract.

Parameter	303K						323K						343K					
Inhibitor conc. g/l	0.0	0.2	0.4	0.6	0.8	1.0	0.0	0.2	0.4	0.6	0.8	1.0	0.0	0.2	0.4	0.6	0.8	1.0
Weight loss (g)	0.027	0.017	0.013	0.007	0.007	0.007	0.043	0.027	0.027	0.02	0.02	0.013	0.063	0.04	0.037	0.03	0.03	0.023
CR (mg/cm^2hr)	0.084	0.053	0.041	0.022	0.022	0.022	0.134	0.084	0.084	0.063	0.063	0.041	0.197	0.125	0.116	0.094	0.094	0.072
IE (%)		37.04	51.85	74.07	74.07	74.07		37.21	37.21	53.49	53.49	69.77		36.51	41.27	52.38	52.38	63.49

Appendix **B** 20: Data of corrosion inhibition of Al in $H_2S0_4$with *Chromolena odorata* leaves extract.

Parameter	303K						323K						343K					
Inhibitor conc. g/l	0.0	0.2	0.4	0.6	0.8	1.0	0.0	0.2	0.4	0.6	0.8	1.0	0.0	0.2	0.4	0.6	0.8	1.0
Weight loss (g)	0.02	0.013	0.013	0.01	0.01	0.007	0.023	0.017	0.013	0.013	0.01	0.01	0.033	0.027	0.023	0.023	0.02	0.02
CR (mg/cm^2hr)	0.125	0.081	0.081	0.062	0.062	0.044	0.144	0.106	0.081	0.081	0.062	0.062	0.206	0.169	0.144	0.144	0.125	0.125
IE (%)		35	35	50	50	65		26.09	43.48	43.48	56.52	56.52		18.18	30.3	30.3	39.39	39.39

Appendix **B** 21: Data of corrosion inhibition of Al in $H_2S0_4$with *Newbouldia leavis* leaves extract.

Parameter	303K						323K						343K					
Inhibitor conc. g/l	0.0	0.2	0.4	0.6	0.8	1.0	0.0	0.2	0.4	0.6	0.8	1.0	0.0	0.2	0.4	0.6	0.8	1.0
Weight loss (g)	0.040	0.020	0.013	0.010	0.007	0.007	0.060	0.033	0.027	0.023	0.017	0.013	0.090	0.050	0.047	0.040	0.033	0.030
CR (mg/cm^2hr)	0.083	0.042	0.027	0.021	0.016	0.016	0.125	0.069	0.056	0.048	0.035	0.027	0.188	0.104	0.098	0.083	0.069	0.063
IE (%)		50.50	67.5	75	82.5	82.5		45	55	61.67	71.67	78.33		44.44	47.78	55.56	63.33	66.67

Appendix **B** 22: Data of corrosion inhibition of Al in $H_2S0_4$with Dennettia tripetala leaves extract.

Parameter	303K						323K						343K					
Inhibitor conc. g/l	0.0	0.2	0.4	0.6	0.8	1.0	0.0	0.2	0.4	0.6	0.8	1.0	0.0	0.2	0.4	0.6	0.8	1.0
Weight loss (g)	0.027	0.017	0.013	0.013	0.01	0.01	0.043	0.027	0.027	0.023	0.02	0.02	0.063	0.04	0.037	0.033	0.03	0.03
CR (mg/cm^2hr)	0.084	0.053	0.041	0.041	0.0313	0.0313	0.134	0.084	0.084	0.072	0.063	0.063	0.197	0.125	0.116	0.103	0.094	0.094
IE (%)		50.00	57.50	75.00	82.50	82.50		45.00	55.00	61.67	66.67	71.67		44.44	47.78	55.56	58.89	63.33

Appendix **B** 23: Data of corrosion inhibition of Al in H_2S0_4 with Dialium guineense leaves extract.

Parameter	303K						323K						343K					
Inhibitor conc. g/l	0.0	0.2	0.4	0.6	0.8	1.0	0.0	0.2	0.4	0.6	0.8	1.0	0.0	0.2	0.4	0.6	0.8	1.0
Weight loss (g)	0.040	0.020	0.017	0.010	0.007	0.007	0.06	0.033	0.027	0.023	0.020	0.017	0.090	0.050	0.047	0.040	0.037	0.033
CR (mg/cm^2hr)	0.083	0.042	0.035	0.021	0.015	0.015	0.125	0.069	0.056	0.048	0.042	0.035	0.188	0.104	0.098	0.083	0.077	0.069
IE (%)		50.00	57.50	75.00	82.50	82.50		45.00	55.00	61.67	66.67	71.67		44.44	47.78	55.56	58.89	63.33

Appendix **B** 24: Data of corrosion inhibition of Al in H_2S0_4 with *Vitex doniana* leaves extract.

Parameter	303K						323K						343K					
Inhibitor conc. g/l	0.0	0.2	0.4	0.6	0.8	1.0	0.0	0.2	0.4	0.6	0.8	1.0	0.0	0.2	0.4	0.6	0.8	1.0
Weight loss (g)	0.027	0.017	0.013	0.013	0.01	0.01	0.043	0.027	0.027	0.023	0.02	0.02	0.063	0.04	0.037	0.033	0.03	0.03
CR (mg/cm^2hr)	0.084	0.053	0.041	0.041	0.0313	0.0313	0.134	0.084	0.084	0.072	0.063	0.063	0.197	0.125	0.116	0.103	0.094	0.094
IE (%)		50.00	57.50	75.00	82.50	82.50		45.00	55.00	61.67	66.67	71.67		44.44	47.78	55.56	58.89	63.33

Appendix **B** 25: Data of corrosion inhibition of Mild steel in KOH with *Aspilia africana* leaves extract.

Parameter	303K						323K						343K					
Inhibitor conc. g/l	0.0	0.2	0.4	0.6	0.8	1.0	0.0	0.2	0.4	0.6	0.8	1.0	0.0	0.2	0.4	0.6	0.8	1.0
Weight loss (g)	0.04	0.027	0.023	0.023	0.02	0.017	0.05	0.037	0.033	0.033	0.027	0.027	0.06	0.047	0.04	0.04	0.037	0.037
CR (mg/cm^2hr)	0.125	0.084	0.072	0.072	0.062	0.053	0.156	0.116	0.103	0.103	0.084	0.084	0.187	0.147	0.125	0.125	0.116	0.116
IE (%)	37.04	51.85	74.07	74.07	74.07		37.21	37.21	53.49	53.49	69.77		36.51	41.27	52.38	52.38	63.49	

Appendix **B** 26: Data of corrosion inhibition of Mild steel in KOH with *Chromolena odorata* leaves extract.

Parameter	303K						323K						343K					
Inhibitor conc. g/l	0.0	0.2	0.4	0.6	0.8	1.0	0.0	0.2	0.4	0.6	0.8	1.0	0.0	0.2	0.4	0.6	0.8	1.0
Weight loss (g)	0.053	0.03	0.027	0.023	0.02	0.02	0.063	0.04	0.037	0.033	0.03	0.027	0.077	0.06	0.047	0.043	0.04	0.04
CR (mg/cm^2hr)	0.110	0.063	0.056	0.048	0.042	0.042	0.131	0.083	0.077	0.069	0.063	0.056	0.160	0.125	0.098	0.090	0.083	0.083
IE (%)		50	67.5	75	82.5	82.5		45	55	61.67	66.67	71.67		44.44	47.78	55.56	63.33	66.67

Appendix **B** 27: Data of corrosion inhibition of Mild steel in KOH with *Newbouldia leavis* leaves extract.

Parameter	303K						323K						343K					
Inhibitor conc. g/l	0.0	0.2	0.4	0.6	0.8	1.0	0.0	0.2	0.4	0.6	0.8	1.0	0.0	0.2	0.4	0.6	0.8	1.0
Weight loss (g)	0.02	0.013	0.013	0.01	0.01	0.01	0.027	0.02	0.02	0.017	0.017	0.013	0.037	0.03	0.027	0.027	0.023	0.023
CR (mg/cm^2hr)	0.125	0.081	0.081	0.063	0.063	0.063	0.169	0.125	0.125	0.106	0.106	0.081	0.231	0.188	0.169	0.169	0.144	0.144
IE (%)		35	35	50	65	65		26.09	43.48	43.48	56.52	56.52		18.18	30.3	30.3	39.39	39.39

Appendix **B** 28: Data of corrosion inhibition of Mild steel in KOH with Dennettia tripetala leaves extract.

Parameter	303K						323K						343K					
Inhibitor conc. g/l	0.0	0.2	0.4	0.6	0.8	1.0	0.0	0.2	0.4	0.6	0.8	1.0	0.0	0.2	0.4	0.6	0.8	1.0
Weight loss (g)	0.04	0.027	0.023	0.023	0.02	0.017	0.05	0.037	0.033	0.033	0.027	0.027	0.06	0.047	0.04	0.04	0.037	0.037
CR (mg/cm^2hr)	0.125	0.084	0.072	0.072	0.062	0.053	0.156	0.116	0.103	0.103	0.084	0.084	0.187	0.147	0.125	0.125	0.116	0.116
IE (%)	37.04	51.85	74.07	74.07	74.07		37.21	37.21	53.49	53.49	69.77		36.51	41.27	52.38	52.38	63.49	

Appendix **B** 29: Data of corrosion inhibition of Mild steel in KOH with Dialium guineense leaves extract.

Parameter	303K						323K						343K					
Inhibitor conc. g/l	0.0	0.2	0.4	0.6	0.8	1.0	0.0	0.2	0.4	0.6	0.8	1.0	0.0	0.2	0.4	0.6	0.8	1.0
Weight loss (g)	0.053	0.03	0.027	0.023	0.02	0.02	0.063	0.04	0.037	0.033	0.03	0.027	0.077	0.06	0.047	0.043	0.04	0.04
CR (mg/cm^2hr)	0.110	0.063	0.056	0.048	0.042	0.042	0.131	0.083	0.077	0.069	0.063	0.056	0.160	0.125	0.098	0.090	0.083	0.083
IE (%)		50	67.5	75	82.5	82.5		45	55	61.67	66.67	71.67		44.44	47.78	55.56	63.33	66.67

Appendix **B** 30: Data of corrosion inhibition of Mild steel in KOH with *Vitex doniana* leaves extract.

Parameter	303K						323K						343K					
Inhibitor conc. g/l	0.0	0.2	0.4	0.6	0.8	1.0	0.0	0.2	0.4	0.6	0.8	1.0	0.0	0.2	0.4	0.6	0.8	1.0
Weight loss (g)	0.02	0.013	0.013	0.01	0.01	0.01	0.027	0.02	0.02	0.017	0.017	0.013	0.037	0.03	0.027	0.027	0.023	0.023
CR (mg/cm^2hr)	0.125	0.081	0.081	0.063	0.063	0.063	0.169	0.125	0.125	0.106	0.106	0.081	0.231	0.188	0.169	0.169	0.144	0.144
IE (%)		35	35	50	65	65		26.09	43.48	43.48	56.52	56.52		18.18	30.3	30.3	39.39	39.39

Appendix **B** 31: Data of corrosion inhibition of Mild steel in NaOH with *Aspilia africana* leaves extract.

Parameter	303K						323K						343K					
Inhibitor conc. g/l	0.0	0.2	0.4	0.6	0.8	1.0	0.0	0.2	0.4	0.6	0.8	1.0	0.0	0.2	0.4	0.6	0.8	1.0
Weight loss (g)	0.02	0.013	0.013	0.01	0.007	0.007	0.023	0.017	0.013	0.013	0.013	0.01	0.03	0.023	0.023	0.02	0.02	0.017
CR (mg/cm^2hr)	0.037	0.027	0.027	0.017	0.017	0.013	0.053	0.04	0.033	0.03	0.027	0.027	0.057	0.047	0.037	0.037	0.03	0.03
IE (%)		37.74	47.17	62.26	66.04	73.58		31.58	38.6	50.88	56.14	66.67		3030	41.67	48.33	55	60

Appendix **B** 32: Data of corrosion inhibition of Mild steel in NaOH with *Chromolena odorata* leaves extract.

Parameter	303K						323K						343K					
Inhibitor conc. g/l	0.0	0.2	0.4	0.6	0.8	1.0	0.0	0.2	0.4	0.6	0.8	1.0	0.0	0.2	0.4	0.6	0.8	1.0
Weight loss (g)	0.037	0.027	0.027	0.017	0.017	0.013	0.053	0.04	0.033	0.03	0.027	0.027	0.057	0.047	0.037	0.037	0.03	0.03
CR (mg/cm^2hr)	0.116	0.084	0.084	0.053	0.053	0.041	0.166	0.125	0.103	0.094	0.084	0.084	0.178	0.147	0.116	0.116	0.094	0.094
IE (%)		39.68	59.52	75.4	76.19	77.78		36.3	59.26	69.63	69.63	75.56		34.75	54.61	62.41	62.91	63.12

Appendix **B** 33: Data of corrosion inhibition of Mild steel in NaOH with *Newbouldia leavis* leaves extract.

Parameter	303K						323K						343K					
Inhibitor conc. g/l	0.0	0.2	0.4	0.6	0.8	1.0	0.0	0.2	0.4	0.6	0.8	1.0	0.0	0.2	0.4	0.6	0.8	1.0
Weight loss (g)	0.05	0.03	0.023	0.02	0.017	0.013	0.06	0.037	0.033	0.03	0.027	0.023	0.07	0.05	0.04	0.037	0.033	0.033
CR (mg/cm^2hr)	0.104	0.063	0.048	0.042	0.035	0.027	0.125	0.077	0.069	0.063	0.056	0.048	0.146	0.104	0.083	0.077	0.069	0.069
IE (%)		46.58	67.08	78.88	80.75	82.42		45.56	65.68	73.37	75.15	76.33		44	60.57	66.29	66.46	66.69

Appendix **B** 34: Data of corrosion inhibition of Mild steel in NaOH with Dennettia tripetala leaves extract.

Parameter	303K						323K						343K					
Inhibitor conc. g/l	0.0	0.2	0.4	0.6	0.8	1.0	0.0	0.2	0.4	0.6	0.8	1.0	0.0	0.2	0.4	0.6	0.8	1.0
Weight loss (g)	0.02	0.013	0.013	0.01	0.007	0.007	0.023	0.017	0.013	0.013	0.013	0.01	0.03	0.023	0.023	0.02	0.02	0.017
CR (mg/cm^2hr)	0.037	0.027	0.027	0.017	0.017	0.013	0.053	0.04	0.033	0.03	0.027	0.027	0.057	0.047	0.037	0.037	0.03	0.03
IE (%)		37.74	47.17	62.26	66.04	73.58		31.58	38.6	50.88	56.14	66.67		3030	41.67	48.33	55	60

Appendix **B** 35: Data of corrosion inhibition of Mild steel in NaOH with Dialium guineense leaves extract.

Parameter	303K						323K						343K					
Inhibitor conc. g/l	0.0	0.2	0.4	0.6	0.8	1.0	0.0	0.2	0.4	0.6	0.8	1.0	0.0	0.2	0.4	0.6	0.8	1.0
Weight loss (g)	0.037	0.027	0.027	0.017	0.017	0.013	0.053	0.04	0.033	0.03	0.027	0.027	0.057	0.047	0.037	0.037	0.03	0.03
CR (mg/cm^2hr)	0.116	0.084	0.084	0.053	0.053	0.041	0.166	0.125	0.103	0.094	0.084	0.084	0.178	0.147	0.116	0.116	0.094	0.094
IE (%)		39.68	59.52	75.4	76.19	77.78		36.3	59.26	69.63	69.63	75.56		34.75	54.61	62.41	62.91	63.12

Appendix **B** 36: Data of corrosion inhibition of Mild steel in NaOH with *Vitex doniana* leaves extract.

Parameter	303K						323K						343K					
Inhibitor conc. g/l	0.0	0.2	0.4	0.6	0.8	1.0	0.0	0.2	0.4	0.6	0.8	1.0	0.0	0.2	0.4	0.6	0.8	1.0
Weight loss (g)	0.05	0.03	0.023	0.02	0.017	0.013	0.06	0.037	0.033	0.03	0.027	0.023	0.07	0.05	0.04	0.037	0.033	0.033
CR (mg/cm^2hr)	0.104	0.063	0.048	0.042	0.035	0.027	0.125	0.077	0.069	0.063	0.056	0.048	0.146	0.104	0.083	0.077	0.069	0.069
IE (%)		46.58	67.08	78.88	80.75	82.42		45.56	65.68	73.37	75.15	76.33		44	60.57	66.29	66.46	66.69

Appendix **B** 37: Data of corrosion inhibition of Mild steel in HCL with *Aspilia africana* leaves extract.

Parameter	303K						323K						343K					
Inhibitor conc. g/l	0.0	0.2	0.4	0.6	0.8	1.0	0.0	0.2	0.4	0.6	0.8	1.0	0.0	0.2	0.4	0.6	0.8	1.0
Weight loss (g)	0.1	0.06	0.04	0.04	0.03	0.03	0.113	0.07	0.063	0.047	0.04	0.04	0.14	0.097	0.07	0.067	0.057	0.057
CR (mg/cm^2hr)	0.313	0.187	0.125	0.125	0.094	0.094	0.353	0.219	0.197	0.147	0.125	0.125	0.438	0.303	0.219	0.209	0.178	0.178
IE (%)		40	60	60	70	70		38.05	44.25	58.41	64.6	64.6		30.71	50	52.14	59.29	59.29

Appendix **B** 38: Data of corrosion inhibition of Mild steel in HCL with *Chromolena odorata* leaves extract.

Parameter	303K						323K						343K					
Inhibitor conc. g/l	0.0	0.2	0.4	0.6	0.8	1.0	0.0	0.2	0.4	0.6	0.8	1.0	0.0	0.2	0.4	0.6	0.8	1.0
Weight loss (g)	0.137	0.07	0.05	0.03	0.023	0.02	0.147	0.08	0.063	0.047	0.04	0.033	0.2	0.13	0.093	0.08	0.07	0.067
CR (mg/cm^2hr)	0.285	0.146	0.104	0.062	0.048	0.042	0.306	0.167	0.131	0.098	0.083	0.069	0.417	0.271	0.194	0.167	0.146	0.140
IE (%)		48.91	63.50	78.10	83.21	85.40		44.06	55.94	67.13	72.03	76.92		35	53.5	60	65	66.5

Appendix **B** 39: Data of corrosion inhibition of Mild steel in HCL with *Newbouldia leavis* leaves extract.

Parameter	303K						323K						343K					
Inhibitor conc. g/l	0.0	0.2	0.4	0.6	0.8	1.0	0.0	0.2	0.4	0.6	0.8	1.0	0.0	0.2	0.4	0.6	0.8	1.0
Weight loss (g)	0.057	0.037	0.03	0.02	0.023	0.017	0.067	0.047	0.04	0.037	0.03	0.027	0.077	0.057	0.05	0.04	0.037	0.037
CR (mg/cm^2hr)	0.356	0.231	0.188	0.125	0.144	0.106	0.419	0.294	0.25	0.231	0.188	0.169	0.481	0.356	0.313	0.25	0.231	0.231
IE (%)		35.09	47.37	64.91	59.65	70.18		29.85	40.3	44.78	55.22	59.7		25.97	35.06	48.05	51.95	51.95

Appendix **B** 40: Data of corrosion inhibition of Mild steel in HCL with Dennettia tripetala leaves extract.

Parameter	303K						323K						343K					
Inhibitor conc. g/l	0.0	0.2	0.4	0.6	0.8	1.0	0.0	0.2	0.4	0.6	0.8	1.0	0.0	0.2	0.4	0.6	0.8	1.0
Weight loss (g)	0.1	0.06	0.04	0.04	0.03	0.03	0.113	0.07	0.063	0.047	0.04	0.04	0.14	0.097	0.07	0.067	0.057	0.057
CR (mg/cm^2hr)	0.313	0.187	0.125	0.125	0.094	0.094	0.353	0.219	0.197	0.147	0.125	0.125	0.438	0.303	0.219	0.209	0.178	0.178
IE (%)		40	60	60	70	70		38.05	44.25	58.41	64.6	64.6		30.71	50	52.14	59.29	59.29

Appendix **B** 41: Data of corrosion inhibition of Mild steel in HCL with Dialium guineense leaves extract.

Parameter	303K						323K						343K					
Inhibitor conc. g/l	0.0	0.2	0.4	0.6	0.8	1.0	0.0	0.2	0.4	0.6	0.8	1.0	0.0	0.2	0.4	0.6	0.8	1.0
Weight loss (g)	0.137	0.07	0.05	0.03	0.023	0.02	0.147	0.08	0.063	0.047	0.04	0.033	0.2	0.13	0.093	0.08	0.07	0.067
CR (mg/cm^2hr)	0.285	0.146	0.104	0.062	0.048	0.042	0.306	0.167	0.131	0.098	0.083	0.069	0.417	0.271	0.194	0.167	0.146	0.140
IE (%)		48.91	63.50	78.10	83.21	85.40		44.06	55.94	67.13	72.03	76.92		35	53.5	60	65	66.5

Appendix **B** 42: Data of corrosion inhibition of Mild steel in HCL with *Vitex doniana* leaves extract.

Parameter	303K						323K						343K					
Inhibitor conc. g/l	0.0	0.2	0.4	0.6	0.8	1.0	0.0	0.2	0.4	0.6	0.8	1.0	0.0	0.2	0.4	0.6	0.8	1.0
Weight loss (g)	0.057	0.037	0.03	0.02	0.023	0.017	0.067	0.047	0.04	0.037	0.03	0.027	0.077	0.057	0.05	0.04	0.037	0.037
CR (mg/cm^2hr)	0.356	0.231	0.188	0.125	0.144	0.106	0.419	0.294	0.25	0.231	0.188	0.169	0.481	0.356	0.313	0.25	0.231	0.231
IE (%)		35.09	47.37	64.91	59.65	70.18		29.85	40.3	44.78	55.22	59.7		25.97	35.06	48.05	51.95	51.95

Appendix **B** 43: Data of corrosion inhibition of Mild steel in H_2S0_4 with *Aspilia africana* leaves extract.

Parameter	303K						323K						343K					
Inhibitor conc. g/l	0.0	0.2	0.4	0.6	0.8	1.0	0.0	0.2	0.4	0.6	0.8	1.0	0.0	0.2	0.4	0.6	0.8	1.0
Weight loss (g)	1.3	0.72	0.53	0.37	0.31	0.30	1.38	0.79	0.59	0.43	0.40	0.38	1.43	0.89	0.75	0.5	0.497	0.48
CR (mg/cm^2hr)	2.708	1.5	1.104	0.771	0.646	0.625	2.875	1.646	1.229	0.896	0.833	0.792	2.979	1.854	1.563	1.042	1.035	1
IE (%)		44.62	59.23	71.54	76.15	76.92		42.75	57.25	68.84	71.01	72.46		37.76	47.55	65.034	65.24	66.43

Appendix **B** 44: Data of corrosion inhibition of Mild steel in H_2S0_4 with *Chromolena odorata* leaves extract.

Parameter	303K						323K						343K					
Inhibitor conc. g/l	0.0	0.2	0.4	0.6	0.8	1.0	0.0	0.2	0.4	0.6	0.8	1.0	0.0	0.2	0.4	0.6	0.8	1.0
Weight loss (g)	0.52	0.32	0.27	0.25	0.213	0.21	0.56	0.36	0.327	0.27	0.24	0.22	0.58	0.38	0.37	0.29	0.29	0.25
CR (mg/cm^2hr)	3.25	2	1.688	1.563	1.331	1.313	3.5	2.25	2.044	1.688	1.5	1.375	3.625	2.375	2.313	1.812	1.812	1.563
IE (%)		38.46	48.08	51.92	59.04	59.62		35.71	41.61	51.79	57.14	60.71		34.48	36.21	50	50	56.9

Appendix **B** 45: Data of corrosion inhibition of Mild steel in H_2S0_4 with newbouuldia leavis leaves extract.

Parameter	303K						323K						343K					
Inhibitor conc. g/l	0.0	0.2	0.4	0.6	0.8	1.0	0.0	0.2	0.4	0.6	0.8	1.0	0.0	0.2	0.4	0.6	0.8	1.0
Weight loss (g)	0.93	0.527	0.453	0.31	0.303	0.3	0.99	0.62	0.53	0.4	0.36	0.35	1.02	0.713	0.57	0.42	0.413	0.39
CR (mg/cm^2hr)	2.906	1.647	1.416	0.969	0.947	0.938	3.094	1.938	1.656	1.25	1.125	1.094	3.188	2.228	1.781	1.312	1.291	1.327
IE (%)		43.33	51.29	66.67	67.42	67.74		37.37	46.46	59.6	63.64	64.65		30.1	44.12	58.82	59.51	61.76

Appendix **B** 46: Data of corrosion inhibition of Mild steel in H_2S0_4 with Dennettia tripetala leaves extract.

Parameter	303K						323K						343K					
Inhibitor conc. g/l	0.0	0.2	0.4	0.6	0.8	1.0	0.0	0.2	0.4	0.6	0.8	1.0	0.0	0.2	0.4	0.6	0.8	1.0
Weight loss (g)	1.3	0.72	0.53	0.37	0.31	0.30	1.38	0.79	0.59	0.43	0.40	0.38	1.43	0.89	0.75	0.5	0.497	0.48
CR (mg/cm^2hr)	2.708	1.5	1.104	0.771	0.646	0.625	2.875	1.646	1.229	0.896	0.833	0.792	2.979	1.854	1.563	1.042	1.035	1
IE (%)		44.62	59.23	71.54	76.15	76.92		42.75	57.25	68.84	71.01	72.46		37.76	47.55	65.034	65.24	66.43

Appendix **B** 47: Data of corrosion inhibition of Mild steel in H_2S0_4 with Dialium guineense leaves extract.

Parameter	303K						323K						343K					
Inhibitor conc. g/l	0.0	0.2	0.4	0.6	0.8	1.0	0.0	0.2	0.4	0.6	0.8	1.0	0.0	0.2	0.4	0.6	0.8	1.0
Weight loss (g)	0.52	0.32	0.27	0.25	0.213	0.21	0.56	0.36	0.327	0.27	0.24	0.22	0.58	0.38	0.37	0.29	0.29	0.25
CR (mg/cm^2hr)	3.25	2	1.688	1.563	1.331	1.313	3.5	2.25	2.044	1.688	1.5	1.375	3.625	2.375	2.313	1.812	1.812	1.563
IE (%)		38.46	48.08	51.92	59.04	59.62		35.71	41.61	51.79	57.14	60.71		34.48	36.21	50	50	56.9

Appendix **B** 48: Data of corrosion inhibition of Mild steel in H_2S0_4 with *Vitex doniana* leaves extract.

Parameter	303K						323K						343K					
Inhibitor conc. g/l	0.0	0.2	0.4	0.6	0.8	1.0	0.0	0.2	0.4	0.6	0.8	1.0	0.0	0.2	0.4	0.6	0.8	1.0
Weight loss (g)	0.93	0.527	0.453	0.31	0.303	0.3	0.99	0.62	0.53	0.4	0.36	0.35	1.02	0.713	0.57	0.42	0.413	0.39
CR (mg/cm^2hr)	2.906	1.647	1.416	0.969	0.947	0.938	3.094	1.938	1.656	1.25	1.125	1.094	3.188	2.228	1.781	1.312	1.291	1.327
IE (%)		43.33	51.29	66.67	67.42	67.74		37.37	46.46	59.6	63.64	64.65		30.1	44.12	58.82	59.51	61.76